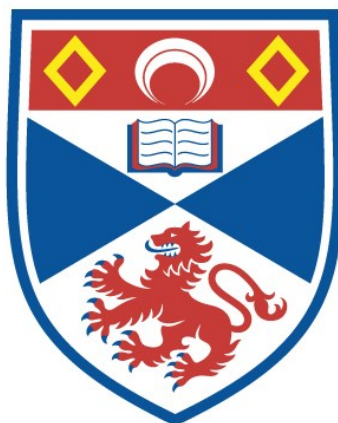


ENANTIOSELECTIVE FLUORINATION OF BIOACTIVE AMINES AND  
SUCCINIC ACIDS FOR SELECTED BIOASSAYS

Yohann Jean Gilles Renault

A Thesis Submitted for the Degree of PhD  
at the  
University of St Andrews



2023

Full metadata for this item is available in  
St Andrews Research Repository

<http://research-repository.st-andrews.ac.uk/>

Identifiers to use to cite or link to this thesis:

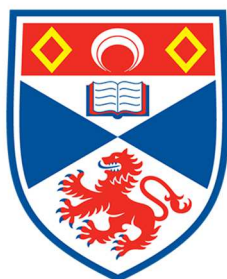
DOI: <https://doi.org/10.17630/sta/612>

<http://hdl.handle.net/10023/28396>

This item is protected by original copyright

# Enantioselective Fluorination of Bioactive Amines and Succinic Acids for Selected Bioassays

Yohann Jean Gilles Renault



University of  
St Andrews

This thesis is submitted in partial fulfilment for the degree of  
Doctor of Philosophy (PhD)  
at the University of St Andrews

April 2023

## **Candidate's declaration**

I, Yohann Jean Gilles Renault, do hereby certify that this thesis, submitted for the degree of PhD, which is approximately 47,000 words in length, has been written by me, and that it is the record of work carried out by me, or principally by myself in collaboration with others as acknowledged, and that it has not been submitted in any previous application for any degree. I confirm that any appendices included in my thesis contain only material permitted by the 'Assessment of Postgraduate Research Students' policy.

I was admitted as a research student at the University of St Andrews in September 2018.

I received funding from an organisation or institution and have acknowledged the funder(s) in the full text of my thesis.

Date 8<sup>th</sup> of September 2023

## **Supervisor's declaration**

I hereby certify that the candidate has fulfilled the conditions of the Resolution and Regulations appropriate for the degree of PhD in the University of St Andrews and that the candidate is qualified to submit this thesis in application for that degree. I confirm that any appendices included in the thesis contain only material permitted by the 'Assessment of Postgraduate Research Students' policy.

Date 8<sup>th</sup> of September 2023

Signature of supervisor

## **Permission for publication**

In submitting this thesis to the University of St Andrews we understand that we are giving permission for it to be made available for use in accordance with the regulations of the University Library for the time being in force, subject to any copyright vested in the work not being affected thereby. We also understand, unless exempt by an award of an embargo as requested below, that the title and the abstract will be published, and that a copy of the work may be made and supplied to any bona fide library or research worker, that this thesis will be electronically accessible for personal or research use and that the library has the right to migrate this thesis into new electronic forms as required to ensure continued access to the thesis.

I, Yohann Jean Gilles Renault, confirm that my thesis does not contain any third-party material that requires copyright clearance.

The following is an agreed request by candidate and supervisor regarding the publication of this thesis:

**Printed copy**

No embargo on print copy.

**Electronic copy**

No embargo on electronic copy.

Date 8<sup>th</sup> of September 2023

Date 8<sup>th</sup> of September 2023

Signature of supervisor

## **Underpinning Research Data or Digital Outputs**

### **Candidate's declaration**

I, Yohann Jean Gilles Renault, understand that by declaring that I have original research data or digital outputs, I should make every effort in meeting the University's and research funders' requirements on the deposit and sharing of research data or research digital outputs.

Date 8<sup>th</sup> of September 2023

### **Permission for publication of underpinning research data or digital outputs**

We understand that for any original research data or digital outputs which are deposited, we are giving permission for them to be made available for use in accordance with the requirements of the University and research funders, for the time being in force.

We also understand that the title and the description will be published, and that the underpinning research data or digital outputs will be electronically accessible for use in accordance with the license specified at the point of deposit, unless exempt by award of an embargo as requested below.

The following is an agreed request by candidate and supervisor regarding the publication of underpinning research data or digital outputs:

No embargo on underpinning research data or digital outputs.

Date 8<sup>th</sup> of September 2023

Date 8<sup>th</sup> of September 2023

Signature of supervisor

## Abstract

Since its isolation by Henri Moissan in 1886, fluorine has garnered a growing interest within many fields of chemistry. This attention is a result of the unique properties of fluorine, explained by it being the most electronegative element in the Periodic Table.

Chapter I introduces the principal characteristics of fluoro-compounds. A description of the different synthetic processes that have been developed to afford fluoro-organic molecules is then detailed. Finally, a brief history of fluoro-containing drugs is reviewed, including the impact of fluorine regarding essential parameters that are necessary in their design, such as lipophilicity, acidity, and hydrogen bonding.

Chapter II gives an overview of the three different methodologies of enantioselective  $\alpha$ -fluorination of aldehydes that were developed in 2005. This is followed by development of a new approach to the determination of enantiomeric ratios (er) of fluoro-amines using  $^{19}\text{F}\{^1\text{H}\}$ -NMR. Finally, the optimisation of  $\alpha$ -fluorination of aldehydes toward the synthesis of the fluoro-bioactives will be explored in this chapter.

Chapter III focuses on GABA, the principal neurotransmitter inhibitor of the central nervous system, detailing its mode of action and its importance in treating many diseases, alongside its existing analogues. This chapter includes a shorter enantioselective synthesis of 3-F-GABA developing from previous synthesis.

Chapter IV explores calcium-sensing receptors (CaSR), their existing modulators and previous enantioselective synthesis of F-cinacalcet. An optimised  $\alpha$ -fluorination of aldehydes is explored towards a 2 step 1 pot synthesis of F-cinacalcet (( $^{\text{F}}\text{S},\text{R}$ )-**269**, ( $^{\text{F}}\text{R},\text{R}$ )-**269**) and other fluoro allosteric modulators (( $^{\text{F}}\text{S},\text{R}$ )-**280**, ( $^{\text{F}}\text{R},\text{R}$ )-**280**, ( $^{\text{F}}\text{S},\text{R}$ )-**281**, ( $^{\text{F}}\text{R},\text{R}$ )-**281**, ( $^{\text{F}}\text{S},\text{R}$ )-**286**, ( $^{\text{F}}\text{R},\text{R}$ )-**286**). The potency of these new F-cinacalcet analogues is assessed in a CaSR bioassay giving an insight into the active molecular conformation.

Chapter V gives a general introduction to the importance of isocitrate lyase (ICL) as a drug target for tuberculosis (TB). The design and synthesis of 4 fluoro-succinic acids (**S**)-**315**, (**R**)-**315**, **316** and **317** as potential ICL inhibitors is achieved. Finally, a ICL bioassay with (**S**)-**315**, (**R**)-**315**, and **316** is utilised to assess their mode of action.

## Acknowledgement

First, I would like to thank my supervisor Prof David O'Hagan, for welcoming me within his research group and for all his advice given throughout my Ph.D. degree. I would like also to thank the University of St Andrews for the studentship (financial support). This work was supported by University of St Andrews (School of Chemistry).

I would like to thank all technical and support staff of the University of St Andrews School of Chemistry, for their amazing work helping to provide the data needed for this Ph.D. A particular thank you to Dr. Thomas Lébl and Dr. Siobhan Smith for the NMR service, Dr. David Cordes for X-Ray data and Caroline Hosburgh Mass Spec.

I would like also to express my gratitude toward all my colleagues, Ph.D. students and Post Doc within the O'Hagan lab for their help, support, and friendship over these four and a half years. I want thanks Dr. Phillip Lowe and Dr. Qingzhi Zhang especially, for their help and patience over these years. I would like to particularly thank my colleagues and friends, Luca Dobson, Maria Papa, Guillaume Poss, Clementine Wachter and Alan Obled for all great moments spent together.

I am also thankful to the Archery Club of the University of St Andrews for all the great times and experiences. In particular, I am thankful to Josephine Stewart, Janine Smithies, and Murray Elliot for their support, advice, and for always creating a great atmosphere on the shooting line all over these years spent together.

I would like to give a special thanks to Paul Jackson for his love and support. There are not enough words to describe how happy I am to have you in my life.

Finalement, dans ma langue d'origine, je souhaite remercier toute ma famille, mes parents, Jean et Jacqueline Renault, mon frère Kevin Renault, ma sœur Manuella Renault, et ma marraine Sophie Rousset, pour leur soutien moral et financier tout au long de mes études supérieures. Je tiens également à remercier tous mes amis qui sont resté en France mais qui ont toujours été là pour moi en toutes circonstances, Aurélie Mons, Roxane Baron, Laura Geoffroy, Camille Vicente, Chloé Larrue, Celine Gâtel, Alexis Bourdet, Florian Rohart. Pour finir, j'aimerais remercier tout spécialement mon professeur de chimie, Valery Cavyn, pour son soutien et son amitié tout au long de mes études supérieures.

## **Research Data/Digital Outputs access statement**

Research data underpinning this thesis are available at  
<https://doi.org/10.17630/32c1ff4b-4d39-4bed-8518-4499b21a31c4>



## Abbreviations

$[\alpha]^{20}_D$	Optical rotation
$\delta$	Chemical shift
$\mu$	Micro
ADME	Absorption, Distribution, Metabolism, Excretion
ADP	Adenosine diphosphate
Ala	Alanine
amu	Atomic mass unit
Arg	Arginine
Arom	Aromatic
ATP	Adenosine triphosphate
BBB	Blood brain barrier
Boc	<i>tert</i> -Butyloxycarbonyl
Bn	Benzyl
CaSR	Calcium sensing receptor
CNS	Central nervous system
CoA	Coenzyme A
COVID-19	Coronavirus disease 2019
CR	Cysteine rich domain
Cys	Cysteine
d	doublet
DAST	Diethylaminosulfur trifluoride
DCE	1,2-Dichloroethane
DCM	Dichloroethane
de	Diastereomeric excess
DFMBA	<i>N,N</i> -Diethyl- $\alpha,\alpha$ -difluoro-3- methylbenzylamine
DIBAL	Diisobutylaluminium hydride
DMF	Dimethylformamide
DMP	Dess-Martin periodinane
DMPU	<i>N,N'</i> -Dimethylpropyleneurea

DMS	Dimethyl sulfide
DNA	Deoxyribonucleic acid
dr	Diastereomeric ratio
E <sub>1</sub> CB	Elimination unimolecular conjugate base
ECD	Extracellular domain
EC <sub>50</sub>	Half maximal effective concentration
ee	Enantiomeric excess
equiv	Equivalent
ESI	Electrospray
er	Enantiomeric ratio
5'FDA	5'-Fluorodeoxyadenosine
FDA	Food and Drug Administration
GABA	γ-Aminobutyric acid
GABA-T	4-Aminobutyrate transaminase
GABOB	γ-Amino-β-hydroxybutyric acid
GAD	Glutamic acid decarboxylase
Glu	Glutamic acid
Gln	Glutamine
HCV	Hepatitis C virus
HCV-NS5B	HCV-non encoded 5B protein
HEK	Human embryonic kidney
HFIP	1,1,1,3,3,3-Hexafluoro-2-propanol
His	Histidine
HIV	Human immunodeficiency viruses
HOMO	Highest occupied molecular orbital
HPT	Hypothalamus-pituitary-thyroid
HSV-1	Herpes simplex virus
5-HT <sub>1D</sub>	5-Hydroxytryptamine receptor 1D
ICD	Intracellular domain
IC <sub>50</sub>	Half maximal inhibitory concentration
ICL	Isocitrate lyase
IDH	Isocitrate dehydrogenase
<i>i</i> -Pr	Isopropyl

IR	Infra red
$J$	Spin-spin coupling constant
$K_a$	Acid dissociation constant
$K_B$	Binding dissociation constant
LB	Ligand binding site
LDA	Lithium diisopropylamine
LDH	Lactate dehydrogenase
Leu	Leucine
$\log \alpha\beta$	Cooperativity
$\log D$	Distribution coefficient
$\log P$	Partition coefficient
LUMO	Lowest unoccupied molecular orbital
$m$	Multiplet
mCPBA	<i>meta</i> -Chloroperbenzoic acid
Me	Methyl
MIC	Minimum inhibitory concentration
m.p.	Melting point
MS	Malate synthase
MS	Mass spectrometry
$m/z$	Mass / charge ratio
NAD	Nicotinamide adenine dinucleotide
NADP	Nicotinamide adenine dinucleotide phosphate
NAM	Negative allosteric modulator
NBS	<i>N</i> -Bromosuccinamide
NFBB	<i>N</i> -fluoro- <i>N</i> -( <i>tert</i> -butyl)- <i>tert</i> -butanesulfonamide
NFOBS	<i>N</i> -Fluoro- <i>o</i> -benzenedisulfonimide
NFSI	<i>N</i> -Fluorobenzenesulfonimide
NIC	( <i>2R,3S</i> )-2-Hydroxy-3-(nitromethyl)succinic acid
NMR	Nuclear magnetic resonance
3-NP	3- Nitropropionic acid

NP	Natural product
ODS	Ozone-depleting substances
<i>p</i>	Para
PAM	Positive allosteric modulators
PFC	Perfluorocarbons
pH	Potential of hydrogen
Phe	Phenylalanine
PivCl	Pivaloyl chloride
pK <sub>a</sub>	Negative log of K <sub>a</sub>
pK <sub>B</sub>	Negative log of K <sub>B</sub>
PLP	Pyridoxal phosphate
PTFE	Polytetrafluoroethylene
PTH	Parathyroid hormone
<i>p</i> -TSA	<i>p</i> -Toluenesulfonic acid
PyFluor	2-Pyridinesulfonyl fluoride
Pyr	Pyridine
q	Quartet
RNA	Ribonucleic acid
RT	Room temperature
s	Singlet
SAM	( <i>S</i> )-Adenosyl methionine
Selectfluor <sup>®</sup>	1-(Chloromethyl)-4-fluoro-1,4-diazabicyclo[2.2.2]octane-1,4-dium ditetrafluoroborate
SEM	Standard error of mean
S <sub>N</sub> <sup>2</sup>	Substitution nucleophilic bimolecular
SPS	Solvent purification system
SSA	Succinic semialdehyde
SSADH	Succinic semialdehyde dehydrogenase
t	triplet
TB	Tuberculosis
TBAF	<i>N</i> -tetrabutylammonium fluoride
TCA	Tricarboxylic acid cycle

TFE	Tetrafluoroethylene
THF	Tetrahydrofuran
TMD	Trans membrane domain
TREAT-HF	Triethylamine trihydrofluoride
Trp	Tryptophan
Ts	Tosyl
VIC	2-Vinyl-D-isocitrate
WHO	World health organisation
WWII	World war two

# Contents

Abstract .....	i
Acknowledgement.....	ii
Abbreviations.....	iv
Contents.....	ix
<b>Chapter I Introduction.....</b>	<b>1</b>
<b>1.1. The fluorine atom.....</b>	<b>5</b>
<b>1.2. The carbon-fluorine bond .....</b>	<b>6</b>
<b>1.3. Stereoelectronic effects of fluorine in organic molecules .....</b>	<b>9</b>
<b>1.3.1. <i>Gauche</i> effect.....</b>	<b>9</b>
<b>1.3.2. Electrostatic <i>gauche</i> effect .....</b>	<b>10</b>
<b>1.4. Effect of fluorine on boiling point (bp) .....</b>	<b>12</b>
<b>1.5. Fluorination reactions .....</b>	<b>14</b>
<b>1.5.1. First fluorination reactions.....</b>	<b>14</b>
<b>1.5.2 Strategies for mono-fluorination reactions .....</b>	<b>16</b>
<b>1.5.2.1. Nucleophilic fluorination .....</b>	<b>16</b>
<b>1.5.2.2. Electrophilic fluorination.....</b>	<b>22</b>
<b>1.6. Fluorine in natural products.....</b>	<b>30</b>
<b>1.7. Fluorine in Medicinal chemistry .....</b>	<b>33</b>
<b>1.7.1. Fluorine containing drugs .....</b>	<b>33</b>
<b>1.7.2. Influence of fluorine properties in drugs development.....</b>	<b>37</b>
<b>1.7.2.1. Lipophilicity .....</b>	<b>37</b>
<b>1.7.2.2. The Fluorous Phase .....</b>	<b>42</b>
<b>1.7.2.3. Hydrogen bonding .....</b>	<b>43</b>
<b>1.7.2.4. Acidity.....</b>	<b>44</b>
<b>1.8. Conclusion .....</b>	<b>49</b>
<b>Chapter II <math>\alpha</math>-Fluorination of aldehydes .....</b>	<b>50</b>
<b>2.1. Importance of molecule enantiopurity in pharmaceuticals .....</b>	<b>50</b>
<b>2.2. Different approaches to the <math>\alpha</math>-fluorination of aldehydes .....</b>	<b>52</b>
<b>2.2.1. Preparation of <math>\beta</math>-fluoro alcohols .....</b>	<b>52</b>
<b>2.2.2. Preparation of <math>\beta</math>-fluoro amines<sup>119</sup> .....</b>	<b>56</b>
<b>2.3. Optimisation of <math>\alpha</math>-fluorination of aldehydes to afford <math>\beta</math>-fluoro-alcohols and <math>\beta</math>-fluoro-amines .....</b>	<b>59</b>
<b>2.4. New approach to <sup>19</sup>F NMR enantiomeric excess (ee) determination .....</b>	<b>64</b>

2.5. Conclusion .....	70
<b>Chapter III 2<sup>nd</sup> Generation synthesis of 3-F-GABA stereoisomers.....</b>	<b>71</b>
3.1. Role of GABA and GABA receptors.....	71
3.2. GABA analogues .....	78
3.3. 3-F-GABA synthesis and assay .....	81
3.3.1. First synthesis of 3-F-GABA <sup>166</sup> .....	81
3.3.2 Previous synthesis of 3-F-GABA enantiomers <sup>28</sup> .....	81
3.3.3 Synthesis of 3-F-GABA adapting the Lindsley protocol. ....	84
3.4. Conclusion .....	94
<b>Chapter IV Selective fluorination of calcium sensing receptor(CaSR) agonists ..</b>	<b>95</b>
4.1. Extracellular calcium sensing receptors (CaSR) .....	95
4.2. Calcium receptors agonists .....	99
4.2.1. Orthosteric ligands.....	99
4.2.2. Allosteric modulators of CaSR.....	101
4.3. Development of F-cinacalcet and other fluoro allosteric modulators.....	108
4.3.1 F-Cinacalcet <sup>248</sup> .....	108
4.3.2 Synthesis of F-cinacalcet analogues adapting the Lindsley protocol...	112
4.3.3 CaR receptor assays .....	121
4.4. Conclusion .....	124
<b>Chapter V Targeting isocitrate lyase (ICL).....</b>	<b>125</b>
5.1. Introduction.....	125
5.1.1. Introduction to ICL.....	129
5.1.2. Existing inhibitors of ICL.....	133
5.1.2.1 Non-covalent inhibitors.....	133
5.1.2.2 Covalent inhibitors of ICL.....	139
5.2. Synthesis and assay of potential inhibitors.....	148
5.2.1 Synthesis of fluorosuccinic acid targets.....	148
5.2.1.1 Mono fluorosuccinic acids.....	151
5.2.1.2 Difluorosuccinic acids .....	155
5.3. ICL assay experiments .....	166
5.3.1. Enzyme assay of (S)/(R)-2-F-succinic acids.....	166
5.3.2. Enzyme assay of <i>erythro</i> -2,3-difluorosuccinic acid.....	171
5.4. Conclusion .....	177
<b>Chapter VI Experimental.....</b>	<b>178</b>
6.1 General experimental .....	178

<b>6.2 Synthetic procedure and characterisation of compounds</b> .....	180
<b>References</b> .....	223
Annexe 1.....	239
Annexe 2.....	240
Annexe 3.....	241



## Chapter I Introduction

'Fluor' comes from the latin *fluere*, translating to "flux", because fluorite ( $\text{CaF}_2$ ) was used as a flux (a substance added to a metal to purify and promote fluidity) in metallurgy due to its low melting point ( $1402\text{ }^\circ\text{C}$ ).<sup>1</sup> Hydrofluoric acid (HF) was first prepared in 1771 thanks the work of Carl-Willhem Scheele but he never managed to isolate HF; <sup>2</sup> however, it was subsequently purified in 1809 by Joseph Louis Gay-Lussac and Louis Jacques Thénard.<sup>2</sup> Following the isolation of HF, Humphry Davy carried out electrolytic experiments to afford anhydrous HF between 1813-1814.<sup>2</sup> Davy observed a normal electric current while the HF contained water, whereas without water the conductivity disappeared.<sup>2</sup> His methodology helped him to obtain some pure HF at low temperature; however, the HF evaporated rapidly, creating a very dangerous environment.<sup>2</sup> Other work on HF isolation was carried out by Aimé (1833) and the Knox brothers (1836) without success and this also led to incidents of severe injury while trying to handle HF and discovering its properties.<sup>2</sup> Later in 1854, Edmond Frémy carried out the electrolysis of liquid  $\text{CaF}_2$  at high temperature and observed on the anode the formation of a gas which quickly degraded the platinum covering of the electrode. In 1869, George Gore determined some properties of HF, such as its boiling point and its behaviour in reactions with other acids or metals, using the HF production methodology developed Frémy.<sup>2</sup> The work of Gore was qualified as "remarkable by its exactitude" by Henri Moissan.<sup>2</sup> Finally in 1886, Henri Moissan (Figure 1.1) manage to isolate  $\text{F}_2$  thanks to the electrolysis of HF with KF added as an electrolyte, and for this achievement he was awarded the 1906 Nobel Prize.<sup>2,3</sup>

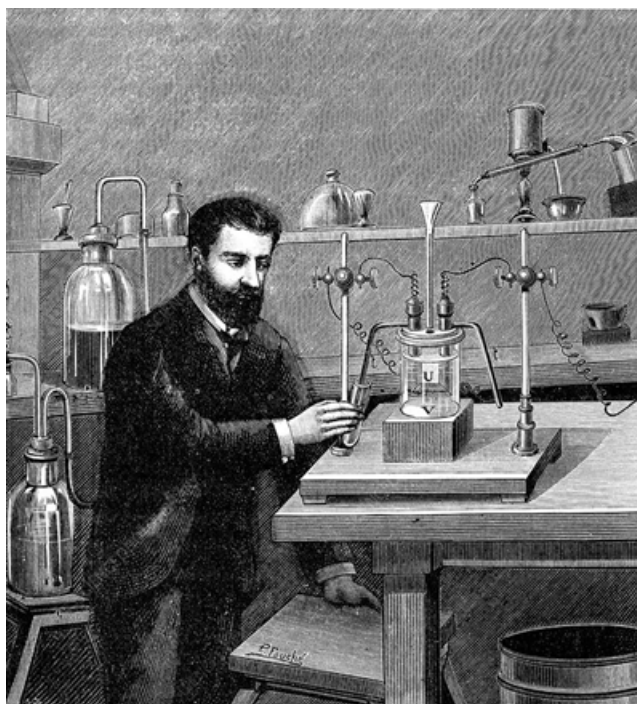
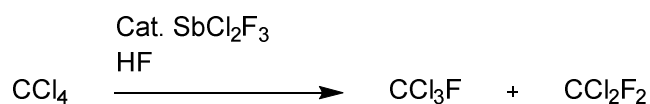


**Figure 1.1** Drawing from Paul Fouché of Henri Moissan (1852-1907) next to the electrolysis apparatus used for the isolation of  $F_2$ .<sup>4</sup>

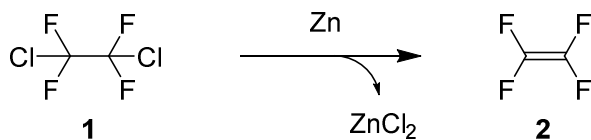
The history of fluorinated organic compounds in industry started in 1928, with the desire of General Motors to find substitute engine coolants due to the high flammability and/or toxicity of current products.<sup>5,6</sup> This effort led to the synthesis of  $CCl_2F_2$  by Midgley *et al.*, using  $CCl_4$  and  $SbF_3$ . The work of Midgley was used to develop compounds which were commercialised by DuPont, and in particular  $CCl_2F_2$  (commercialised under the name Freon<sup>®</sup>) using  $CCl_4$ , HF and catalysed by in-situ generated  $SbCl_2F_3$  (Scheme 1.1).<sup>6-8</sup>



**Scheme 1.1** Synthesis of Freon<sup>®</sup> using  $CCl_4$  and HF/ $SbF_3$ , developed by DuPont.

Research on the development of new refrigerants progressed and led to the discovery of (poly)-tetrafluoroethylene (PTFE) by Plunkett, a chemist working at DuPont, a polymer generated from tetrafluoroethylene (TFE) **2**, itself generated from Freon<sup>®</sup> 114 **1** (Scheme

1.2). PTFE remains a significant polymer today as it is chemically and moisture resistant.<sup>6,7,9,10</sup>



**Scheme 1.2** Synthesis of TFE **2** starting from Freon<sup>®</sup> 114 **1**.

During WWII (Manhattan Project), UF<sub>6</sub> was investigated as a gaseous derivative for separating U<sup>235</sup> from U<sup>238</sup> and success here led to the development of the atomic bomb. UF<sub>6</sub> was obtained from the reaction between UO<sub>2</sub> and HF to afford UF<sub>4</sub>, and this product was then treated with fluorine gas to afford UF<sub>6</sub>. The Manhattan Project also accelerated the development of new fluorocarbon compounds in order to have surfaces which were resistant to UF<sub>6</sub>.<sup>11</sup>

After WWII, the patent rights for Freon<sup>®</sup>'s were acquired by the 3M company, and they carried on the development and commercialisation of highly fluorinated compounds as adhesives.<sup>6</sup> At the same time (1948), Dupont commercialised PTFE under the name Teflon<sup>®</sup> and this was used for its non-stick properties on cookware coatings and as a polymeric material for stain repellent.<sup>6,7</sup>

In the 1960s the world woke up to the environmental impact of certain chemicals such as inorganic mercuric compounds.<sup>6</sup> In order to produce NaOH, mercury was replaced by fluorine-containing ion exchange membranes.<sup>12,13</sup> Due to the stability of the C-F bond, these membranes proved very resistant to corrosive chemicals.

In 1974 it became obvious that there was a depletion in atmospheric ozone, and that an ozone hole was growing in the Southern hemisphere. The problem was connected to chlorine radicals being generated from chlorofluorocarbon refrigerants, and such compounds presented a major problem to the environment.<sup>14</sup> The environmental impact of these chemicals led to one of the rare times when all UN countries united to ratify The Montreal Protocol in September 1987. The Montreal Protocol required the lowering consumption and production of ozone depleting substances (ODS), following a managed

timeline. Thanks to this global effort the Protocol has contributed to the reversal of ozone depletion and a full recovery is estimated by 2050.<sup>15</sup>

Agrochemicals containing fluorine were developed in the 1930s with aryl-CF<sub>3</sub> compounds emerging as herbicides and insecticides.<sup>16,17</sup> Nowadays, fluoro compounds are used across a wide range of industries such as electronics, materials and pharmaceuticals. However due to the growing challenge toward protecting our environment it is important to study the consequences of fluorine containing compounds and to take their bio-degradation into consideration.

## 1.1. The fluorine atom

The fluorine atom is the most electronegative in the Periodic Table. This electronegativity is enhanced by the high nuclear charge linked to its small atomic radius. Due to its electronegativity, removing an electron from fluorine ( $1s^2 2s^2 2p^5$ ) to form  $F^+$ , is a high energy process ( $+401.2 \text{ kcal.mol}^{-1}$ ) due to the 2p orbitals being close to the nucleus. For comparison it is easier to remove an electron (oxidise) from oxygen ( $+312.9 \text{ kcal.mol}^{-1}$ ) as the nucleus is less positively charged with only eight rather than nine protons. On the other hand, adding an electron to a fluorine atom to form  $F^-$  (fluoride) is relatively straightforward ( $-78.3 \text{ kcal.mol}^{-1}$ ) as the electron is stabilised by the nuclear charge.

Fluorine has a van der Waals radius between oxygen and hydrogen, and thus fluorine can replace a hydrogen or an oxygen atom without significantly sterically impacting a given molecule (Table 1.1). This replacement changes other properties such as lipophilicity and polarity. It is also the next smallest atom to hydrogen that forms stable bonds to carbon, and this has found wide use in pharmaceuticals.

**Table 1.1** Comparison of the electronegativity and the Van er Waals radius of H, O and F.<sup>18,19</sup>

	<b>H</b>	<b>O</b>	<b>F</b>
<b>Electronegativity (pauling)</b>	2.1	3.5	4.0
<b>Van der waals radius (Å)</b>	1.2	1.52	1.47

## 1.2. The carbon-fluorine bond

The C-F bond is considered to be the strongest in organic chemistry. This strength is explained by the electronegativity difference between carbon ( $\delta^+$ ) and fluorine ( $\delta^-$ ) enhancing an ionic character resulting in high polarisation of the bond. This strength can be observed when comparing the energy dissociation between C-F and other C-X halogen bonds or the C-O and C-H bonds (Table 1.2).

**Table 1.2** Comparison of the C-F bond length and bond dissociation energy to C-H, C-O, C-Cl bonds.<sup>19</sup>

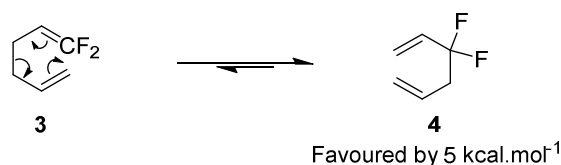
	<b>C-F</b>	<b>C-H</b>	<b>C-O</b>	<b>C-Cl</b>
<b>Bond length (Å)</b>	1.35	1.09	1.43	1.77
<b>Bond dissociation energy (kcal.mol<sup>-1</sup>)</b>	105.4	98.8	84	78.5

The sequential addition of one to four fluorines on the same carbon increases the strength and progressively decreases the length of the bond (Table 1.3), which can be explained by a progressively increasing partial charge on carbon.<sup>19</sup>

**Table 1.3** Correlation between the increasing number of fluorines and the bond length and bond dissociation energies of the C-F bond.

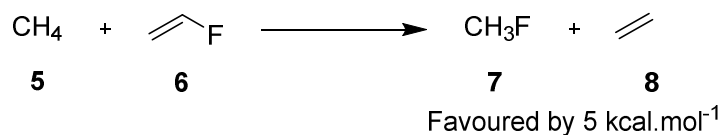
	<b>CH<sub>3</sub>F</b>	<b>CH<sub>2</sub>F<sub>2</sub></b>	<b>CHF<sub>3</sub></b>	<b>CF<sub>4</sub></b>
<b>C-F Bond length (Å)</b>	1.385	1.357	1.332	1.319
<b>C-F Bond dissociation energy (kcal.mol<sup>-1</sup>)</b>	109.9	119.5	127.5	130.5

In 1987 Dolbier *et al.*, while exploring the Cope rearrangement (Scheme 1.3), demonstrated the preference of fluorine to bind to a  $sp^3$  over a  $sp^2$  hybridised carbon.<sup>20</sup> The preference is explained by the ability of fluorine to attract more electrons from the more polarisable  $sp^3$  orbitals, which have increased p-orbital density.



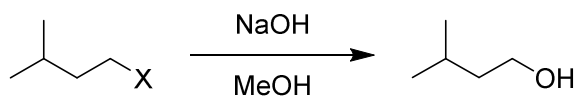
**Scheme 1.3** Cope rearrangement of **3** illustrating the preference of fluorine to bond to a sp<sup>3</sup> carbon.<sup>20</sup>

The phenomenon was also observed in 2006 by Pieniazek *et al.*, in a computational isodesmic reaction comparing the overall energies of vinyl fluoride **5** and methane **6** relative to fluoromethane **7** and ethylene **8** (Scheme 1.4).<sup>21</sup>



**Scheme 1.4** Isodesmic reaction between **5** + **6** and **7** + **8**, illustrating the preference of fluorine to bond to a sp<sup>3</sup> carbon.<sup>21</sup>

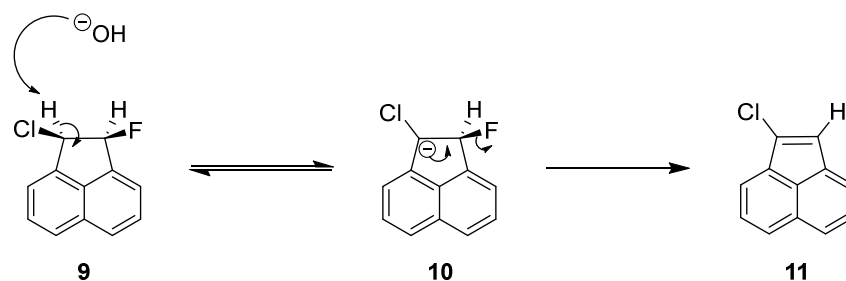
Due to the high strength of the C-F bond, it follows that fluorine is a poor leaving group in S<sub>N</sub>2 reactions. This is illustrated in the rate data in Figure 1.2, which shows the relative rates of different alkyl halides in S<sub>N</sub>2 reactions with hydroxide ion.<sup>19</sup>



X	Relative rate
F	1
Cl	71
Br	3500
I	4500

**Figure 1.2** Relative rate comparison of halides as a leaving group.<sup>19</sup>

On the other hand, due to the high polarisation of the C-F bond, the elimination of fluoride can occur by an E<sub>1</sub>cb mechanism starting with the deprotonation of a hydrogen β to a fluorine.<sup>22</sup> This anion is stabilised by the inductive electron withdrawing effect of the fluorine, and this promotes a two-step elimination process (Scheme 1.5).<sup>22</sup>



**Scheme 1.5** Non-concerted E<sub>1</sub>cb elimination of hydrogen fluoride from **9**.



### 1.3. Stereoelectronic effects of fluorine in organic molecules

#### 1.3.1. *Gauche* effect

The *gauche* effect describes the tendency of 1,2-difluoroethane **12** to prefer a conformation where the fluorines are *gauche* ( $60^\circ$ ) rather than *anti* ( $180^\circ$ ) to each other.<sup>23</sup> This conformation is energetically more favourable than other conformations by  $0.8 \text{ kcal.mol}^{-1}$  in the gas phase. This is perhaps unexpected as sterics might anticipate that the larger substituents would prefer to be *anti*-periplanar to each other (*anti*) (Figure 1.3). For example, 1,2-dichloroethane **12** prefers such an *anti*-conformation.

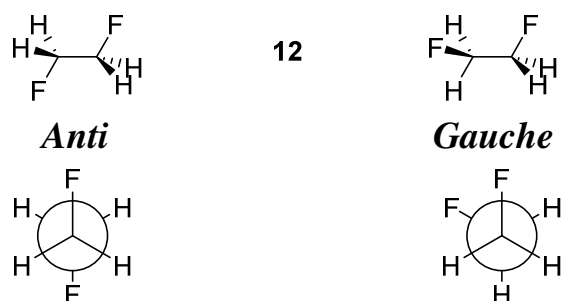


**Figure 1.3**                      *Anti* and *gauche* conformations of difluoroethane **12**.

Several reasons have been proposed over the years for this preference. The most widely accepted explanation involves hyperconjugation between the electron rich C-H  $\sigma$  orbitals (HOMO) and the  $\sigma^*$  antibonding orbitals of the C-F bonds (LUMO), which act as an electron acceptor. Only the *gauche* conformation allows good overlap between these two orbitals and the interactions occur in both direction as there are two fluorine atoms (Figure 1.4).<sup>24</sup>

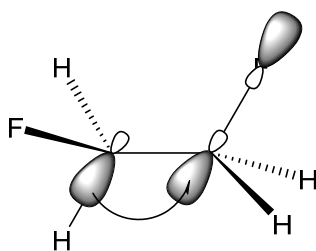


**Figure 1.4**                      Overlap between the C-H  $\sigma$  orbital and the antibonding  $\sigma^*$  of C-F.

### 1.3.2. Electrostatic *gauche* effect

The “electrostatic *gauche* effect” is an extension of the *gauche* effect in that the conformational preference is supported by an additional electrostatic attraction between fluorine and a positive charge. The classical “*gauche* effect” has an energy difference between *anti* and *gauche* conformers of around  $\sim 0.5 - 1.0 \text{ kcal.mol}^{-1}$ , whereas this increases for the “electrostatic *gauche* effect” to between  $4.0 - 8.0 \text{ kcal.mol}^{-1}$ ,<sup>25</sup> similar to the strength of a conventional hydrogen bond.<sup>26</sup>

The electrostatic *gauche* effect can have an important influence on the preferred conformation of charged molecules. This is seen for example with the fluoroethylpyridinium cation **13** which has a strong *gauche* preference ( $3.8 \text{ kcal.mol}^{-1}$ )<sup>25,26</sup> or the axial preference ( $5.4 \text{ kcal.mol}^{-1}$ ) observed for fluorine in 3-fluoropiperidinium **14** ring systems (Figure 1.5).

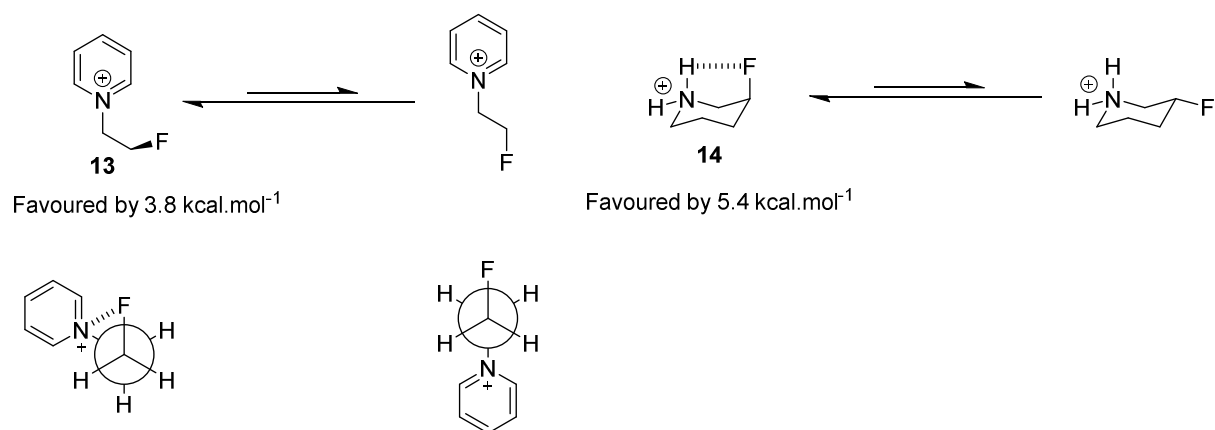


**Figure 1.5** Electrostatic *gauche* effect of fluoroethylpyridinium **13** and fluoropiperidinium salt **14**<sup>19,27</sup>

A study by the O’Hagan group in 2007,<sup>28</sup> explored the influence of the electrostatic *gauche* effect on the conformation of 3-fluoro *gamma*-aminobutyric acids **16** and **17** (3-fluoro GABA) analogues (Figure 1.6).

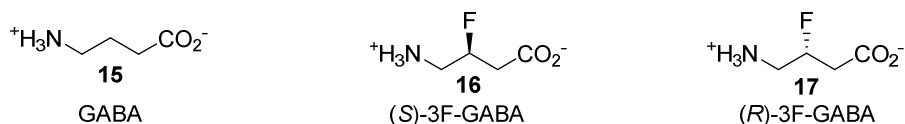


**Figure 1.6** GABA **15** and its 3-fluorinated enantiomers **16** and **17**.

The study was carried out by assaying both enantiomers of 3-fluoro GABA **16** and **17** on the enzyme GABA transaminase (GABA-T). 3-Fluoro-(*S*)-GABA **16** was a significantly better substrate for the enzyme than 3-fluoro-(*R*)-GABA **17**. It was argued that the (*S*)-enantiomer could more easily access the binding conformation **A** than the (*R*)-enantiomer, due to the electrostatic *gauche* effect, as illustrated in Figure 1.7.

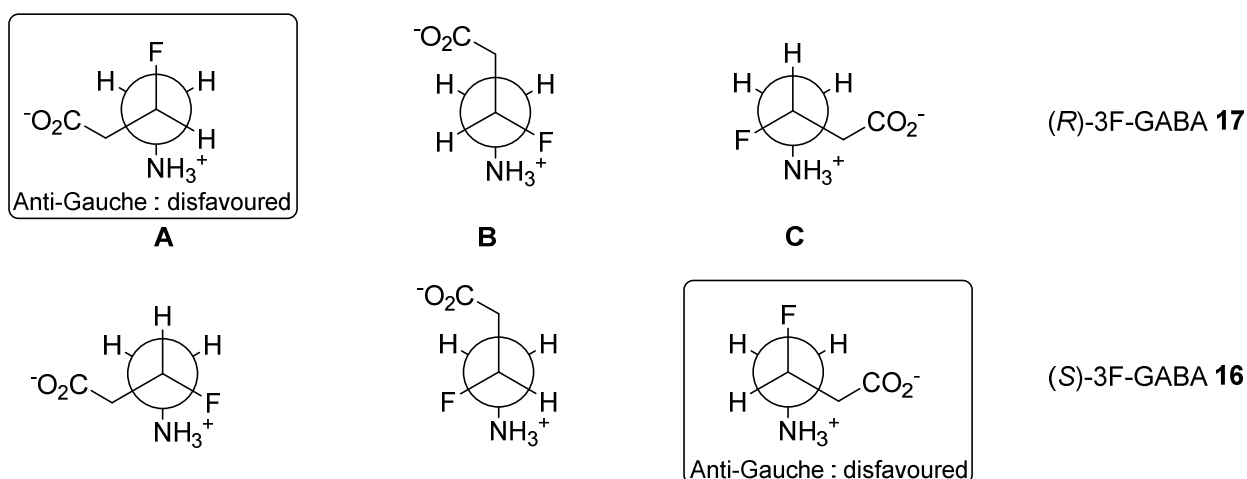


**Figure 1.7** Conformations of (*R*)-3F-GABA **17** and (*S*)-3F-GABA **16**.

For conformation **A** the (*R*)-enantiomer would have to adopt an *anti* conformation which is disfavoured, whereas the (*S*)-enantiomer can readily access this conformation as it is stabilised by the electrostatic *gauche* effect. A comparison between the activity of both enantiomers, helped to understand the preferred binding conformation to the enzyme.<sup>28,19</sup>

#### 1.4. Effect of fluorine on boiling point (bp)

The unique polarisation of the C-F bond impacts on the relative boiling points of classes of fluoro-carbons. Considering short chain alkanes (eg. methane, ethane, propane and butane) it is observed that the replacement of a hydrogen by a halogen decreases the vapor pressure (increases boiling point) following the increase in mass (Figure 1.8). The mass increase results in more energy needed to transition from the liquid phase to the gas phase.

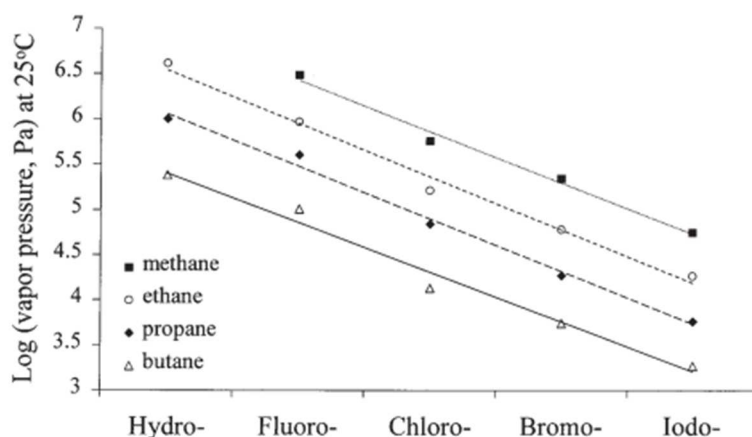


**Figure 1.8** Influence of monohalogenations of short chains alkanes on vapor pressure (boiling point).<sup>29</sup>

Regarding progressive halogenation of methane, it is again observed with chlorine, bromine, and iodine that there is a constant increase in the boiling point corresponding to the increase of mass. However, in the case of fluorine the phenomenon is only observed for  $\text{CH}_3\text{F}$  and  $\text{CH}_2\text{F}$  and the opposite is observed for  $\text{CHF}_3$  and  $\text{CF}_4$  (Figure 1.9).

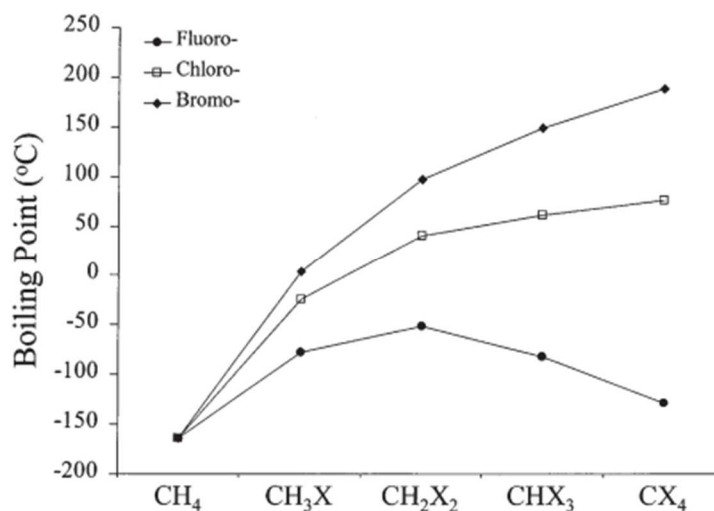


**Figure 1.9** Comparison of the boiling points of halogenated methanes.<sup>29</sup>

This unusual evolution of boiling point can be explained by the inability of carbon bound fluorine to form intermolecular interactions, and progression to CF<sub>4</sub> leads to increased volatilisation. This behaviour extends to higher order perfluorocarbons such as C<sub>4</sub>F<sub>10</sub> which has a very low boiling point relative to hexadecane (Table 1.4).

**Table 1.4** Comparison of boiling points between decafluorobutane and hexadecane.<sup>29</sup>

	C <sub>4</sub> F <sub>10</sub> (238 g.mol <sup>-1</sup> )	C <sub>16</sub> H <sub>34</sub> (226.5 g.mol <sup>-1</sup> )
<b>Boiling points</b> (°C)	4	287

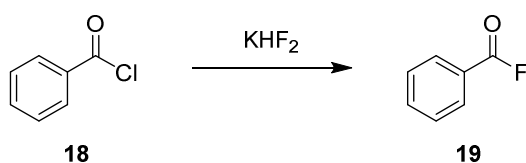
To summarise we have seen that the introduction of fluorine within hydrocarbons generally involves an increase in the boiling, in correlation with increased mass and dipole moment. However, in the case of perfluorocarbons a decrease of the boiling point is observed correlating with a decrease of the dipole moment and reduction in intermolecular interactions.

## 1.5. Fluorination reactions

As indicated, there is a growing demand for organofluorine products in many different fields (**I.1**). As such it is important to outline the variety of strategies available to afford fluorinated products. The first methods used to introduce fluorine into organic molecules typically involved hazardous reagents and conditions such as  $F_2$  and HF. Moreover, the first fluorination reactions were usually not selective, and this represented a challenge.

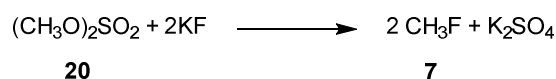
### 1.5.1. First fluorination reactions

The first fluorination reaction was carried out in 1835 and was later published in 1862 by Borodin *et al.* The reaction involved the conversion of acyl chloride **18** to acyl fluoride **19** using  $KHF_2$  (Scheme 1.6).<sup>30,6</sup>



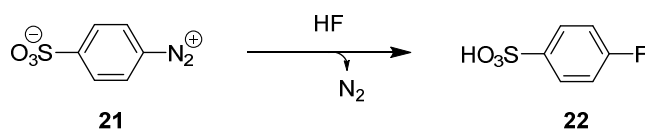
**Scheme 1.6** First reported fluorination reaction as described by Borodin *et al.*<sup>30</sup>

The first organofluorine compound reported was described by Dumas *et al* in 1835, which detailed the production of fluoro-methane **7** using potassium fluoride and dimethyl sulfate (Scheme 1.7).<sup>31,7</sup>



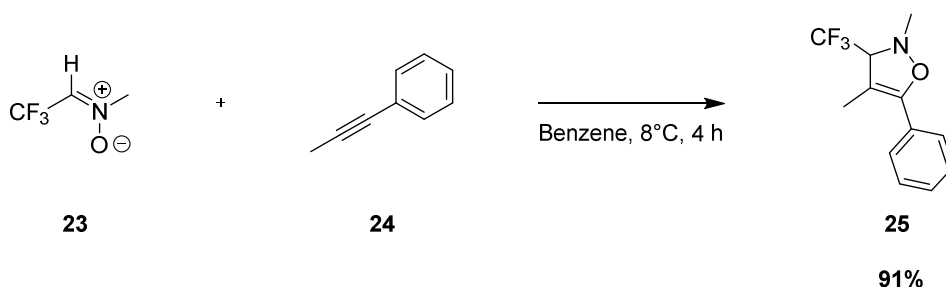
**Scheme 1.7** Production of fluoro-methane **7** from dimethyl sulfate and KF as described by Dumas *et al.*<sup>31</sup>

The fluorination of an aromatic ring was first carried out in 1870 by Schmitt *et al.*, using an aromatic diazonium cation **21**, whereby the diazonium ion was substituted with fluorine using HF to afford **22** (Scheme 1.8).<sup>7</sup>



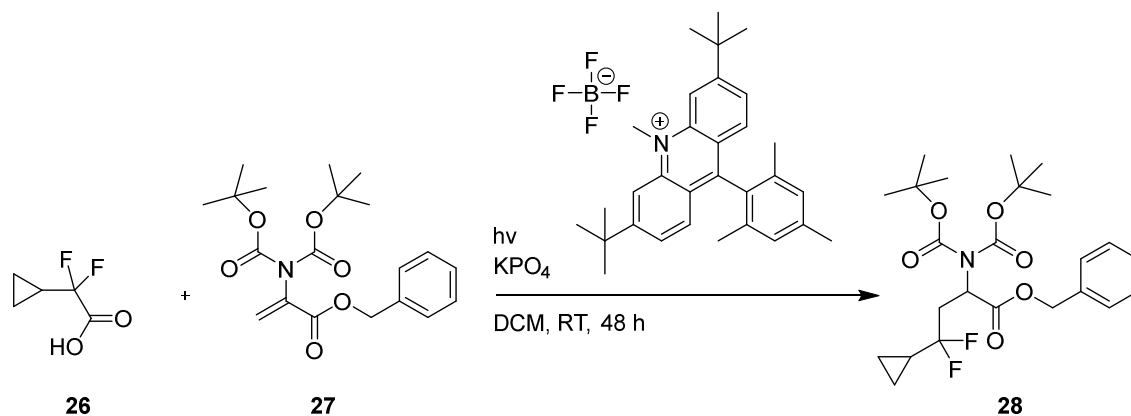
**Scheme 1.8** Diazonium substitution by fluorine carried out by Schmitt *et al.*<sup>7</sup>

Carbon tetrafluoride was successfully synthesised in 1926 by Lebeau and Damiens,<sup>32</sup> and was further characterised in 1930 by Keim *et al.*<sup>33</sup> Generally, the introduction of fluorine into a molecule can be achieved using one of two strategies. Firstly, this involved the use of a pre-established fluorinated building block reacting with a complementary molecule to afford the desired product. In this context, in 1988, Tanaka *et al.* reported a [3+2] cycloaddition of a trifluoromethyl-1,3-dipolar substrate **23** with an arylacetylene to generate a trifluoromethyl functionalised heterocycles **25** (Scheme 1.9).<sup>34</sup>



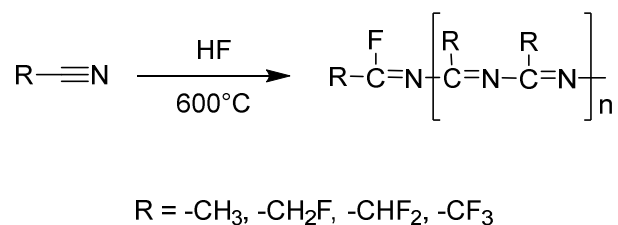
**Scheme 1.9** Synthesis of isoxazole **25** from the building block (Z)-2,2,2-trifluoro-N-methylethan-1-imine oxide **23**.<sup>34</sup>

Fluorination using fluoro-building blocks is still widely used to acquire novel fluorinated molecules. For instance, a recent contribution reported the use of  $\alpha$ -fluorinated carboxylic acids to afford alkyl fluorides and fluorine containing amino acids, in a photoactivated decarboxylative radical reaction (Scheme 1.10).<sup>35</sup>



**Scheme 1.10** Synthesis of protected amino acid **28** from building block **26**.<sup>35</sup>

A second general strategy to afford fluoro-organic molecules involves direct fluorination. One of the first reported, stable, direct fluorinations of an organic molecule containing an hetero atom was published in 1952 using gaseous HF as the fluorinating reagent (Scheme 1.11).<sup>36</sup>



**Scheme 1.11** Fluorination of the nitrile group.<sup>36</sup>

Cuculo *et al.*, reported that polymerisation of the final product led to a stable material which resisted the elimination of fluoride at temperatures up to 600°C.<sup>36</sup>

## 1.5.2 Strategies for mono-fluorination reactions

### 1.5.2.1. Nucleophilic fluorination

Nucleophilic fluorination reagents release fluoride anion and include HF-amine complexes or reagents like DAST, Deoxofluor and DFMBBA (Figure 1.12). Common



fluoride anion sources include KF, CsF and AgF. These metal fluoride salts are not always useful due to their poor solubility in organic solvents, and they often act as bases promoting elimination rather than substitution reactions.<sup>37</sup> In order to circumvent poor solubility stable quaternary ammonium complexes were developed, the most prominent being TBAF **29** (Figure 1.10), which is generally soluble in organic solvents.

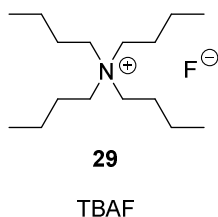


**Figure 1.10** Tetrabutylammonium fluoride (TBAF) **29**.

A general challenge can be the stability of selectively fluorinated products under basic conditions. In 2012 Kim *et al.* studied the impact of solvent (acetonitrile versus tert-amyl butanol) on the effect of substitution versus elimination using TBAF **29** in reactions with alkylchloride **30** (Figure 1.11).<sup>38</sup> The polar protic solvent promoted substitution over elimination, by reducing the basicity of the fluoride ion showing only 3% of the elimination product **32** whereas this could be contrasted with ~ 40% in acetonitrile (Figure 1.11).

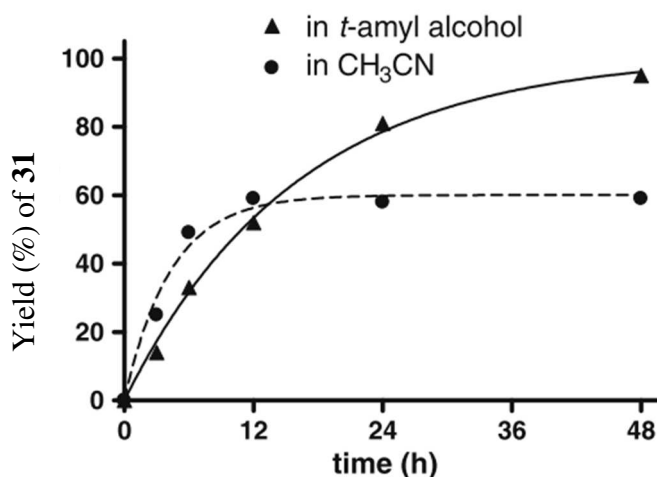
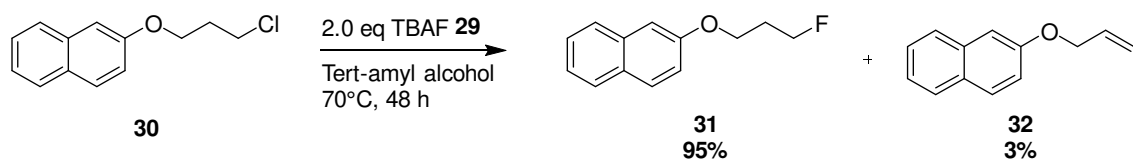
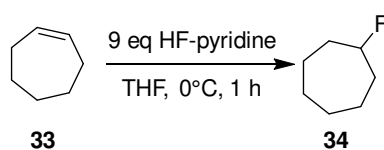


**Figure 1.11** Solvent effect on substitution versus elimination using TBAF with **30**, monitored by the production of **31**.<sup>38</sup>

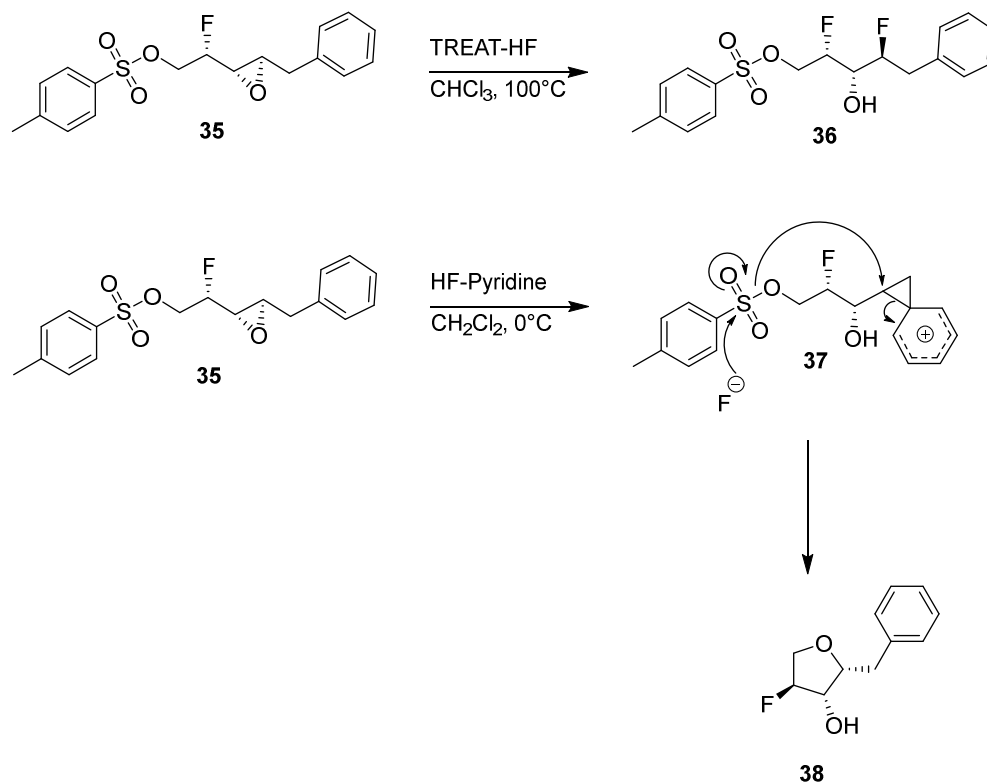
Other nucleophilic reagents include hydrofluoric acid combined with pyridine or alkylamines. HF-pyridine (70/30, w/w) also known as Olah's reagent, was introduced in 1979.<sup>39</sup> This reagent was developed as a liquid form of HF and has a range of reactivities including the addition of HF to double bond (Scheme 1.12).



**Scheme 1.12** Fluorination of cycloheptene **33** with HF-pyridine.

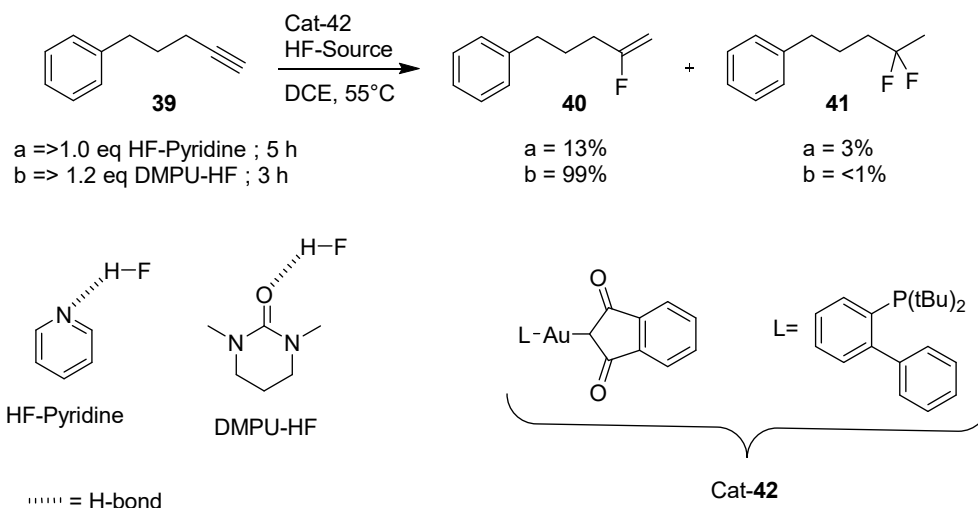
Triethylamine/3HF complex (TREAT-HF) is a derivative of Olah's reagent, but with a lower acidity, therefore it can be a more selective reagent. Brunet *et al.*,<sup>40</sup> reported in 2009 an example of TREAT-HF fluorination of **35** resulting in the desired epoxide opening to afford **36**, whilst using Olah's reagent resulted in the formation of tetrahydrofuran ring

**38**, Brunet *et al.* proposed that this was obtained from the cyclisation of the alkoxide-phenonium intermediate **37** (Scheme 1.13).<sup>40</sup>



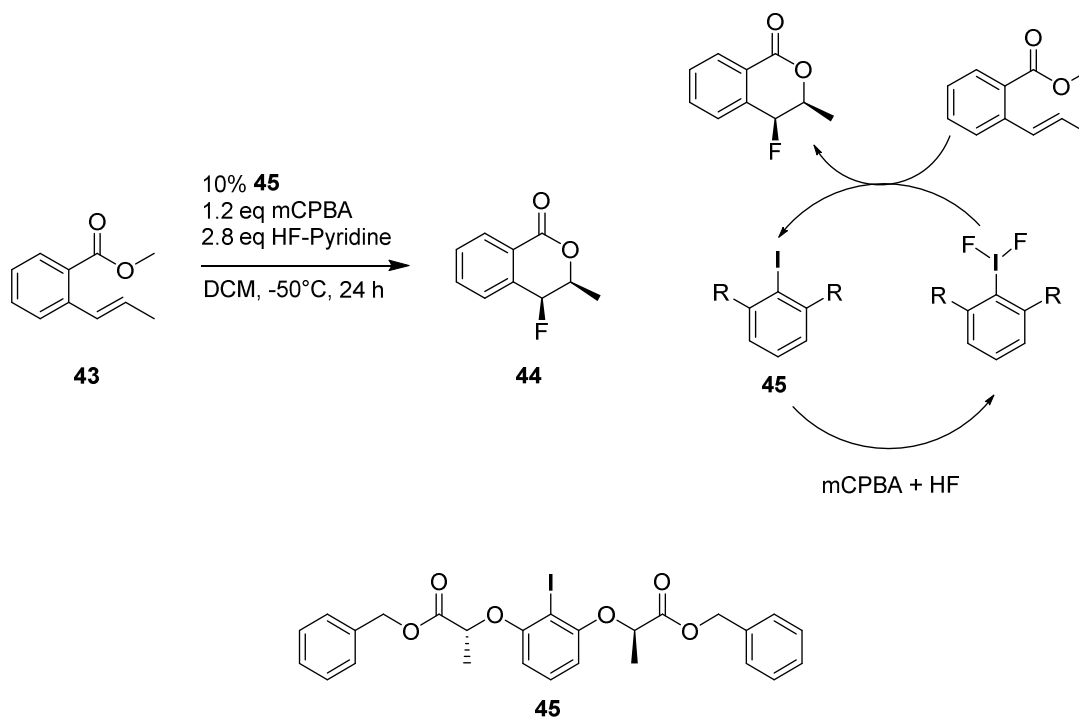
**Scheme 1.13** Different reactions outcomes of epoxide **35** using HF-pyridine or TREAT-HF.<sup>40</sup>

To improve the reactivity and stability of Olah's reagent, specifically regarding selective fluorination using a metal catalyst such as gold, Okoromoba *et al.* replaced pyridine with DMPU.<sup>41</sup> DMPU is less basic and a better hydrogen bond acceptor than pyridine and triethylamine, making the DMPU-HF complex more acidic and more reactive. DMPU is also a weak coordinator to metal catalysts and a weak nucleophile. The poor nucleophilicity of DMPU helps to avoid any competition with HF nucleophilic fluorination. Considering these properties, and its ease of use, the DMPU-HF complex represents a promising candidate for highly selective metal-catalysed fluorination (Scheme 1.14).<sup>41</sup>



**Scheme 1.14** Comparison between Olah's reagent and DMPU-HF in reactions with pent-4-yn-1-ylbenzene **39**.

In 2016, Woerly *et al.*, developed a method for the enantioselective fluorination of an alkene with HF-pyridine, resulting in 86% yield and 95% ee (Scheme 1.15),<sup>42</sup> proving its utility in novel fluoro-drug development.



**Scheme 1.15** Enantioselective fluorination of alkenes reported by Woerly *et al.*<sup>42</sup>

Other regularly used reagents for nucleophilic fluorination are DFMBA **46**, Deoxofluor **47** and DAST **48** (Figure 1.12).

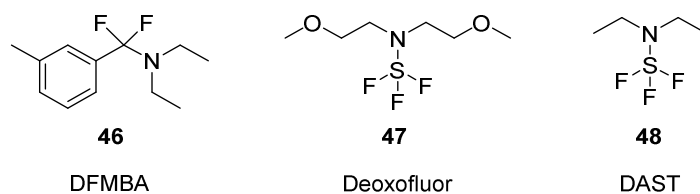
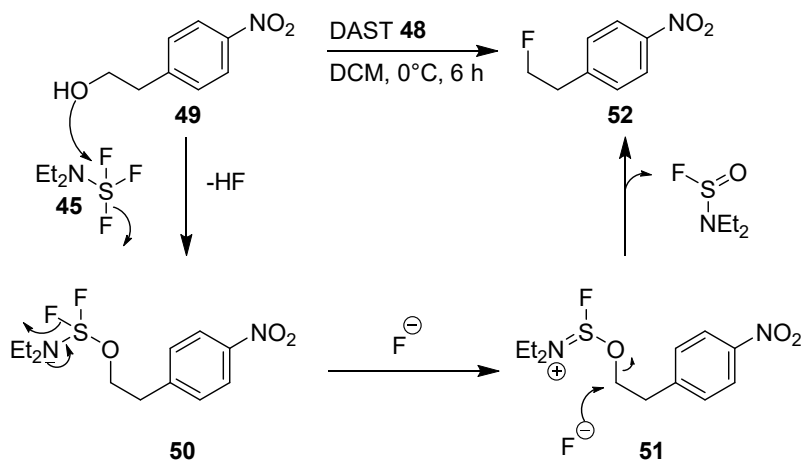


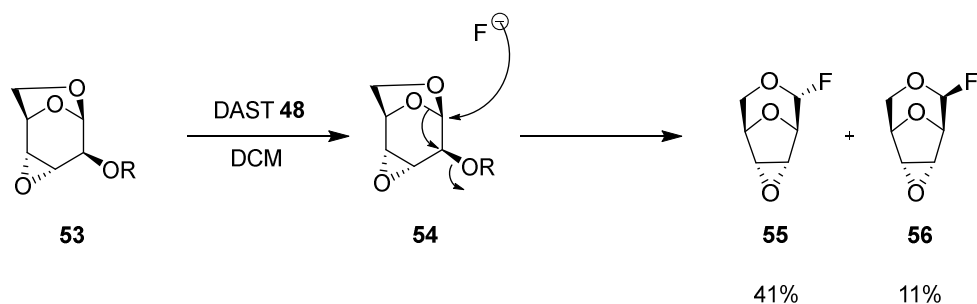
**Figure 1.12** Common fluorination reagents.

DAST **48** is used to carry out deoxyfluorination of alcohols and carbonyls (Scheme 1.16) and has found extensive use for selective fluorinations in the development of new pharmaceuticals.



**Scheme 1.16** Deoxyfluorination reaction of alcohol **49**.<sup>43</sup>

DAST **48** is widely used; however, it can generate side products due to molecular rearrangements of intermediate carbocations (Scheme 1.17).<sup>44</sup>



**Scheme 1.17** DAST mediated rearrangement of **53** as described by Kaźmierczak *et al.*<sup>44</sup>

Reagents less prone to such rearrangements have been developed such as Deoxofluor<sup>®</sup> **57**, Pyfluor **58** and Fluolead **59** (Figure 1.13).<sup>45,46</sup>

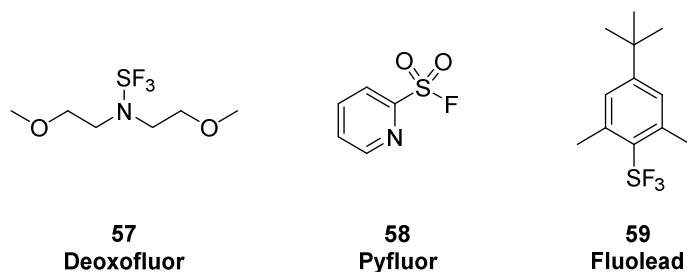


**Figure 1.13** Deoxofluor **57**, Pyfluor **58** and Fluolead **59**.

### 1.5.2.2. Electrophilic fluorination

An electrophilic fluorination reaction relies on reagents that can provide the equivalent of an F<sup>+</sup> cation. The most common reagents for electrophilic fluorination are the N-F reagents Selectfluor<sup>®</sup> **60**, NFOBS **61**, NFSI **62** and N-fluoropyridinium salts such as **63** (Figure 1.14).<sup>47</sup>

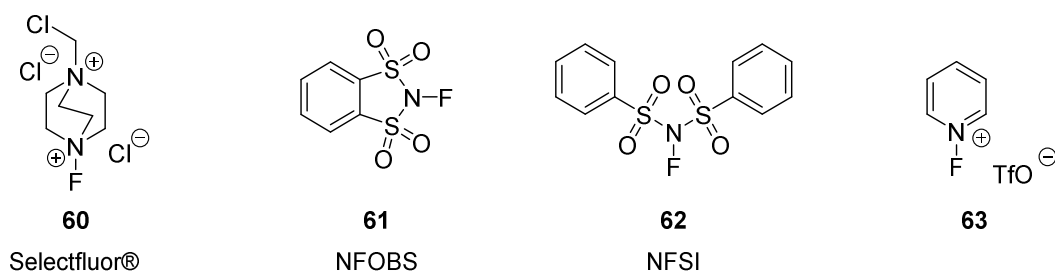


**Figure 1.14** Structure of common electrophilic fluorination reagents.

These reagents have been proven to be efficient for the fluorination of aromatics, alkenes enolates and aldehydes. Selectfluor® **60** was first introduced in 1992 by Banks *et al.*, for the fluorination of aromatic,  $\alpha$ -ketones,  $\alpha$ -esters and sterols (Figure 1.15).<sup>48</sup>

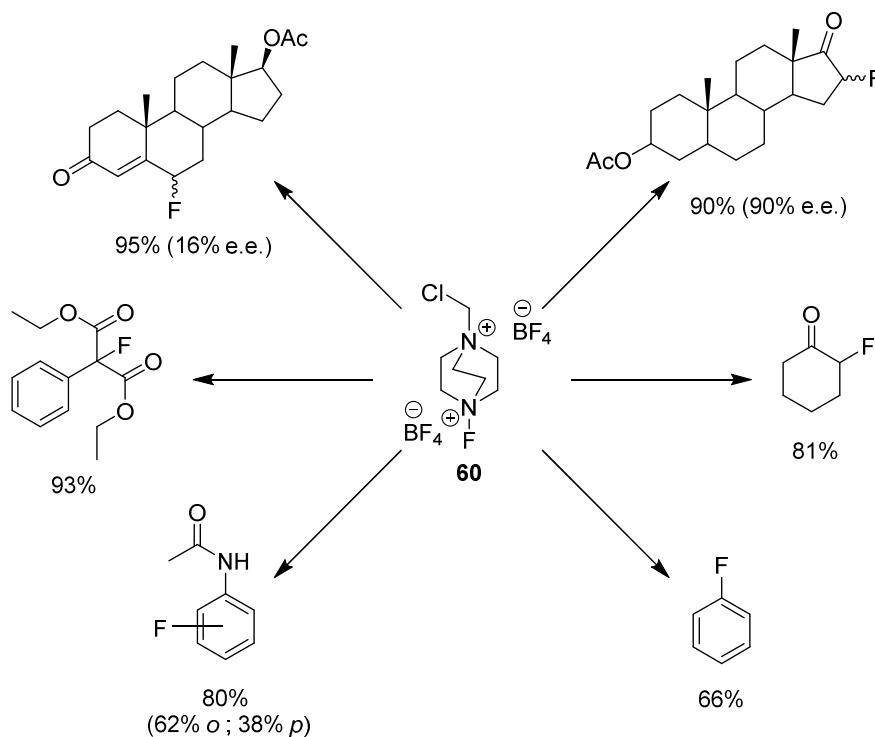
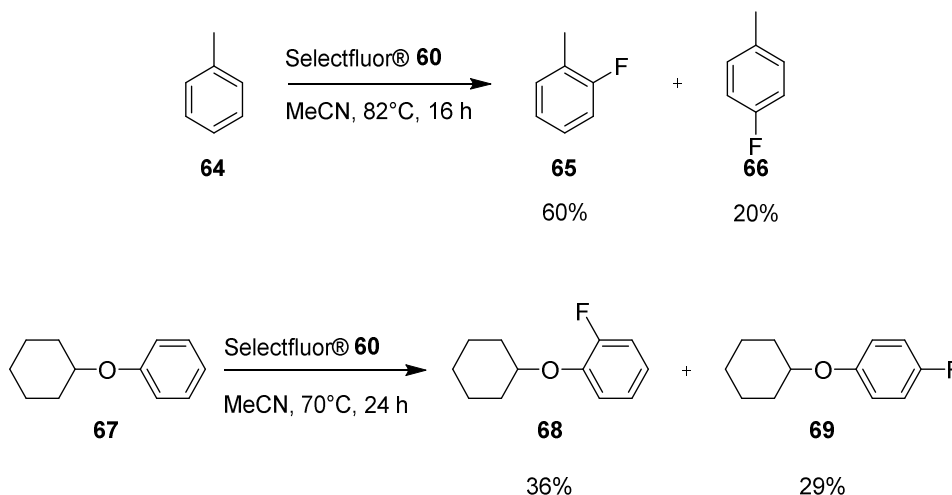


**Figure 1.15** Range of applications with Selectfluor® introduced by Banks *et al.*, in 1992.<sup>48</sup>

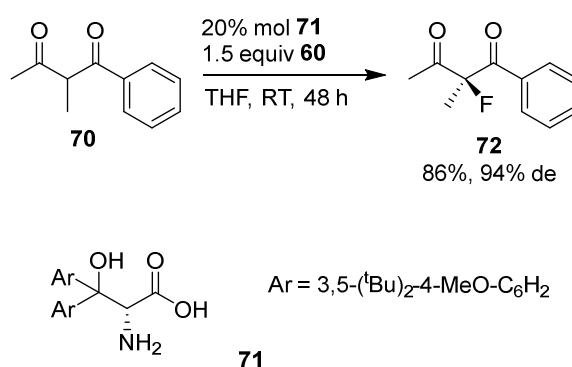
In 1998 Banks *et al.* studied the selectivity of fluorination using Selectfluor® whilst exploring fluorinations on toluene **64** and (cyclohexyloxy)benzene **67** (Scheme 1.18).<sup>49</sup> Fluorination at the *ortho* position to the methyl group of **64** was preferred, whilst no preferences were observed with the cyclohexyl ether **67**.<sup>49</sup> The difference in selectivity

can be explained by the C<sub>6</sub>H<sub>11</sub>-O- of **67** being a much bulkier group than the methyl of **64**, increasing fluorination at the *para* position.



**Scheme 1.18** Regioselectivity fluorinations with Selectfluor<sup>®</sup>.<sup>49</sup>

Selectfluor<sup>®</sup> **60** is still frequently used as the fluorine source in enantioselective fluorinations. Poorsadeghi *et al.* reported the fluorination of diketone **70** in high yields and enantioselectivity using **71** as catalyst (Scheme 1.19).<sup>50</sup>

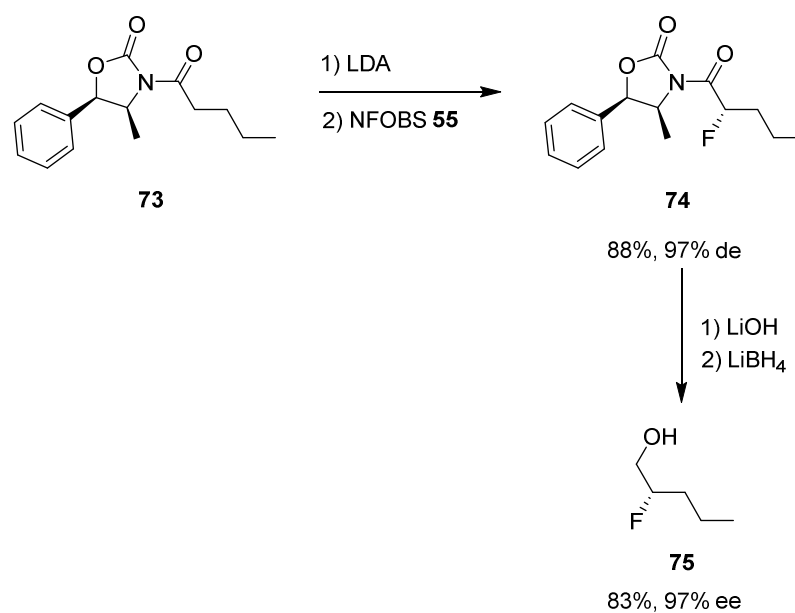


**Scheme 1.19** Recent example of Selectfluor<sup>®</sup> for the fluorination of diketone **70** reported by Poorsadeghi *et al.*<sup>50</sup>

Regarding NFOBS **61**, Davis *et al.* reported an electrophilic fluorination with NFOBS, along with an Evans oxazolidinone auxiliary to influence the stereoselectivity, and to

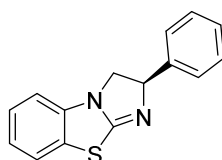
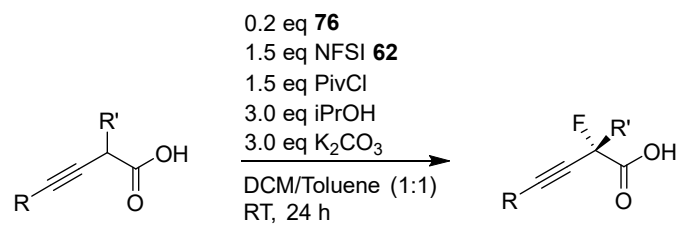


afford a  $\beta$ -fluoro alcohol product in good enantiomeric purity (86-95% ee), (Scheme 1.20).<sup>51</sup>

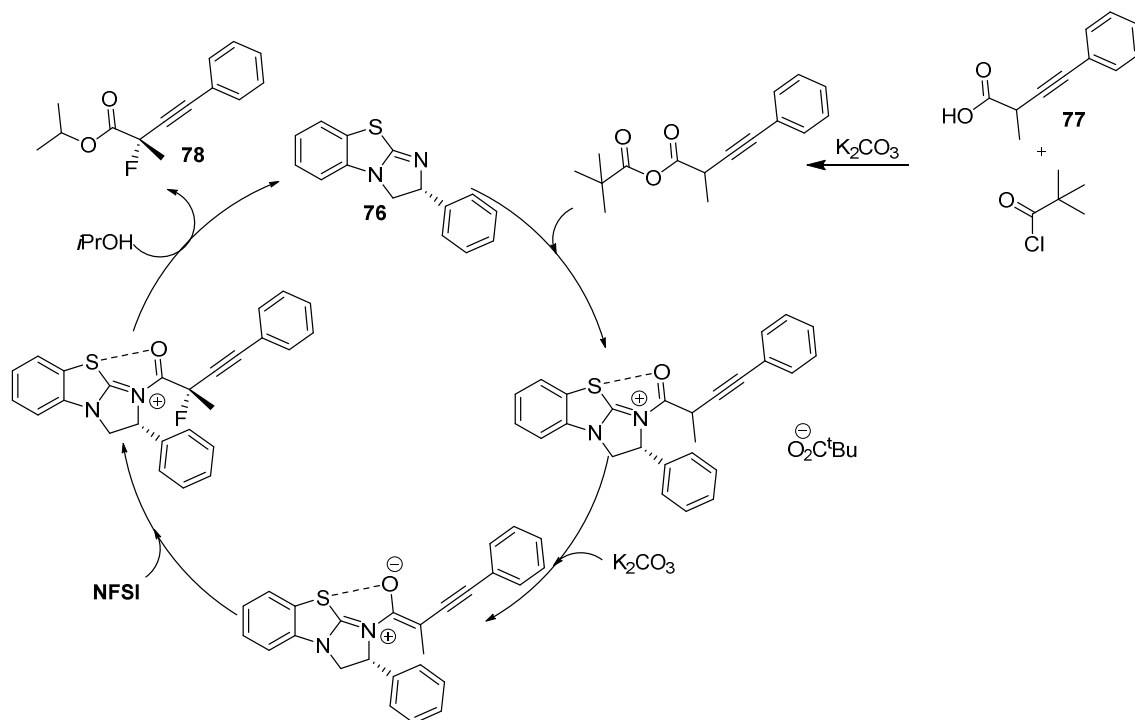


**Scheme 1.20** NFOBS fluorination to afford  $\beta$ -fluoro alcohol **75**.<sup>51</sup>

Finally, NFSI **62** is readily available and widely used. A recent report demonstrated the enantioselective  $\alpha$ -fluorination of carboxylic acids (Scheme 1.21), and this methodology proved to be efficient with yields averaging 77% and with high stereoselectivities up to 97% ee.<sup>52</sup>



**76**



**Scheme 1.21** Mechanism of an asymmetric fluorination with NFSI **62** to afford enantioselective  $\alpha$ -fluorocarboxylic acids.<sup>52</sup>

A recent example of NFSI fluorination by ball milling was reported by Hernandez *et al.*<sup>53</sup> Ball milling is a mechanical process that can carry out organic synthesis reactions in solid state without the use of any solvent (Figure 1.16).

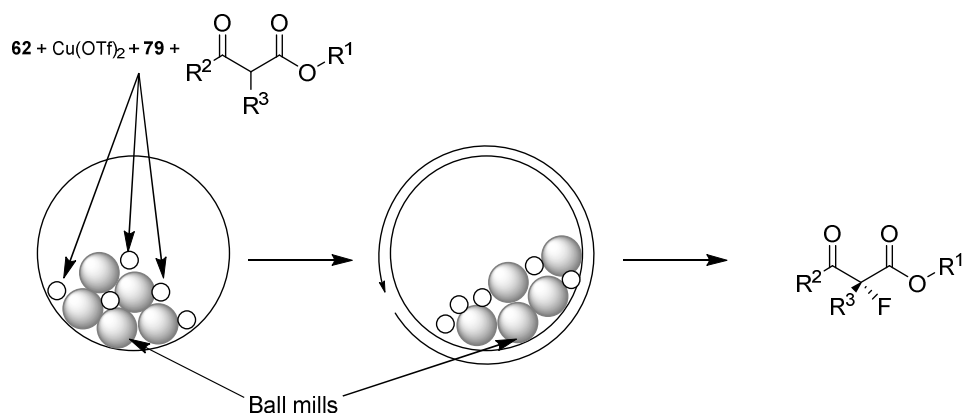
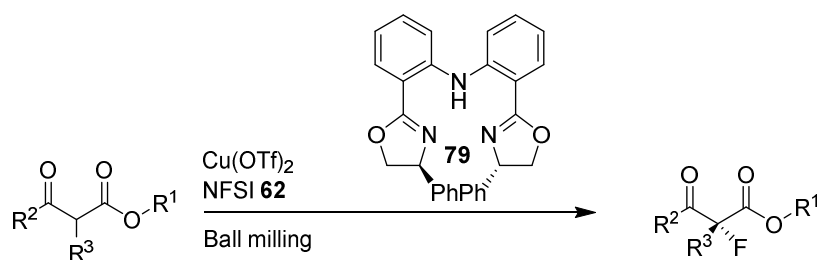


**Figure 1.16** Representation of a ball milling process for the NFSI fluorination developed by Hernandez *et al.*

This process helps the development of sustainable chemical transformations (without solvent).<sup>54</sup> Reagent **62** was utilised here, to carry out the asymmetric fluorination of  $\beta$ -keto esters with the chiral ligand **77** (Scheme 1.22).<sup>53</sup>



**Scheme 1.22** Enantioselective fluorination of  $\beta$ -keto esters using a **79**-Cu complex and NFSI **62**.<sup>53</sup>

NFSI **62** is typically used in enantioselective syntheses to afford fluorine containing bioactives, as a result of its low cost and relative safety. Novel electrophilic fluorination reagents continue to be developed, such as NFBB **80**, an analogue of NFSI **62** which has been demonstrated to be more efficient in terms of yield and selectivity and they are

deemed to be particularly safe with a high detonation threshold relative to other N-F reagents. Examples of transformation using the recently reported NFBB are illustrated in Figure 1.17.<sup>55</sup>

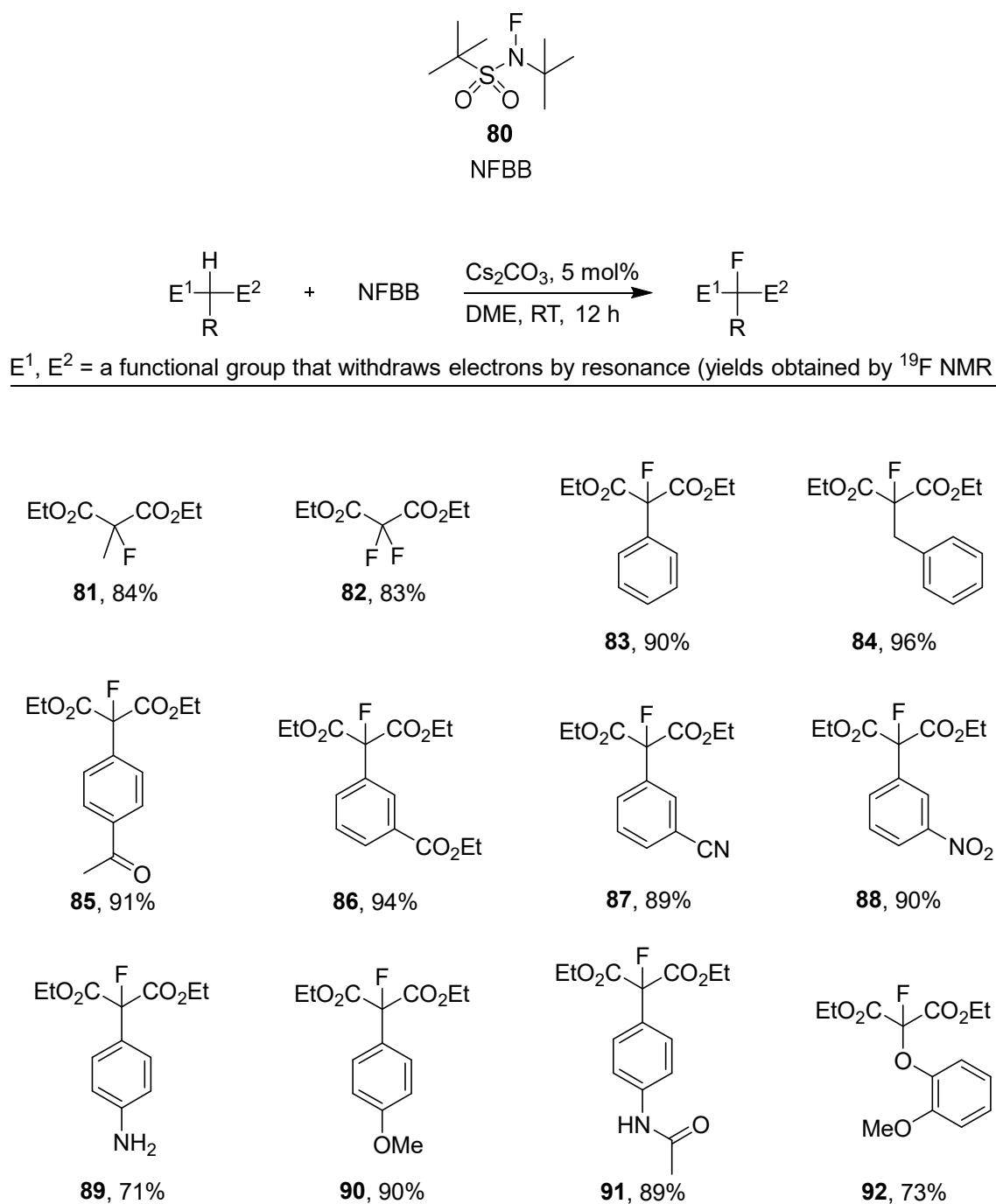


**Figure 1.17** NFBB fluorinations reported by Yang *et al.*<sup>55</sup>

The improved outcomes with NFBB **80**, compared to NFSI **62**, appear to arise from *in-situ* generation of  $[\text{tBuSO}_2\text{N}^t\text{Bu}]^-$  and this facilitates the fluorination-deprotonation cycle to maintain a “self-sustaining fluorination” mechanism. On the other hand the equivalent NFSI derived intermediate  $[\text{PhSO}_2\text{NSO}_2\text{Ph}]^-$  is more stable due delocalisation of the charge and is thus less reactive (Figure 1.18).<sup>55</sup>

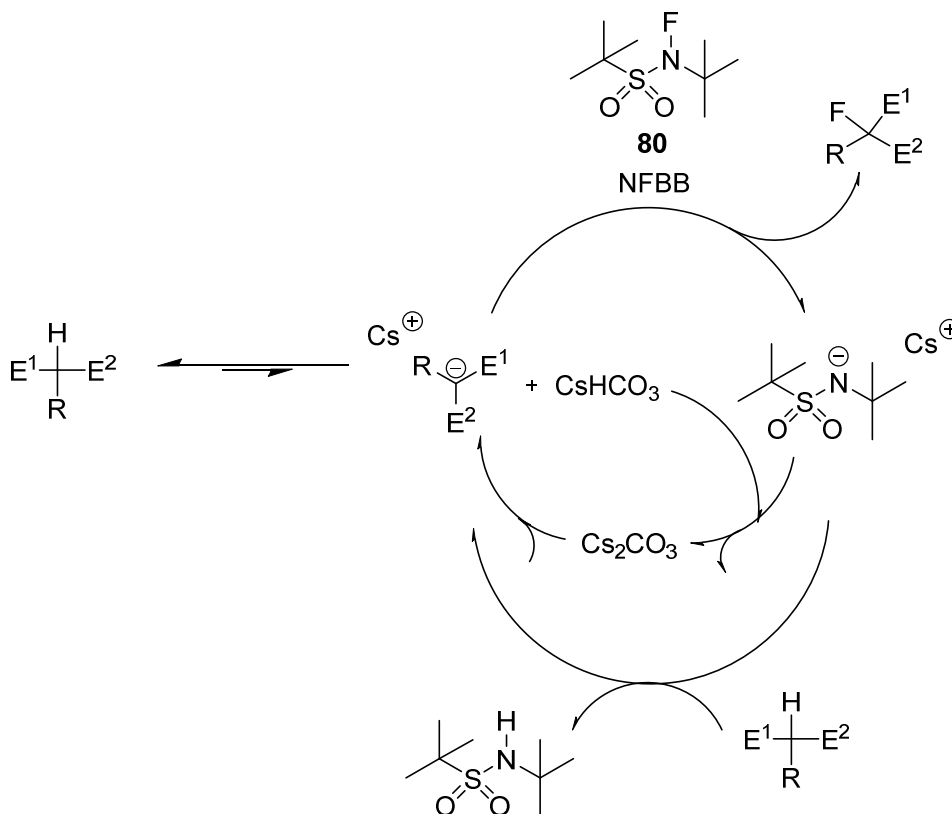
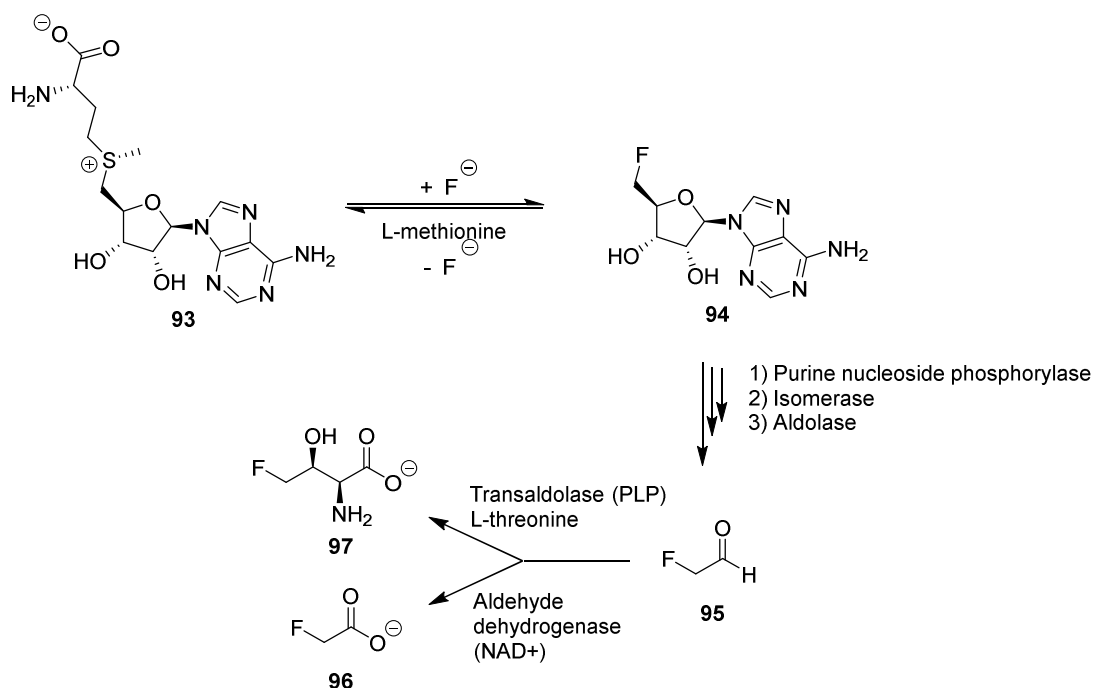


**Figure 1.18** Proposed NFBB **80** fluorination mechanism catalysed by  $\text{Cs}_2\text{CO}_3$  by Yang *et al.*<sup>55</sup>

## 1.6. Fluorine in natural products

Fluorine is the most abundant halogen on earth and the 13<sup>th</sup> most abundant element. Fluorine is usually found within minerals such as fluorite (CaF<sub>2</sub>). Within natural products (NP) only five fluorine containing compounds are known from an estimated 130,000 entities which have been structurally characterised.

The most abundant fluorinated natural product is fluoroacetate **96**, a toxin found in a wide range of tropical plants on all Southern hemisphere continents (S. America, Africa and Australasia).<sup>56,57</sup> Fluoroacetate is also found in bacteria, and was first identified alongside 4-fluorothreonine **97** from the *Streptomyces cattleya*. The co-metabolites **96** and **97**, are produced following five enzymatic steps, starting from the fluorinase enzyme that catalyse the reversible S<sub>N</sub>2 reaction transforming S-adenosyl methionine **93** (SAM) to 5'-fluorodeoxyadenosine **94** (FDA).<sup>58</sup> FDA **94** is then progressed through three enzymatic reactions to fluoroacetaldehyde **95** and then to fluoroacetate **96** by the action of an NAD dependent acetaldehyde dehydrogenase. Separately fluoroacetaldehyde **95** is transformed to 4-F-L-threonine **97** by the action of a pyridoxal phosphate (PLP) dependent transaldolase, and utilising L-threonine also as a substrate (Scheme 1.23).<sup>58</sup>



**Scheme 1.23** Enzymatic pathway from SAM **93** to fluorometabolites **96** and **97** established by O'Hagan *et al.*<sup>58</sup>

F-citrate **98** (Figure 1.19) is another fluorine containing natural product found in fluoroacetate **96** producing toxic plants. Fluoroacetate's **96** toxicity comes from its transformation to a single isomer of F-citrate due to it being processed by acetyl-CoA synthase and then citrate synthase.<sup>59</sup> F-citrate **98** then inhibits aconitase, an enzyme of the citric cycle, and this arrests energy production and compromises respiration.<sup>60</sup>

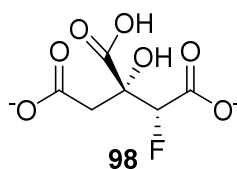


**Figure 1.19** Structure of the isomer of F-citrate obtained from the metabolism of fluoroacetate.

In 1960,  $\omega$ -fluoro-oleic acid **99** (Figure 1.20) was discovered within the seeds of the West African plant, *Datura toxicarium*. Many other fluoro fatty acids were also discovered in

these seeds but all in lower concentrations than **99** as they are assumed to be arise from the metabolism of **99**.<sup>61</sup>

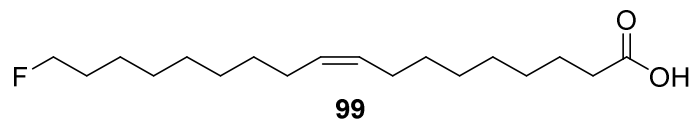


**Figure 1.20** Structure of  $\omega$ -fluoro-oleic acid isolated from *Datura toxicarium*.

Finally, nucleocidin **100** (Figure 1.21), a product of the soil bacterium *Streptomyces calvus* was isolated as an antibiotic and antitrypanosomal agent.<sup>62</sup> The fluorine in nucleocidin is distinct from the fluoromethyl metabolites and it has a separate biosynthesis; however, the C-F bond forming enzyme involved in the biosynthesis of **100** is still unknown.

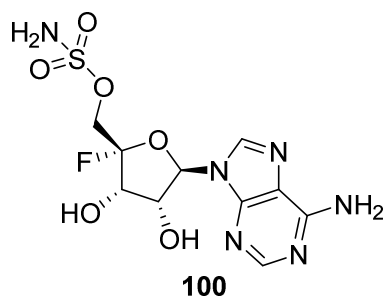


**Figure 1.21** Structure of nucleocidin, **100** from *Streptomyces calvus*.



## 1.7. Fluorine in Medicinal chemistry

### 1.7.1. Fluorine containing drugs

Fluorohydrocortisone **101** (Figure 1.22) was the first fluorine containing drug and it was demonstrated to be potent against rheumatoid arthritis in 1954.<sup>63</sup>

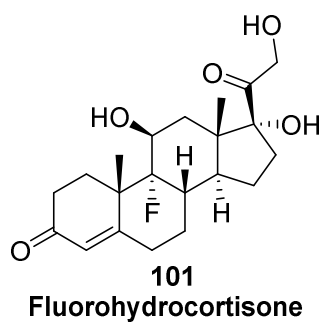
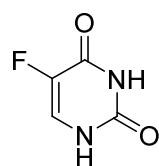


**Figure 1.22** Fluorohydrocortisone **101**; the first fluorine containing drug in the clinic.

A year later Borman, Dinger and Numerof discovered that fluorohydrocortisone **101** and its analogue, chlorohydrocortisone, also possess activities against adrenal insufficiency and postural hypotension.<sup>64</sup> In 2023, fluorohydrocortisone **101** is still widely used and has been reported to be potent also against 21-hydroxylase deficiency (disorder enhancing the decreased production of hormones causing disruption in sexual development).<sup>65</sup> Another important fluorine containing drug, which was developed in the 1950s, is 5-fluorouracil **102** (Figure 1.23), an anti-cancer drug, commercialised as Adrucil **102**.



**102**

**5-fluorouracil**

**Figure 1.23** Structure of the anticancer drug 5-fluorouracil **102**.

Adrucil **102** is a chemotherapy medication used for several types of cancers such as colorectal, esophageal, stomach, pancreas, breast and cervical cancers. Adrucil **102** was patented in 1956 and has been in clinical use since 1962.<sup>66</sup> Adrucil **102** acts as an inhibitor of thymidylate synthase preventing the incorporation of thymidine into DNA, and this leads to suppression of DNA and RNA synthesis, resulting in cell death.<sup>67</sup> Adrucil **102** is still employed as a treatment of various diseases. A study in 2020 (reviewed recently in 2022)<sup>68</sup> described its action towards the incidence of recurrence of odontogenic keratocyst and inferior alveola nerves paresthesia.<sup>68,69</sup>

These two molecules, **101** and **102**, demonstrate the importance of fluorine within drug discovery and helped inspire a continuing and increased focus on fluorine in the development of medicinal compounds. This is evidenced by the increased percentage of approved drugs for the clinic which carry fluorine, from 14% in 1997 to 43% in 2019 (Figure 1.24).<sup>70</sup>

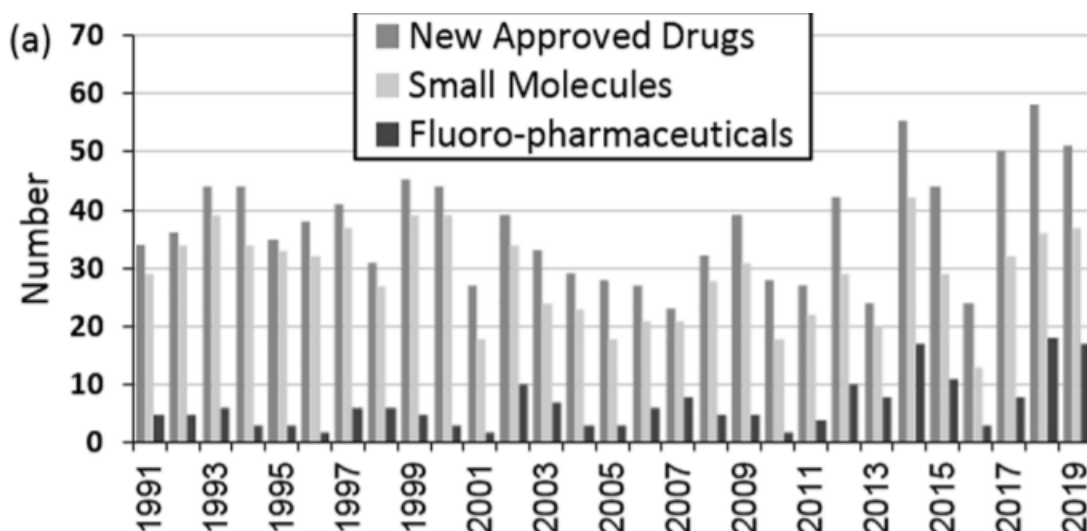


**Figure 1.24** Numbers of fluorine containing drugs approved by the FDA over the past two decades.<sup>70</sup>

The important hepatitis C (HCV) anti-viral, Sovaldi, known also as Sofosbuvir<sup>®</sup> **103** (Figure 1.25) was disclosed in 2007 by Michael Sofia and his collaborators. Sofosbuvir<sup>®</sup> is a prodrug and nucleotide analogue, which inhibits HCV viral replication.

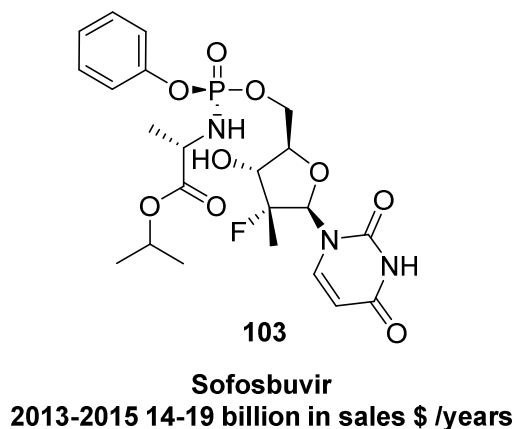


**Figure 1.25** Structure of antiviral Sofosbuvir **103** used for the treatment of HCV.

More specifically Sofosbuvir<sup>®</sup> inhibits HCV NS5B polymerase and acts as a chain terminator which interrupts the life cycle of HCV and stops its replication. Sofosbuvir<sup>®</sup> was approved by the FDA and generated between \$14 - 19 million during the period

between 2013 to 2015.<sup>71</sup> In this context it has proven to be among the most commercially successful drugs of all time.<sup>72</sup>

In 2021, 18% of new drugs approved by the FDA contained at least one fluorine (Figure 1.26).<sup>73,74</sup>

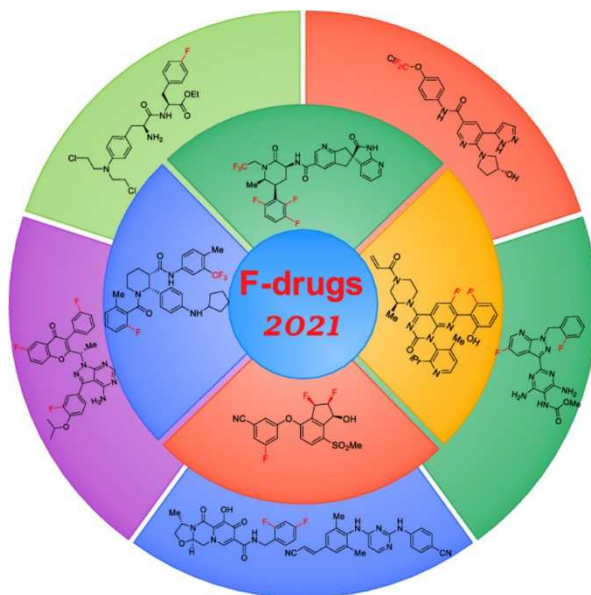


**Figure 1.26** Fluoro drugs approved by the FDA in 2021.<sup>74</sup>

One of these is Scemblix® **104** (Figure 1.27) an anti-cancer medication used to treat chronic myeloid leukaemia (CML). It acts as an allosteric inhibitor of tyrosine kinase BCR-ABL1.<sup>75</sup>

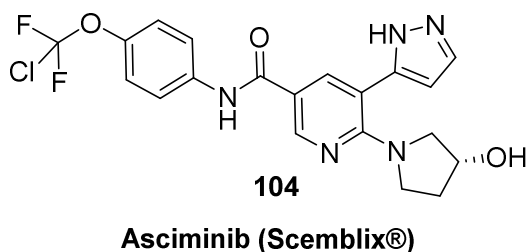


**Figure 1.27** Scemblix **104** approved by the FDA 2021.

## 1.7.2. Influence of fluorine properties in drugs development

One of the most important considerations for the development of a small molecule drug is its pharmacokinetic profile. The requirements to meet appropriate pharmacokinetics have been summarised in the Lipinski rule of 5, which offers guidelines relating to the profile that a molecule must generally have to emerge as a marketable oral pharmaceutical (Figure 1.28).

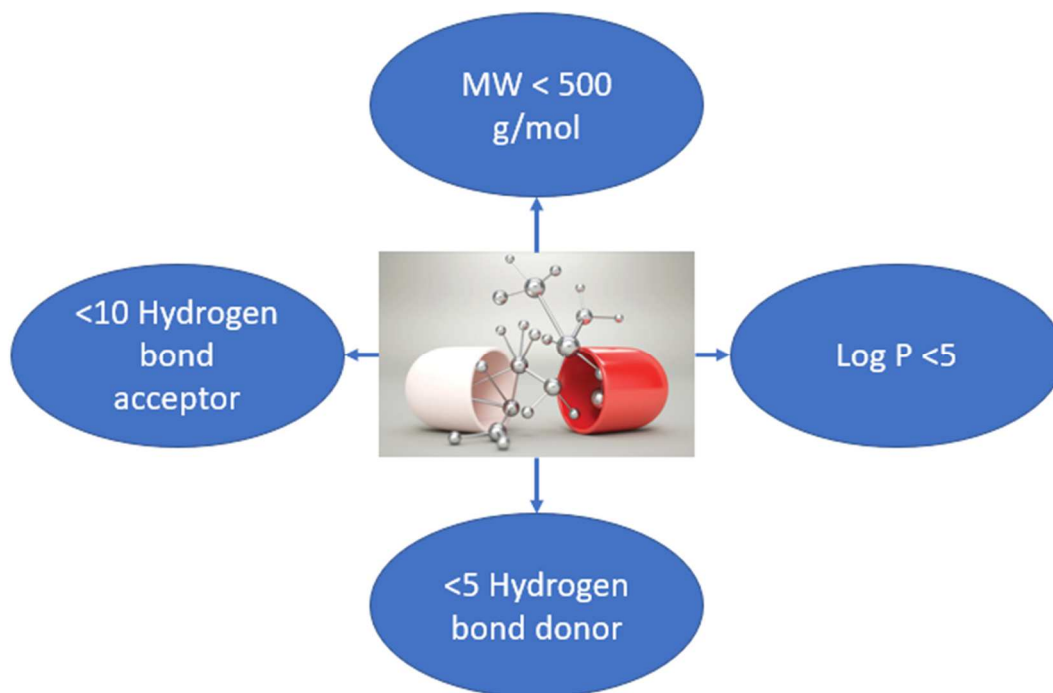


**Figure 1.28** Lipinski rule of 5 for oral absorption of drugs.<sup>76</sup>

The introduction of a fluorine atom can play an important impact in tailoring a potential drug to the guidelines outlined by Lipinski.

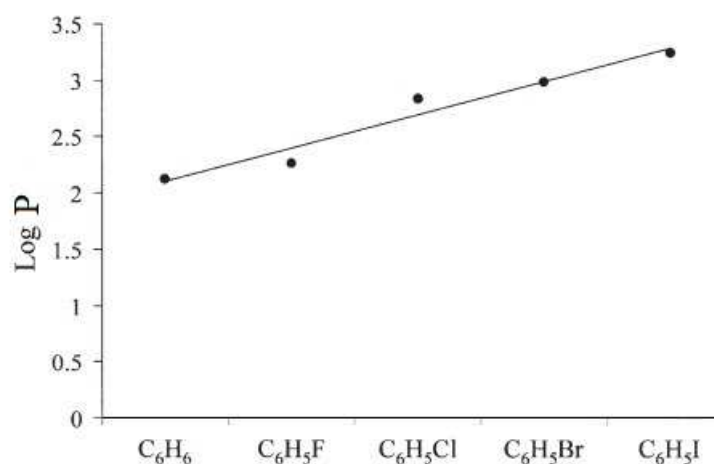
### 1.7.2.1. Lipophilicity

Lipophilicity is fundamentally important for the development of new pharmaceuticals. Tuning lipophilicity is important for a drug to be able to pass through cell membranes and reach its target. When the drugs reach the target, lipophilicity also plays an important role regarding its binding affinity to target proteins. Too hydrophobic a drug reduces its solubility in water and increases its adsorption to lipophilic proteins such as albumin,

reducing overall bioavailability. Thus, the balance between lipophilicity and polarity is important. Fluorine can help regulate the lipophilicity of a lead compound by tuning acidity and basicity, tuning inherent lipophilicity and polarity, and it can be used as a tool to block metabolism and increase *in vivo* efficacy for longer.<sup>77</sup>

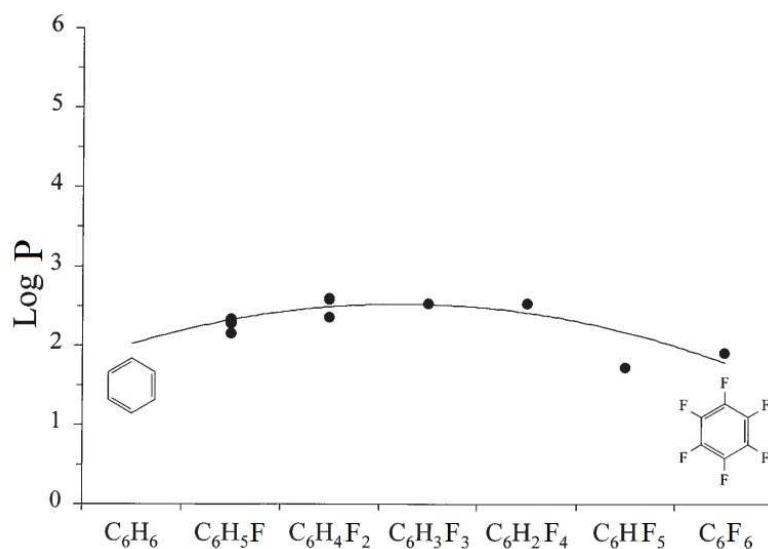
In order to describe the lipophilicity of a molecule the partition coefficient between octanol and water, log P and log D, are used. The Log P value translates to the relative solubility of non-ionizable molecules in octanol and water, while the log D value translates to the relative solubility of ionizable molecules in octanol and water (usually at pH = 7.4, log D<sub>7.4</sub> ~ log P). The higher the log P value the more lipophilic the molecule.

The correlation between lipophilicity and fluorine is complex. Indeed, for single fluorinated aromatic compounds there is generally an increase in the log P value (Figure 1.29), related to the increase of the molar volume or surface area.<sup>29</sup>



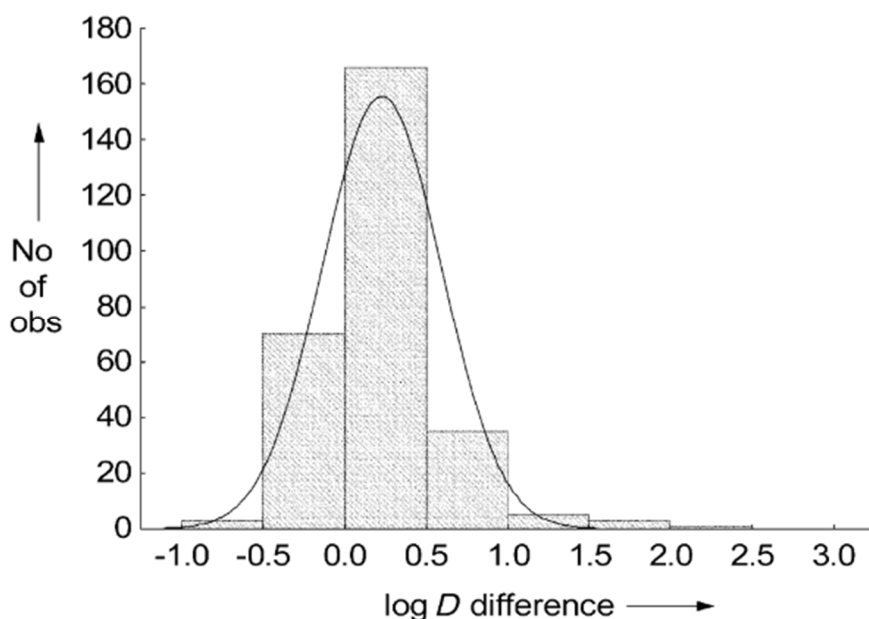
**Figure 1.29** Partition coefficient's at 25°C of mono-halogenated benzenes.<sup>29</sup>

On the other hand, progressive fluorination of benzene results in an increase in lipophilicity up to the fourth fluorine, but for the fifth and sixth fluorines there is an observed decrease in lipophilicity (Figure 1.30).<sup>29,78-82</sup>



**Figure 1.30** Partition coefficients (Log P) at 25°C for multiple fluorinated benzenes (data collected from different references, assembled together by Ellis *et al.*).<sup>29</sup>

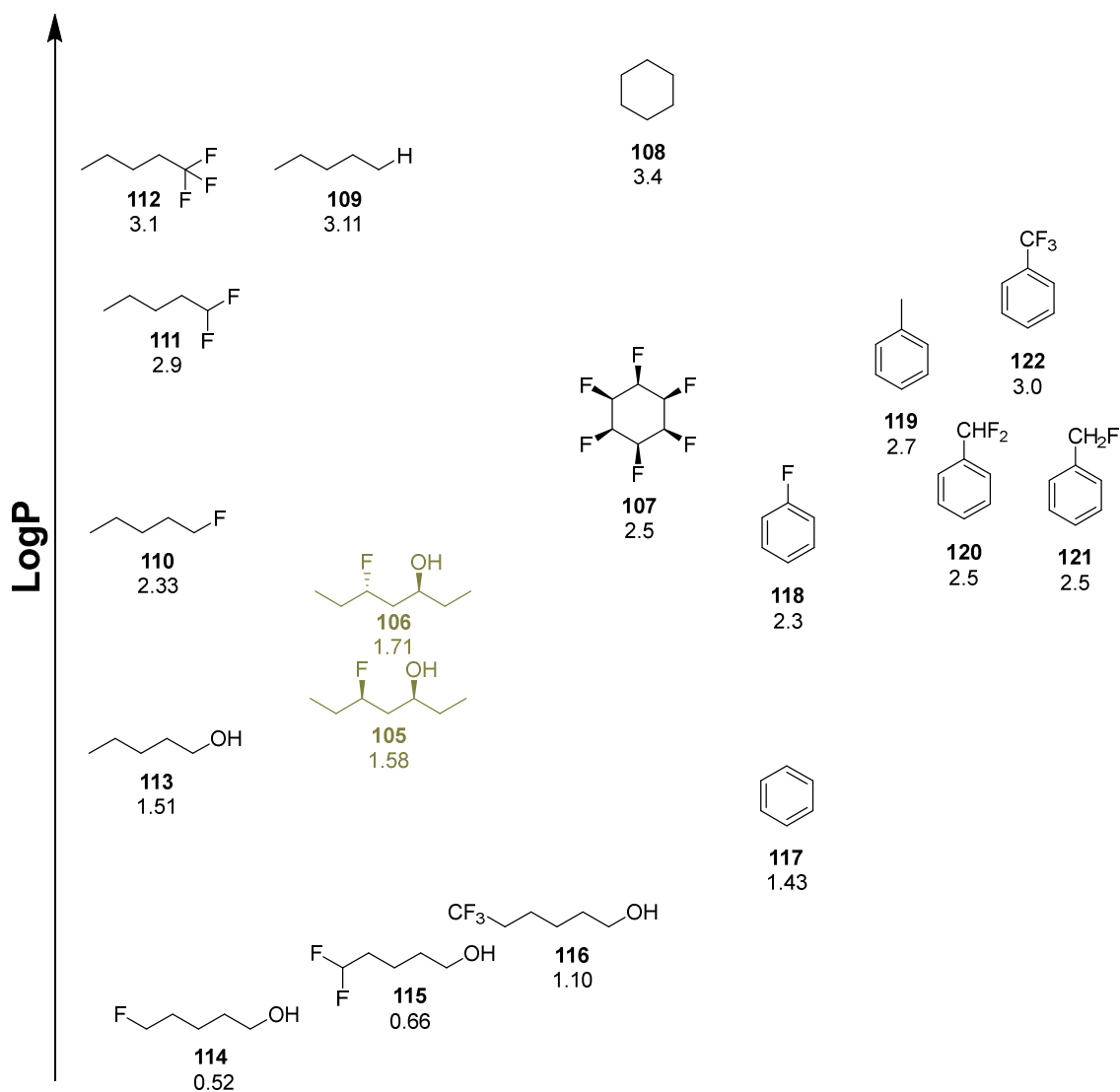
Böhm *et al.*, carried out a study with 293 pairs of non-fluorinated and then selectively fluorinated molecules, to highlight global trends regarding the effect of fluorine on lipophilicity. The results are summarised in Figure 1.31 and demonstrate that selective fluorination can both increase and also decrease lipophilicity, and thus the outcome is structure dependent.<sup>83</sup> Many of these compounds are aromatics where fluorination leads to an increase in lipophilicity and particularly with  $\text{CF}_3$ . However selective fluorination on aliphatics can result in a significant increase in hydrophilicity.



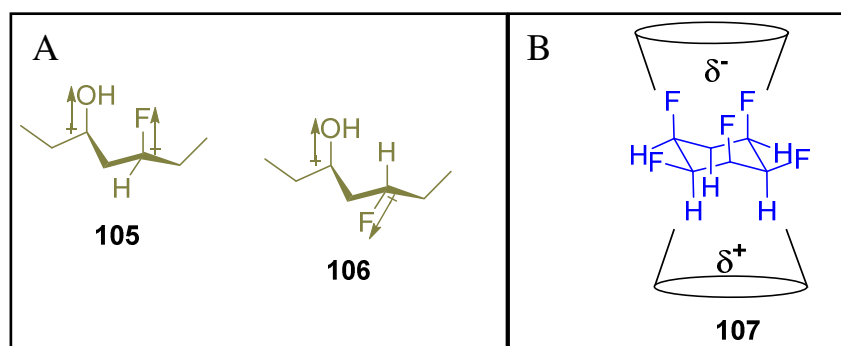
**Figure 1.31** Histogram of change in log  $D$  observed upon substitution of a hydrogen atom by a fluorine atom. On average, log  $D$  is increased by roughly 0.25.<sup>83</sup>

Figure 1.32 below summarises the effect of fluorine incorporation into some compounds on their lipophilicity. For non-chiral compounds the first replacement of a hydrogen by fluorine results in a decrease in lipophilicity but an increase of lipophilicity is observed with the replacement of a second and third hydrogen with fluorine. Regarding chiral fluoro-alcohols **105**, **106**, and **107** a stereochemical influence is observed. The *cis*-diastereoisomer **105** is less lipophilic than the *anti*-diastereoisomer **106**. This difference is explained by the greater polarity of the *cis*-diastereoismer due to the alignment of the two C-O/C-F dipoles, while for the *anti*-diastereoisomers the two dipoles face in opposite directions causing an overall a reduction in polarity (Figure 1.33 ; A).<sup>84</sup> Finally, with *cis*-1,2,3,4,5,6-hexafluorocyclohexane **107** a significant drop in lipophilicity is observed compared to cyclohexane **108**, as the C-F bond is the most polarized covalent bond and having all fluorine in *cis* conformation enhances polarisation of this molecules thus decreasing its lipophilicity (Figure 1.33 ; B).<sup>85</sup>





**Figure 1.32** Lipophilicity (Log P) trends of a selection of fluorinated compounds.<sup>84-87</sup>



**Figure 1.33** Influence of the C-F bond polarity on linear A) **105**, **106** and cyclic B) **107** fluoroaliphatics<sup>84,85</sup>

### 1.7.2.2. The Fluorous Phase

A special situation arises for perfluoroalkyl chains. Perfluorocarbon liquids such as perfluorodecalin or perfluorocyclohexane are immiscible with organic solvents and also water. This results in the creation of a third liquid phase which has been termed the “fluorous” phase. When a biphasic mixture of an organic solvent and a perfluorocarbon liquid are heated then they become miscible, and on cooling they partition again (Figure 1.34).<sup>88</sup> Therefore a catalyst for a reaction can be appended with perfluorocarbon chains ‘ponytails’ to make it soluble in a perfluorocarbon solvent. If reagents and products are soluble in the organic solvent, then the catalyst can be removed into the fluorous phase and recovered from the reaction after cooling.

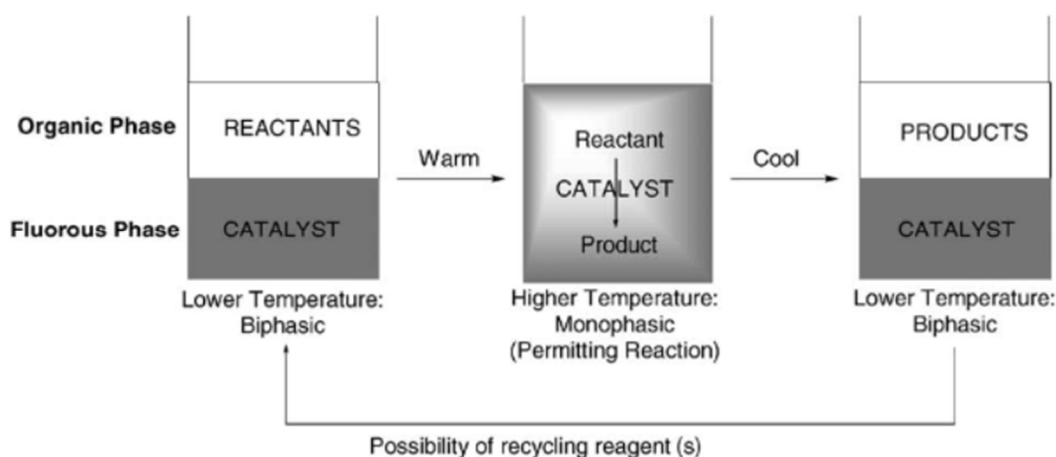
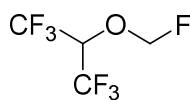


**Figure 1.34** Example of fluorous biphasic catalysis set-up reported by Dobbs *et al.*<sup>88</sup>

Perfluorocarbons are also good at dissolving small molecules and particularly gases (CO, CO<sub>2</sub>, NO, O<sub>2</sub>) and they have therefore found roles, particularly as blood substitutes for transport and delivery of bioactive gases for therapeutic purposes.<sup>89–92</sup> It was demonstrated that PFCs are able to dissolve 50 times more oxygen and 2.9 times more Sevoflurane<sup>®</sup> **123** (commonly used volatile anaesthetic, Figure 1.35) than blood plasma.<sup>91,93</sup> PFCs are biological inert materials with low toxicity.<sup>94</sup> PFCs avoid any risk of infections, a complication of blood transfusion.<sup>95,96</sup>



**123**  
**Sevoflurane**

**Figure 1.35** Sevoflurane **123**, a commonly used anaesthetic that dissolves in PFCs.

### 1.7.2.3. Hydrogen bonding

Despite having three lone pairs of electrons and a high electronegativity, fluorine is a poor hydrogen bond acceptor. It has been shown that the strength of a hydrogen bond between a fluorine and a proton from a hydroxy group (C-F...H-O-) is almost three times weaker (~2.5 kcal/mol) than a “conventional” hydrogen bond (5-10 kcal/mol) between C-O...H-X, where X can be an oxygen or a nitrogen atom.<sup>97</sup> Hydrogen bonding plays a fundamental role in ligand binding (eg. drugs) in biological and chemical systems. Despite fluorine being a poor hydrogen bond acceptor, weak hydrogen bonding interactions with fluorine can help stabilise interactions of drugs within an enzyme’s active site, when the fluorine can contact a hydrogen bond donor. For example as illustrated in Figure 1.36 there is a moderate to weak hydrogen bonding interaction within the active site of isomerase FKBP12 .<sup>98,99</sup>

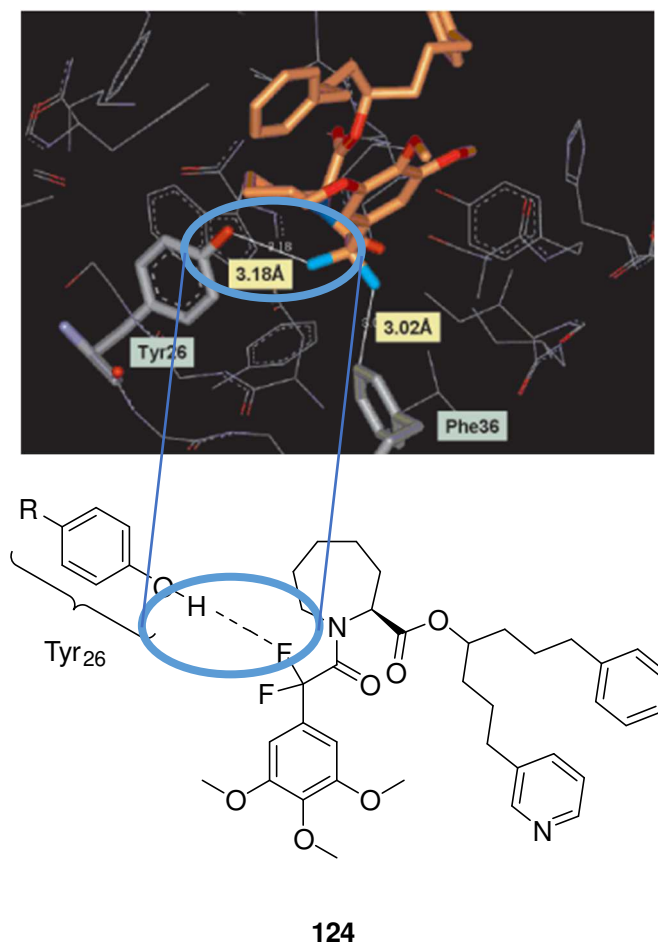


**Figure 1.36** Hydrogen bonding interaction with fluorine between drug V-10 **124** and a tyrosine residue of isomerase FKBP12.<sup>99</sup>

#### 1.7.2.4. Acidity

Due to the strong negative inductive effect of fluorine, fluoroalkyls are considered to be electron withdrawing groups, which results in the neighbouring hydrogen atoms becoming more acidic or suppressing the lone pair donor ability of heteroatoms, as demonstrated for the carboxylic acids and amines respectively in Table 1.5.

**Table 1.5** Impact of fluorine on the pK<sub>a</sub> of carboxylic acids and amines.

	pK <sub>a</sub>
<b>Carboxylic acids</b>	
CH <sub>3</sub> -COOH	4.76
CH <sub>2</sub> F-COOH	2.6
CHF <sub>2</sub> -COOH	1.3
CF <sub>3</sub> -COOH	0.5
<b>Ammoniums</b>	
CH <sub>3</sub> CH <sub>2</sub> NH <sub>3</sub> <sup>+</sup>	10.7
CH <sub>2</sub> FCH <sub>2</sub> NH <sub>3</sub> <sup>+</sup>	9
CHF <sub>2</sub> CH <sub>2</sub> NH <sub>3</sub> <sup>+</sup>	7.3
CF <sub>3</sub> CH <sub>2</sub> NH <sub>3</sub> <sup>+</sup>	5.9

The basicity of alkyl amines is significantly diminished by the progressive replacement of vicinal hydrogens by fluorine, as represented in Table 1.5. The impact of the introduced fluorine on the pK<sub>a</sub> has been widely used in drug discovery to tailor potency towards their possible targets, mainly due to pharmacokinetics and the resultant effects on solubility and bioavailability. Some examples from Neil *et al.*, have demonstrated an increase of bioactivity due to the introduction of fluorine on the propyl side chain of the 3-(3-(piperidin-1-yl)propyl)indoles as illustrated in Figure 1.37. Fluoro analogues of **127**, **128**, and **129** were synthesised to reduce the pK<sub>a</sub> and favour oral absorption thus allowing for an increase in bioactivity while avoiding any impact on the selectivity for the target, a subtype of the receptor 1D of 5-hydroxytryptamine (5-HT<sub>1D</sub>).<sup>100</sup>

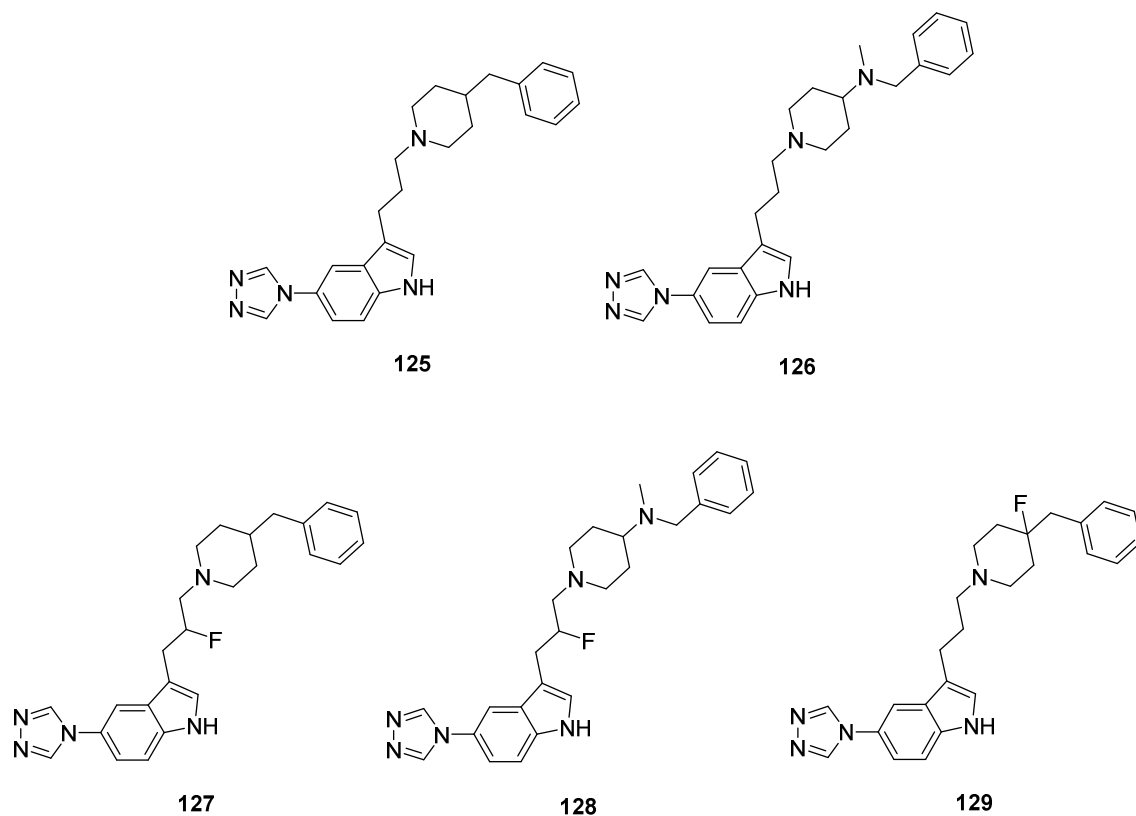


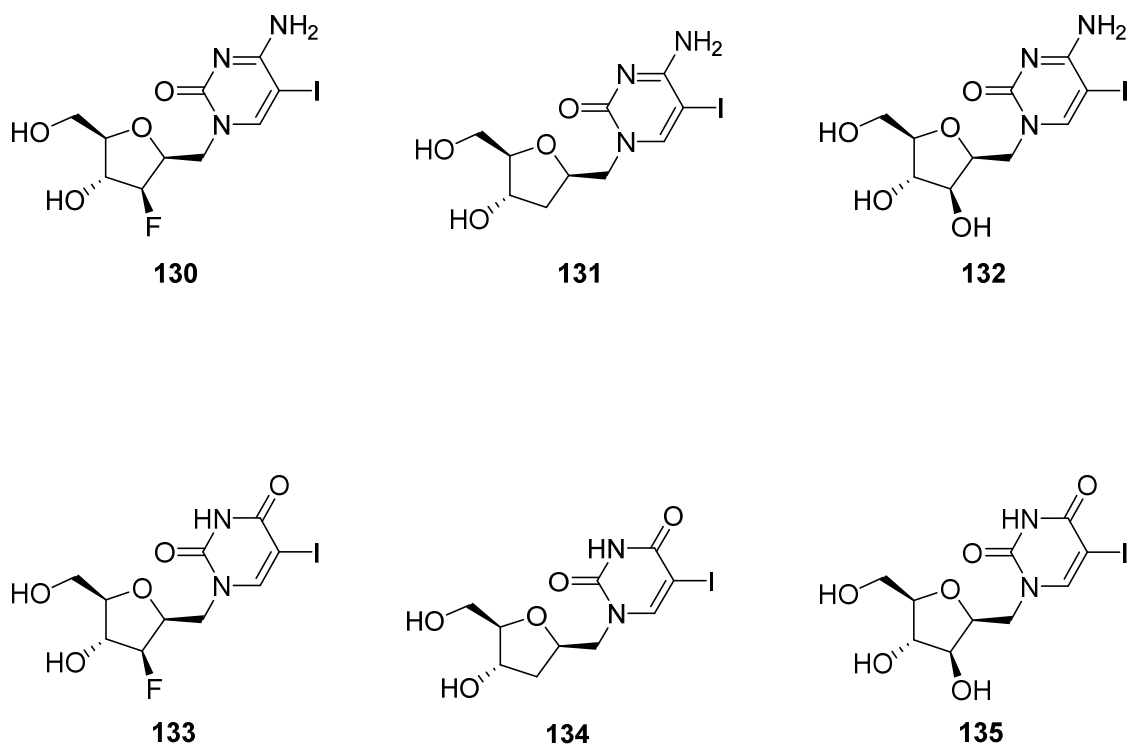
**Figure 1.37** 3-(3-(Piperidin-1-yl)propyl)indoles **125**, **126**, **127**, **128** and **129**.

The data in Table 1.6 indicates that **129** has a better absorption than its non-fluoro analogue **125** and fluoro analogue **127** also possesses an improved absorption. This trend is also observed with for **126** and its fluoro analogue **128**, a trend which correlates with a reduction in  $pK_a$  (Table 1.6).

**Table 1.6** Comparison of  $pK_a$  and absorption properties of anti-Migraines analogues<sup>100</sup>

Compounds	$pK_a$	Absorption after 30 min	
		hpv	Systemic
<b>125</b>	9.7	$25 \pm 4$	<2
<b>126</b>	9.3	$4 \pm 1$	<1
<b>129</b>	8.8	$570 \pm 119$	$52 \pm 21$
<b>128</b>	8.7	$781 \pm 171$	$196 \pm 60$
<b>127</b>	8.5	$57 \pm 15$	$2 \pm 1$

In 1979, Watanabe *et al.* disclosed the inhibitory properties of some 2'-F-2'-deoxyarabinofuranosylpyrimidines (Figure 1.38) toward an enzyme responsible for the replication step of the herpes simplex virus (HSV-1). It was demonstrated that fluoro analogue **130** was more active than **131** and **132**. It has also demonstrated that the fluoro compound **133** was also more effective than its non-fluorinated analogues **134** and **135**.<sup>101</sup>



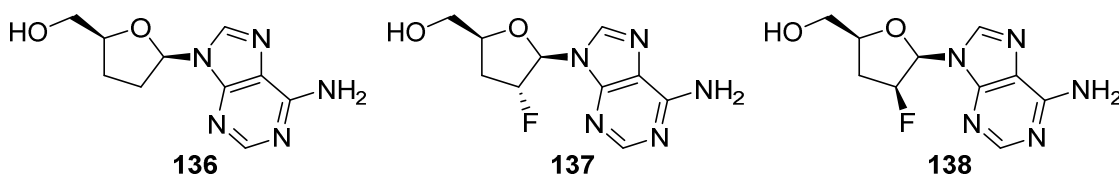
**Figure 1.38** 2'-F-2'-Deoxyarabinofuranosyl-pyrimidines targeting herpes virus, HSV-1.<sup>101</sup>

Table 1.7 below clearly shows the impact of the fluorine towards the bioactivity of **130-135** against HSV-1.

**Table 1.7**Bioactivity of compound **118** to **123** on HSV-1.

Compounds	ID <sub>50</sub> µg/mL	
	LS178Y	P815
<b>130</b>	48	14
<b>131</b>	>100	>100
<b>132</b>	0.2	0.08
<b>133</b>	0.9	0.8
<b>134</b>	4.2	0.9
<b>135</b>	30	16

Another example, from Marquez *et al.*, in 1987, explored the stability of the two fluoro analogues **137** and **138** as illustrated in Figure 1.39. Both analogues showed a better stability at pH = 1 than **136** without any observed decomposition over 24 h, presumably as the fluorine was stabilising amination hydrolysis and base removal. While compound **137** was observed to be 13% less effective than the non-fluoro analogue on HIV, its diastereoisomer **138** had similar durable antiviral properties to **136**.<sup>102</sup>

**Figure 1.39**Anti-HIV nucleoside therapies **136**, **137** and **138**.<sup>102</sup>



## 1.8. Conclusion

Natural products containing fluorine are rare and there are no naturally occurring fluorinated compounds that can be used as starting materials for synthesis programmes, therefore any development of new fluorinated molecules requires the deployment of synthetic fluorination methodologies.

As such, there has been a continuous focus on organic chemistry methodology aimed at the development and optimisation of new fluorination strategies. This focus has led to the discovery of numerous fluorinating reagents and catalysts including methods for enantioselective fluorinations. Additionally, the growing demand from the pharmaceuticals industry to develop new fluorinated compounds by environmentally compatible processes leaves a lot of room for future innovation in fluorine chemistry.

Some of the synthetic methods developed for asymmetric  $\alpha$ -fluorination of aldehydes will be investigated in this thesis in order to design new synthetic routes to fluoro-analogues of bioactives and novel fluorine containing bioactives.

## Chapter II $\alpha$ -Fluorination of aldehydes

This chapter describes the two key reactions that are utilised in this research, concerning the asymmetric  $\alpha$ -fluorination of aldehydes and then their reduction or reductive aminations to afford  $\beta$ -fluoro alcohols or  $\beta$ -fluoro amines respectively. It was an objective of the project to modify the reaction protocols to adapt them to the synthesis of specific fluorinated bioactive targets.

### 2.1. Importance of molecule enantiopurity in pharmaceuticals

In 2002, enantiomeric drugs represented an important portion of all existing drugs (56%), with 44% of these being sold as enantiopure compounds. It is perhaps striking that 56% are sold as racemic mixtures.<sup>103,104</sup> The enantiopurity aspect of a drug is important as they can clearly have very different biological properties as they make diastereoisomeric interactions with proteins targets. Spatial orientation in binding affinity to the active sites of enzymes and receptors enhances or diminishes binding interactions. A clear concern is adverse effects of the less active enantiomer. In 1960s this problem was dramatically observed in the well documented case of thalidomide (Figure 2.1).

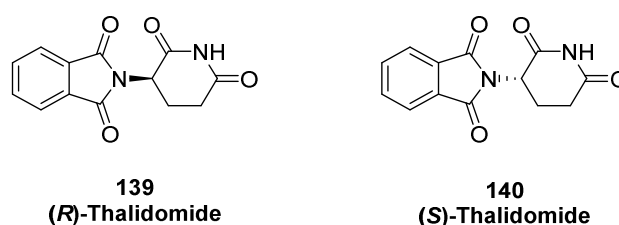


**Figure 2.1** Enantiomers of thalidomide. The (*S*) enantiomer **140** was responsible for embryo-toxicity while the (*R*) enantiomer **139** has sedative properties.

Thalidomide was initially administered in a racemic formulation when first commercialised in 1956,<sup>105</sup> and it was used for the treatment of insomnia due to its sedative properties.<sup>106</sup> It was widely employed due to its apparent lack of undesired effects.<sup>106</sup> It was then used for its anti-emetic effect on pregnant women, becoming very popular, and in 1960 approximately 14.6 tons of thalidomide was sold worldwide.<sup>107</sup>

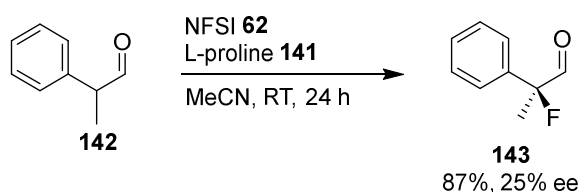
However, in 1961 some doctors started to make a connection between the drug and congenital malformations.<sup>108,109</sup> Later, it was discovered that the toxicity of thalidomide arose from the (*S*) enantiomer **140**, which is embryo-toxic while the sedative effect was attributed to the (*R*) enantiomer **139**.<sup>110,111</sup> One option was to resolve the enantiomers; however, it was discovered that such purification was futile due to a ready racemisation that occurs *in vivo*.<sup>110</sup>

## 2.2. Different approaches to the $\alpha$ -fluorination of aldehydes

### 2.2.1. Preparation of $\beta$ -fluoro alcohols

In 2005, three different research groups published their work regarding the enantioselective  $\alpha$ -fluorination of aldehydes.<sup>112, 113, 114</sup> Barbas,<sup>112</sup> Jørgensen<sup>113</sup> and MacMillan<sup>114</sup> independently described the first asymmetric organo-catalytic protocols for the preparation of  $\alpha$ -fluoroaldehydes by electrophilic fluorination.  $\alpha$ -Fluoroaldehydes are usually more volatile and unstable than the parent aldehydes, and they are more prone to hydration, and thus purification can be challenging.<sup>115</sup> As such, these three research groups carried out *in-situ* reductions with NaBH<sub>4</sub> to generate the corresponding  $\beta$ -fluoroalcohols, thus allowing the yields and stereoselectivity of each reaction to be assessed.

Initially, Barbas used L-proline **141** as a catalyst. L-proline **141** and its derivatives had previously proven to be efficient regarding the  $\alpha$ -chlorination of aldehydes.<sup>116–118</sup> Barbas started to investigate optimal electrophilic fluorinating reagents and found NFSI **62** to be the most efficient and enantioselective, eg. affording an 87% yield and 25% ee for alcohol **143** (Scheme 2.1), while other fluorination reagents, such as Selectfluor<sup>®</sup> gave significantly inferior outcomes with an enantioselectivity of 4% ee reported for **143**.



**Scheme 2.1** Barbas fluorination of aldehyde **142** to afford **143** using NFSI **62** and L-proline **141** as an organo-catalyst.<sup>112</sup>

Barbas *et al.*<sup>112</sup> explored the impact of solvent on the reaction outcome. Acetonitrile was most commonly used for such fluorination reactions, but they found THF to be a more suitable solvent, achieving a 94% yield and an enantioselectivity of 28% ee. Although THF gave good outcomes over-fluorination was a problem and it could be replaced by DMF as this reduced difluorinated side product **144** (Figure 2.2).

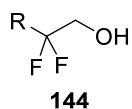


**Figure 2.2** Difluorinated side product **144**, obtained from over-fluorination while using THF.

The best catalyst for the fluorination of  $\alpha$ -substituted aldehydes proved to be the proline derivative **145** which gave **146** in 98% yield and a 38% ee. For unsubstituted, linear aldehydes such as decanal the imidazolidinone analogue **148** was the better catalyst generating products such as **149** in a 30% yield and an 88% ee (Figure 2.3).

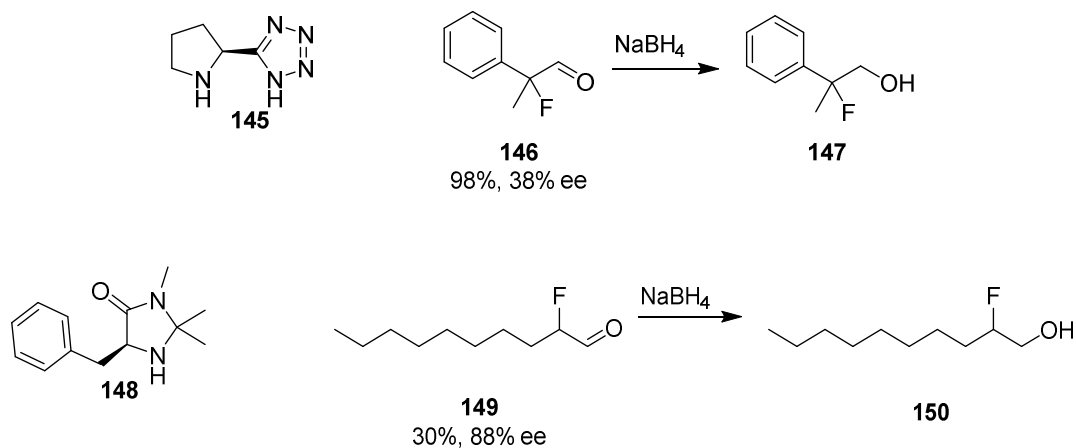


**Figure 2.3** Catalysts and product outcomes as reported by *Barbas et al.*<sup>112</sup>

*Barbas et al.*,<sup>112</sup> also investigated the impact of temperature on stereoselectivity, carrying out fluorinations at  $-20\text{ }^{\circ}\text{C}$  in an attempt to slow down the reaction and increase the stereoselectivity. It was found that decreasing the temperature to  $-20\text{ }^{\circ}\text{C}$  did slow down the reaction time but, it did not impact the stereoselectivity. At the same time an increase of temperature was observed to afford more side products, presumed to be self-aldol products. Various aldehydes with different functionalities were explored and for example from products **151** and **153**, corresponding alcohols **152** and **154** were isolated in modest to good yields and also modest to good enantioselectivities, as exemplified in Figure 2.4.

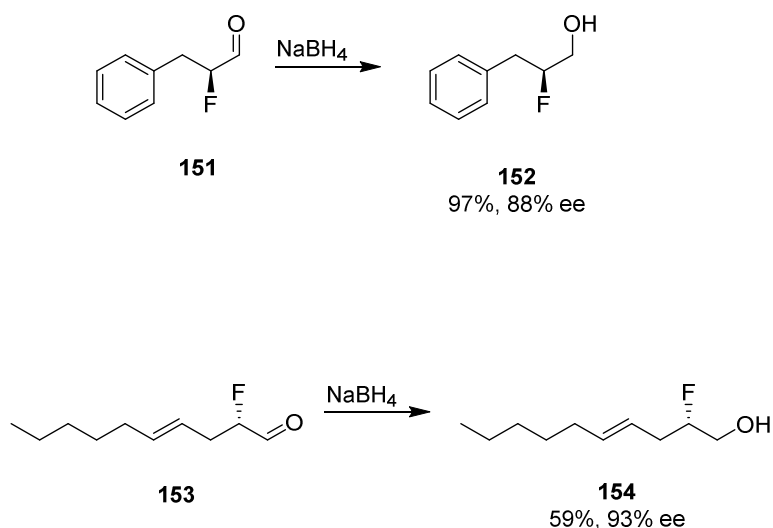
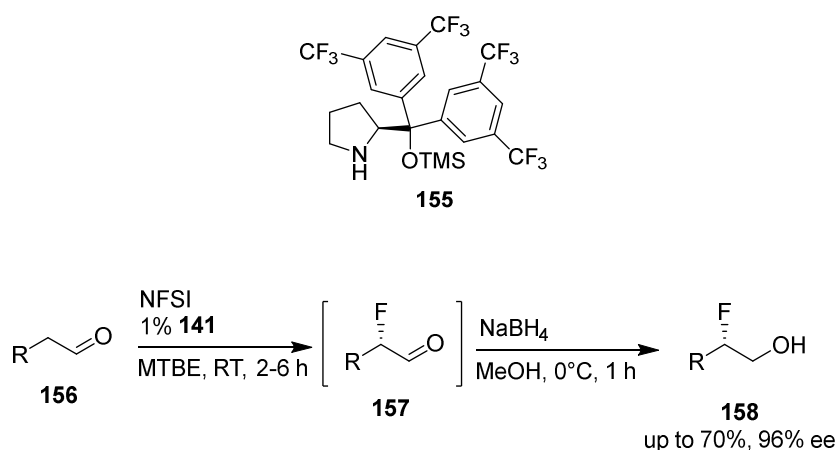


**Figure 2.4** Examples of Barbas  $\alpha$ -fluorinations.<sup>112</sup>

Jørgensen *et al.*,<sup>113</sup> developed an asymmetric  $\alpha$ -fluorination reaction of aldehydes using  $\alpha,\alpha$ -diarylpyrrolidine silyl ethers as catalysts. In this case the particularly bulky aryl groups should influence the enantioselectivity of the reaction. After catalyst screening, pyrrolidine **155** was found to be the optimal catalyst for the reaction with for example around 70% yield and 96% ee for product **158** (Scheme 2.2).



**Scheme 2.2**  $\alpha$ -Fluorination of aldehydes reported by Jørgensen *et al.*<sup>113</sup>

In this study solvent (MeCN, DCM, MTBE) did not have much impact on the reactivity of **155** as a catalyst. Optimised yields required a slight excess of the aldehyde and 1 mol% of catalyst could be used. In general, **155** led to shorter reaction times relative to the methods of Barbas and MacMillan due to its high reactivity, while the yield and selectivity were slightly lower than that obtained by the other protocols. On the other hand, the MacMillan catalyst (*S*)-Cat and (*R*)-Cat worked better in terms of stereoselectivity with a larger loading (2.5-100 mol%) see below.

MacMillan *et al.*,<sup>114</sup> commenced their investigation into this reaction by developing an  $\alpha$ -chlorination of aldehydes,<sup>116</sup> and then they progressed to  $\alpha$ -fluorination using their signature catalysts (*S*)-Cat and (*R*)-Cat (Figure 2.5).<sup>114</sup>

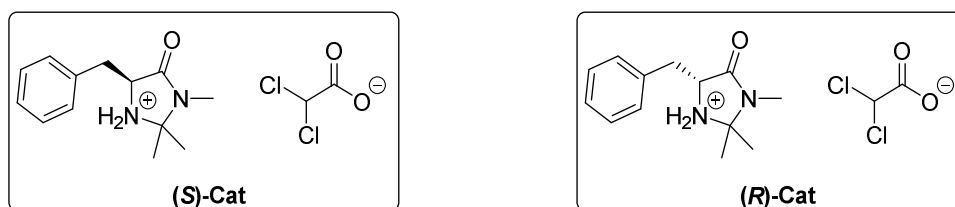
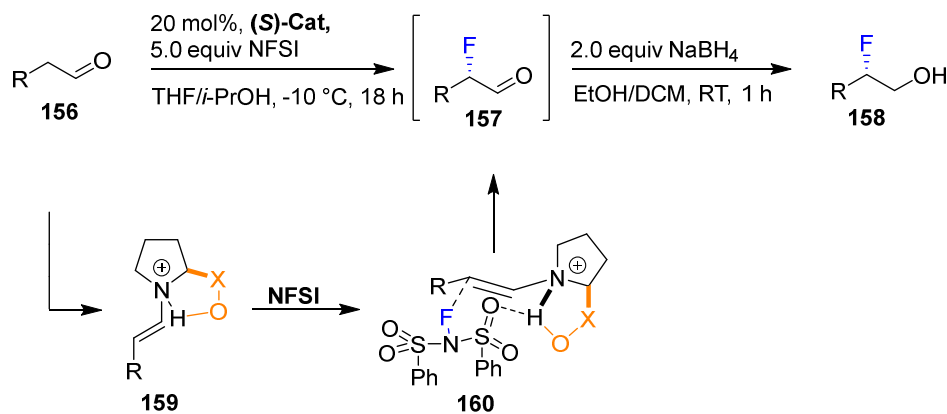


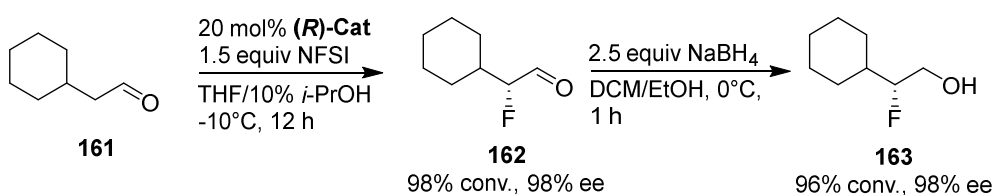
**Figure 2.5** MacMillan catalysts (*S*)-Cat and (*R*)-Cat.

The choice of NFSI, as the fluorination reagent, was made due to its low cost, stable solid state, and the ability of to participate toward the formation of complex **160** facilitating fluor/enamine activation (Scheme 2.3).



**Scheme 2.3** Mechanism proposed by MacMillan *et al.*, for their  $\alpha$ -fluorination of aldehydes.<sup>114</sup>

MacMillan *et al.*<sup>114</sup> investigated the influence of different catalyst, solvents, temperature and reaction times. Optimal result was found at 20 mol% catalyst (**S**)/(**R**)-Cat (best compromise between stereoselectivity and yield), THF and 10% *i*-PrOH at -10 °C and a 12 h reaction time. For example, this afforded  $\alpha$ -fluoroaldehyde **162** in 98% conversion and 98% ee (scheme 2.4).



**Scheme 2.4**  $\alpha$ -Fluorination of aldehyde **161** to **162** (98% conv, 98% ee), and final conversion to the alcohol **163**.<sup>114</sup>

These conditions were applied to a wide range of aldehydes, with differing functional groups, and the method proved generally efficient with yield up to 96% and ee's up to 94%.

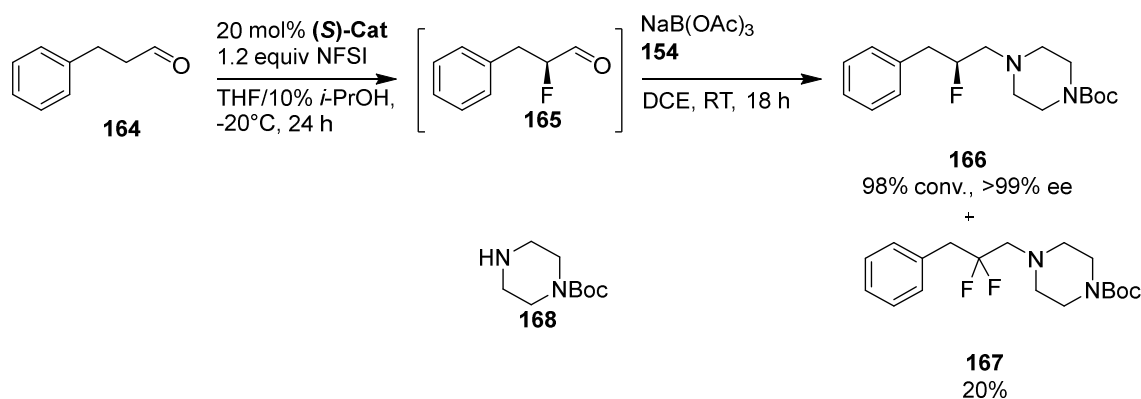
Of these 2005 disclosures,<sup>112–114</sup> the most promising one, in terms of adaptability towards different functional groups and consistent high yields and enantioselectivity, appears to be the MacMillan protocol.<sup>114</sup> As such, this method was selected in the project for the production of  $\alpha$ -fluoroaldehydes which would then be converted directly to  $\beta$ -fluoroamines, by reductive amination, by adapting a protocol of Lindsley *et al.*<sup>119</sup>

### 2.2.2. Preparation of $\beta$ -fluoro amines<sup>119</sup>

In 2009 Lindsley *et al.*,<sup>119</sup> reported a reductive amination of  $\alpha$ -fluoroaldehydes generated from the asymmetric organocatalytic protocol of MacMillan and this afforded  $\beta$ -fluoroamines in a step one pot reaction. This offered a direct approach to the preparation of enantiomers of  $\beta$ -fluoroamines, a class of molecules which will respond to the electrostatic *gauche* effect, and should have some level of conformational stability as described in Section 1.3.2.



Lindsley *et al.*,<sup>119</sup> optimised the fluorination step by exploring the equivalence of NFSI, solvents, temperature and the reaction time. Their best results were obtained with 1.2 equivalent of NFSI, in THF as a solvent containing 10% *i*-PrOH. A temperature of -20 °C and a reaction time of 24 h afford products in a 99% conversion and in some cases >99% ee (Scheme 2.5).



**Scheme 2.5** Lindsley *et al.*, asymmetric fluorination-reductive amination of aldehydes.<sup>119</sup>

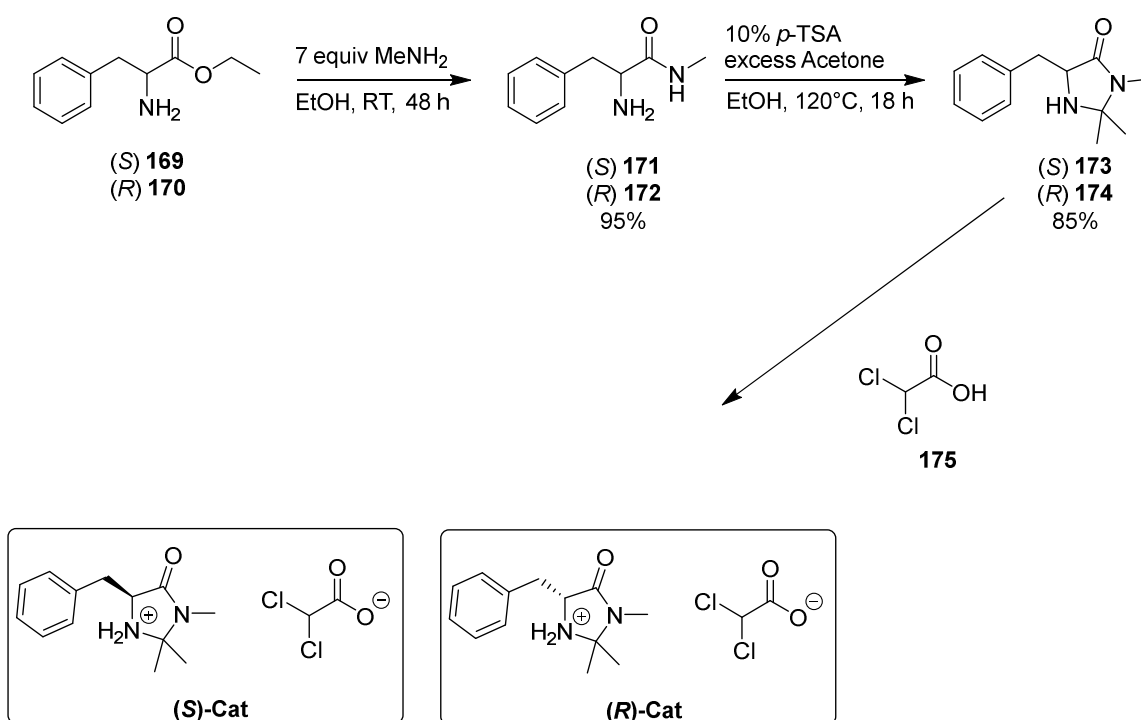
However, side products were observed, and particularly the over-fluorinated  $\alpha,\alpha$ -product **167** which for example was generated at 20% in the typical example illustrated in Scheme 2.5. The  $\alpha$ -aldehyde is converted to an enamine in combination with the added amine, in this instance *tert*-butyl piperazine-1-carboxylate **168**, and this is reduced *in-situ* with sodium triacetoxyborohydride. Different amines were assessed and all afforded yields between 68-82% and with a good stereoselectivity >95% ee. The catalysts **145** and **155** from the Barbas and Jørgensen protocols were also assessed but these generated poorer results than MacMillan's catalyst **(S)-Cat** and **(R)-Cat**, in terms of yields and enantioselectivity.

With these results in mind, it was decided to apply this protocol to the synthesis of selected bioactives and particularly to use dibenzylamine as the amine for reductive amination. This amine in particular acts as a masked free amine, as a straightforward hydrogenation should cleave the *N,N*-dibenzyl group to afford a primary amine. Dibenzylamine was used in only one example of the Lyndsey paper, and subsequent hydrogenations of this or any amine was not explored. There was a clear opportunity to

achieve a shorter route to the enantiomers of 3-F-GABA (**16** and **17**), and similar fluoro-analogues of other bioactive amines using this deprotection.

### 2.3. Optimisation of $\alpha$ -fluorination of aldehydes to afford $\beta$ -fluoro-alcohols and $\beta$ -fluoro-amines

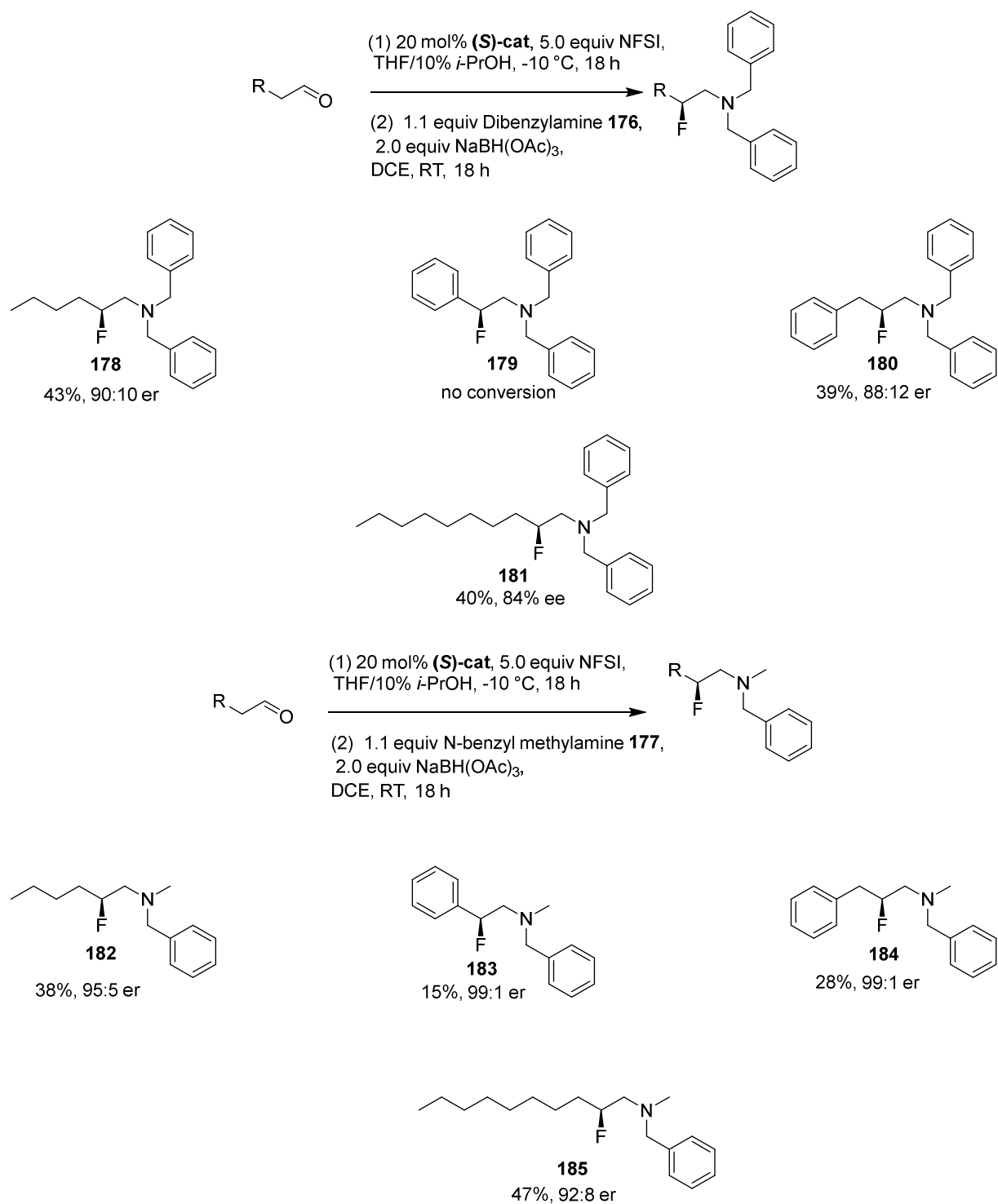
The MacMillan catalysts (**S**)-Cat and (**R**)-Cat required for  $\alpha$ -fluorination reactions of aldehyde substrates were synthesised in house (Scheme 2.6). They are relatively expensive (£250 for 2g) and both enantiomers were required. The synthesis of enantiomer **171** started from the amidation of (*S*)-ethyl 2-amino-3-phenylpropionate hydrochloride salt **169**, using methylamine. Similarly (*R*)-ethyl 2-amino-3-phenylpropionate hydrochloride salt **170** was used for the synthesis of enantiomer **172**. In both cases yield was high, around 95%. The resulting amides were treated with acetone/*p*-TSA to afford imidazoles **173** and **174**, with an average yield of 85%. Finally, **173** and **174** were acidified with dichloroacetic acid **175** to afford the final MacMillan catalysts (**S**)-Cat and (**R**)-Cat.



**Scheme 2.6** Synthesis of MacMillan catalysts (**S**)-Cat and (**R**)-Cat.

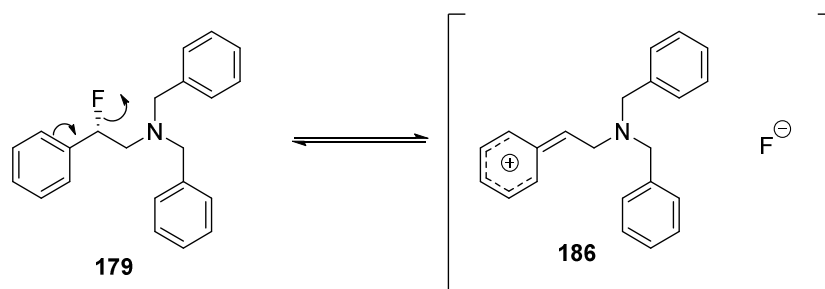
The Lindsley protocol<sup>119</sup> has been primarily explored on a range of readily available aldehydes. In order to become acquainted with and gain a better understanding of the

reaction, initial experiments were carried out on aldehydes such as, hexanal, decanal, phenylpropanal and phenylacetaldehyde. Benzyl amines such as, dibenzylamine **176** and *N*-methylbenzylamine **177** were then used for the subsequent reductive amination step. The outcomes are summarised in Scheme 2.7.



**Scheme 2.7** Exploration of  $\alpha$ -fluorination-reductive amination protocol on selected aldehydes and amines using **(S)-Cat**.

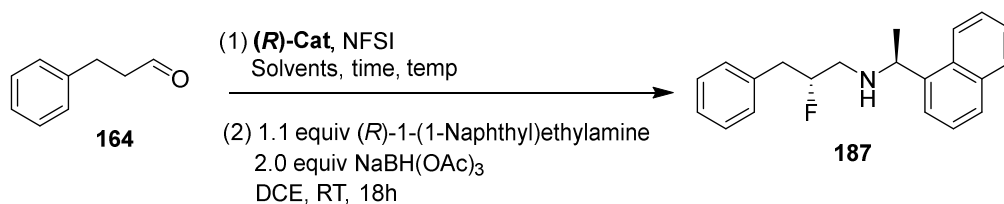
In this substrate scope study, the selectivity and yields obtained were lower than that reported by MacMillan and Lindsley; however, more generally the process worked on most of the aldehydes tested. Lower yields can generally be explained due to over fluorination and generation of significant levels of the corresponding  $\alpha,\alpha$ -difluoro products. This side product was also observed by Barbas<sup>112</sup> while developing that  $\alpha$ -fluorination strategy (2.2.1). No conversion was observed from phenyl acetaldehydes to afford **179** and a very low reactivity to afford **183**. This is most likely due the introduction of a benzylic fluorine which can be vulnerable to elimination for example through intermediate **186** in the case of **179** (Scheme 2.8).



**Scheme 2.8** Putative fluoride elimination from **179** reduces recovery.

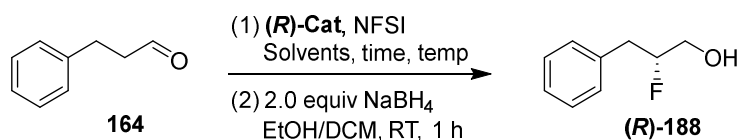
With these results, the decision to re-optimize the reaction for the purpose of targeted bioactives synthesis of products such as 3-F-GABA and F- cinacalcet, was undertaken. Optimization was explored particularly with phenylpropanal **164** as a substrate to afford  $\beta$ -fluoroamine **187** and  $\beta$ -fluoroalcohol (*R*)-**188**. Changes in solvent, catalyst loading, amount of NFSI, temperature and time of the reaction were varied to different extents. Throughout this optimization the key indicators that were considered were, the reaction conversion, the ratio between mono and difluoro compounds and the isolated yield (Tables 2.1 and 2.2).

**Table 2.1** Optimisation of  $\alpha$ -fluorination-reductive amination protocol for the synthesis of  $\beta$ -fluoroamine **187**.



Entry	solvent	Cat (%)	NFSI (equiv)	Temp (°C)	Time (h)	Conversion (%)	Ratio CHF:CF <sub>2</sub>	Yield (%)	dr (%)
1	THF	20	1	-10	18	83	85:15	41	84:16
2	THF	30	1	-10	18	80	94:6	40	96:4
3	THF	20	1.5	-10	18	97	81:19	35	86:14
4	THF	20	1	-10	24	59	31:69	N/A	N/A
5	THF	20	1.5	-20	3	99	16:84	N/A	N/A
6	HFIP	30	1	24	18	15	N/A	N/A	N/A
7	THF	30	1 slow	-10	18	87	97:3	71	98:2
8	THF	30	1.5 slow	-10	18	99	90:10	53	90:10

**Table 2.2** Optimisation of MacMillan protocol exploring various factors.



Entry	solvent	Cat (%)	NFSI (equiv)	Temp (°C)	Time (h)	Conversion (%)	Ratio CHF:CF <sub>2</sub>	Yield (%)	er (%)
1	THF	20	1	-10	18	83	85:15	38	79:21
2	THF	30	1	-10	18	80	91:9	69	99:1
3	THF	20	1.5	-10	18	97	88:12	42	86:14
4	THF	20	1	-10	24	59	31:69	N/A	N/A
5	THF	20	1.5	-20	3	99	16:84	N/A	N/A
6	HFIP	30	1	24	18	15	N/A	N/A	N/A
7	THF	30	1 slow	-10	18	87	97:3	78	97:3
8	THF	30	1.5 slow	-10	18	99	93:7	54	93:7

Entries 1 to 3 (Table 2.1 and 2.2) show little influence of NFSI equivalents in the range from 1 to 1.5 and also the catalyst loading % did not improve conversion in the range of 20 to 30%. Entry 2 (Table 2.1 and 2.2) shows a slightly better yield and better stereoselectivity regarding dr and er. Both Lindsley and MacMillan reported that their fluorinations at room temperature were only marginally inferior to reactions at -10 °C, but in this optimisation fluorinations at room temperature resulted primarily in an increase on the production of the difluorinated products (Entry 5, Table 2.1 and 2.2). Guided by a recent report, regarding  $\alpha$ -chlorination of aldehydes,<sup>120</sup> HFIP/water was explored as a solvent system; however, this did not show any conversion (Entry 6, Table 2.1 and 2.2).

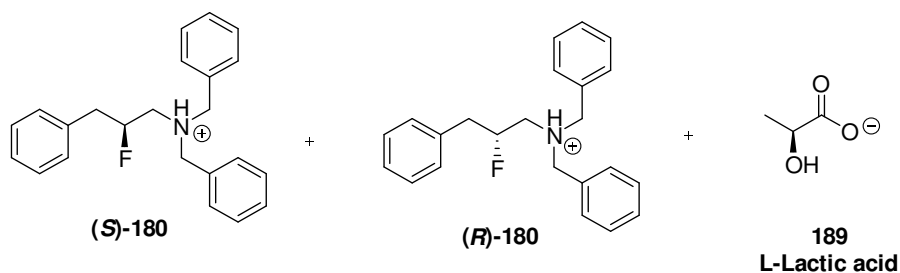
This paper also reported on the impact of the slow addition of the halogenated reagents using a syringe pump over 20 min, to significantly decrease the levels of any dichloro-compound, and to optimise  $\alpha$ -chlorination. An attempt was undertaken to carry out the addition of NFSI (1.0 equiv) in THF over 30 min using a syringe pump. This proved very successful (Entry 7) with a ratio of over 90% of the mono- versus di- fluorinated products, an 87-89% yield and a relatively high stereoselectivity at 97:3 er for alcohol (**R**)-**188**, and 98:2% dr for the amine **187**. These conditions were repeated and gave similar results in each run. Having taken care to reduce the production of difluoro side product, a new set of conditions was explored with 1.5 equivalents of NFSI added by syringe pump over 45 min (Entry 8). The conversion did improve from 89% to 99% but unfortunately these conditions generated more difluorinated product relative to Entry 7. Jørgensen and co-workers,<sup>113</sup> described in their work that a higher yield can be obtained with an excess of the starting aldehyde, but after trialling this our experience was that the non-fluorinated compounds, which contaminated the product mixture proved too challenging to separate by chromatography from the mono and difluoro products.

## 2.4. New approach to $^{19}\text{F}$ NMR enantiomeric excess (ee) determination

An important aspect when involved in the synthesis of chiral organic molecules and bioactives is determining enantioselectivity. Enantiomeric excess can be determined with methods such as: polarimetry, chiral HPLC, chiral gas chromatography (GC) or NMR analyses with chiral dilution/solvating agents. Other methods (for example lanthanide shift reagents) require the product to be isolated before measurement. Polarimetry was for a long time widely used but can be difficult to reproduce as concentration, solvent and temperature must all be rigorously controlled, and the compound must have been isolated previously to obtain the absolute rotation values. The most commonly used methodology nowadays, chiral GC and chiral HPLC, are very accurate if a resolution can be achieved but, they can be time-consuming. To this end, the project focused on developing a technique for assessing the enantiopurity of the prepared fluoro-compounds er using  $^{19}\text{F}\{^1\text{H}\}$ -NMR.

It is often possible to determine diastereoisomeric excess of fluorinated diastereoisomers by integration of the  $^{19}\text{F}\{^1\text{H}\}$ -NMR signals. So, I decided to work on a method for determining enantiomeric excess of fluorinated compounds using H-decoupled  $^{19}\text{F}\{^1\text{H}\}$ -NMR appeared to offer an attractive method for the compounds in this project. Since amines form salts with carboxylic acids it was decided to explore the addition of an enantiopure carboxylic acid to analytical samples for NMR. This method here consisted of the introduction of L-lactic acid directly into the NMR tube to create a more complex chiral medium that would simulate the presence of diastereoisomers due to electrostatic interactions between the fluoroamine enantiomers and the carboxylic acid (Figure 2.6).





A)



B)

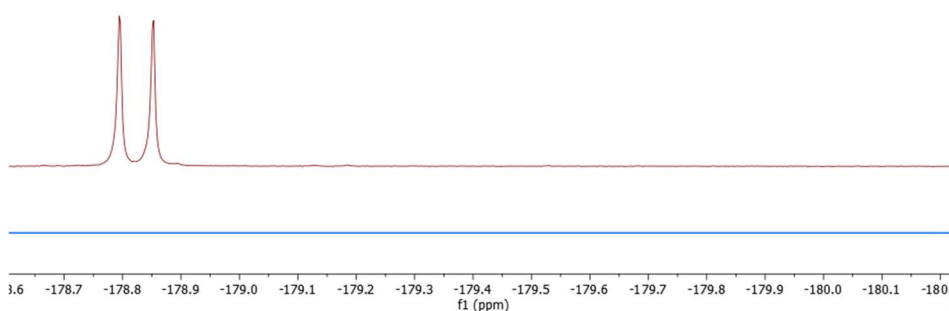


**Figure 2.6**  $^{19}\text{F}\{^1\text{H}\}$ -NMR of racemic mixture (*S*)/(*R*)-**180** : **A**) without L-lactic acid **188**; **B**) with 5.0 equiv of L-lactic acid **189**.

In order to apply this method, analyses were carried out on (*S*)-*N,N*-dibenzyl-2-fluoro-3-phenylpropan-1-amine (**S**)-**180** and (*R*)-*N,N*-dibenzyl-2-fluoro-3-phenylpropan-1-amine (**R**)-**180**, produced after the  $\alpha$ -fluorination-reductive amination protocols from phenylpropanal **164** and dibenzylamine **176** respectively.

First, L-lactic acid **189** was gradually added to the NMR tubes (from 0.5 to 5 equivalent, at 0.5 equivalent increments) to a racemic mixture containing (*S*)- $\beta$ -fluoroamine (**S**)-**180** and (*R*)- $\beta$ -fluoroamine (**R**)-**180** (Figure 2.7).

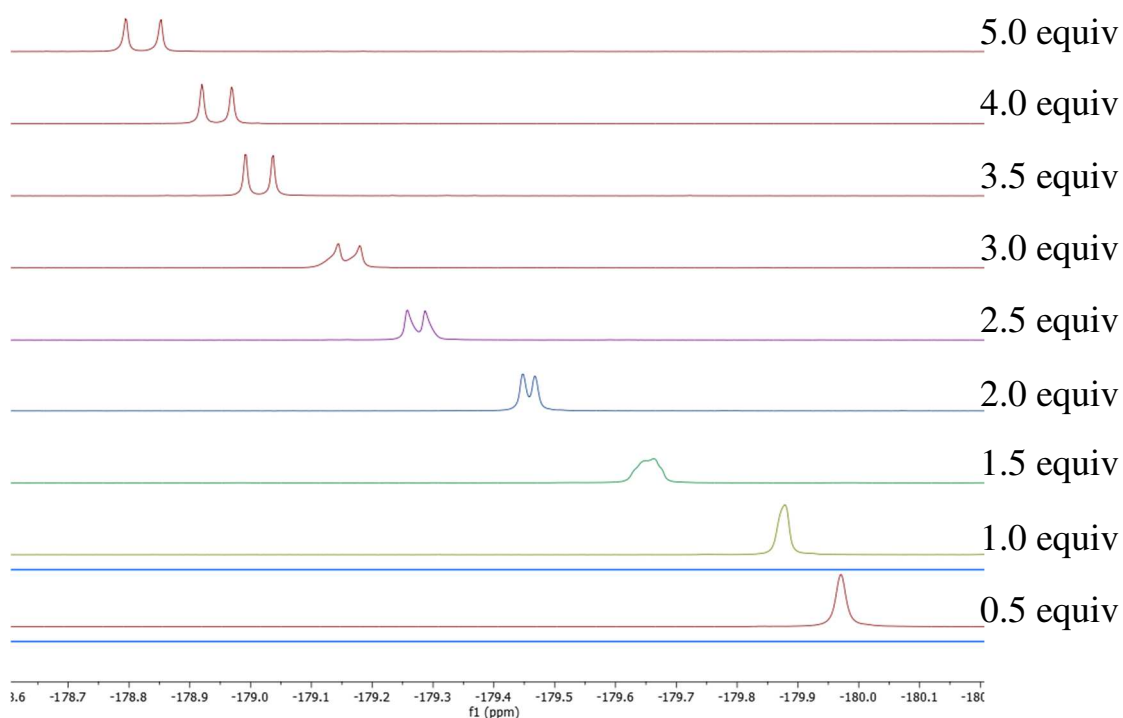


**Figure 2.7**  $^{19}\text{F}\{^1\text{H}\}$ -NMR of racemic mixture of (*S*)-**180** and (*R*)-**180** obtained through Lindsley protocol with L-lactic acid increase from 0.5 to 5.0 equivalent, showing clear peak dissociation at 3.0 equivalent.

For the racemate in Figure 2.7 it is clear that the signals resolve as two peaks corresponding to both enantiomers, when the quantity of L-lactic acid **189** reaches 4.0 equivalents, with a baseline separation such that the peaks could be separately integrated.

This protocol was then explored with a non-racemic mixture of (*S*)-*N,N*-dibenzyl-2-fluoro-3-phenylpropan-1-amine (*S*)-**180** (Figure 2.8), and (*R*)-*N,N*-dibenzyl-2-fluoro-3-phenylpropan-1-amine (*R*)-**180** (Figure 2.9). Each spectra show correlated results, with an integration of the two enantiomers peak revealing an 93:7 er in both cases. This provided confidence in the methodology.

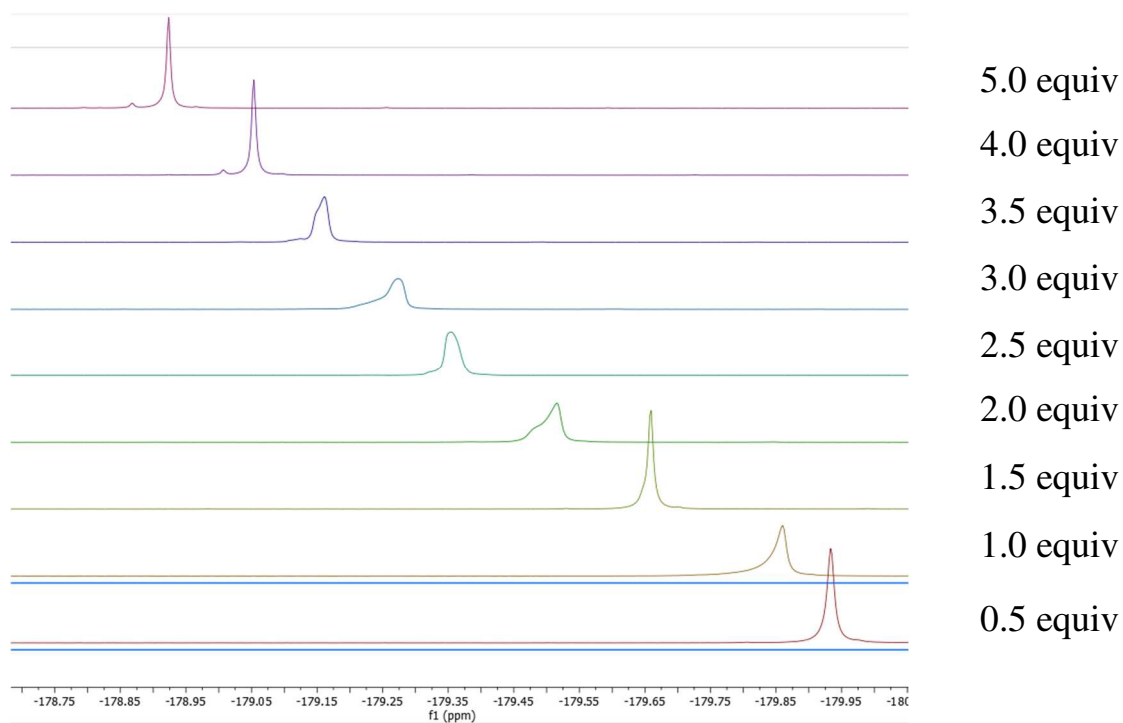


**Figure 2.8**  $^{19}\text{F}\{^1\text{H}\}$ -NMR (*S*)-**180** with an L-lactic acid increase from 0.5 to 5.0 equivalent, showing clear peak dissociation at 4.0 equivalent with the major peak corresponding to isomer (*S*)-**180**, and the minor peak to the isomer (*R*)-**180** revealing 93:7 er.

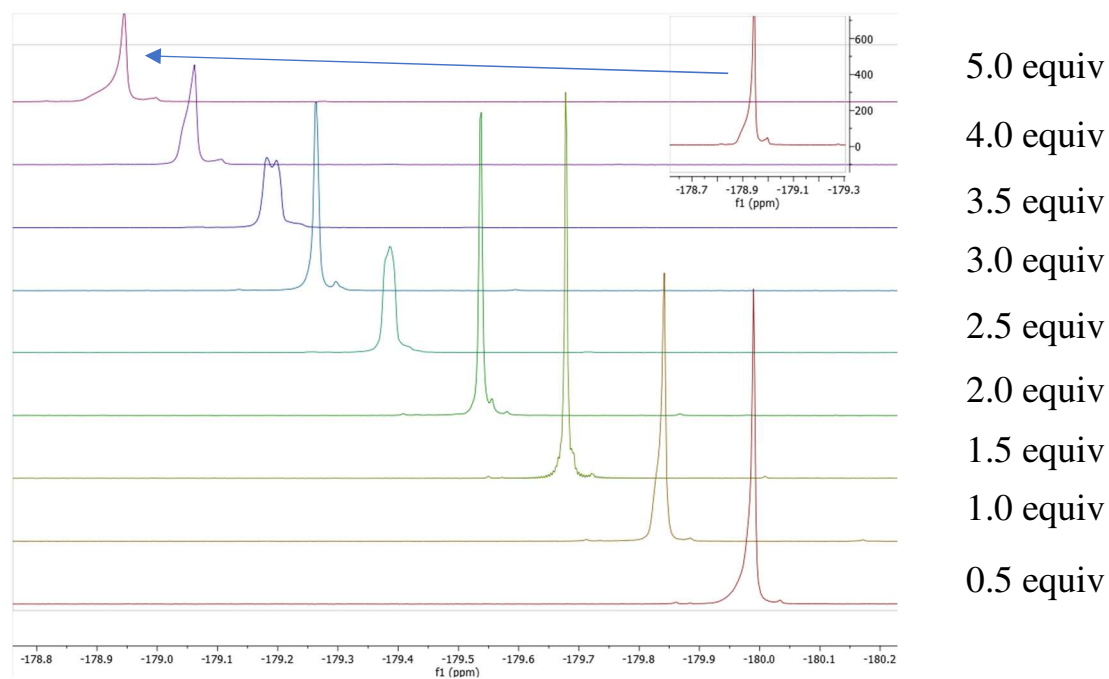


**Figure 2.9**  $^{19}\text{F}\{^1\text{H}\}$ -NMR of (*R*)-**180** obtained through Lindsley protocol with L-lactic acid increase from 0.5 to 5.0 equivalent, showing clear peak dissociation at 4.0 equivalent with the major peak corresponding to the isomer (*R*)-**180** minor peak to the isomer (*S*)-**180** revealing 93:7 er.

The protocol was applied also to (*S*)-*N,N*-dibenzyl-2-fluorodecan-1-amine **181** (Figure 2.10).

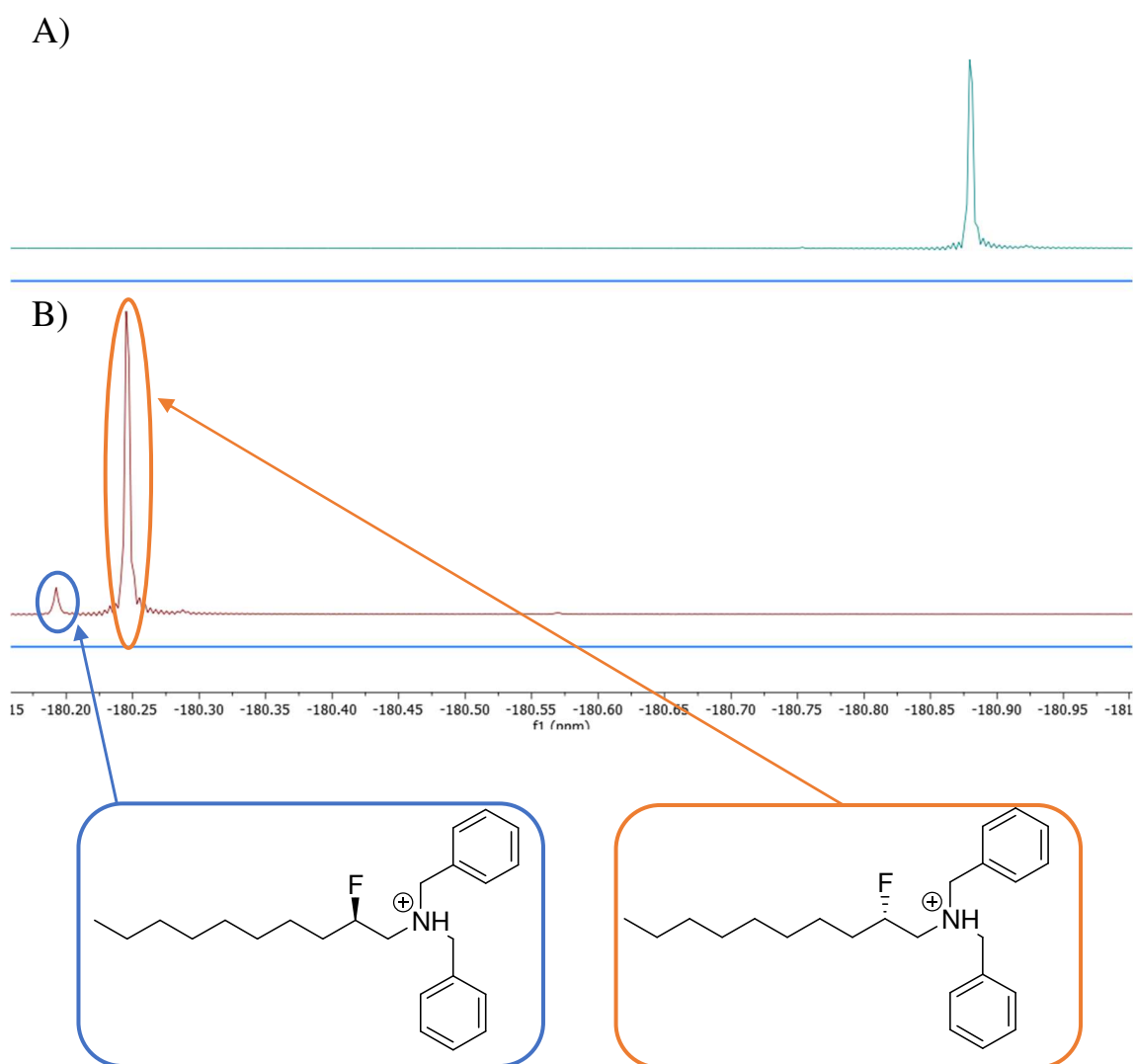
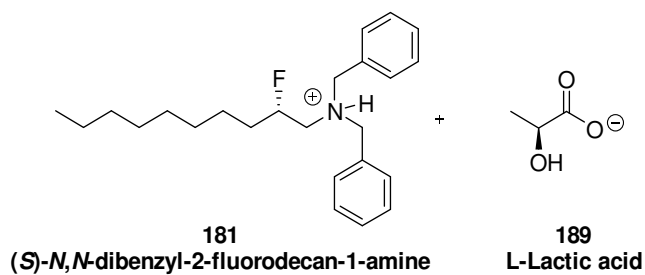


**Figure 2.10**  $^{19}\text{F}\{^1\text{H}\}$ -NMR of **181** : **A)** without L-lactic acid **189** ; **B)** with 5.0 equiv of L-lactic acid **189** to fluoroamine **181** revealing 92:8% er.

Again, the experiment resulted in the resolution of two  $^{19}\text{F}\{^1\text{H}\}$ -NMR signals corresponding to the diastereisomeric salts in solution. Integration of the two peaks, each corresponding to one enantiomer, gives a ratio and thus the enantiomeric excess of 92:8 er (Figure 2.10).

## 2.5. Conclusion

In the chapter an  $\alpha$ -fluorination of aldehydes followed by a reductive amination protocol was explored following the earlier work of the MacMillan and Lindsley laboratories. In this way the Lindsley protocol represented an attractive approach to introduce a fluorine at the  $\beta$  position of a benzyl protected amine that can then be hydrogenated in a one step process to afford the  $\beta$ -fluoro free amine.

Reaction conditions were explored and optimised. In addition, a method of analysis of the enantiopurity of the products  $\beta$ -fluoroamines was established by adding L-lactic acid to the NMR solutions.

This protocol has been applied in the next Chapter to explore a shorter synthesis of 3-fluoroGABA and in Chapter IV will be applied to the preparation of a range of F-cinacalcet analogues.

## Chapter III 2<sup>nd</sup> Generation synthesis of 3-F-GABA stereoisomers

### 3.1. Role of GABA and GABA receptors

$\gamma$ -Aminobutyric Acid or GABA **15** (Figure 3.1), is an inhibitory neurotransmitter of the central nervous system (CNS).

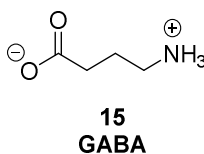
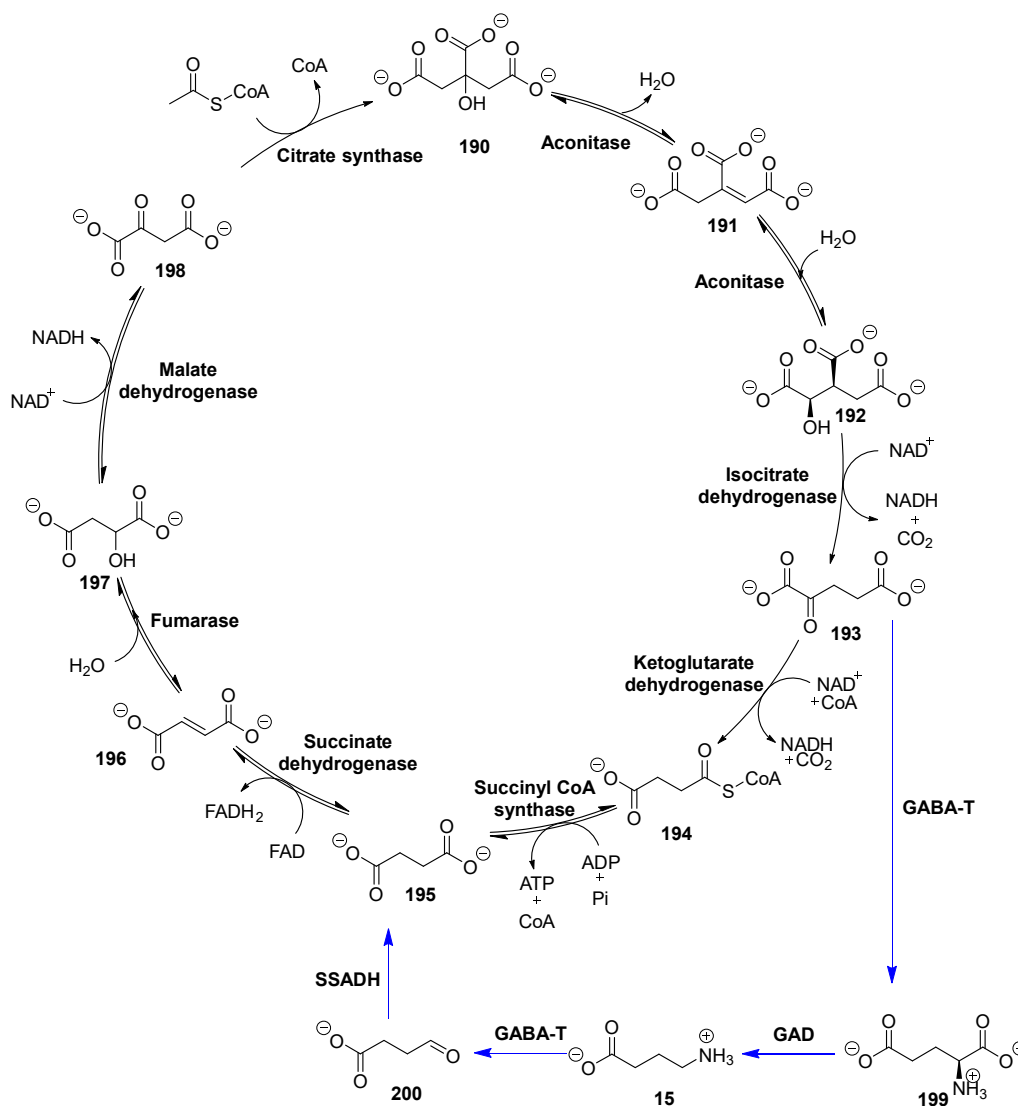


**Figure 3.1**  $\gamma$ -Aminobutyric acid **15** (GABA).

GABA was first isolated from extracts of mammalian brain in 1956 by Bazemore *et al.*,<sup>121</sup> and in the same year it was also found to block sensory discharge (potential released by the action of a neuron or a group of neurons) of the Crayfish stretch receptor.<sup>122</sup> The first report on the mode of action of GABA was described by Kuffler *et al.*, in 1957.<sup>123</sup> GABA works as an inhibitory messenger stopping specific neuron signals (adenylate cyclase and voltage-gated calcium channels) and producing a calming effect.<sup>124</sup> As such, use of GABA and its derivatives represent a promising treatment for disorders such as anxiety, stress and fear.<sup>125</sup>

Within the body, GABA **15** is synthesised from L-glutamate **199**, the main excitatory neurotransmitter of the CNS, by the enzyme L-glutamic acid decarboxylase (GAD). GABA is then transformed to succinic semialdehyde **200** by GABA transaminase (GABA-T). When this occurs  $\alpha$ -ketoglutarate **193** is also produced and it can be processed back to L-glutamate **199**. Succinic semialdehyde **200** is then transformed to succinate by succinic semialdehyde dehydrogenase. Succinate concentration is an important factor of the citric acid cycle as it has inhibitory properties against GAD if the concentration exceeds the amount needed by the citric acid cycle (Scheme 3.1). Dysregulation of this process, with an overly high concentration of GABA **15** or low concentration of L-glutamate **199**, can lead to abnormalities within the transfer of neuronal signals the

consequences of which can contribute to the onset of diseases/conditions such as Parkinson, Alzheimer, epilepsy and depression.



**Scheme 3.1** Citric acid cycle and GABA shunt (blue arrows).<sup>126</sup>

It is valuable to have active sites structures of GABA<sub>A</sub> and GABA<sub>B</sub> receptors to understand how to target them. Such studies could inform on the development of new GABA **15** analogue drugs capable of binding these receptors. GABA<sub>A</sub> is an ion channel receptor which mediates permeability of chloride ions across the cell membrane.<sup>127</sup> Once



GABA **15** binds, the GABA<sub>A</sub> receptor allows chloride to enter and hyperpolarise the cell leading to the inhibition of the postsynaptic activity of the neuron (Figure 3.2).<sup>128</sup>

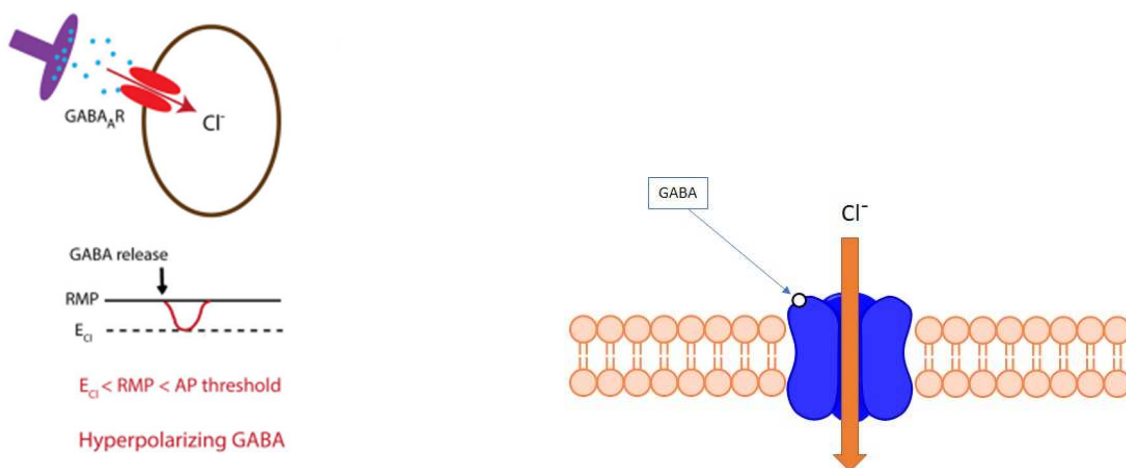


**Figure 3.2** The level of intracellular chloride concentration dictates the polarity of the current through GABA<sub>A</sub> receptors. If Cl<sup>-</sup> concentration is low, the potential of Cl<sup>-</sup> (E<sub>Cl</sub>) becomes negative compared to the resting membrane potential (RMP). In this condition the receptor mediates an inward Cl<sup>-</sup> current that results in hyperpolarization of the cell membrane.<sup>129</sup>

One of the most common GABA<sub>A</sub> antagonists is bicuculine **201** (Figure 3.3). Studies on bicuculine activity in the 70s helped to prove the role of GABA as an inhibitory neurotransmitter.<sup>130,131</sup>

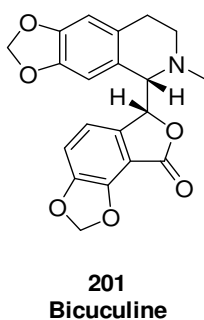


**Figure 3.3** Bicuculine **201** a GABA<sub>A</sub> antagonist.

Due to the structural complexity of GABA<sub>A</sub> receptors, prior to 2014 and the work of Sigel *et al.*, there was no crystal structure of the receptor. The elucidation of the structure

(Figure 3.4) has enabled a deeper understanding of the active site, providing an insight into the GABA agonist binding mode.<sup>132</sup> Prior to the crystal structure, the nature of this receptor was informed using a homologous protein structures and computational modelling in order to gain an understanding of the different binding sites.<sup>133</sup>

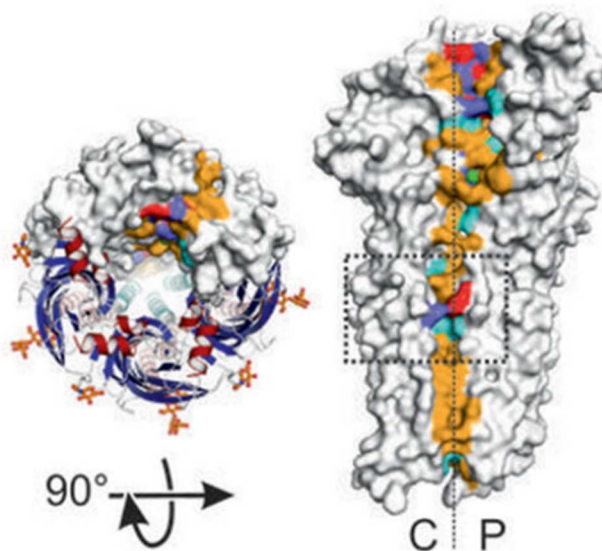


**Figure 3.4** Crystal structure GABA<sub>A</sub> receptor determined by Miller *et al.*<sup>132</sup>

The structural complexity of the receptor is linked to its multimeric composition. Indeed, GABA<sub>A</sub> receptors are composed of 5 subunits (Figure 3.5) that are part of a collection containing 16 subunits ( $\alpha_1$ - $\alpha_6$ ,  $\beta_1$ - $\beta_3$ ,  $\gamma_1$ - $\gamma_3$ ,  $\delta$ ,  $\epsilon$ ,  $\pi$ ,  $\theta$ ). This number of subunits allows the expression of 30 different functional iso-forms of GABA<sub>A</sub> receptors that are expressed within CNS. Each of the 30 possible GABA<sub>A</sub> receptors have distinct physiological and pharmacological properties, explaining the wide range of actions and related diseases that the receptor is associated with and thus its importance as a pharmaceutical target.<sup>134</sup>

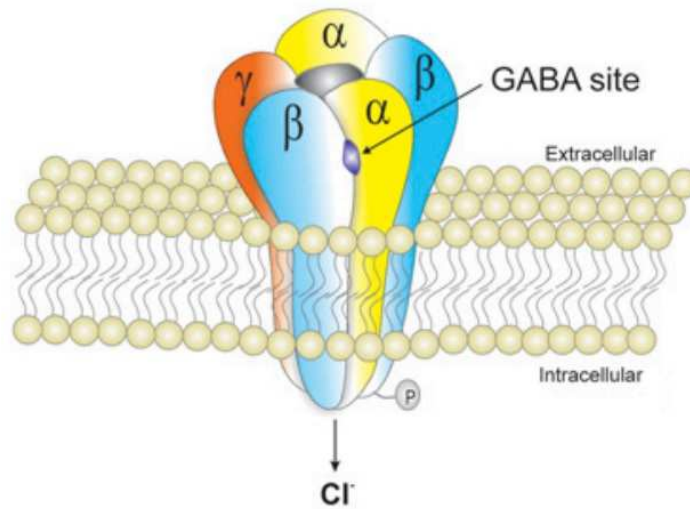


**Figure 3.5** Structure of GABA<sub>A</sub> receptor composed of 5 subunits with binding site.<sup>135</sup>

The GABA<sub>A</sub> receptor binding site was initially thought to be located at the interface of the α and β subunits; however, recently, Sigel *et al.*,<sup>136</sup> discovered that the presence of α subunits is not necessary to obtain a response from GABA binding. In their revised GABA<sub>A</sub> receptor configuration the GABA binding site is instead situated at the interface of two β subunits (Figure 3.6).<sup>136</sup>

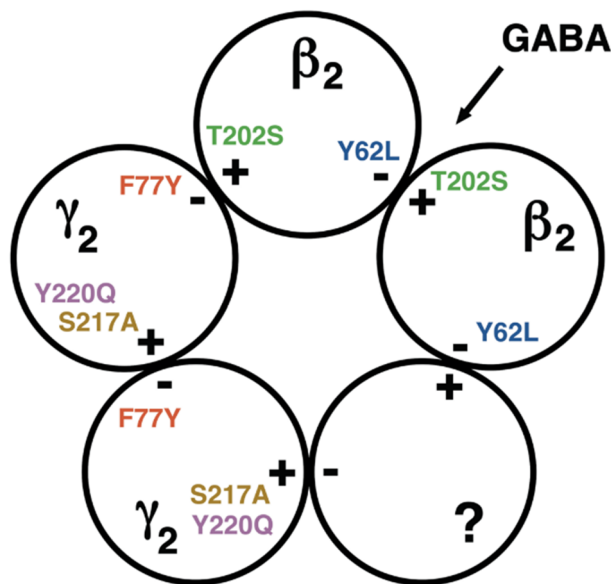


**Figure 3.6** GABA<sub>A</sub> receptor composed of β and γ subunits with the GABA binding site as described by Sigel *et al.*<sup>136</sup>

GABA<sub>B</sub> receptors operate as G protein coupled receptors, the G protein in this instance linking GABA<sub>B</sub> to K<sup>+</sup> and Ca<sup>2+</sup> ion channels (Figure 3.7).

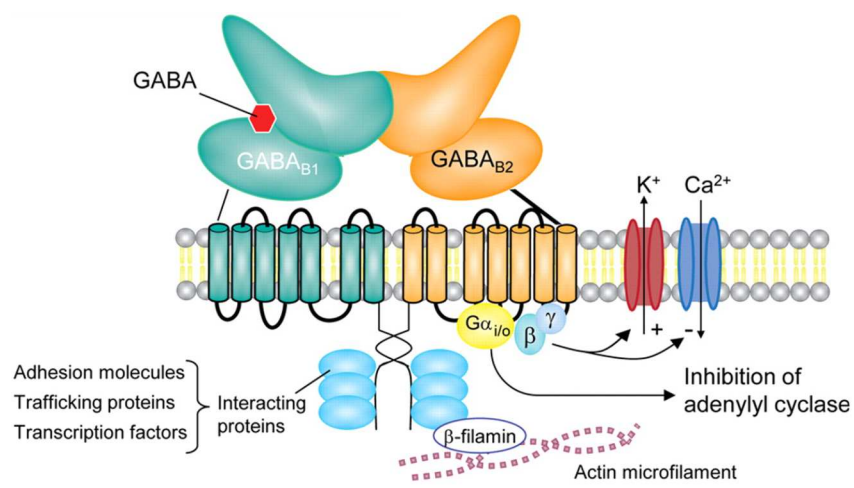


**Figure 3.7** Schematic of a G coupled GABA<sub>B</sub> receptor with GABA binding site.<sup>137</sup>

The pharmacology of GABA<sub>B</sub> receptors is not yet well developed. Indeed, as of 2018 the only marketed drug targeting GABA<sub>B</sub> was baclofen **202** (Figure 3.8).<sup>138</sup>

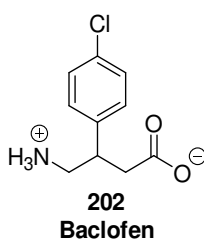


**Figure 3.8** Baclofen **202** a GABA<sub>B</sub> antagonist, sold as racemic mixture.

Baclofen **202** is used in the treatment of many different diseases, such as spasticity due to spiral cord injury,<sup>139</sup> cerebral palsy and sclerosis.<sup>140</sup> Baclofen **202** was first discovered in 1962 by Henrich Keberle while working for the Ciba-Geigy company,<sup>139,141–143</sup> and subsequently it entered the market in 1972. Agonists and antagonists of GABA<sub>B</sub> are still

being studied, such as saclofen **203**, hydroxy saclofen **204** and phaclofen **205** (Figure 3.9); however, due to difficulties permeating the blood-brain barrier (BBB) they possess low potencies.<sup>140</sup>

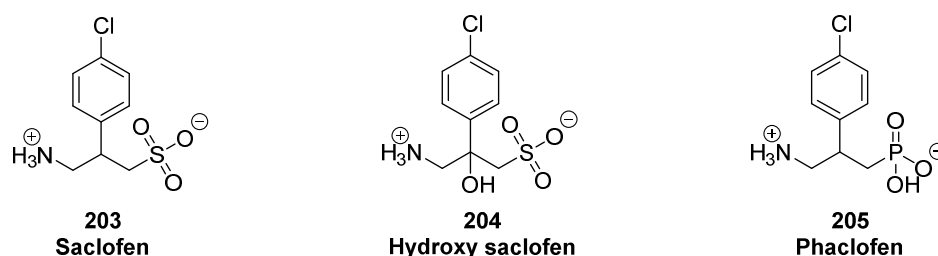


**Figure 3.9** Saclofen **203**, hydroxy saclofen **204** and phaclofen **205**, three GABA<sub>B</sub> agonists, the three of them sold as racemic mixture.

Some phosphonic acid derivatives, **206**, **207**, **208** and **209** (Figure 3.10), that pass through the BBB, have recently shown promising IC<sub>50</sub>'s toward GABA<sub>B</sub> receptors, in the nM - μM range and are now referred to as “first generation” GABA<sub>B</sub> receptors antagonists.<sup>140</sup>

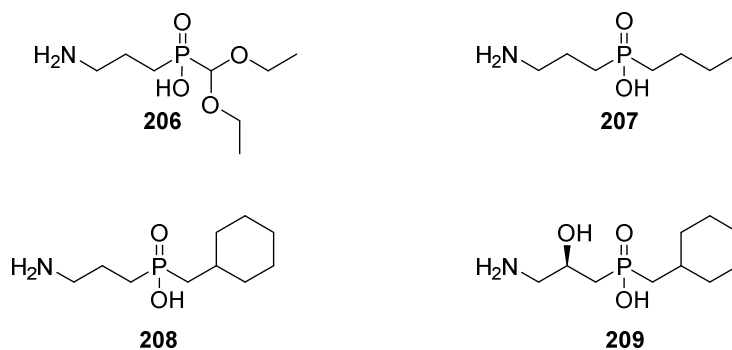


**Figure 3.10** “First generation” GABA<sub>B</sub> receptor agonists **206**, **207**, **208** and **209**.

### 3.2. GABA analogues

As outlined in Section 3.1., GABA is an important inhibitory neurotransmitter linked to the cause and treatment of many diseases. Over years many GABA analogues have been synthesised to regulate GABA<sub>A</sub> action, with some, such the steroid ganaxolone **210** (Figure 3.11) (FDA approved in 2022 for epilepsy),<sup>144</sup> having no structural similarity with GABA but are still capable of mimicking its effect on the receptors.<sup>145–147</sup>

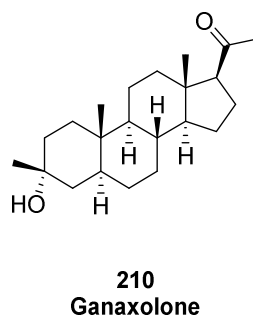


**Figure 3.11** Ganaxolone **210**, a drug targeting the GABA<sub>A</sub> for the treatment of epilepsy.

This study will focus on GABA analogues with a similar structure to GABA **15**. GABA<sub>B</sub> receptor agonists phenibut **211** and tolibut **212**<sup>148</sup> (Figure 3.12), two analogues of baclofen **202**, were developed in the 60s in the Soviet Union,<sup>149</sup> with the aim of treating anxiety,<sup>150,151</sup> insomnia,<sup>152</sup> and depression.<sup>153</sup>

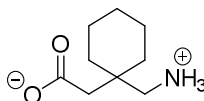


**Figure 3.12** GABA agonists phenibut **211** and tolibut **212**, both sold as racemic mixture.

Analogues **211** and **212** are less potent than baclofen and require a higher concentrations in order to obtain similar activity.<sup>154</sup> Agonists **211** and **212** also stimulate dopamine

biosynthesis which results in an enhanced feeling of excitement as well as reducing anxiety.<sup>155</sup>

Gabapentin **213** (Figure 3.13), is another GABA analogue, first synthesised in 1977 by Hartensteir and Stazinger.<sup>156</sup> Gabapentin **213** was approved by the FDA in 1993 for the treatment of bipolar disorder,<sup>157,158</sup> non-neuropathic pain and anxiety.<sup>159</sup>

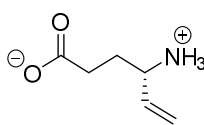


**213**  
**Gabapentin**

**Figure 3.13** Gabapentin **213**, drug analogue of GABA **15** approved by the FDA in 1993 for the treatment of bipolar disorder, non-neuropathic pain and anxiety.

Gabapentin **213** has also had an important impact toward helping people with alcoholism.<sup>160</sup> In 2004 the sales associated with prescriptions of gabapentin were \$3 billion and in 2020 gabapentin was still ranked in the top 10 drugs by sales, used in the U.S.

Vigabatrin **214** (Figure 3.14), is a GABA analogue used in the treatment of epilepsy.<sup>161</sup> It was approved by the FDA in 2009 and acts as GABA-T inhibitor.<sup>162</sup>



**214**  
**Vigabatrin**

**Figure 3.14** Vigabatrin **214** a GABA analogue approved by the FDA in 2009 to treat epilepsy.

The inhibition of GABA-T results in an increase in the concentration of GABA within the brain, leading to a reduction in neuronal activity and thus reduced levels of seizures.

Finally, GABOB **215** (Figure 3.15), another anti-convulsant GABA analogue used in the treatment of epilepsy, was first reported as having an effect by Wada *et al.*, in 1961.<sup>163</sup>

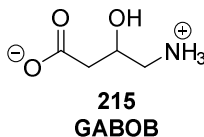


**Figure 3.15** GABOB **215**, drug analogue of GABA **15** used for the treatment of epilepsy.

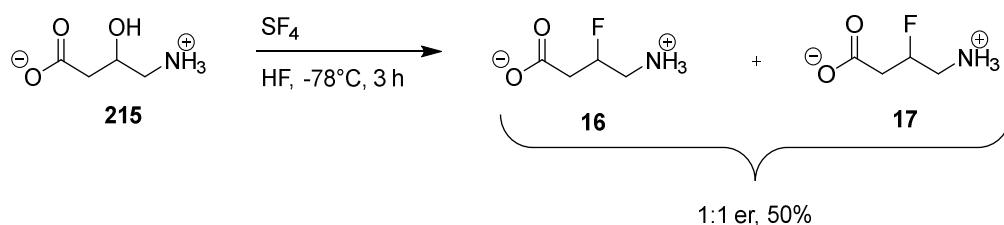
It was determined that the (*S*)-GABOB enantiomer was a GABA<sub>A</sub> agonist while (*R*)-GABOB was a GABA<sub>B</sub> agonist. The drug is sold as a racemic mixture and acts on both receptors.<sup>164</sup> Due to the ability of these GABA analogues to cross the blood-brain barrier, they are more potent than GABA **15** itself.<sup>165</sup>



### 3.3. 3-F-GABA synthesis and assay

#### 3.3.1. First synthesis of 3-F-GABA<sup>166</sup>

(*R*)/(*S*)-3-F-GABA **16/17** was first synthesised by Kollonitsch *et al.*, in 1979,<sup>166</sup> using a straight-forward synthetic pathway starting from GABOB **215**. The alcohol was treated directly with SF<sub>4</sub> at -78°C for three hours in HF to afford **16/17**. The reaction was quantitative, and the product was then purified by ion exchange chromatography, eluting with 4N HCl. Recrystallisation from ethanol afforded **16/17** in a yield of 50% and as a racemic mixture (Scheme 3.2).



**Scheme 3.2** Synthesis of 3-F-GABA **16/17** from GABOB **215** by Kollonitsch *et al.*<sup>166</sup>

This methodology is efficient; however, DAST reactions are generally not stereoselective<sup>167-170</sup> and due to the toxicity of the reagents this route does not represent an attractive strategy to afford 3-F-GABA in enantiomeric forms (**16** and **17**). It is important for any biological/pharmaceutical purposes to develop an enantioselective approach, as the efficacy of the enantiomers requires to be assessed separately as they will have different effects.

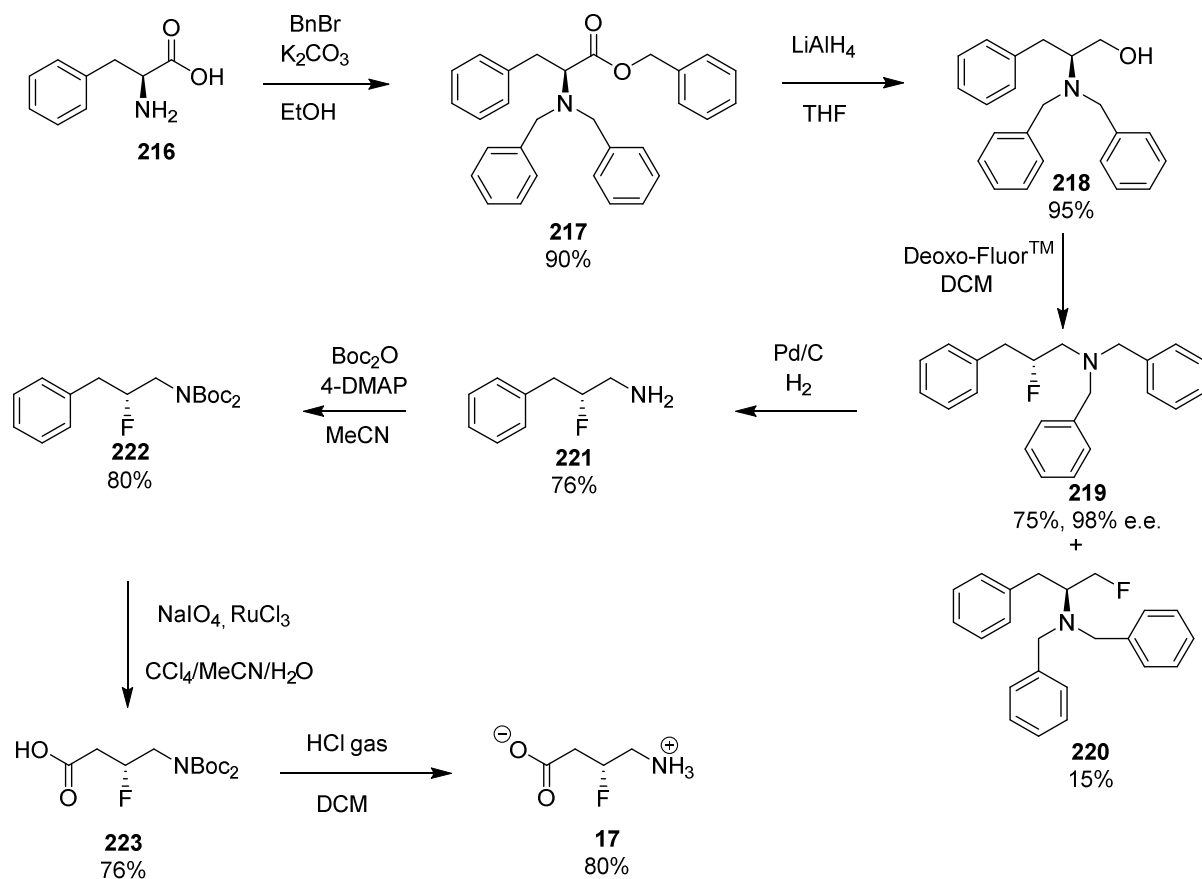
#### 3.3.2 Previous synthesis of 3-F-GABA enantiomers<sup>28</sup>

In 2007 at St Andrews, Deniau *et al.* (O'Hagan Lab), carried out the first enantioselective synthesis of 3-F-GABA. This synthesis was developed for several purposes. Firstly, it was explored to prepare individual samples of **17** and **16** (Figure 3.16). The enantiomers were then used individually to determine their relative bioactivity on GABA<sub>A</sub> and GABA<sub>B</sub> receptors. The outcomes here were then used to assess the impact of the electrostatic *gauche* effect in determining the conformation of **17** and **16**.



**Figure 3.16** Enantiomers of 3-F-GABA.

The route involved a seven-step pathway starting with a three way benzyl protection of the (*R*) or (*S*) phenylalanine **216** to afford **217** (Scheme 3.3). The benzyl ester was then reduced with LiAlH<sub>4</sub> in THF. The resulting alcohol **218** was treated with Deoxo-fluor to give the fluorinated side product **220** which was isolated along with the desired product **219**, obtained by the rearrangement arising from the ring opening of an intermediate aziridinium ring by fluoride. The two N-benzyl groups of **219** were then removed by hydrogenation using Pd/C to afford **221**. After Boc protection of amine **211**, an exhaustive oxidation of the phenyl group was carried out (NaIO<sub>4</sub>/ RuCl<sub>3</sub>) on **222** to generate carboxylic acid **223**. Finally, **17** was afforded the two Boc groups being removed in acid conditions using HCl gas.



**Scheme 3.3** First route to (*R*)-3-F-GABA **17** from (*S*)-phenylalanine (*S*)-**216**, developed by Deniau *et al.*<sup>28</sup>

The enantiomers **16** and **17**, were individually assayed *in vitro* with the human GABA<sub>A</sub> receptor and *in vivo* within more a complex whole animal model (*X. laevis*). The bioassay using cloned human GABA<sub>A</sub> receptor shown no major difference in potency between the enantiomers (Figure 3.17), and although active they were poorer agonists than GABA **15**.

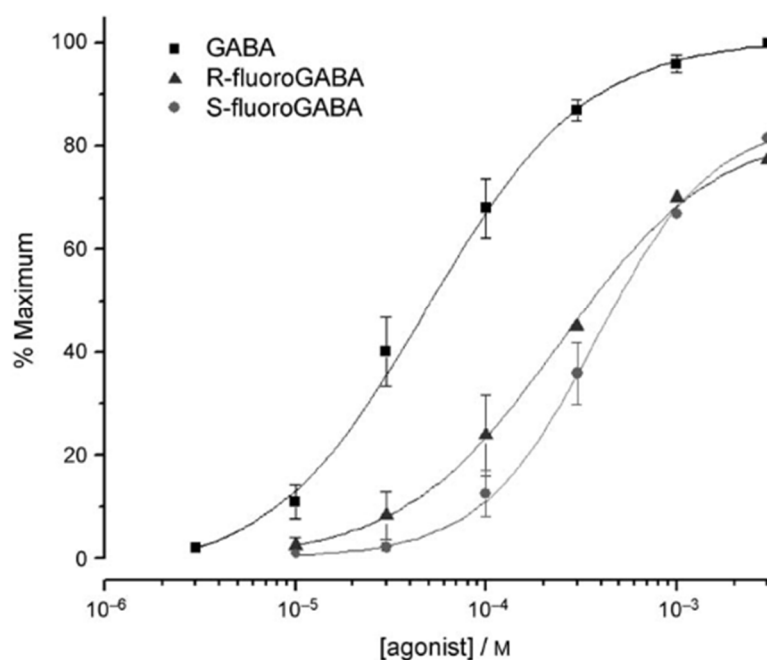
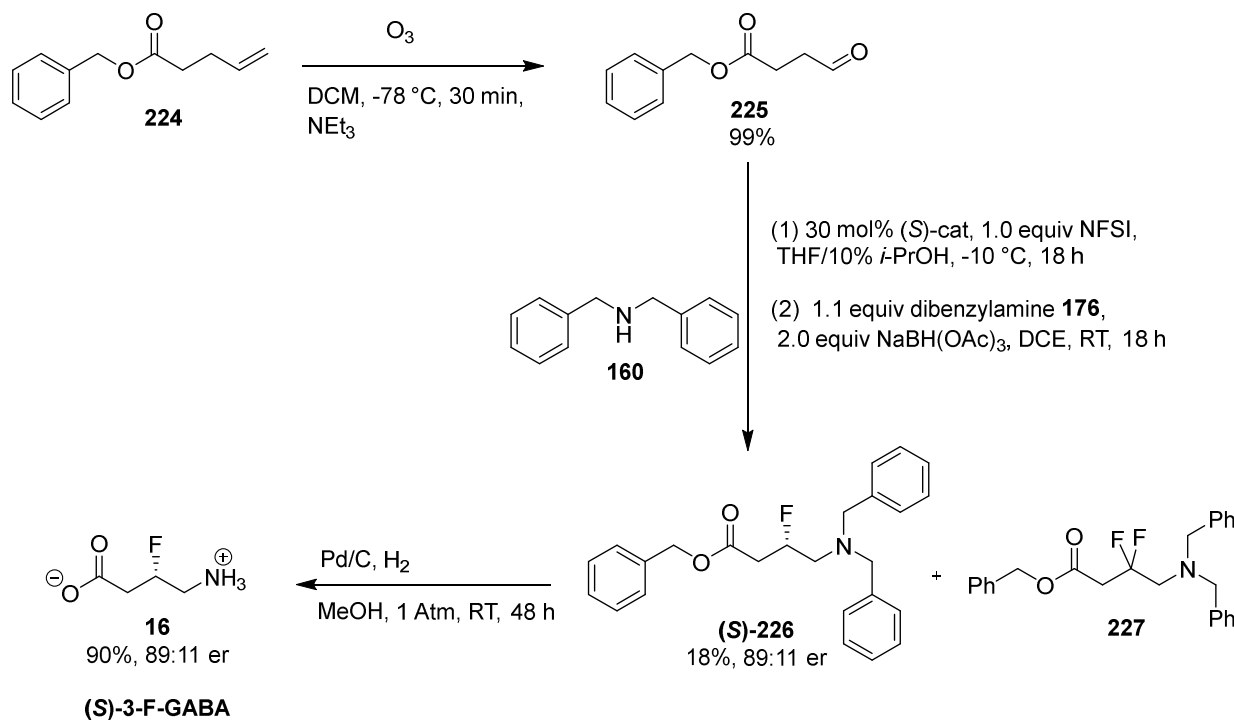


**Figure 3.17** Assays of GABA **15**, (*R*)-3-F-GABA **17** and (*S*)-3-F-GABA **16** on human GABA<sub>A</sub> receptors.

However, in the *in vivo* bioassay **16** showed a better potency than **17**. The difference of potency in intact *X. laevis* cells may be due to a greater metabolism of the **17** enantiomers when compared to **16**, although this could not be unambiguously determined.

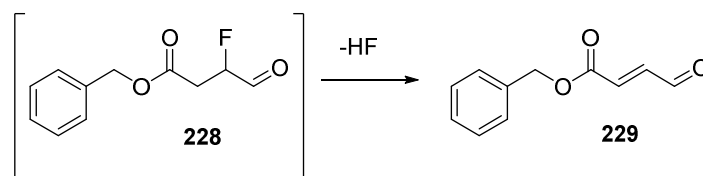
### 3.3.3 Synthesis of 3-F-GABA adapting the Lindsley protocol.

Due to an ongoing interest in exploring the bioactivity of 3-F-GABA, and a lack of available material due to the impractical nature of the synthesis, an effort was made to shorten the route. In this project it became an objective to explore a 1-pot - two-step synthesis of  $\beta$ -fluoro amines, and then apply that to the synthesis of **16** and **17**. To this end an organocatalytic asymmetric  $\alpha$ -fluorination of aldehydes was explored coupled to a reductive amination using conditions described by Lindsley *et al.*<sup>119</sup> The work of Deniau *et al.*<sup>28</sup> had already demonstrated that enantiomer **16** was the more potent of the two, thus the synthesis protocol was developed around this enantiomer (Scheme 3.4).



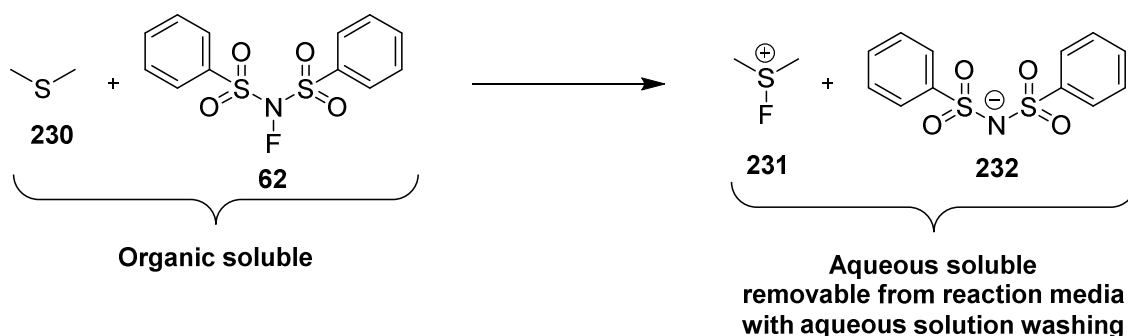
**Scheme 3.4.** First attempted of (*S*)-3-F-GABA **16** synthesis using non-optimised Lindsley protocol starting from the benzyl protected aldehyde **225**.

The route started with benzyl esterification of pentenoic acid to afford ester **224**. The terminal alkene was then oxidised using ozone at  $-78^\circ\text{C}$  to afford aldehyde **225**. This proved to be very efficient and **225** was isolated in a 99% yield. After quick filtration through a pad of silica, **225** was added to a  $-10^\circ\text{C}$  solution of THF and 10% *i*-PrOH, containing 20% mol of MacMillan catalyst (*S*)-Cat, and 5.0 equivalents of NFSI. The reaction was left to stir typically overnight in order to afford  $\alpha$ -fluoroaldehyde (*S*)-**228**. This  $\alpha$ -fluoroaldehyde is susceptible to elimination to **229** as illustrated in Scheme 3.5.



**Scheme 3.5** Aldehyde **228** is susceptible to HF elimination.

As such, (*S*)-**228** was subjected to rapid work up and progressed directly to the reductive amination step. The work up consisted of precipitation of the catalyst with diethyl ether and then filtration through a pad of silica before adding dimethyl sulfide **230** (DMS). DMS here reacts with the excess of NFSI **62** (Scheme 3.6) avoiding any over production of the difluoro side-product **227** (Scheme 3.4).<sup>171</sup>



**Scheme 3.6** Action of DMS **230** on the inactivation of excess NFSI **62**.

The organic solution was then washed three times with a saturated solution of  $\text{NaHCO}_3$  and then brine. After concentration under vacuum, the crude  $\alpha$ -fluoroaldehyde (*S*)-**228** was immediately added to the reductive amination medium containing the dibenzylamine **176** in 1,2-dichloroethane (DCE) which was followed by the addition of  $\text{NaHB}(\text{OAc})_3$  to afford the benzyl protected fluoro GABA (*S*)-**226** with 18% yield and 78% ee (Scheme 3.4)

The enantiomeric excess was determined by the  $^{19}\text{F}\{^1\text{H}\}$ -NMR methodology described in Section 2.3. Figure 3.18 shows the clear peak dissociation after addition of 5.0 equivalent of L-lactic acid to the columned enantiomer mixture of (*S*)-**226**, the minor peak corresponding to (*R*)-**226**. The absolute configuration was assumed regarding the previous worked carried out on the  $\alpha$ -fluorination of aldehydes with (*S*)-Cat and (*R*)-Cat.<sup>113,114</sup>

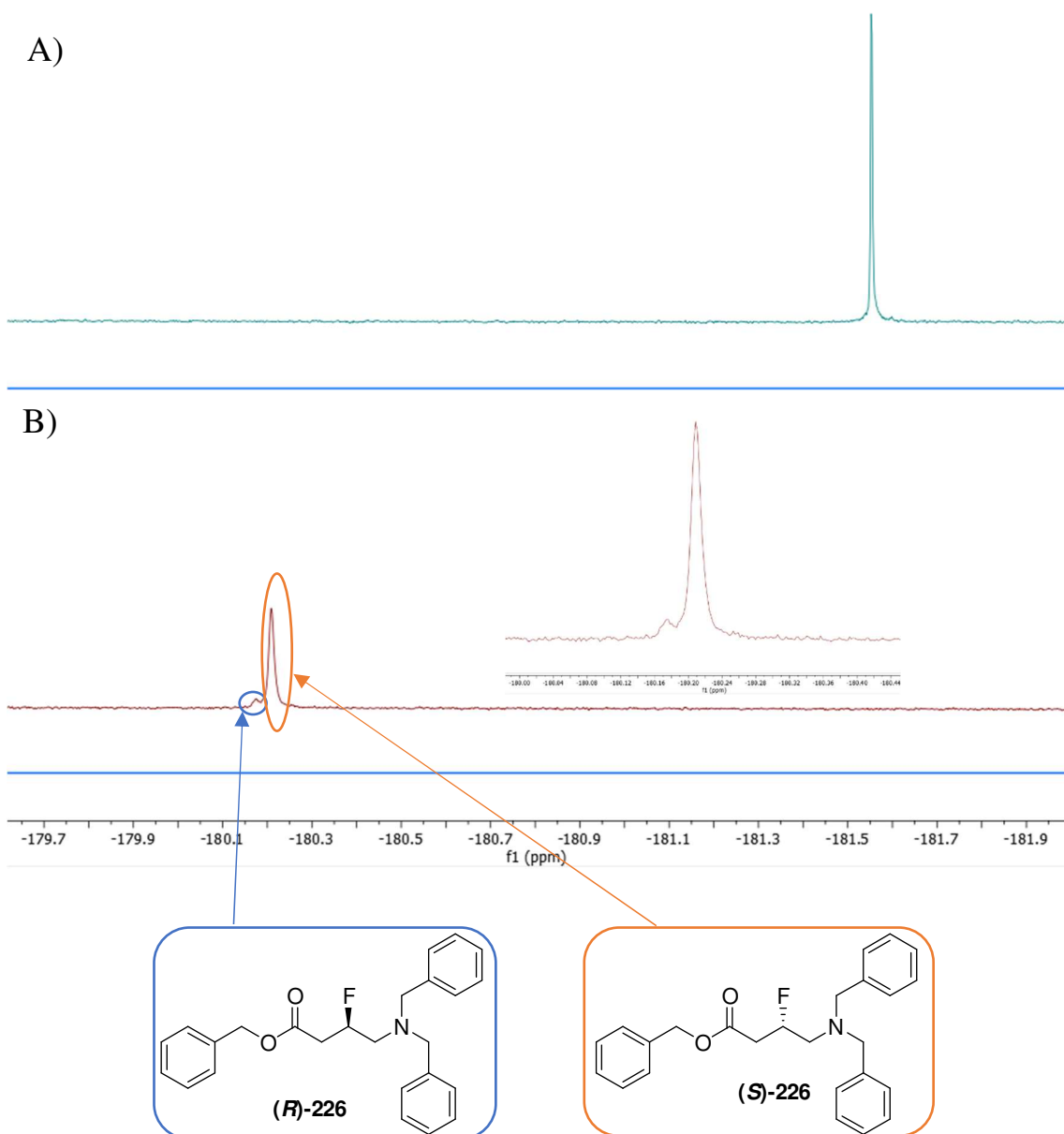


**Figure 3.18**  $^{19}\text{F}\{^1\text{H}\}$ -NMR of (*S*)-**226** after column chromatography : **A**) Without L-lactic acid ; **B**) With 5.0 equivalent of L-lactic acid showing the minor isomer (*R*)-**226**, integration of both peaks reveal 89:11 dr.

Finally, (*S*)-**226** was deprotected using  $\text{Pd}(\text{OH})_2/\text{C}$  and  $\text{H}_2$  to afford the final product **16**, after reverse phase column purification, in a 90% yield. The overall process afforded (*S*)-3-F-GABA **16** with 16% yield and 89:11 er (Scheme 3.4). The main loss in the yield was due to the over production of the difluoro product **227** and other unidentified side products (Figure 3.19), the same problem observed within the simple aldehydes tested in Section 2.4.

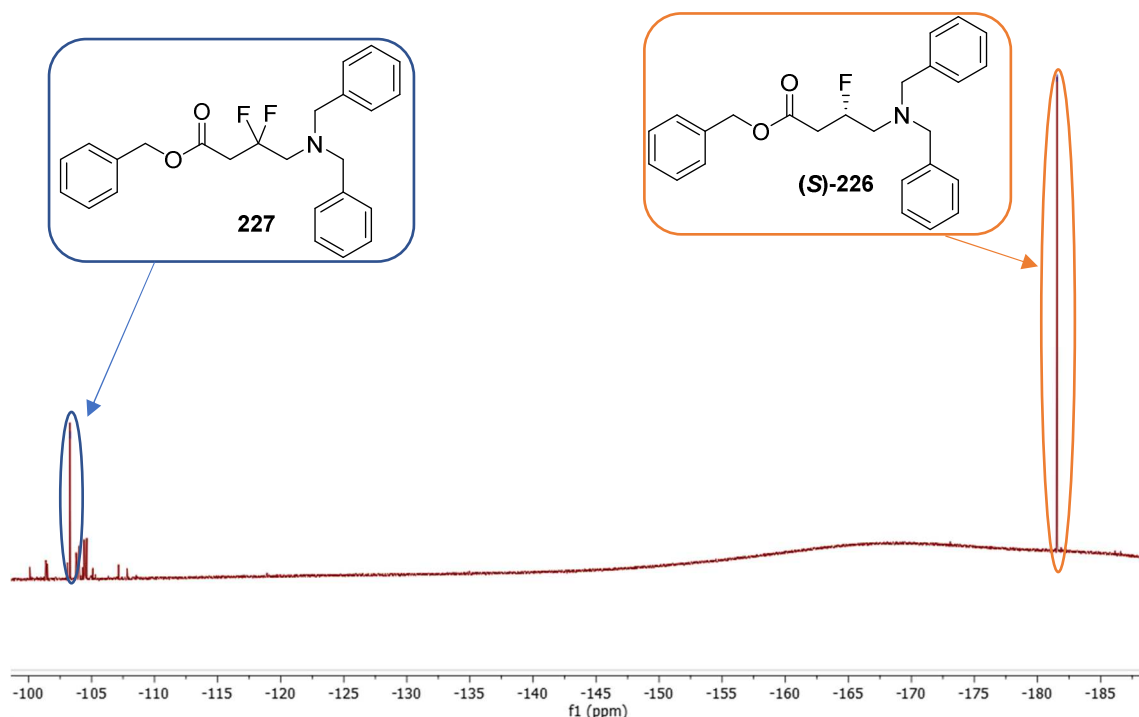
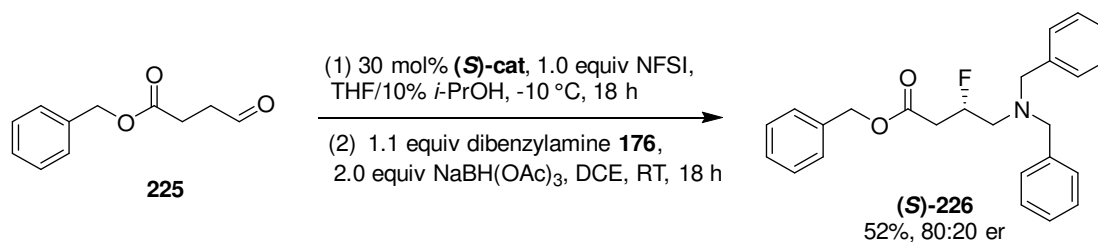


**Figure 3.19**  $^{19}\text{F}\{^1\text{H}\}$ -NMR of unpurified (*S*)-**226** highlighting the difluoro side product **227** at -103 ppm, and other minor unidentified side products.

The same synthetic pathway was trialed with the optimised conditions established in Section 2.4. (30% (*S*)-Cat, 1.0 equivalent of NFSI over 30 min) while using a syringe pump for addition of NFSI over 30 min (rate of  $2.5 \text{ g}\cdot\text{h}^{-1}$ ), to limit the production of the side product (*R*)-**226**. With these conditions  $\beta$ -fluoro amine step afforded (*S*)-**226** with 52% yield and a lower selectivity than the previous condition with 80:20 er (scheme 3.7).



**Scheme 3.7** Synthesis of (*S*)-**226** using the optimised Lindsley protocol conditions determined in Section 2.3.



Again, the enantioselectivity were determined by the addition of 5.0 equivalent of L-lactic to the purified (*S*)-**226** (Figure 3.20).

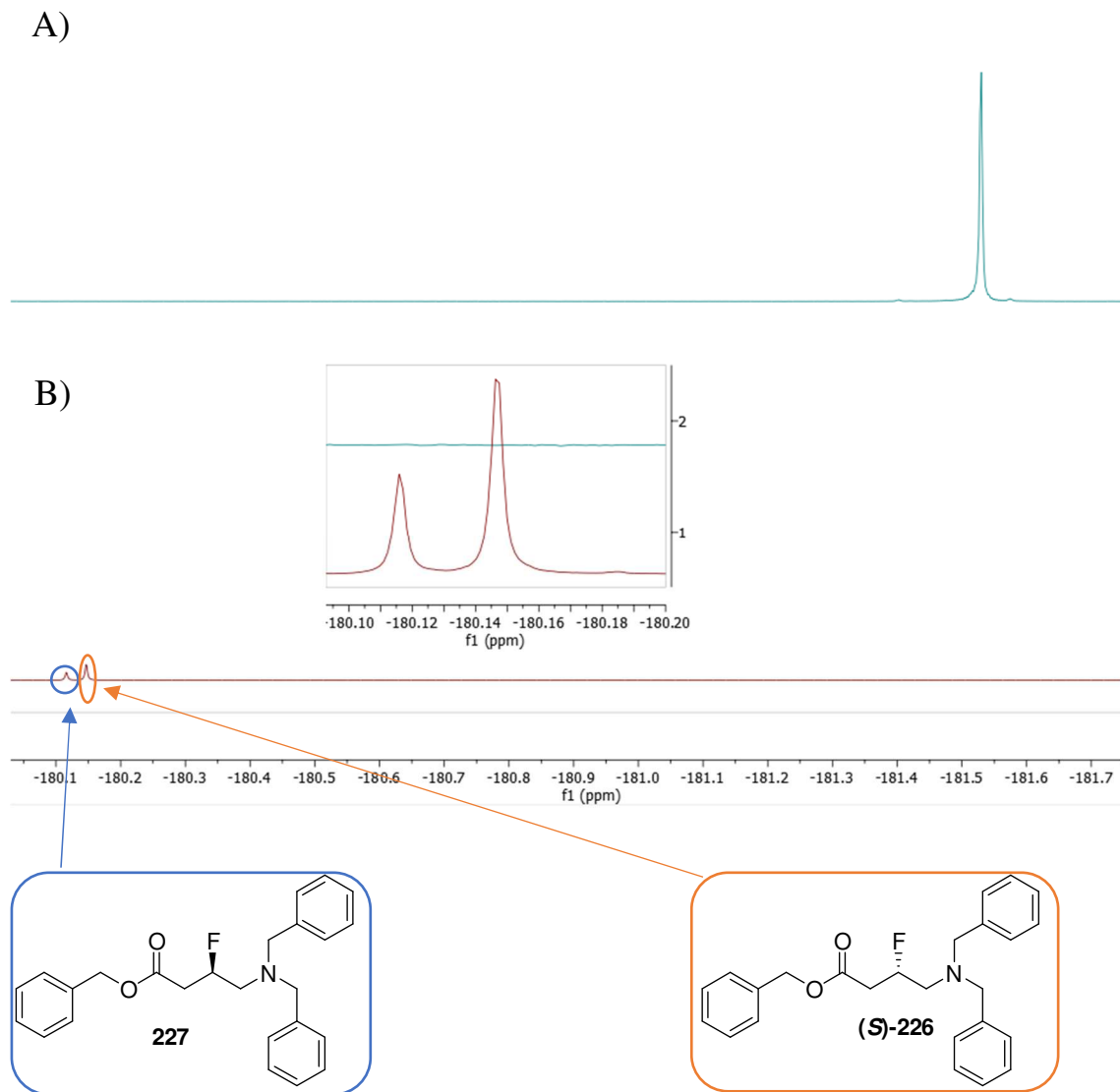


**Figure 3.20**  $^{19}\text{F}\{^1\text{H}\}$ -NMR of (*S*)-**226** synthesised with optimised Lindsley protocol conditions : **A**) Without L-lactic acid ; **B**) With 5.0 equivalent of L-lactic acid showing the minor isomer (*R*)-**226**, integration of both peaks reveal 80:20 dr.

The increase in yield can be explained by a lower production of the difluoro product that can be observed, by  $^{19}\text{F}\{^1\text{H}\}$ -NMR of the crude products (Figure 3.21). The decrease of **227** production is explained by the reaction being slowed down due to slow addition of NFSI.

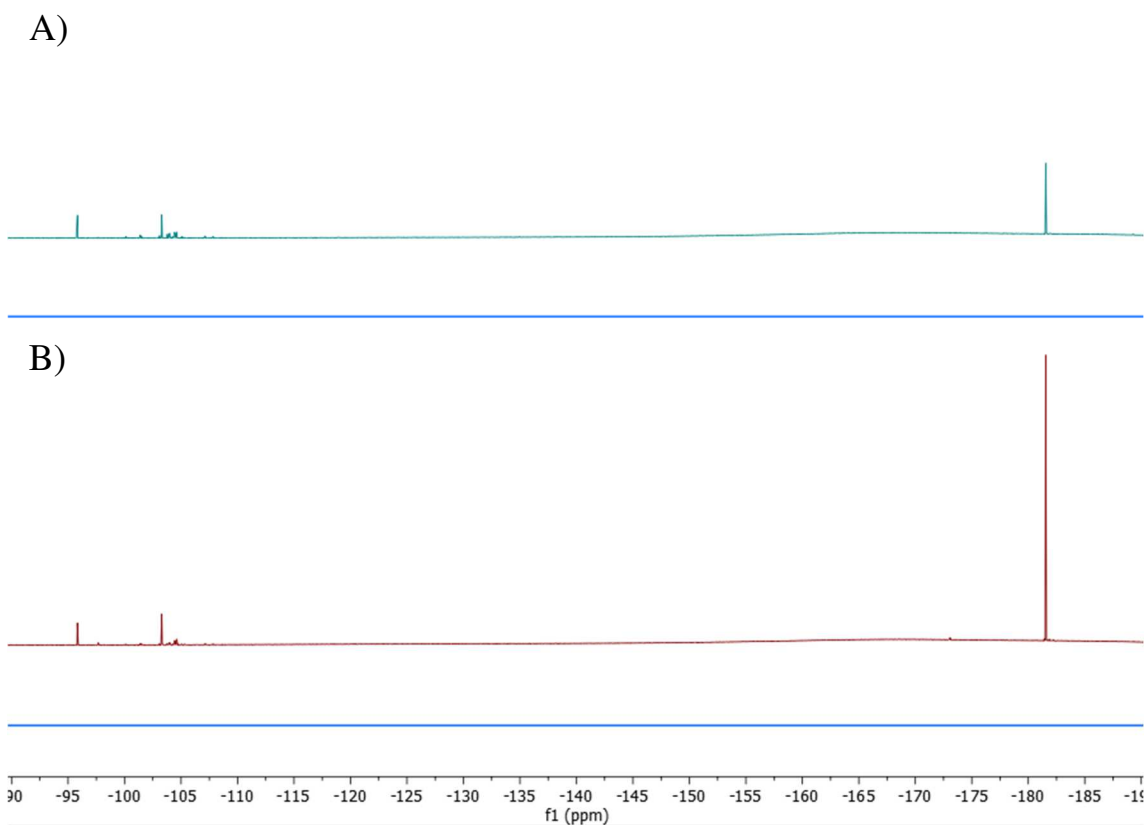


**Figure 3.21**  $^{19}\text{F}\{^1\text{H}\}$ -NMR comparison of the two Lindsley protocols tested over the synthesis of (*S*)-**226** (-181 ppm) : **A**) Unoptimised protocol ; **B**) Optimised protocol showing less difluoro side product **227** -103 ppm and also less unidentified side products.

With these optimised conditions the overall yield increased from 16% to 46% yield which represents an improvement regarding the methodology used by Deniau *et al.*, in 2007.<sup>28</sup>

For both protocols tested (Scheme 3.4 and Scheme 3.7), column chromatography purification managed to remove most of the difluoro side product **227** and the other unidentified side products. As an example, for the protocol described Scheme 3.7, before purification 12% of the difluoro compound **227** was observed, while only 1% was observed after purification (Figure 3.22). For the protocol described in Scheme 3.4, before purification 20% of the difluoro product was observed, while only 1% was observed after purification.

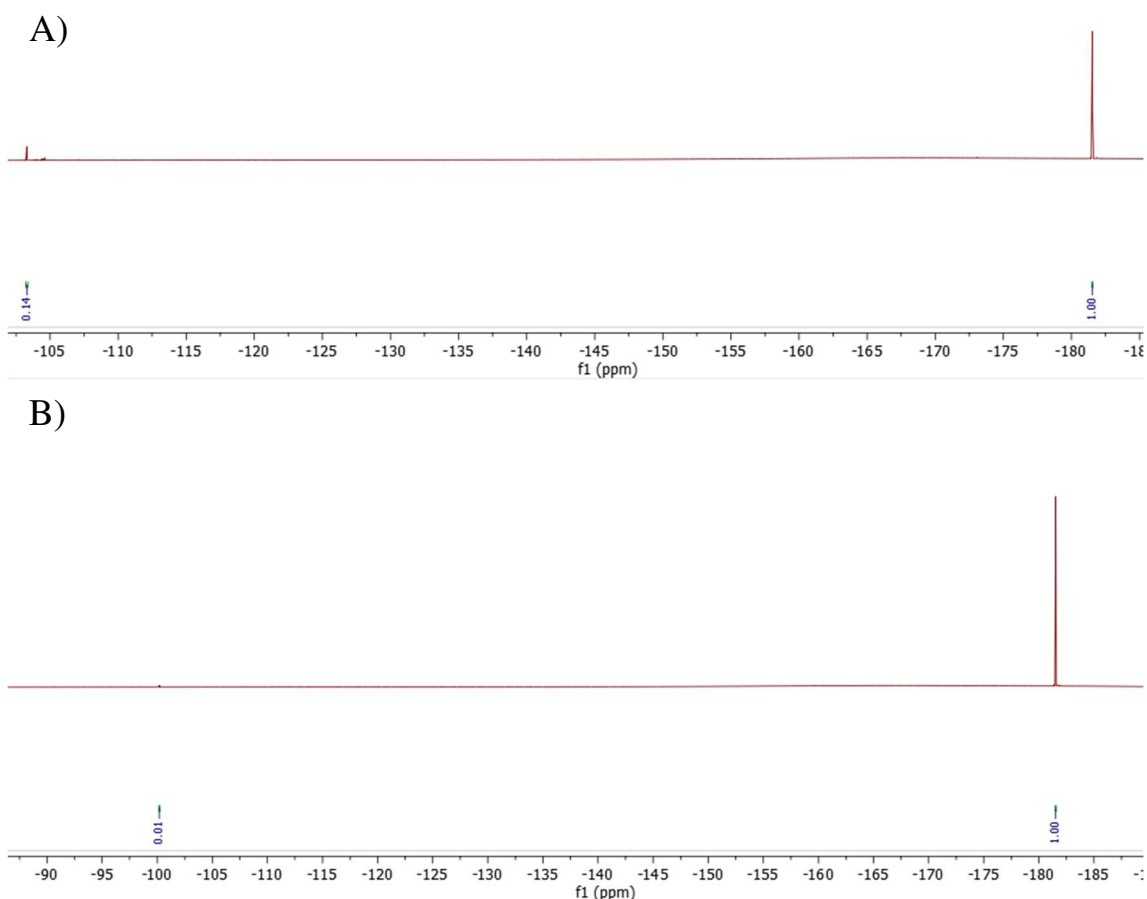


**Figure 3.22**  $^{19}\text{F}\{^1\text{H}\}$ -NMR of (*S*)-**226** (-181 ppm) synthesised from the optimised Lindsley protocol : **A**) Before purification showing 12% of **227** (-103 ppm) ; **B**) After Purification showing 1% of **227** (-103 ppm).

Overall the reactivity and enantioselectivity obtained was lower compared to that reported by Lindsley *et al.*<sup>119</sup> This lower reactivity could be linked to the impact of the electron attracting inductive effect of the benzyl ester, which lowers the nucleophilicity of the carbon  $\alpha$  to the aldehyde resulting in a lower activity (Figure 3.23). This is also exacerbated by the steric impact of the benzyl group impacting the approach of NFSI to the enamine moiety of the aldehyde reacting with the MacMillan catalyst (Figure 3.23).

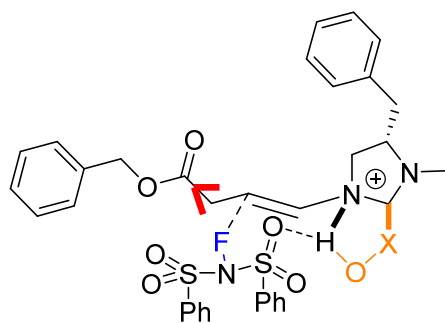


**Figure 3.23** Representation of the transition state between the enamine formed from the (*S*)-**Cat** and aldehyde **225**, and NFSI **62**. This image highlights the withdrawing inductive effect (red arrow) decreasing the nucleophilic property of the enamine.

The benzyl group represented a promising motif in the original strategy due the ease of deprotection by hydrogenation.

To increase the diastereoselectivity after purification, chiral benzyl amines were explored instead of dibenzyl amines to afford diastereoisomers product and increase the possibility of a better separation by column chromatography. For this new reductive amination strategy, the amines used were (*R*)-1-phenylethan-1-amine **230**, (*R*)-1-(naphthalen-2-yl)ethan-1-amine **231** and (*R*)-*N*-benzyl-1-phenylethan-1-amine **232** (Figure 3.24).

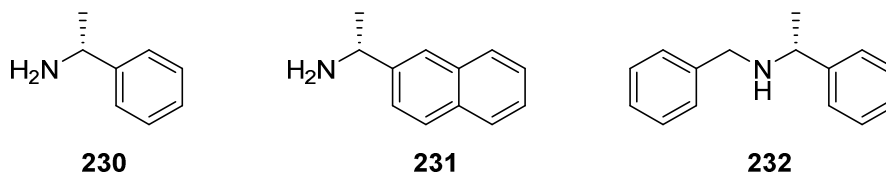
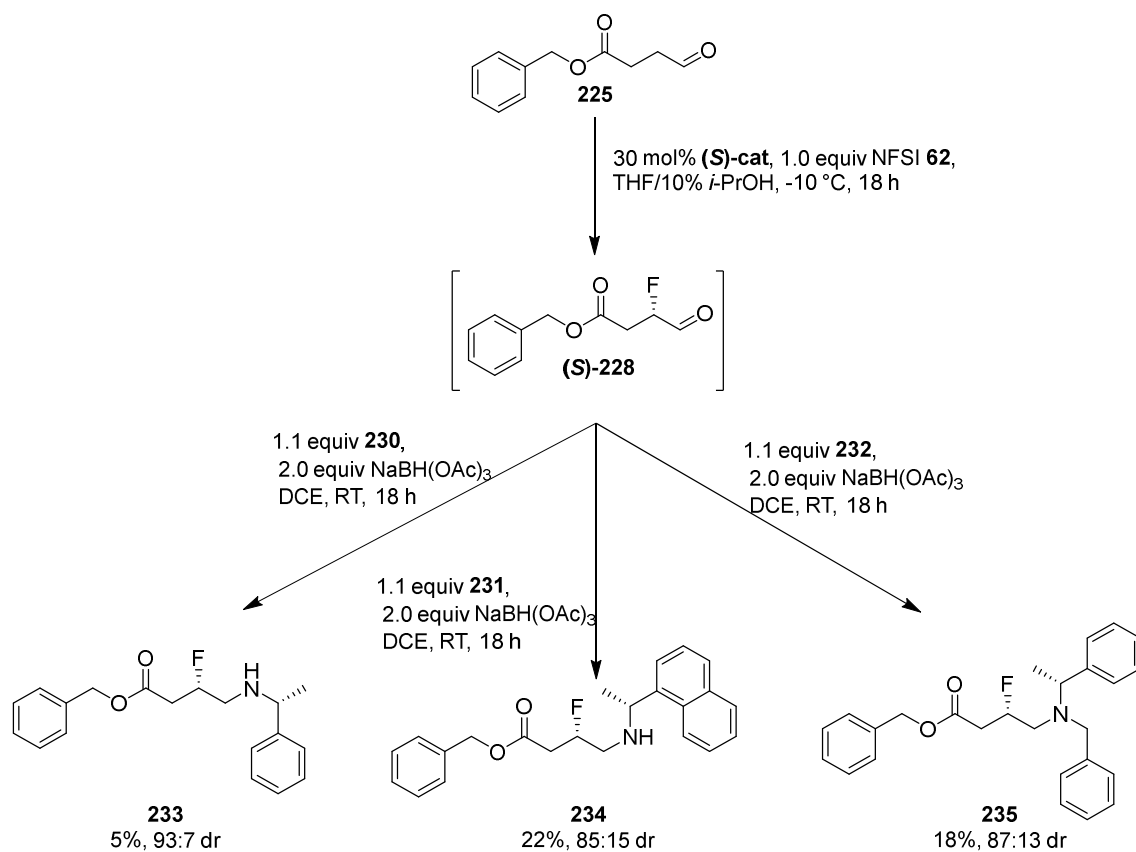


**Figure 3.24** Amines used for the synthesis of diastereoisomers **230**, **231** and **232**.

These three amines afforded the final products **233**, **234** and **235** (Scheme 3.8).



**Scheme 3.8** Synthesis of diastereoisomers **233**, **234** and **235**, using the optimised Lindsley protocol established Section **2.3**.

Product **233** was obtained in 5% yield, 93:7 dr, and 1% of the difluoro product. Product **234** was obtained with 22% yield, 85:15 dr, and 10% of the difluoro product. Finally, **235** was obtained with 18% yield, 87:13 dr, and <1% difluoroproduct. Of the three chiral amines the compound representing the best compromise is compound **235** (Table 3.1).

**Table 3.1** Comparison of CF<sub>2</sub> contamination, de and yield of diastereoisomers **233**, **234** and **235** synthesised with optimised Lindsley protocol.

Compounds	CF <sub>2</sub> (%)	dr	Yield (%)
<b>233</b>	1	93:7	5
<b>234</b>	10	85:15	22
<b>235</b>	<1	87:13	18

### 3.4. Conclusion

In this chapter we overviewed the importance of GABA and its analogues towards the treatment of many neurological diseases, was reviewed. The synthesis of the 3-fluoro analogue of GABA has been of interest, notably due to the impact of fluorine, in pharmaceutical studies. After an initial non-stereoselective synthesis of 3-F-GABA, the O'Hagan lab developed a seven step enantioselective synthesis of both enantiomers of 3-F-GABA, **16** and **17**, with an overall yield of 23% but with good stereoselectivity of 98% ee. This project explored a more efficient synthetic approach using the  $\alpha$ -fluorination of aldehydes, followed by a reductive amination, to develop a three step strategy. The methodology provided an increase in the overall yield of up to 46% however, the stereoselectivity dropped significantly. Attempts to introduced chiral amines instead of dibenzyl amines were trialled to improve the stereoselectivity through generating diastereoisomers, for chromatography purification. These chiral amines helped to increase the stereoselectivity in some cases but there was a decrease in the overall yield. Despite this, the benefits of the Lindsley protocol toward the synthesis of fluoro bioactives were successfully demonstrated.

## Chapter IV      **Selective fluorination of calcium sensing receptor (CaSR) agonists**

### **4.1. Extracellular calcium sensing receptors (CaSR)**

Calcium sensing receptors are G-coupled protein receptors, a class of receptors first reported in 1980<sup>172-175</sup> and their existence was confirmed in 1993 with the cloning of CaSR from bovine parathyroid.<sup>176</sup> CaSRs play a role in the regulation of the concentration of Ca<sup>2+</sup> in blood and other extracellular fluids.<sup>177</sup>

CaSRs are mainly present in the high quantities in the parathyroid glands,<sup>178</sup> kidney,<sup>179</sup> pancreas,<sup>180</sup> and duodenum<sup>181</sup> but they can be found in lower levels in other organs and tissues of the human body such as brain,<sup>182</sup> digestive system,<sup>183</sup> stomach,<sup>184</sup> respiratory system<sup>185</sup> and renal tubules.<sup>186</sup> CaSRs control the concentration of Ca<sup>2+</sup> within extracellular fluids, usually between 1.2 to 1.4 mM.<sup>187</sup>

In the 1960s the correlation between the secretion of parathyroid hormone (PTH) and calcium was discovered.<sup>188,189</sup> Indeed, CaSRs regulate the production of PTH and the reabsorption of Ca<sup>2+</sup>. When the concentration of Ca<sup>2+</sup> rises, it enhances the CaSR mediated suppression of PTH synthesis. Also when the secretion of PTH decreases the reabsorption of Ca<sup>2+</sup> from bones and the renal ascending limb increases.<sup>190</sup> Within the kidney the process is slightly different as it does not rely on the action of PTH secretion, instead it relies on an over-concentration of Ca<sup>2+</sup>. This leads to a decrease in Ca<sup>2+</sup> reabsorption.<sup>190</sup> In the thyroid an increase of the Ca<sup>2+</sup> concentration stimulates the release of calcitonin *via* the action of the CaSR, leading to the absorption of Ca<sup>2+</sup> in bones.<sup>191</sup>

The CaSRs have many other impacts excluding calciotropic functions. For example, Ohsu *et al.* studied the impact of CaSR agonist ( $\gamma$ -glutamyl peptides and Ca<sup>2+</sup>) on the CaSRs of the taste cells surface and discovered that it was stimulating an appetite reaction, that could be linked to the action of the agonist binding to the receptor and transferring a response to the CNS.<sup>192</sup> In 2017, Babinsky *et al.* reported that CaSRs in the pancreas help maintain blood glucose levels by the contribution of glucose-mediated insulin secretion.<sup>193</sup> Another example reviewing treatments of asthma, showed that CaSRs within the lungs mediate airway defense as airways contract or succumb to inflammation, thanks to the detection of local polyamine fluctuations.<sup>194</sup>

The structure of the CaSR protein is complex (Figure 4.1) but conforms to the general structure of a G-protein coupled receptor. It is encoded by seven exons expressed as a polypeptide containing 1078 amino acids.<sup>195</sup> The extracellular domain (ECD) is encoded by exons 2-6. The transmembrane domain (TMD) is expressed by exon 7.<sup>196,197</sup> The ECD is composed of two lobes (LB1 and LB2) that open or close around the ligand binding cleft. LB1 and LB2 are connected to the TMD through a cysteine-rich domain (CR).<sup>198</sup>

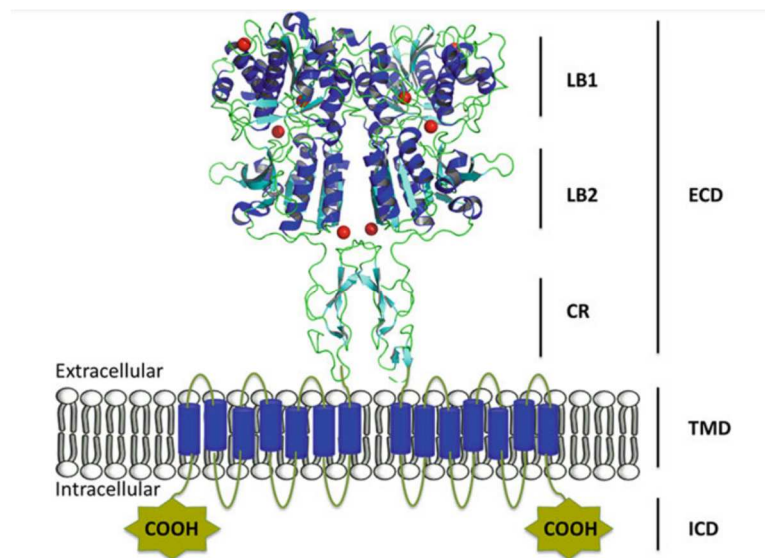


**Figure 4.1** Structure of CaSR with crystal structure of ECD, LB1, LB2,CR and representation of TMD and ICD.<sup>199</sup>

CaSRs responds to many stimuli other than  $\text{Ca}^{2+}$ . Indeed, other ligands can bind to the receptors due to multiple active sites associated with the ECD part of the receptor, as summarised in Figure 4.2.<sup>200</sup>



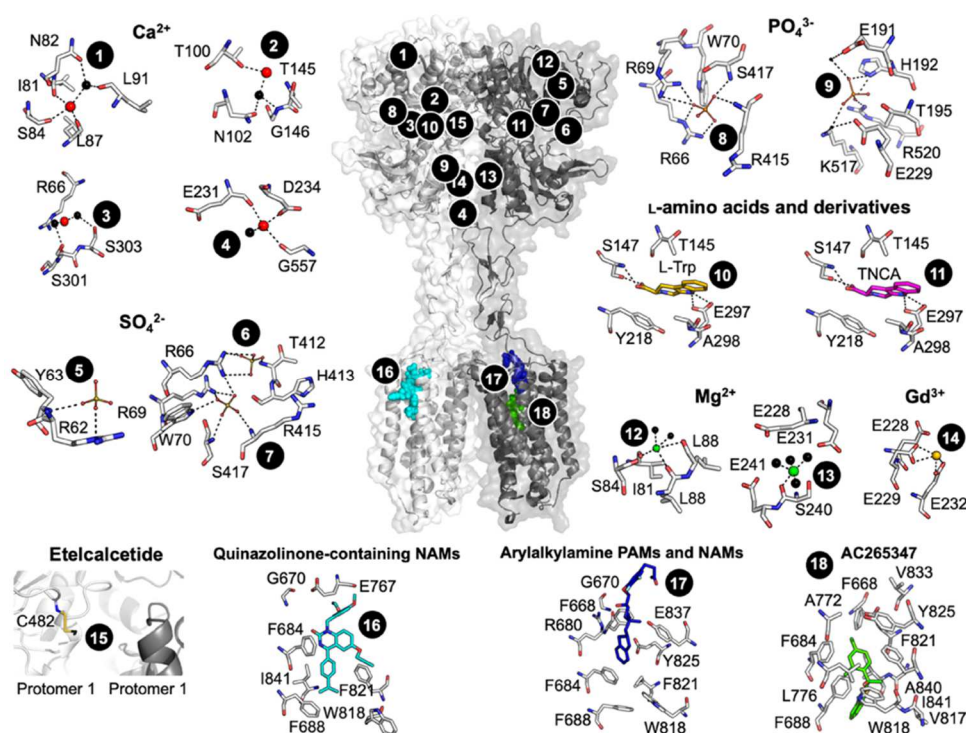


**Figure 4.2** Crystal structure of CaSR with the various binding sites for modulators.<sup>200</sup>

The compounds that can bind to a CaSR are divided into two groups. Type I are termed ‘orthosteric modulators’. They bind to one of the active pockets of the receptor situated within the LB1 and LB2 domains, and they respond to the direct action of the receptors as they are categorised as competitors of  $\text{Ca}^{2+}$ .<sup>197,198,201</sup> Type II are termed ‘allosteric modulators’, and they bind to the TMD.<sup>202</sup> The binding of an allosteric modulator to the receptor enhances a structural modification of the receptor resulting in stabilisation of the receptor into either an active or inactive state (Figure 4.3).<sup>197</sup>

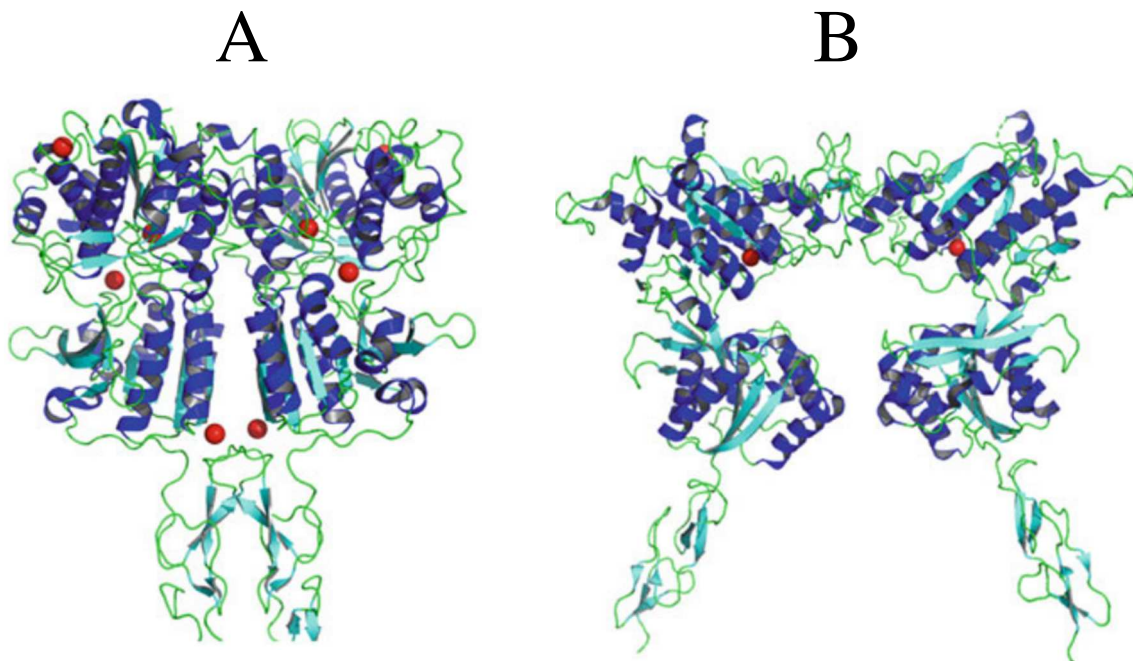


**Figure 4.3** Crystal structure of : **A)** the active conformation ; **B)** the inactive conformation of CaSR.

Mutation of CaSR can enhance a dysregulation of the  $\text{Ca}^{2+}$  balance with the body resulting in hyper- or hypo-calcaemia responsible for several diseases such as hyperparathyroidism (HPT) and osteoporosis.<sup>203,204</sup> CaSR is then recognised as an attractive target for which to explore the development of new pharmaceuticals.

## 4.2. Calcium receptors agonists

### 4.2.1. Orthosteric ligands

As stated (Section 4.1.), orthosteric modulators are essentially direct competitors of  $\text{Ca}^{2+}$  as they bind to the same sites and can enhance the activation of  $\text{Ca}^{2+}$  on their own without  $\text{Ca}^{2+}$  being present. One group of this type of modulator are alternative inorganic cations that bind the  $\text{Ca}^{2+}$  pocket. Such potent cations are  $\text{Gd}^{3+}$ ,  $\text{Al}^{3+}$ ,  $\text{Mg}^{2+}$ ,  $\text{Sr}^{2+}$ ,  $\text{Pb}^{2+}$  and  $\text{Co}^{2+}$ .<sup>205–210</sup> These were assessed on bovine parathyroid cells, and correlations were determined between the charge of the cation and the atomic radius, toward the potency of the modulators. The potency was determined to be  $\text{Gd}^{3+} > \text{La}^{3+} > \text{Ca}^{2+} = \text{Ba}^{2+} > \text{Sr}^{2+} > \text{Mg}^{2+}$ .<sup>174</sup>

Another group of orthosteric modulators of CaSR are polyamines (Figure 4.4).<sup>211</sup> The principal effect of polyamines is to activate CaSR in the absence of  $\text{Ca}^{2+}$ , enhancing inhibition of PTH secretion.<sup>211, 212</sup> However, no binding site has been determined to be specifically associated with polyamine activity.<sup>213</sup> The first polyamines group that showed potency on CaSR, were amines separated by more than two carbons. Spermine **236** is active with an  $\text{EC}_{50} = 150 \mu\text{M}$ , but then spermidine **237** significantly less so ( $\text{EC}_{50} = 2 \text{ mM}$ ) and then cadaverine **238** and putrescine **239** were found to be inactive at concentrations up to 3mM. For this group, a correlation between the potency and the net positive charges of the bioactives is observed.<sup>211</sup>

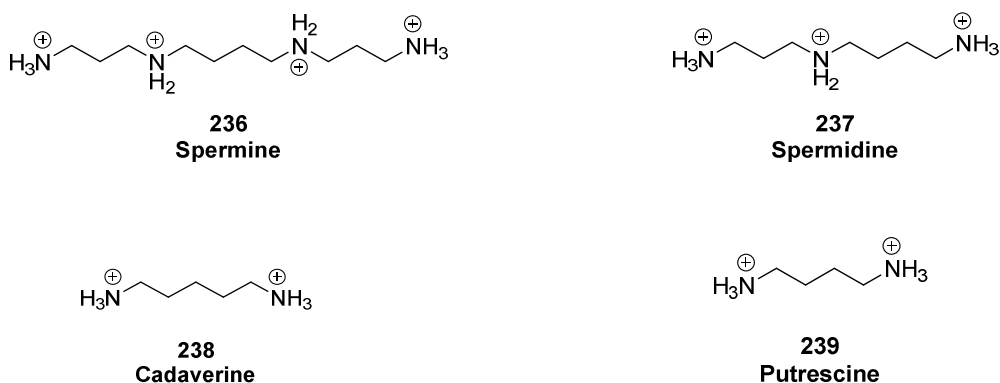


**Figure 4.4** Polyamines associated with CaSR.

Polyamines separated by two carbons were studied on the HEK-293 receptor (Figure 4.5). These polyamines included triethylenetetramine **240** ( $EC_{50} = 8 \text{ mM}$ ), tetraethylenepentamine **241** ( $EC_{50} = 2.5 \text{ mM}$ ) and pentaethylenehexamine **242** ( $EC_{50} = 600 \text{ }\mu\text{M}$ ). Here we can observe that despite the increase in net positive charge the three polyamines are less potent than spermine. With the heterocycle hexacyclen **243** ( $EC_{50} = 20 \text{ }\mu\text{M}$ ) the potency increased about 30 times relative to **7** and 7.5 times compared to spermine **236**.<sup>211</sup>

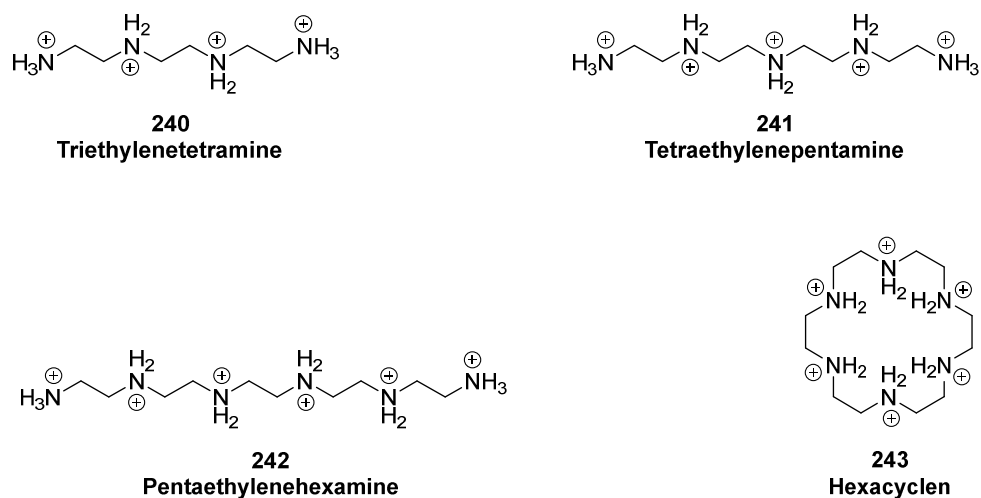


**Figure 4.5** Structure of  $C_2$  spaced polyamines which act as CaSR agonists.

This difference in potency gives an insight into the conformation of the active site where the polyamines interact. Indeed, the net positive charge does not seem to be as important as charge density, and the size of the modulator to the resulting potency of the bioactives.

Finally, another group of orthosteric modulators are the family of aminoglycoside antibiotics (Figure 4.6) which have proven to be active on CaSR. Once again it was determined that the potency depended on the net charge of the modulators. Neomycin B **244** ( $EC_{50} = 20 \text{ }\mu\text{M}$ ) is more potent than gentamicin **245** ( $EC_{50} = 150 \text{ }\mu\text{M}$ ) and bekanamycin **246** ( $EC_{50} = 200 \text{ }\mu\text{M}$ ), which are also more potent than streptomycin **247** ( $EC_{50} = 600 \text{ }\mu\text{M}$ ). However, these antibiotics have shown some toxicity as they inhibit ribosomal protein synthesis while binding to the A-site on 16S ribosomal RNA leading

to the assembly of polypeptides that can enhance cell membrane damage when they are released.<sup>214,215</sup>

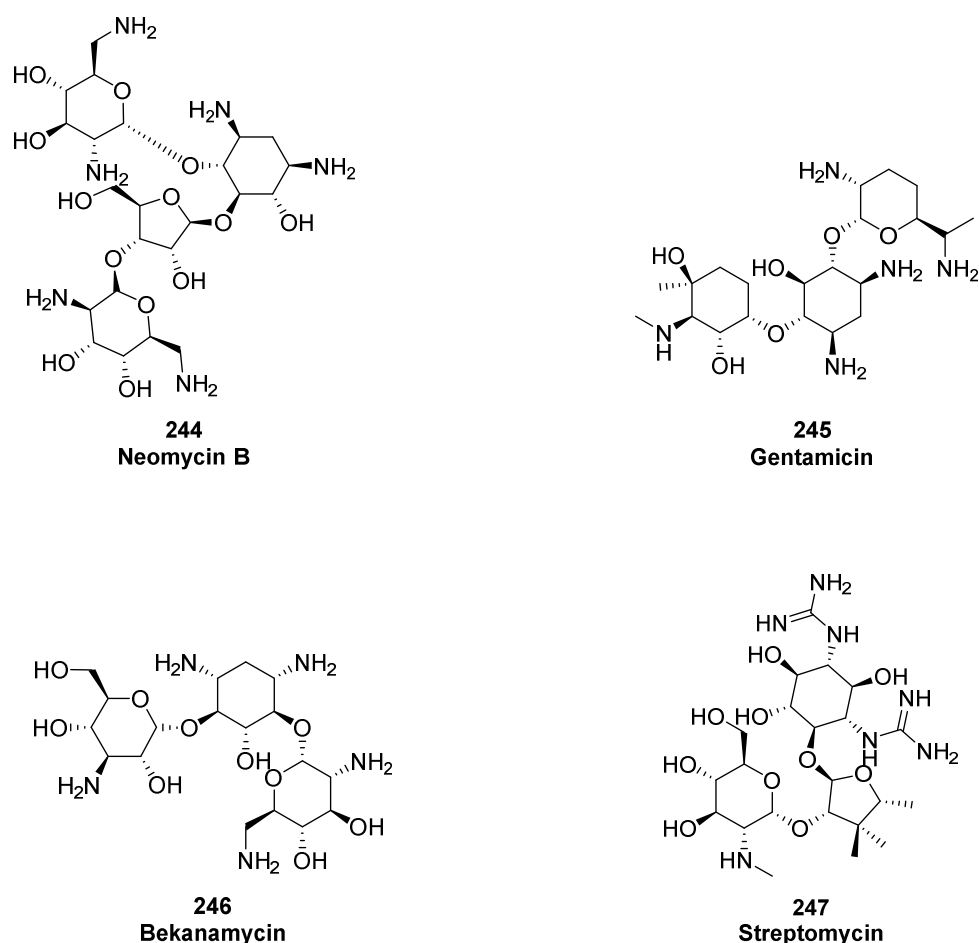


**Figure 4.6** Structures of aminoglycoside antibiotics which act as CaSR agonists.

#### 4.2.2. Allosteric modulators of CaSR

As stated, Type II modulators, or allosteric modulators, bind to the TMD region of the CaSR (Figure 4.2) affecting the conformational equilibrium of the receptor. The modulation of the CaSR structure can be either to the active or inactive state of the receptor (Figure 4.3).<sup>197,200</sup> These allosteric modulators are classified into either positive (PAM) or negative allosteric modulators (NAM) depending on whether they activate or deactivate the receptor.<sup>200</sup>

The first PAMs discovered were the endogenous amino acids, L-tryptophan **248**, L-phenylalanine **216**, L-alanine **249**, L-glutamine **250**, L-arginine **251**, L-leucine **252** and

L-histidine **253**.<sup>216-218</sup> The action of these amino acids increases the sensitivity of the CaSR to inorganic orthosteric modulators enhancing an increase of PTH inhibition. A correlation was observed between an increase in amino acid concentration and secretion inhibition of PTH. This revealed a physiological regulation between PTH synthesis and CaSR activation.<sup>218</sup>

The potencies of the amino acids in CaSR (fura-2IAM-loaded normal human parathyroids cells) are listed in Table 4.1.<sup>216,218</sup> The most potent amino acids are the aromatics one following the order L-Trp **248** > L-Phe **216** > L-His **253** > L-Ala **249** > L-Glu **250** > L-Arg **251** > L-Leu **252** (Table 4.1).

**Table 4.1** EC<sub>50</sub> of potent endogenous amino acids on CaSR fura-2IAM-loaded normal human parathyroid cells.<sup>216,218</sup>

Aminoacids	EC <sub>50</sub> (μM)
<b>L-Trp 248</b>	40
<b>L-Phe 216</b>	60
<b>L-His 253</b>	100
<b>L-Ala 249</b>	410
<b>L-Glu 250</b>	710
<b>L-Arg 251</b>	2700
<b>L-Leu 252</b>	1400

In the same year (2004) the impact of pH on the activity of CaSR was reported. The increase of activity was proposed to be due to protonation of the amines interacting within the active site of the receptor with the negatively charged glutamate and aspartate side chains.<sup>219,220</sup> The net positive charge of inorganic and organic agonists can clearly be influenced by external pH conditions, with more acidic media resulting in an increase of the activity.<sup>219</sup>

The second group of PAMs are phenylalkyl amines. These compounds are known as calcimimetics because they were initially recognized for their ability to inhibit PTH secretion as Ca<sup>2+</sup>, before their mode of action as agonists was fully understood.<sup>221,222</sup> The development of the first calcimimetics was carried out in NPS Pharmaceutical Inc., which started from the study of fendiline **254** (Figure 4.7).<sup>223</sup>

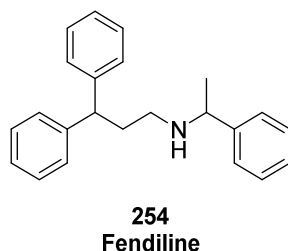


**Figure 4.7** The first PAM, fendiline **254** developed by NPS Pharmaceutical Inc.

Fendiline was first selected due to early knowledge of its activity toward calcium channel receptors<sup>224</sup> and its good balance between ADME and toxicity on bovine parathyroid cells. It had good potency ( $EC_{50} = 15 \mu\text{M}$ ) compared to the other 200 compounds tested over the same screening.<sup>223</sup> Continuing investigations involved the preparation of derivatives which improved understanding of CaSR binding and better modulators emerged. This led to the development of NPS 459 **255** with a higher  $EC_{50} = 30 \mu\text{M}$ .<sup>223</sup> The impact of the substituent on the phenyl amine moiety of fendiline **254** and NPS 459 **255** was then studied, and this resulted in NPS 551 **256** and NPS 467 **257** (Figure 4.8).

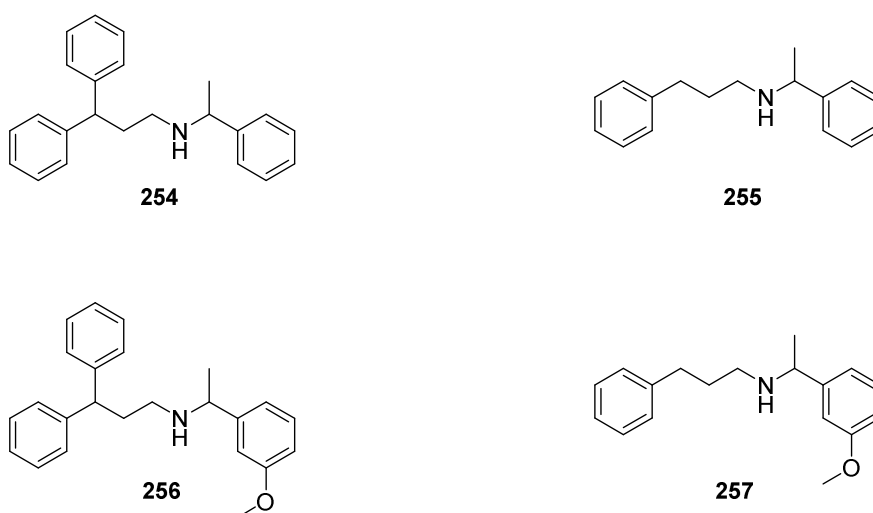


**Figure 4.8** Structures of the first generation PAMs.

An increase in potency was observed with a *meta*-methoxy group ( $EC_{50} = 3.4 \mu\text{M}$  for **256** and  $EC_{50} = 4.1 \mu\text{M}$  for **257**) and there was an observed impact in the potency of individual

enantiomers with a better potency for (*R*)-NPS R-467 **258** ( $EC_{50} = 2.7 \mu\text{M}$ ) (Figure 4.9).<sup>223</sup>

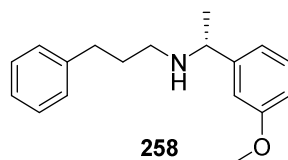


**Figure 4.9**

(*R*)-NPS R-467 **258**.

Modification of the other aryl group with the introduction of an *ortho*-chlorine resulted in NPS R-568 **259** (also called tecalcet, Figure 4.10), which had a better potency ( $EC_{50} = 0.75 \mu\text{M}$ ) than **258**.<sup>223</sup>

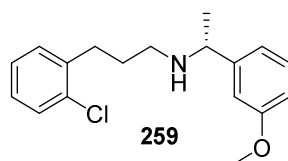


**Figure 4.10**

(*R*)-NPS R-568 **259**.

After an assay of **258** and **259** on mice and rats, NPS R-467 **258** and NPS R-568 **259** were found to be orally active, with NPS R-568 **259** having greater potency compared to NPS R-467 **258**.<sup>223</sup> Exploration of new derivatives of **258** and **259** involved the introduction of amines such as (*R*)-naphthylethylamine in compounds such as NPS 646 **260** ( $EC_{50} = 0.11 \mu\text{M}$ ).<sup>223</sup> Introduction of a trifluoromethyl group in the case of NPS 1440 **261** ( $EC_{50} = 0.32 \mu\text{M}$ ) (Figure 4.11) also led to good drugs. Compounds **260** and **261** both have better potency than **259**.<sup>223</sup>





**Figure 4.11** NPS 646 **260** and NPS 1440 **261**

The combined structure activity profiling of (*R*)-naphthylethylamine and the trifluoro methyl group led to NPS R-1493 **262** (Figure 4.12), more widely known as known as cinacalcet **262**, which resulted in the most potent ( $EC_{50} = 0.049 \mu\text{M}$ ) agonist to date.<sup>223</sup>

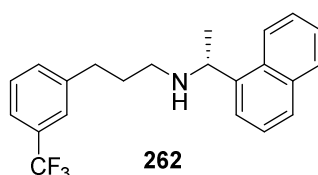


**Figure 4.12** NPS R-1493 (cinacalcet) **262**.

Cinacalcet **262** was approved by the FDA in 2004 for the treatment of hyperparathyroidism and parathyroid carcinoma.<sup>225,226–229</sup> In 2021, Angem reported sales of cinacalcet (Sensipar®/Mimpara™) representing \$84 million.<sup>230</sup>

On the other hand, there are the calcytics modulators NAMs, which stimulate the secretion of PTH and are antagonists of CaSR, unlike cinacalcet **262**. Calcytics modulators were first investigated for the treatment of osteoporosis and pulmonary diseases.<sup>231–239</sup> Their binding sites are situated in the same region as the calcimimetics binding site (TMD, Figure 4.2).<sup>196,202,240,241</sup> Due to a poor understanding of the structure of TMD it is difficult to differentiate the binding sites. One of the first NAMs developed, also by NPS Pharmaceutical Inc., was NPS 2143 **263** (Figure 4.13).<sup>233</sup>

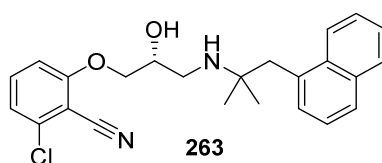


**Figure 4.13**

NPS 2143 **263**.

Compound **263** has a similar core structure to the NPSs PAMs.<sup>202,241</sup> The emergence of **263** led to the development of other NAMs such as ronacaleret **264** and JTT305 **265** (Figure 4.14).<sup>242,243</sup>

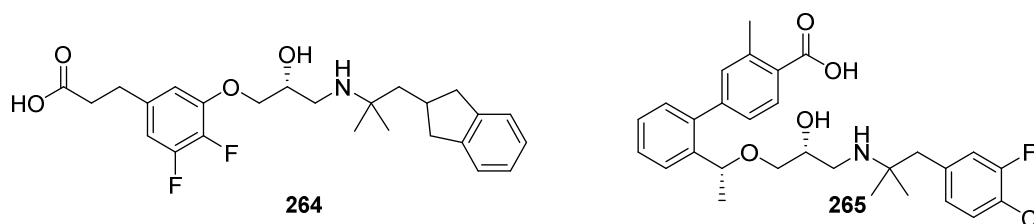


**Figure 4.14**

Representative NAMs, ronacalceret **264** and JTT305 **265**.

Novartis also contributed to the development of NAMs after screening quinazolinone containing bioactives ATF936 **266** and AXT914 **267** (Figure 4.15). ATF936 **266** emerged as the best NAM compared to AXT914 **267** and the original NPS 2143 **263**.<sup>202</sup> Compound **267** again helped an understanding of structure activity relationships towards the development of new NAMs.

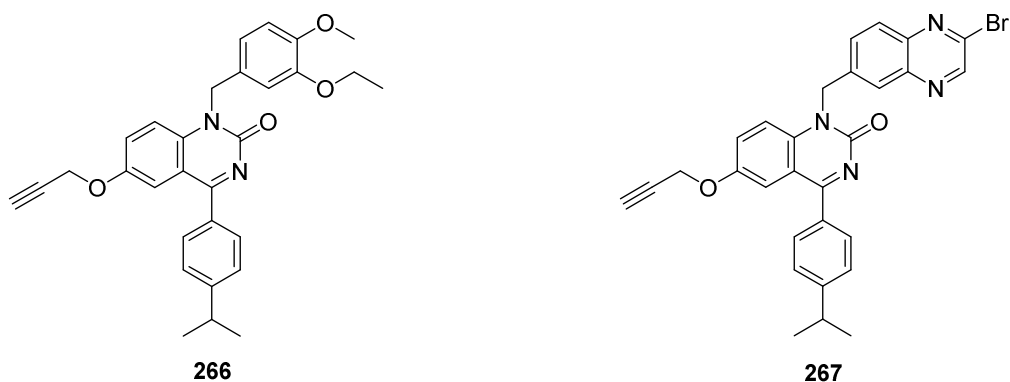


**Figure 4.15** ATF936 **266** and AXT 914 **267** developed by Novartis.

Another interesting allosteric modulator is calhex 231 **268** which has been described both as a PAM and a NAM.<sup>244</sup> Calhex 231 **268** (Figure 4.16) appears to bind the cinacalcet **262** and NPS 2143 **263** binding sites and others PAM/NAM binding sites.<sup>245,246</sup>

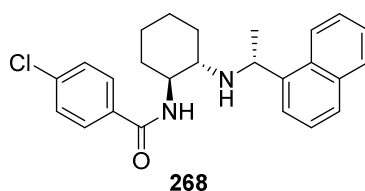


**Figure 4.16** Allosteric modulator calhex 231 **268**.

The ability of **268** to accommodate both binding sites might be explained by the cyclohexane moiety providing flexibility to the structure such that it can adapt two relevant binding conformations.<sup>247</sup>

### 4.3. Development of F-cinacalcet and other fluoro allosteric modulators

#### 4.3.1 F-Cinacalcet<sup>248</sup>

As discussed (4.2.2.), a full crystal structure of the binding sites of allosteric modulators of CaR is unknown (TMD, Figure 4.1-4.2) and thus their mode of binding, of these flexible molecules is not clear.<sup>196,202,233,240,241</sup> The introduction of fluorine offers a useful tool for probing conformation and in particular we wished to exploit the electrostatic *gauche* effect to influence conformation.

In a preliminary study Chai *et al.* (O'Hagan Lab), in 2012, explored the influence of fluorine  $\beta$  to the amine and in a mid-chain position of cinacalcet **262**. To achieve this a first generation synthesis of fluorocinacalcets diastereoisomers **269** and cinacalcet analogue **270** (Figure 4.17) was developed.

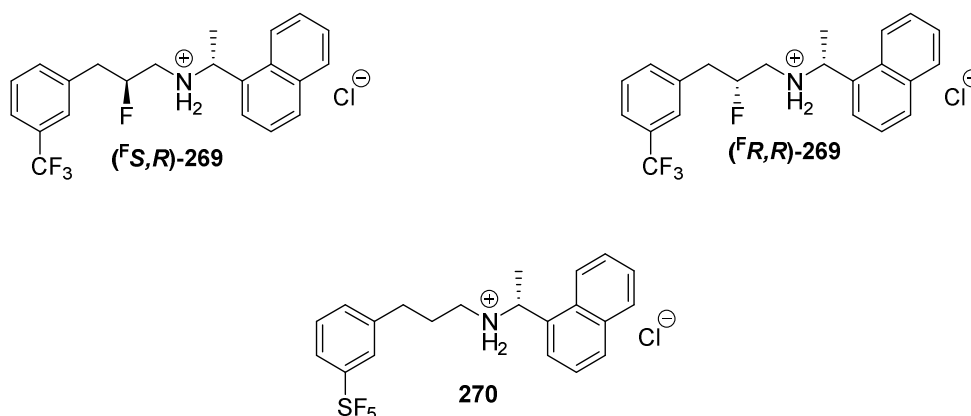
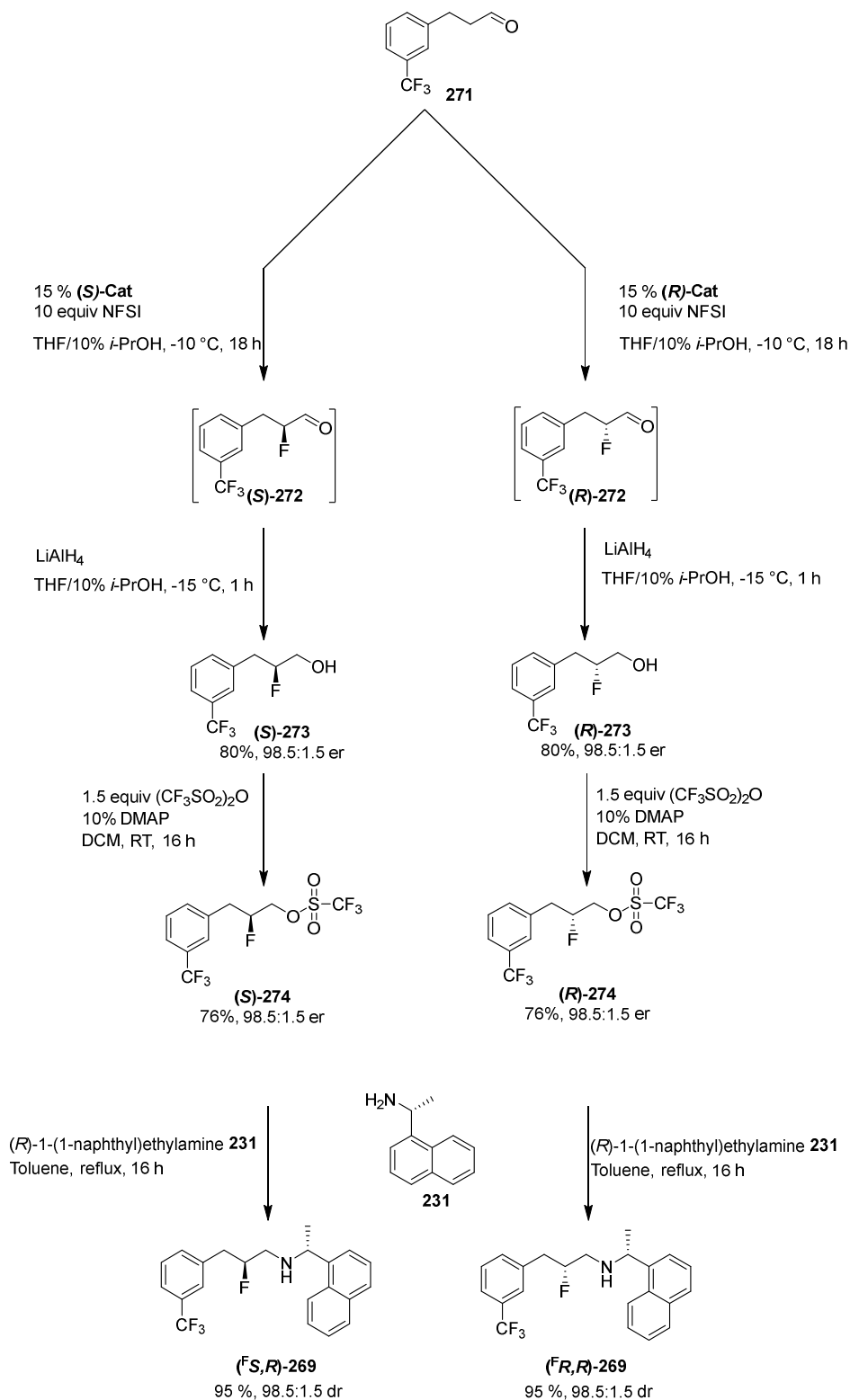


**Figure 4.17** Fluoro-cinacalcet stereoisomers (F<sup>S</sup>,R)-**269** and (F<sup>R</sup>,R)-**269**, and SF<sub>5</sub>-cinacalcet **270**.<sup>248</sup>

The synthesis involved four steps (Scheme 4.1). 3-(Trifluoromethyl)phenyl propanal **271** was fluorinated with an organocatalytic MacMillan  $\alpha$ -fluorination protocol to afford (S)/(R)-**272**. The product aldehyde was reduced to the corresponding  $\beta$ -fluoro alcohol (S)/(R)-**273** with LiAlH<sub>4</sub> in the same reaction media. The alcohol (S)/(R)-**273** was then activated with trifluoromethanesulfonyl, to afford (S)/(R)-**274**, before nucleophilic substitution with (R)-naphthylethylamine **231** to afford the (F<sup>S</sup>,R)-F-cinacalcet (F<sup>S</sup>,R)-**269** with an overall yield of 47% and a stereoselectivity of 98.5:1.5 dr. The synthesis of

the diastereoisomer was obtained following the same methodology to afford (<sup>F</sup>*R,R*)-F-cinacalcet (<sup>F</sup>*R,R*)-**269** with an overall yield of 58% and a stereoselectivity of 98.5:1.5 dr.



**Scheme 4.1** First route to (<sup>F</sup>*S,R*)-F-cinacalcet (<sup>F</sup>*S,R*)-**269** and (<sup>F</sup>*R,R*)-F-cinacalcet (<sup>F</sup>*R,R*)-**269** developed by Chai *et al.*<sup>248</sup>

An X-ray crystal structure analysis was carried out on the chloride salts ( $^F S, R$ )-**276** obtain from ( $^F S, R$ )-**269**, to confirm the relative and absolute configuration. This also revealed the *gauche* alignment of the vicinal C-F and C-N<sup>+</sup> bonds stabilised as a consequence of the electrostatic *gauche* effect between fluorine and the ammonium groups. The structure also indicated a preference for an extended alkyl chain, similar to the original cinacalcet structure (Figure 4.18).

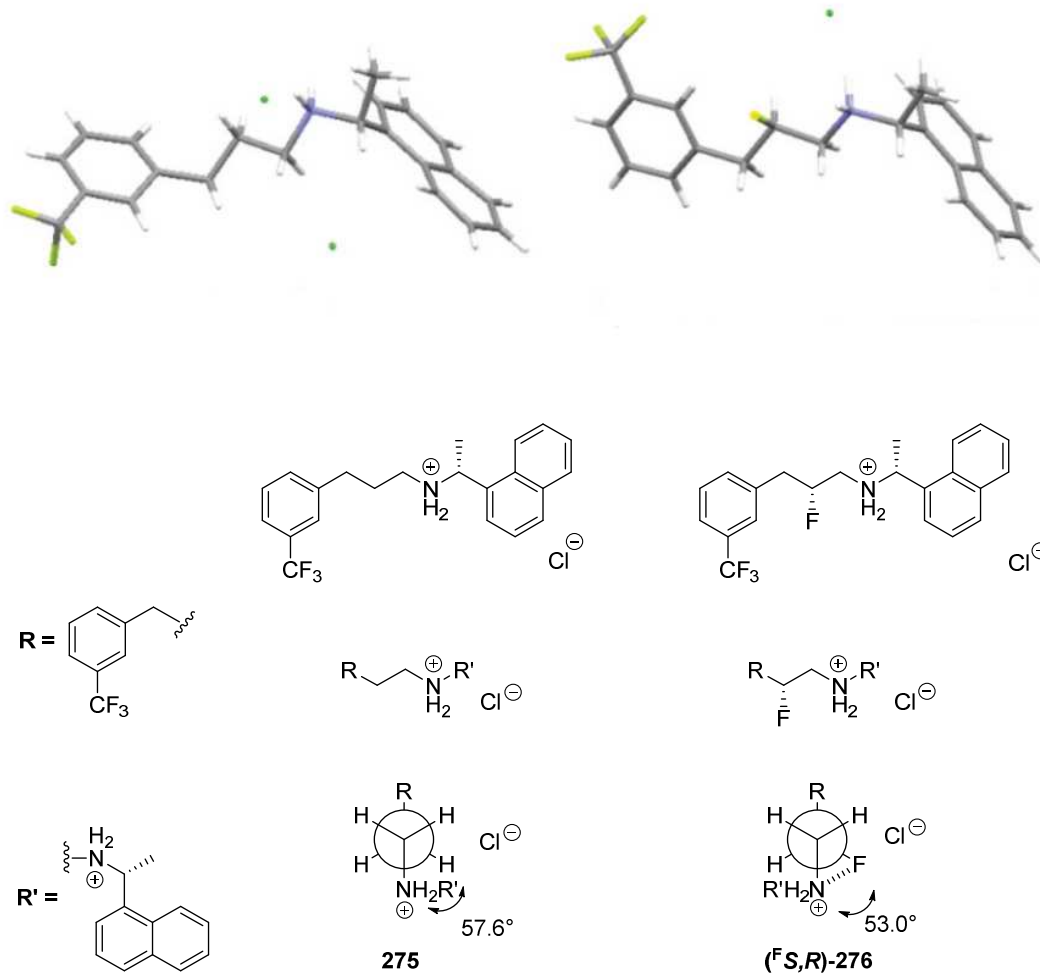
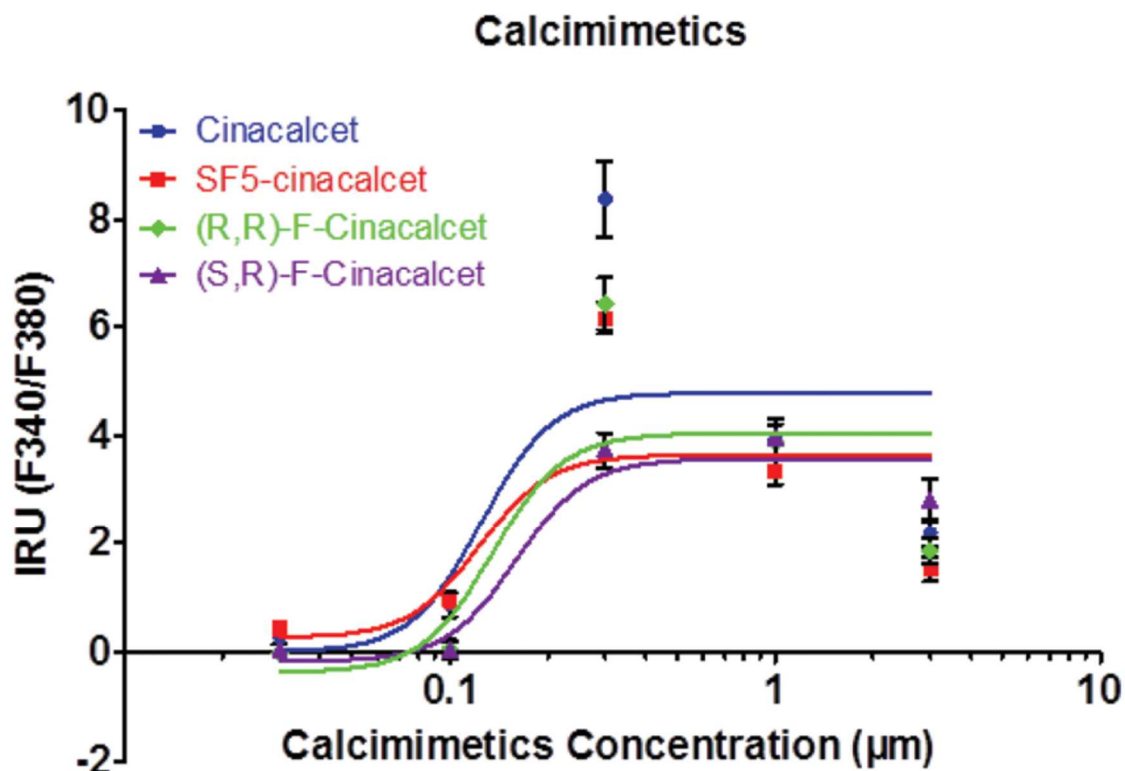


**Figure 4.18** Similarity of the X-ray structure of chloride salt of cinacalcet **275** and fluorinated stereoisomer ( $^F S, R$ )-**276**.<sup>248</sup>

Both diastereoisomers chloride salts ( $(^F S,R)$ -276,  $(^F R,R)$ -276) were assayed against HEK-293 cells, which express human CaSR. The graph in Figure 20 displays the results from that assay, where the integration of the dose response curve and the Hill integration led to the determination of EC<sub>50</sub> values (Figure 4.19).



CaSR agonists	Cinacalcet 275	$(^F S,R)$ -F-Cinacalcet $(^F S,R)$ -276	$(^F R,R)$ -F-Cinacalcet $(^F R,R)$ -276
EC <sub>50</sub> (µM)	0.125	0.135	0.160

**Figure 4.19** Dose response curves of calcimimetics tested and their resultant EC<sub>50</sub> calculated by Chai *et al.*<sup>248</sup>

The Table in Figure 4.19 shows that the two diastereoisomeric salts  $(^F S,R)$ -276 and  $(^F R,R)$ -276 were found to be less potent than the original cinacalcet salt 275 (in the range of 20-25%). This may be due to a reduction of the pK<sub>a</sub> of the amine as a consequence of the electronegative fluorine or perhaps the fluorine having a negative impact on binding. Both diastereoisomers appeared to interact with the CaSR similarly, suggesting that a particular extended conformation is stabilised as indicated also by X-ray structure analysis (Figure 4.20).

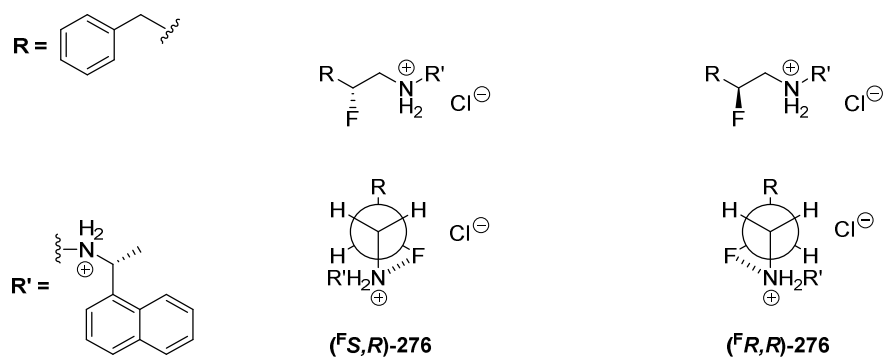


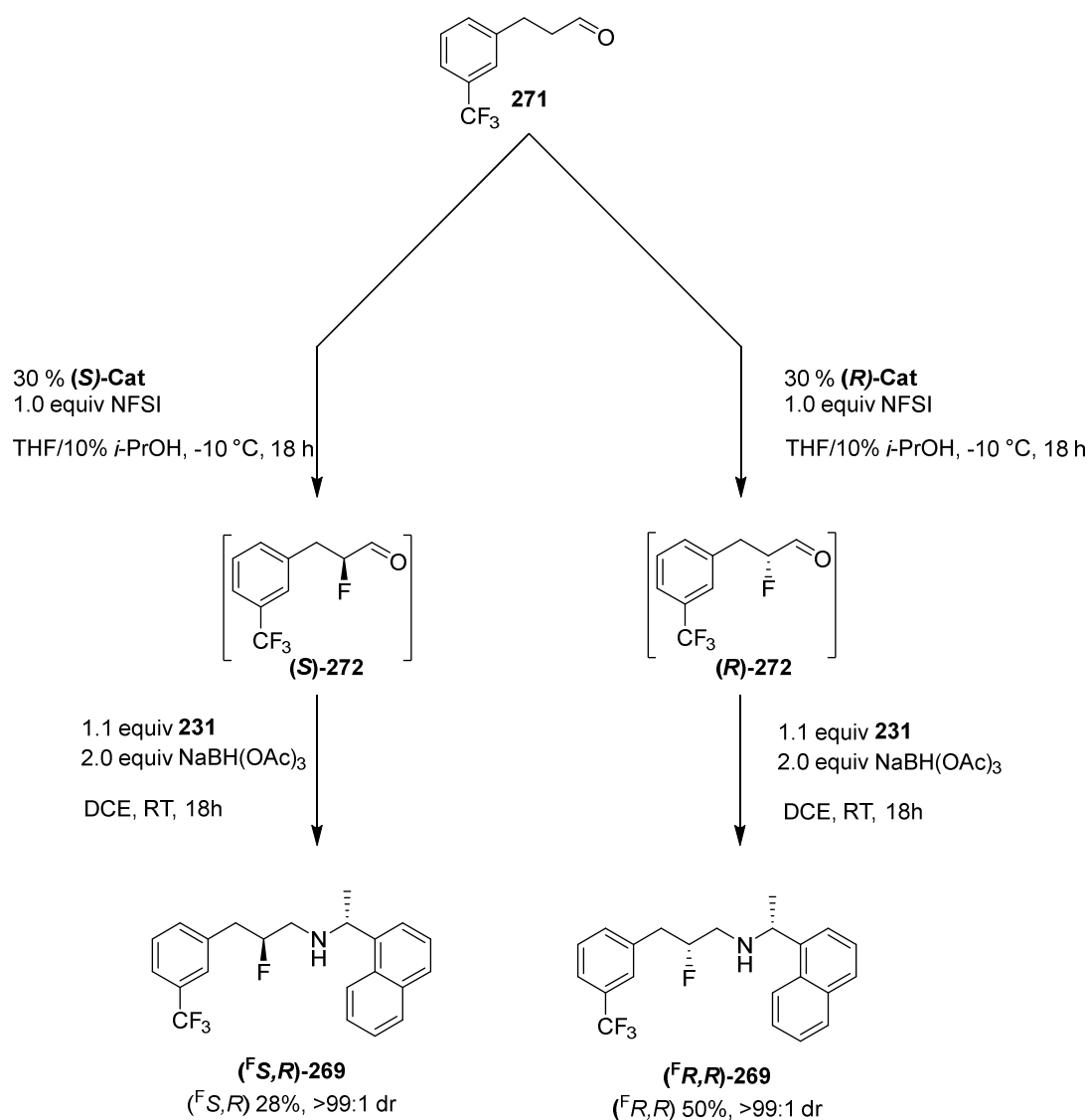
**Figure 4.20** Favoured extended F-cinacalcet conformation illustrated from a Newman perspective.

The similar activity of (<sup>F</sup>*S,R*)-276 and (<sup>F</sup>*R,R*)-276 on CaSR, helped to provide a better understanding of the binding conformation. This strategy was now extended in this project to explore selectively fluorinated analogues of other allosteric modulators such as fendiline **254**, tecalcet **259** and NPS R-467 **258**. To that end a more efficient synthesis was envisaged involving a reductive amination after asymmetric fluorination of an appropriate aldehyde to generate products in a two-step-one-pot protocol.

#### 4.3.2 Synthesis of F-cinacalcet analogues adapting the Lindsley protocol

The project explored the efficiency of the method first developed by Lindsley *et al.*,<sup>119</sup> and optimised in Section 2.3. to afford β-fluoro-arylamines directly. This involved the asymmetric fluorination of aldehydes followed by their reductive amination using sodium triacetoxyborohydride. In this project the approach was applied in the first instance to a synthesis of the F-cinacalcet diastereoisomers (<sup>F</sup>*S,R*)-269 and (<sup>F</sup>*R,R*)-269 (Scheme 4.2).





**Scheme 4.2** Synthetic pathway starting from phenylpropanal **271** and using (*R*)-naphthylethylamine **231** to afford F-cinacalcets (<sup>F</sup>*S*,*R*)-**269** and (<sup>F</sup>*R*,*R*)-**269**.

Here the synthesis started from 3-(trifluoromethyl)phenyl propanal **271**. Accordingly aldehyde **271** was fluorinated using MacMillan catalyst (**S**)-**Cat** (for the synthesis of (<sup>F</sup>*S*,*R*)-**269**) and (**R**)-**Cat** (for the synthesis of (<sup>F</sup>*R*,*R*)-**269**), with NFSI (slowly added over 30 min, 1.2 g·h<sup>-1</sup>) as the electrophilic fluorination reagent. Such reactions tended to be slow and were generally conducted at -10°C overnight. After a quick work up, due to the instability of the α-fluoroaldehyde, the crude product solution was combined with (*R*)-naphthylethylamine **231** followed by the addition of sodium triacetoxy borohydride. The reactions were generally allowed to stir overnight at room temperature and were quenched with saturated NaHCO<sub>3</sub>. Work up afforded the product (<sup>F</sup>*S*,*R*)-F-cinacalcet (<sup>F</sup>*S*,*R*)-**269**.

The yield of the reaction was modest for this two-step protocol, and the best outcome was around 28% yield, however the stereoselectivity was very high with a 99:1 dr. The diastereoselectivity was readily assessed by  $^{19}\text{F}$ -NMR as both diastereoisomers are easily resolved. A synthesis of the other diastereoisomer was obtained following the same methodology but using the (**R**)-Cat in the asymmetric fluorination reaction, and this afforded ( $^{\text{F}}\text{R},\text{R}$ )-F-cinacalcet ( $^{\text{F}}\text{R},\text{R}$ )-**269**. In this case the yields were better up to around 50%, and again with a very high stereoselectivity of 99:1 dr. The decrease of the yield compared to the first synthesis (Section 4.2.1.) can be explained by a second purification carried out on the final compounds ( $^{\text{F}}\text{S},\text{R}$ )-**269** and ( $^{\text{F}}\text{R},\text{R}$ )-**269** to improve the stereoselectivity to 99:1 dr as much as the residue of the difluoro side product **277** (Figure 4.21).

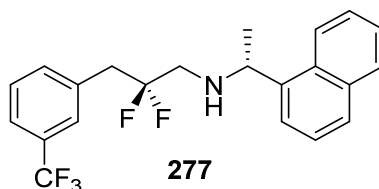
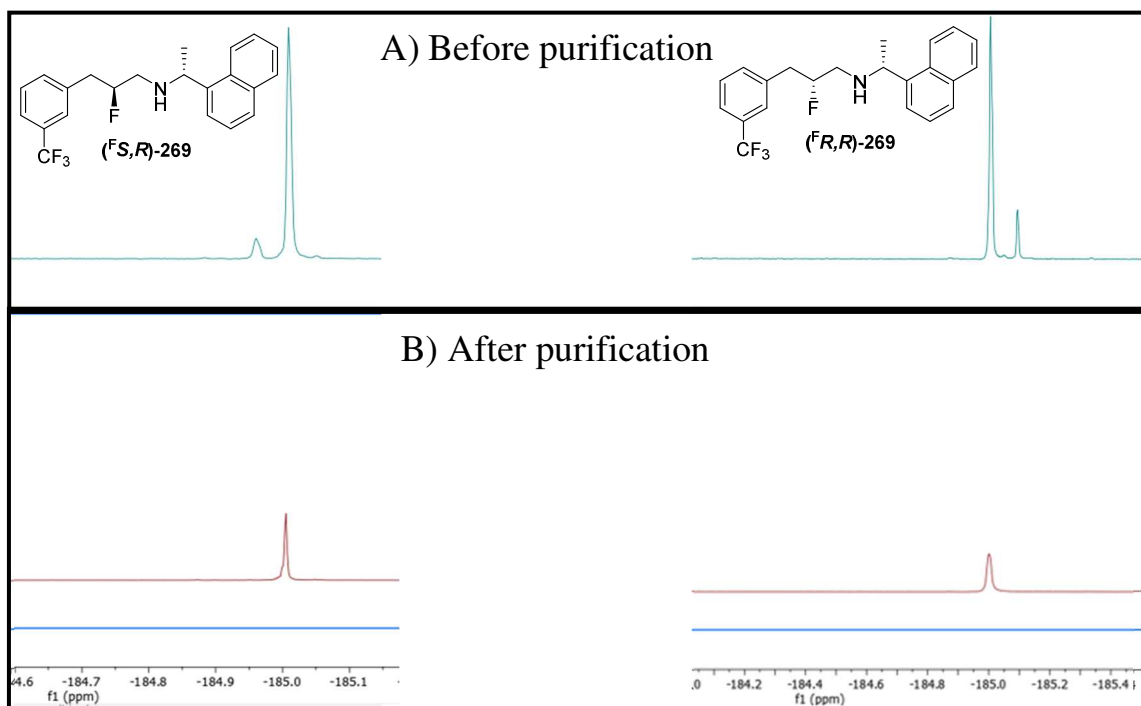


**Figure 4.21** Over-fluorinated side product **277**.

Indeed, before purification the diastereomeric ratios were determined to be 88:12 dr for isomer ( $^{\text{F}}\text{S},\text{R}$ )-**269** and 83:17 dr for isomer ( $^{\text{F}}\text{R},\text{R}$ )-**269** (Figure 4.22).

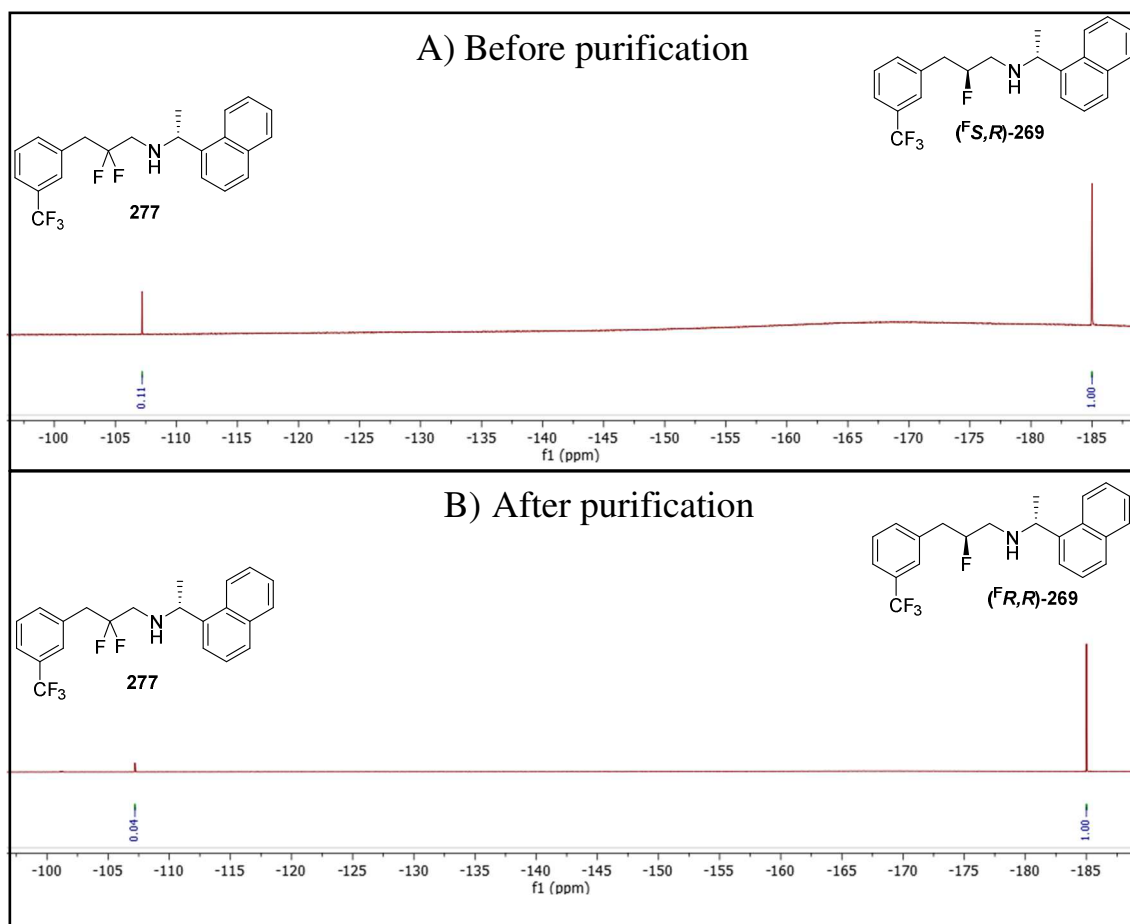


Compounds	dr before purification	dr after purification
( <sup>F</sup> S, <i>R</i> )-269	88:12	99:1
( <sup>F</sup> R, <i>R</i> )-269	83:17	99:1

**Figure 4.22**  $^{19}\text{F}\{^1\text{H}\}$ -NMR of (<sup>F</sup>S,*R*)-269 and (<sup>F</sup>R,*R*)-269 showing the improvement of diastereomeric ratios and Table summarising the results : **A)**  $^{19}\text{F}\{^1\text{H}\}$ -NMR Before purification ; **B)**  $^{19}\text{F}\{^1\text{H}\}$ -NMR after purification.

It is clearly observed in Figure 4.22 that there is a reduction of both minor diastereomeric peaks after purification by column chromatography.

Regarding the difluoro **277** product, it was determined that the mixture contained 5% of **277** for (<sup>F</sup>S,*R*)-269 and 3% for (<sup>F</sup>R,*R*)-269 before purification, while in the case of (<sup>F</sup>S,*R*)-269 the level decrease to 2% after purification (Figure 4.23).



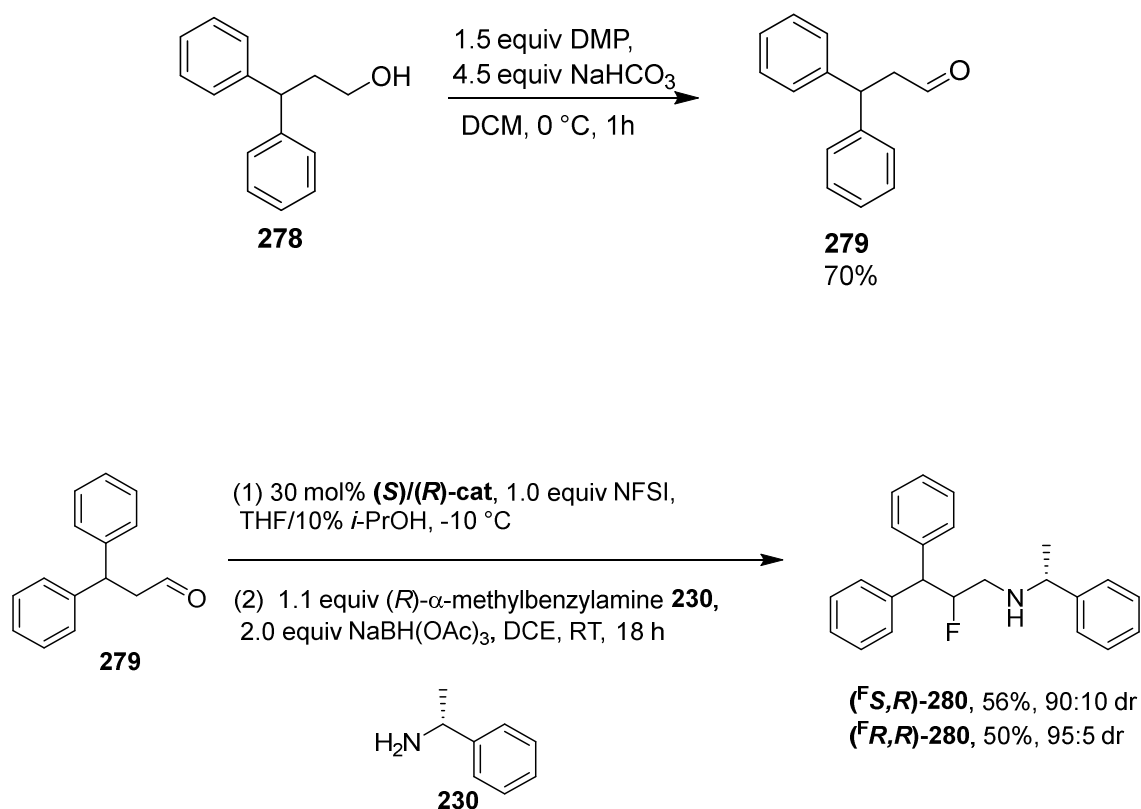
Compounds	% CF <sub>2</sub> before purification	% CF <sub>2</sub> after purification
( <sup>F</sup> S, <sup>R</sup> )-269	5	2
( <sup>F</sup> R, <sup>R</sup> )-269	3	3

**Figure 4.23** <sup>19</sup>F{<sup>1</sup>H}-NMR of (<sup>F</sup>S,<sup>R</sup>)-269 and (<sup>F</sup>R,<sup>R</sup>)-269 showing the difluoro sideproduct **277** and a Table summarising the results : **A)** <sup>19</sup>F{<sup>1</sup>H}-NMR Before purification ; **B)** <sup>19</sup>F NMR after purification.

Encouraged by the good diastereoselectivity obtained after purification and the average yields of the F-cinacalcets it became an objective to extend the approach to other F-cinacalcets analogues. These analogues were the corresponding monofluorinated stereoisomers of a range of established CaR agonists (Section 4.2.2.).

In the first instance the β-fluorostereoisomers of fendiline **254** were addressed. The protocol started from the oxidation of 3-diphenylpropanol **278** to 3-diphenylpropanal **279** with Dess-Martin periodinane (DMP). Aldehyde **279** was then subjected to the optimised

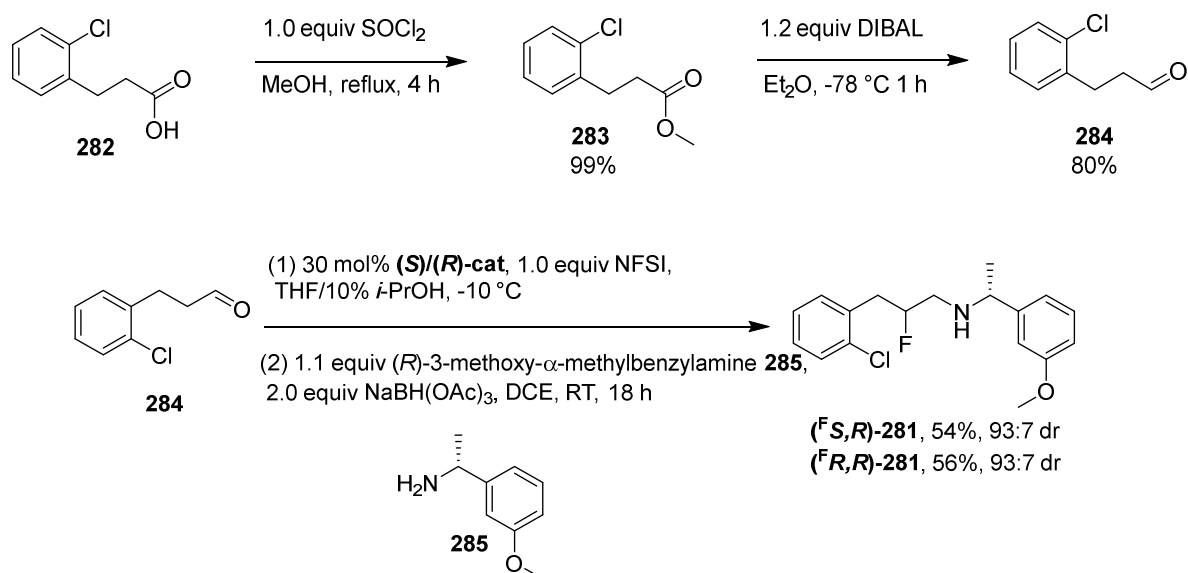
asymmetric fluorination followed by reductive amination, in this case using (*R*)-methylbenzylamine **230** to afford (<sup>F</sup>*S,R*)-F-fendiline (<sup>F</sup>*S,R*)-**280**. In the event the product was recovered in a 56% yield and with 90:10 dr, as determined by <sup>19</sup>F-NMR. Diastereoisomer (<sup>F</sup>*R,R*)-**280** was obtained following the same protocol with the (*R*)-Cat catalyst. This afforded (<sup>F</sup>*R,R*)-F-fendiline (<sup>F</sup>*R,R*)-**280** in a 50% yield and with an 95:5 dr (Scheme 4.3).



**Scheme 4.3** Two-step route to F-fendilines (<sup>F</sup>*S,R*)-**280** and (<sup>F</sup>*R,R*)-**280**.

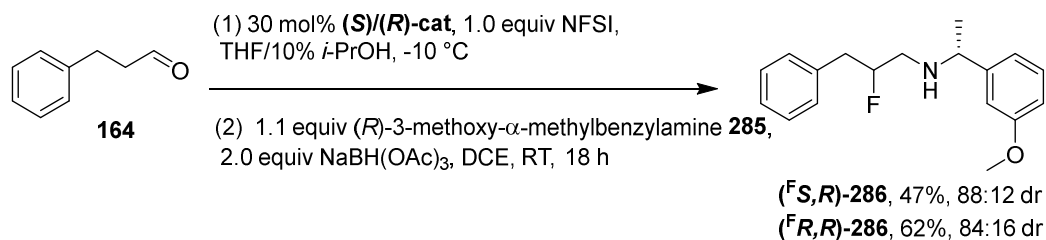
The next target was (<sup>F</sup>*S,R*)-F-tecalcet (<sup>F</sup>*S,R*)-**281** and its diastereoisomer (<sup>F</sup>*R,R*)-F-tecalcet (<sup>F</sup>*R,R*)-**281**. The synthesis of (<sup>F</sup>*S,R*)-**281** and (<sup>F</sup>*R,R*)-**281** started by esterification of carboxylic acid **282** to generate methyl ester **283**. A selective reduction of the ester with DIBAL smoothly generated 3-(2-chlorophenyl)propanal **284**. Aldehyde **284** was then committed to the two step protocol with (*R*)-1-(3-methoxyphenyl)ethylamine **285**, for the reductive amination step. In the event this afforded (<sup>F</sup>*S,R*)-**281** in modest yield (54%) and a diastereoselectivity of 93:7 dr, as determined by <sup>19</sup>F{<sup>1</sup>H}-NMR. The other

diastereoisomer was obtained following the same method but with (*R*)-**Cat** to afford (<sup>F</sup>*R,R*)-**281**. In this case in a 56% yield and with a diastereoselectivity of 93:7 dr (Scheme 4.4).



**Scheme 4.4** Two step route to F-tecalcets (<sup>F</sup>*S,R*)-**281** and (<sup>F</sup>*R,R*)-**281**.

Finally, the diastereoisomers of (<sup>F</sup>*S,R*)-F-NPS R-467 (<sup>F</sup>*S,R*)-**286** and (<sup>F</sup>*R,R*)-F-NPS R-467 (<sup>F</sup>*R,R*)-**286** were synthesised starting from phenylpropanal **164**. Aldehyde **164** was used in combination with (*R*)-1-(3-methoxyphenyl)ethylamine **285** for asymmetric fluorination followed by a reductive amination to afford agonist (<sup>F</sup>*S,R*)-**286**. This reaction resulted in a 47% yield and with a diastereoselectivity of 88:12 dr. The (<sup>F</sup>*R,R*) diastereoisomer (<sup>F</sup>*R,R*)-**286** was obtained following the same protocol but with (*R*)-**Cat**. Although there was a modest yield improvement (62%) there was also a reduction in the diastereoselectivity (84:16 dr). (Scheme 4.5).



**Scheme 4.5** Two step route to F-NPS R-467 (**(<sup>F</sup>S,*R*)-286** and **(<sup>F</sup>R,*R*)-286**).

To summarise, eight CaR calcimimetics stereoisomers were synthesised in modest yields and good to moderate stereoselectivity. The stereoisomeric purity could be improved by column chromatography purification, as the products are diastereoisomers. Column chromatography in some cases could also decrease the level of difluoro side products (Table 4.2).

**Table 4.2** Comparison of F-cinacalcet analogues dr and CF<sub>2</sub> ratio before and after purification through column chromatography.

Compounds	Before Purification		After Purification	
	dr	CF <sub>2</sub> (%)	dr	CF <sub>2</sub> (%)
<b>(<sup>F</sup>S,<i>R</i>)-280</b>	85:5	3	90:10	2
<b>(<sup>F</sup>R,<i>R</i>)-280</b>	80:20	3	95:5	1
<b>(<sup>F</sup>S,<i>R</i>)-281</b>	80:20	3	93:7	3
<b>(<sup>F</sup>R,<i>R</i>)-281</b>	80.5:19.5	6	93:7	<1
<b>(<sup>F</sup>S,<i>R</i>)-286</b>	87:13	3	88:12	<1
<b>(<sup>F</sup>R,<i>R</i>)-286</b>	73.5:26.5	3	84:16	<1

The original fluorocinacalcet (**(<sup>F</sup>S,*R*)-269**) synthesis required four steps for each stereoisomer, and this is now reduced to two steps here which presents some advantage. After synthesis and purification of all F-cinacalcets analogues, they were converted into salts using 1M HCl in diethyl ether and recrystallised in methanol/acetone system.

In this study some of the products were sufficiently crystalline to obtain single crystal X-ray structures, and this analysis was carried out on **(<sup>F</sup>R,*R*)-287**, **(<sup>F</sup>S,*R*)-288** and **(<sup>F</sup>R,*R*)-288**. This allowed the relative and absolute configurations to be confirmed. In each case the structures show a *gauche* alignment consistent with the electrostatic *gauche* effect between fluorine and the ammonium residue and this again (Section 4.3.1.) suggests a

preference for an extended alkyl chain (*anti*-zig-zag) for each stereoisomer (Figure 4.24). The *gauche* angle was measured for the CF-N<sup>+</sup>C angle. The values obtained were 56.9° for (<sup>F</sup>*R,R*)-287, 60.4° for (<sup>F</sup>*S,R*)-288 and 60.6° for (<sup>F</sup>*R,R*)-288 (Figure 4.24).

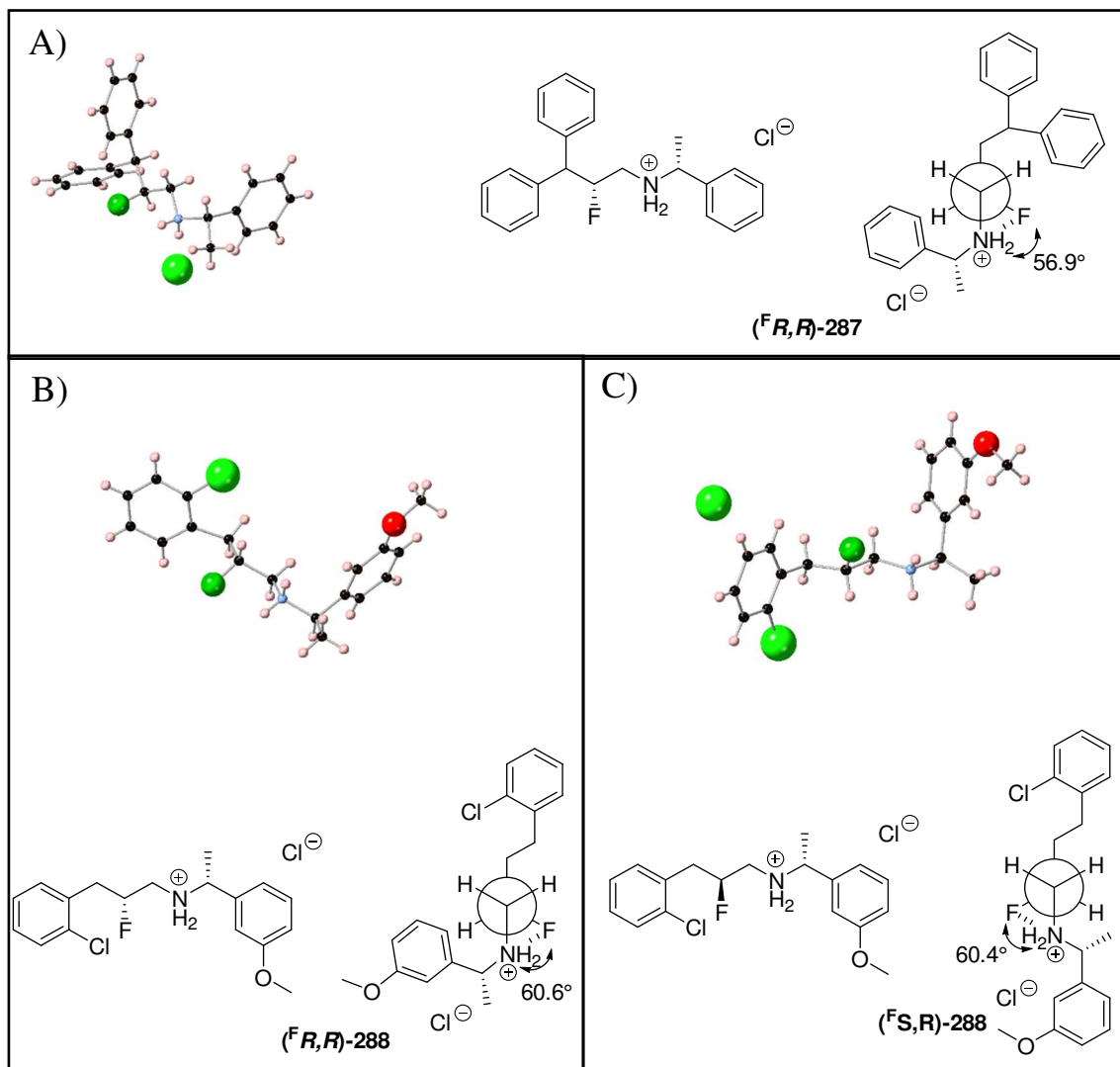


**Figure 4.24** A) Crystal structure of (<sup>F</sup>*R,R*)-287 showing a *gauche* angle of 56.9° ; B) Crystal structure of (<sup>F</sup>*R,R*)-288 showing a *gauche* angle of 60.6° ; C) Crystal structure of (<sup>F</sup>*S,R*)-288 showing a *gauche* angle of 60.4°.

The chloride salt fluoro-isomers were subject to CaR receptor assays at Monash University in the laboratory of Dr. Katie Leach. All eight chloride salt stereoisomers were investigated, and the outcomes are discussed below.

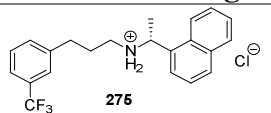
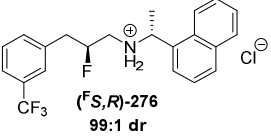
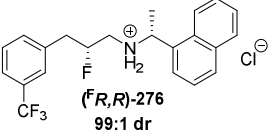
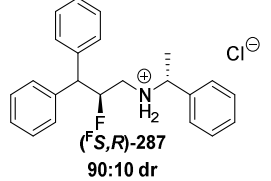
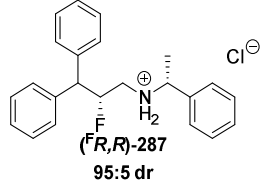
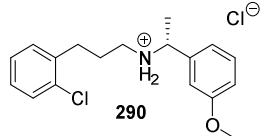
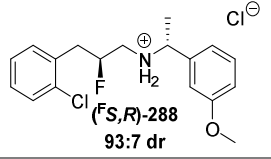
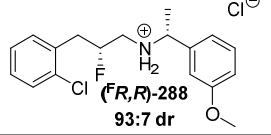
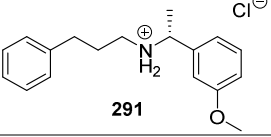
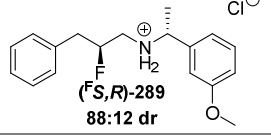
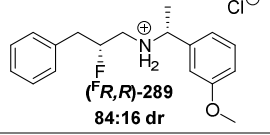


### 4.3.3 CaR receptor assays

The outcomes of the CaR assays are reported in Table 4.3. It is notable that all eight of the fluorinated analogues display reasonable agonist activity. The analysis indicated that they had a similar allosteric cooperativity to cinacalcet, that is when the analogues tested bound to the same allosteric site and they had a similar agonist activity with respect to Ca<sup>2+</sup> binding. The (<sup>F</sup>*S*) absolute configuration ((<sup>F</sup>*S,R*)-**276**, (<sup>F</sup>*S,R*)-**288**, (<sup>F</sup>*S,R*)-**289**) has a slightly higher activity than (<sup>F</sup>*R*) absolute configuration ((<sup>F</sup>*R,R*)-**276**, (<sup>F</sup>*R,R*)-**288**, (<sup>F</sup>*R,R*)-**289**). As an example it is observed that (<sup>F</sup>*S,R*)-F-cinacalcet (<sup>F</sup>*S,R*)-**276** was more active than cinacalcet **275** and (<sup>F</sup>*R,R*)-F-cinacalcet (<sup>F</sup>*R,R*)-**276**. This preference toward the (<sup>F</sup>*S*) configuration compared to (<sup>F</sup>*R*), can also be observed on two other sets of modulators (**288** and **289**).

It is important to keep in mind that, except for (<sup>F</sup>*S,R*)-**276** and (<sup>F</sup>*R,R*)-**276**, none of the F-cinacalcet analogue diastereoisomers were enantiomerically pure (68-90%). Thus a maximum effect will be observed on the cinacalcet set, correlating with the higher level activity observed with (<sup>F</sup>*S,R*)-**276**.

**Table 4.3** Affinity ( $pK_B$ ) and efficacy ( $\text{Log}\alpha\beta$ ) of CaSR PAMs determined in  $\text{Ca}^{2+}$  mobilization assays. Data are mean  $\pm$  SD from the indicated number of independent experiments (n).

Cinacalcets analogues	Affinity : $pK_B \pm \text{SEM}$	Efficacy : $\text{Log}\alpha\beta \pm \text{SEM}$
 275	$5.64 \pm 0.11$	$1.63 \pm 0.15$
 ( <i>S,R</i> )-276 99:1 dr	$6.20 \pm 0.11$	$1.81 \pm 0.12$
 ( <i>R,R</i> )-276 99:1 dr	$5.75 \pm 0.12$	$1.60 \pm 0.11$
 ( <i>S,R</i> )-287 90:10 dr	$4.15 \pm 0.73$	$2.81 \pm 0.68$
 ( <i>R,R</i> )-287 95:5 dr	n.d.	n.d.
 290	$5.82 \pm 0.15$	$1.41 \pm 0.21$
 ( <i>S,R</i> )-288 93:7 dr	$5.75 \pm 0.14$	$2.06 \pm 0.14$
 ( <i>R,R</i> )-288 93:7 dr	$4.19 \pm 0.68$	$2.79 \pm 0.63$
 291	$5.57 \pm 0.13$	$2.03 \pm 0.13$
 ( <i>S,R</i> )-289 88:12 dr	$5.69 \pm 0.14$	$1.86 \pm 0.13$
 ( <i>R,R</i> )-289 84:16 dr	$4.11 \pm 1.21$	$2.92 \pm 1.15$

This assay shows also, due to the similar activity of isomers from the same sets, that both configurations of each set adopts an *anti-zig-zag* conformation **A** or **B** (Figure 4.25). Both **A** and **B** retain a stabilised electrostatic *gauche* effect between fluorine and protonated nitrogen. This is in correlation with the X-ray structure (Figure 4.24) showing *anti-zig-zag* structures. On the other hand, conformation **C** is considered disfavoured due to its higher energy compared to **A** and **B** (Figure 4.25). There is a constant bias observed for the favoured (<sup>F</sup>*S*) configuration that could be explained relative to the R group deviating from a perfect *anti-zig-zag* conformation. This constant bias indicates a favoured binding mode from the conformation where R is directed away from the *anti-zig-zag*, explained by the narrower electrostatic *gauche* angle (conformation **B**, Figure 4.25). In the case of the (<sup>F</sup>*R*) isomers the conformation is closer to an *anti-zig-zag* (conformation **A**, Figure 4.25) orientating the R group to a less favoured orientation, thus achieving a more energetic binding mode. Regarding conformation **C**, due to the energetic barrier (~3-5 kcal.mol<sup>-1</sup>) that needs to be overcome to achieve binding, if it would have been the preferred conformation, neither of the diastereoisomers would have shown good activity.

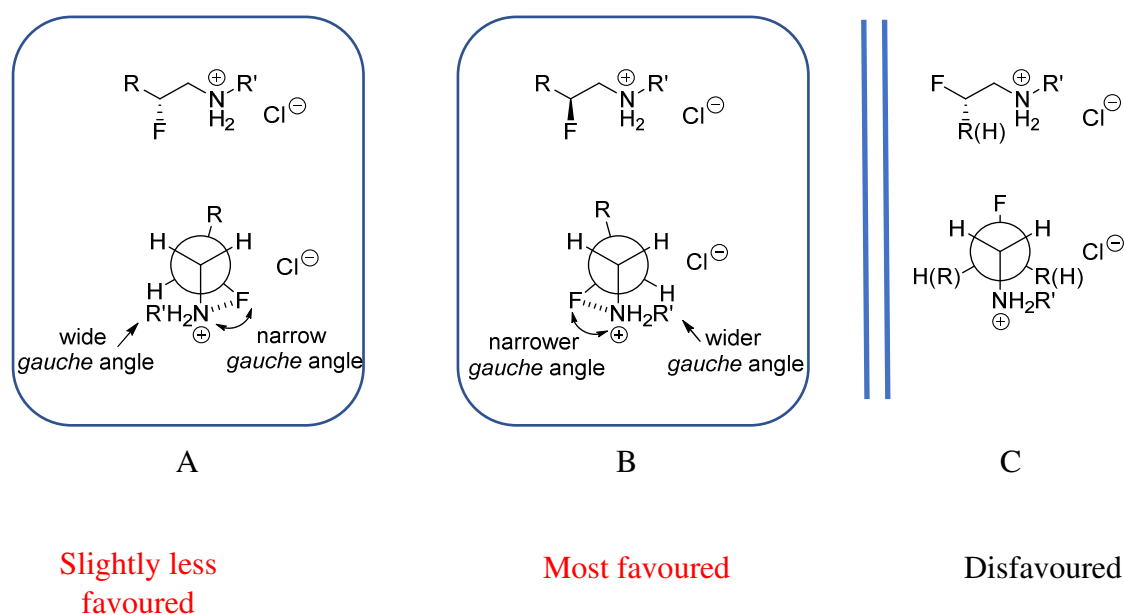


**Figure 4.25** Newman representation of three staggered conformations showing rotation around the F-C-C-N bond. The electrostatic *gauche* effect stabilises conformers **A** and **B** only.

#### 4.4. Conclusion

This chapter focussed on the synthesis of  $\beta$ -fluoro derivatives of established CaSR agonists of the cinacalcin family. Different stereoisomers, inverting the stereochemistry at fluorine centre, offered conformational probes to study the preferred binding mode to the allosteric site of the CaR receptor. A new synthesis to this class of compounds was developed. This involved a two-step protocol which telescoped an organocatalytic asymmetric fluorination reaction of appropriate starting aldehydes, with a reductive amination. Four pairs of stereoisomers were prepared. These eight new calcimimetics proved to have modest to good affinity in CaSR assays, with the most potent being (<sup>F</sup>*S,R*)-F-cinacalcet (**(<sup>F</sup>*S,R*)-276**) (Table 4.3). The CaSR assay also helped to confirm the preferred conformation of the bioactives, by taking into account preferred conformations dictated by the electrostatic *gauche* effect.

## Chapter V Targeting isocitrate lyase (ICL)

### 5.1. Introduction

According to the World Health Organisation (WHO), tuberculosis (TB) was responsible for 1.6 million deaths worldwide in 2021. TB then represents the 13<sup>th</sup> most frequent cause of death and the 2<sup>nd</sup> highest infectious disease in the world (after COVID-19). The causative bacterium is *Mycobacterium tuberculosis* which was discovered in 1882 by Robert Koch<sup>249,250</sup> (Figure 5.1). TB is present in most of the world with 10.6 million people reported to be infected in 2021. A complexity in finding a treatment against TB is the development of resistance of *M. tuberculosis* against the most efficient antibiotics isoniazid **292** and rifampicin **293**, the structures of which are shown in Figure 5.2.



**Figure 5.1** Drug-resistant *Mycobacterium tuberculosis*.<sup>251</sup>

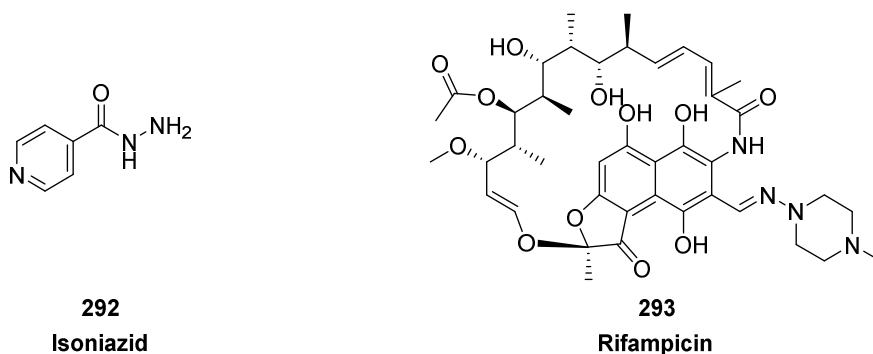


**Figure 5.2** Structures of isoniazide **292** and rifampicin **293**.

Currently, research on TB treatment is leading to a decrease in illness propagation by over 2% per year. However, funding from the Global Fund, US government and BRICS countries (Brazil, Russian Federation, India, China, South Africa), to address TB has decreased in recent years. In 2021 the budget was reduced to \$5.4 billion from \$6.0 billion in 2019. Around 79% (\$4.3 billion) of the Global Fund came from UN countries, with 64% from BRICS countries. The US is one of the major contributors in fighting TB covering 50% of international funding for diagnosis, prevention, treatment and research. The WHO reported that \$13 billion dollars annually would be needed globally to successfully address TB. Up to now, the WHO has set an objective to end the disease by 2030. This will only be achieved if next generation pharmaceuticals are discovered which are able to efficiently target *M. tuberculosis*.

The important antibiotic isoniazid **292** was first synthesised in 1912 and was used as a clinical treatment for TB in 1952.<sup>252-255</sup> Nowadays, isoniazid is used in combination with other antibiotics such as rifampicin **293**, pyrazinamide **294**, streptomycin **295**, or ethambutol **296**, (Figure 5.3) on active and also latent (inactive) forms of tuberculosis.<sup>256,257</sup>

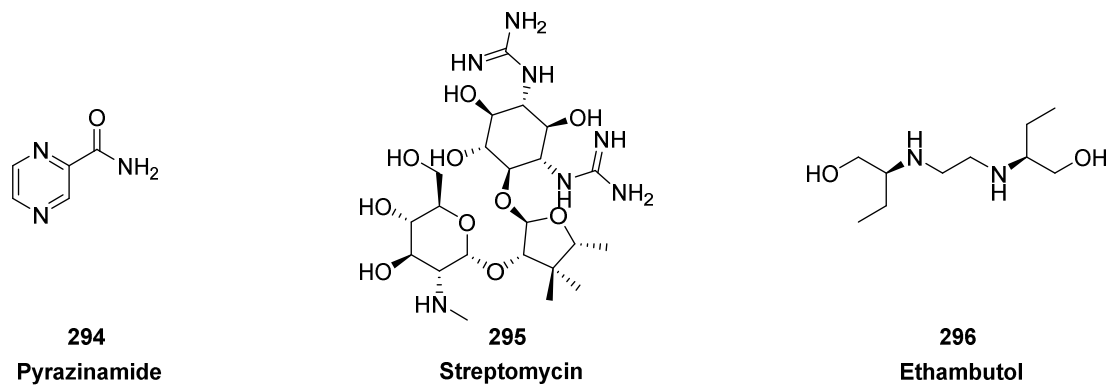


**Figure 5.3** Antibiotics used in combination with isoniazid for the treatment of *M. tuberculosis*.

Within the organism, isoniazid is transformed by the enzyme KatG into radicals **297** that inhibit the synthesis of mycolic acids (Figure 5.4),<sup>258</sup> lipids that are essential for the synthesis of the *M. tuberculosis* cell wall. Over the years *M. tuberculosis* has developed resistance toward the action of isoniazid due to mutations of the *katG*, *inhA*, *kasA* and *ohpC* genes.<sup>259,260</sup> Coupling isoniazid with other antibiotics helps to enhance the overall potency of the antibiotics.<sup>259,260</sup>

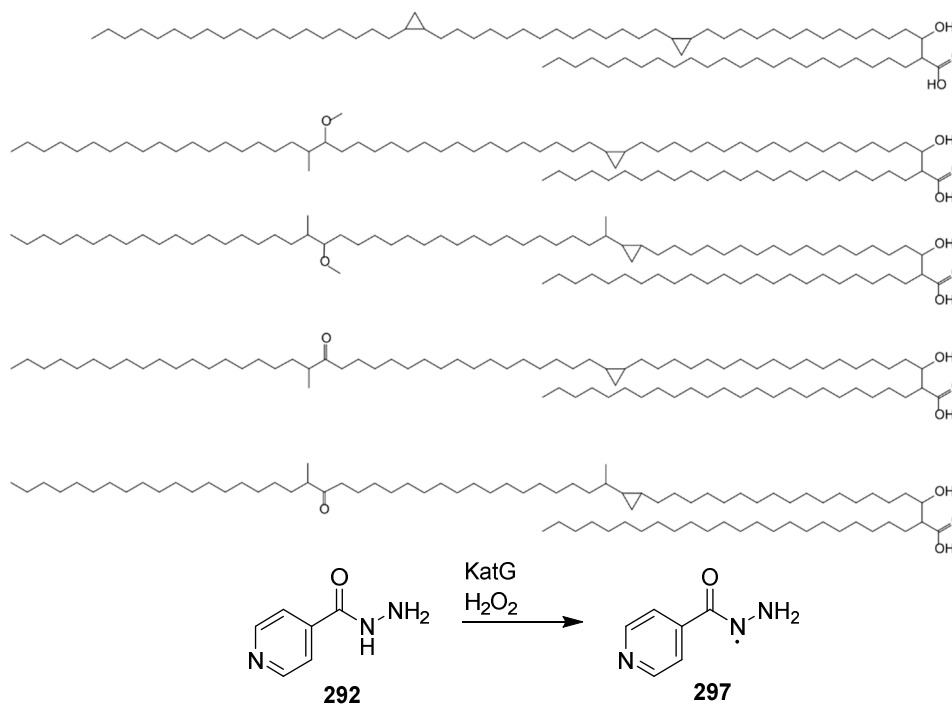


**Figure 5.4** Isoniazide **292** is transformed to radical **297**, by KatG, that inhibits, the synthesis of *M. tuberculosis* mycolic acids essential for cell wall biosynthesis.

Rifampicin **293** is also used in combination with other antibiotics.<sup>261</sup> Rifampicin **293** was discovered in 1965 as a natural product of *Amycolatopsis rifamicinia*, and it was approved by the FDA in 1971 for the treatment of TB.<sup>262</sup> Rifampicin is most effective against latent *M. tuberculosis* and is administered to reduce the risk of progression to the active state of development. Rifampicin acts by inhibition of an RNA polymerase essential for the synthesis of bacterial RNA and DNA (Figure 5.5).<sup>263</sup>



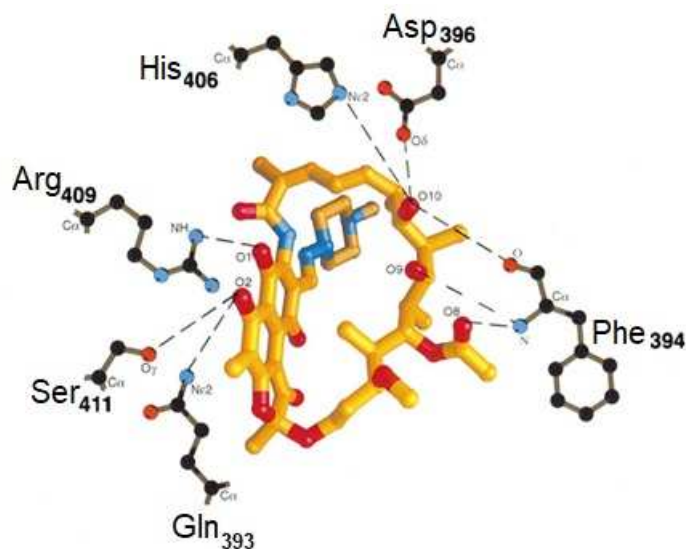


**Figure 5.5** Crystal structure of rifampicin **293** in the RNA polymerase binding site.(red = O, blue = N) <sup>264</sup>

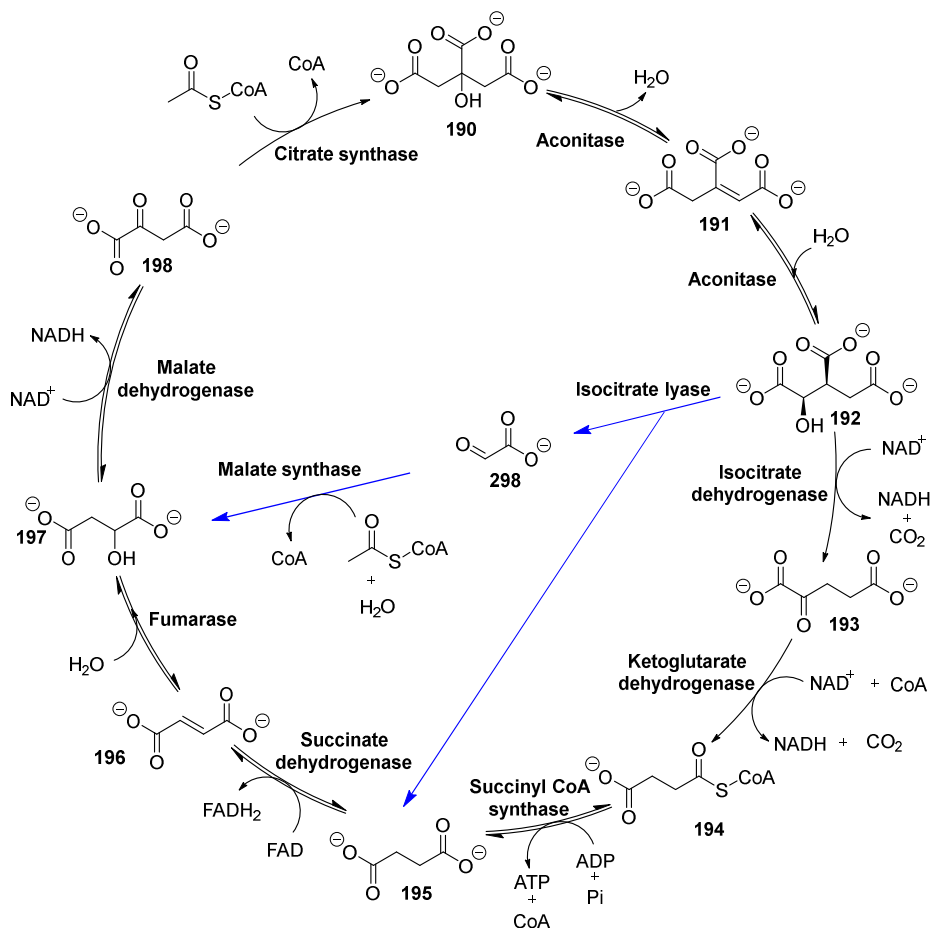
In terms of rifampicin, *M. tuberculosis* has developed resistance due to a mutation of the *rpoB* gene, which encodes the  $\beta$ -subunits of RNA polymerase, where **293** binds. <sup>265</sup>

Isoniazid and rifampicin act on mycolic acid synthase and RNA polymerase respectively. Another important target, that has been recently investigated for the treatment of latent *M. tuberculosis*, is isocitrate lyase (ICL). <sup>266</sup>

### 5.1.1. Introduction to ICL

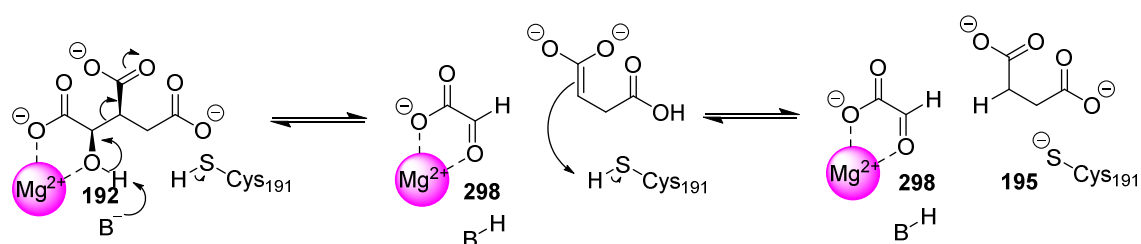
Latent TB has a 5-15% risk to progress to the active phase within the first two years of infection, followed by an additional 5% risk for the rest of the patient's life. These risks mainly depend on personal immunity. <sup>267,268,269</sup> When the bacterium is active it uses the tricarboxylic cycle (TCA cycle) to survive using sugar as its carbon source to generate energy. <sup>270</sup> While in its latent phase, the lack of oxygen and nutrient causes down-regulation of the TCA cycle, and the bacteria up-regulate the enzymes of the glyoxalate cycle that can find its carbon sources from lipids. <sup>270,271</sup> The major difference between both cycles is the conversion of D-isocitrate **192**. Within the TCA cycle, D-isocitrate **192** is converted to  $\alpha$ -ketoglutarate **193** followed by succinyl-CoA **194**, while the glyoxalate cycle by-passes these two decarboxylation steps to directly afford glyoxalate **298** and

succinate **195** (Scheme 5.1).<sup>60</sup> Glyoxalate is then transformed into malate **197** by the action of malate synthase (MS).



**Scheme 5.1** Representation of the TCA (black arrows) and glyoxalate cycles by-passing the two steps of the TCA cycle (blue arrows) used by *M. tuberculosis* in its latent phase.

Isocitrate lyase (ICL) is an  $Mg^{2+}$  dependant enzyme that catalysed the transformation of D-isocitrate **192** to succinate **195** and glyoxalate **298**, through a retro-aldol reaction within the glyoxalate cycle (Scheme 5.2).<sup>271,272</sup>



**Scheme 5.2** Mechanism for the conversion of D-isocitrate **192** to succinate **195** and glyoxalate **298** catalysed by ICL.

ICL exists in multiple organisms such as plants, fungi, and bacteria. Due to the absence of ICL in mammals, this represents an interesting target to explore for selective drug development targeting the bacterium over the human host particularly as *M. tuberculosis* is dependent on ICL for its survival.<sup>273</sup>

ICL exists in two isoforms, ICL<sub>1</sub> (expressed by *icl1*) and ICL<sub>2</sub> (expressed by *aceA*) which share only 27% sequence identity.<sup>249,274</sup> To inhibit the growth of the bacterium, inhibition of both isoforms is required.<sup>273</sup> Up to now most studies have focussed on ICL<sub>1</sub> because ICL<sub>2</sub> is reported to be unstable *in vitro*.<sup>274</sup> Furthermore, many examples of the crystal structure of ICL<sub>1</sub> have been reported (Figure 5.6, **A**), while the first crystal structure of ICL<sub>2</sub> was determined only as recently as 2019 (Figure 5.6, **B-C**).<sup>272,275</sup>

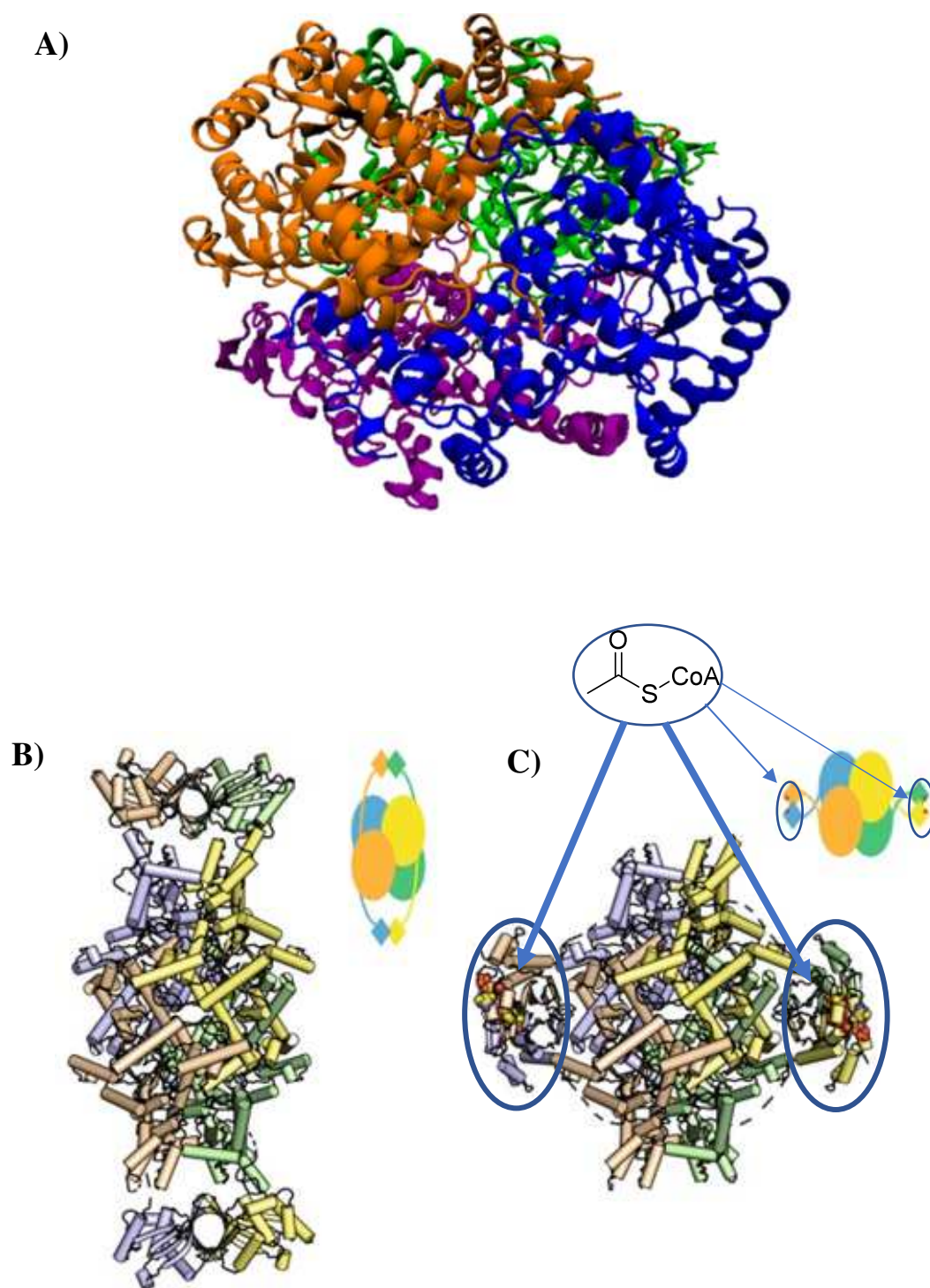


**Figure 5.6** A) Structure of ICL1 determined by Sharma *et al.*<sup>272</sup> Structure of ICL2 determined by Bhusal *et al.*<sup>275</sup> ; B) Structure of ligand-free ICL2. ; C) Structural rearrangement of ICL2 when binding to acetyl-CoA.<sup>275</sup>

### 5.1.2. Existing inhibitors of ICL

The strategies used to identify possible therapies that may inhibit ICL have involved high throughput screening of natural product extracts, and the synthesis of small molecules as potential inhibitors. Compounds are usually first tested against non-*M. tuberculosis* ICL such as ICL from *Pseudomonas indigofera*, *Escherichia coli* or *candida albicans* to avoid exposure risks to *M. tuberculosis*.

In this study we will focus on rationally designed small molecule inhibitors of ICL and the outcomes identified from two categories of inhibitor. The first acted as non-covalent competitive inhibitors, and the second emerged as covalent inhibitors binding to the enzyme.

#### 5.1.2.1 Non-covalent inhibitors

The development of new bioactives often starts from the synthesis of potential pre-existing bioactives. Following this approach, Sriram *et al.*, identified two new groups of ICL inhibitors.<sup>276,277</sup> The first explored derivatives of the antimycobacterial **299** (Figure 5.7).<sup>278-285</sup>

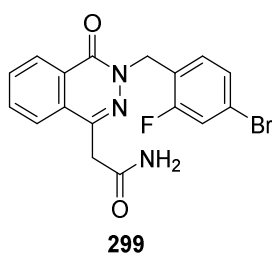


**Figure 5.7** Antimycobacterial **299**, a potent inhibitor of *M. tuberculosis*.<sup>278-285</sup>

Then 24 phthalazin-4-ylacetamides **301** were prepared from the phthalic anhydride **300** (Figure 5.8). It emerged that compound **302** (Figure 5.8) was the most potent of the inhibitors with a minimal inhibitory concentration (MIC) between 0.08 to 5.05  $\mu\text{M}$ , in the *in vivo* and *in vitro* ICL assays tested.<sup>276</sup>

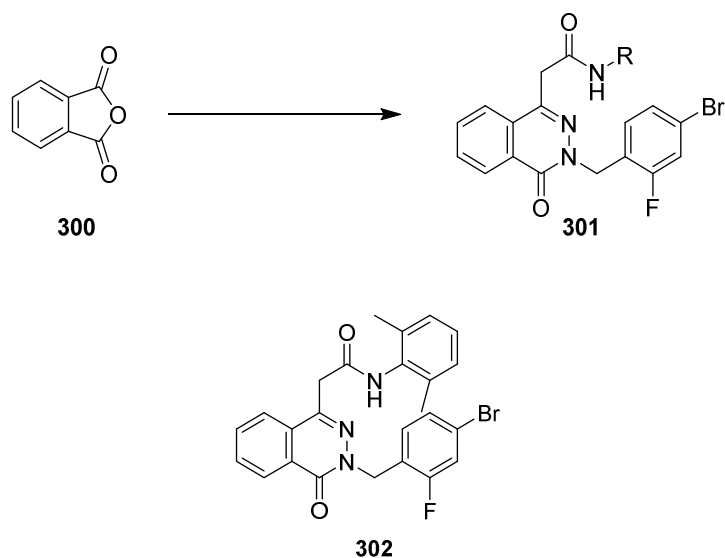


**Figure 5.8** Analogues of the base structure **301** led to the potent ICL inhibitor **302**.<sup>276</sup>

The interaction between **302** and the active site of ICL was identified in a docking study from an X-ray structure of ICL. This revealed multiple interactions including electrostatic, hydrophobic and hydrogen bonding. These interactions included a strong hydrogen bond between the carbonyl of the dimethylbenzyl moiety and the SH from the Cys-191 residue. This residue plays an important role in stabilising **302** within the active site in combination with interactions to Trp-93, Thr-347 and Leu-348 (Figure 5.9).<sup>276</sup>

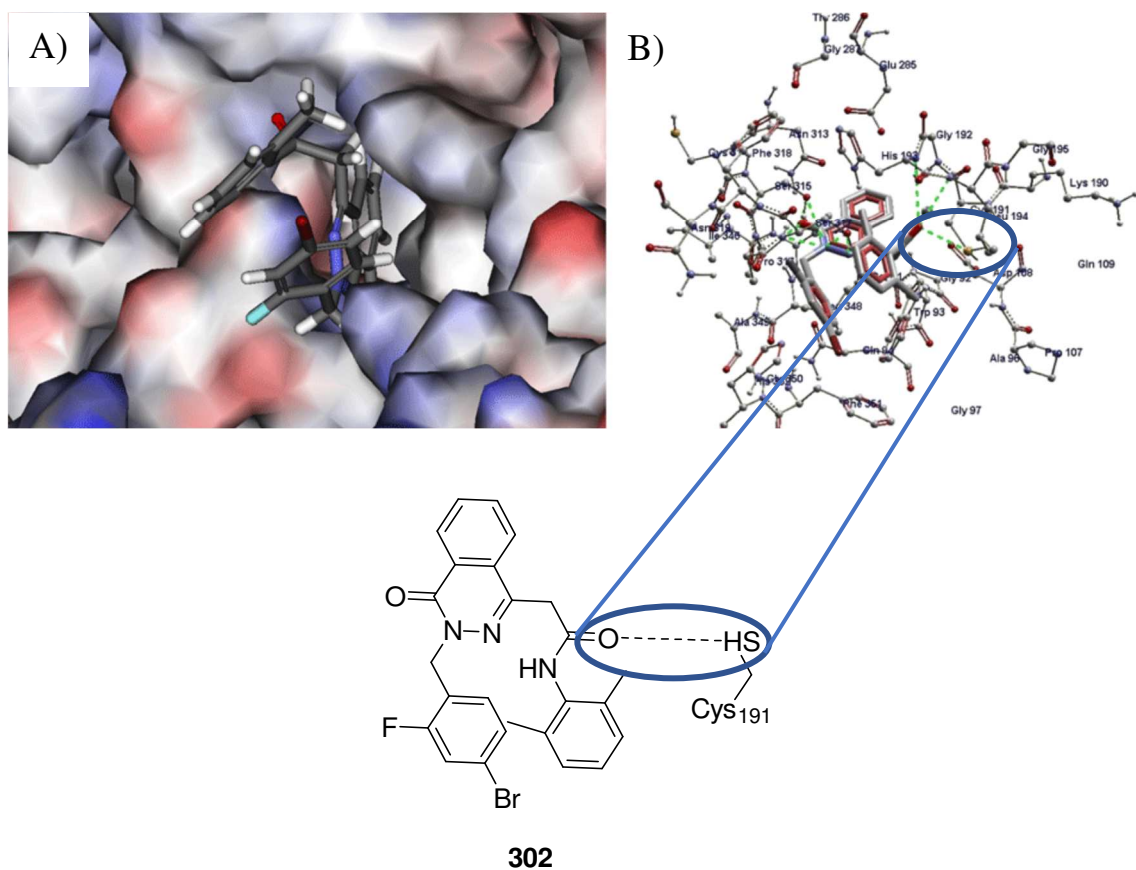


**Figure 5.9** Docked inhibitor **302** within ICL. **A)** Electrostatic surface map ; **B)** Inhibitor binding mode with H-bonds represents in green.<sup>276</sup>

Follow up studies revealed the potency of 5-nitrofuranyl derivatives, 2-[3-(4-bromo-2-fluorobenzyl)-4-oxo-3,4-dihydro-1-phthalazinyl]-acetic acid hydrazones **303** (MIC between 0.09 to 12.25  $\mu\text{M}$ ) and nitrofuranyl amides **304** (MIC between 0.52 to 10.7  $\mu\text{M}$ ) on *M. tuberculosis* (Figure 5.10).<sup>286–288</sup>

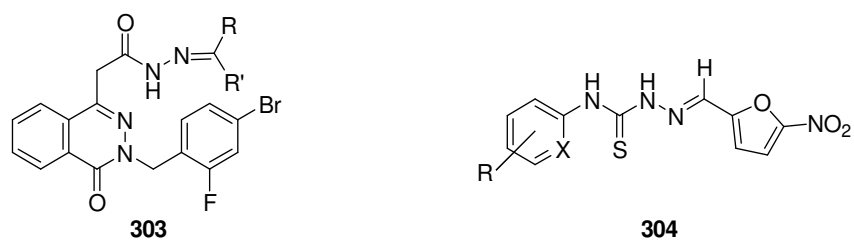


**Figure 5.10** ICL inhibitors **303** and **304** screened by Sriram *et al.*<sup>286–288</sup>

Sriram *et al.* then explored the potential potency of 5-nitrofuran-2-ylidenehydrazones derivatives **305** on *M. tuberculosis* ICL (Figure 5.11).<sup>277</sup> Compound **306** (Figure 5.11) emerged as the most potent with a MICs between 2.7 to 10.6  $\mu\text{M}$  in different ICL assays.<sup>277</sup>

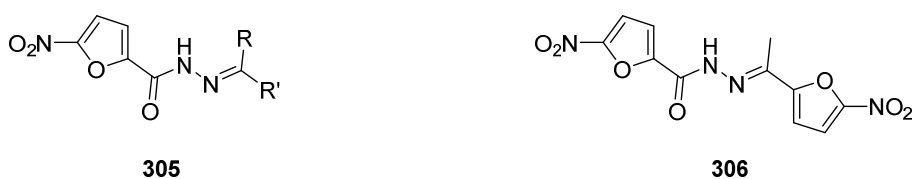


**Figure 5.11** ICL inhibitor **305** led to the more potent compound **306**.<sup>277</sup>

One of the attractive aspects of **306** is its lack of cytotoxicity regarding mammalian cell lines, even at a concentration of 62.5  $\mu\text{M}$  over 72 h incubation.<sup>277</sup> The docking study here reveals strong intermolecular interactions of **306** within the active site of the enzyme. These interactions are stronger than those observed within the inhibitor 3-bromopyruvate and 3-nitropropionic acid,<sup>289,290</sup> consistent with the higher affinity of **306** for the enzyme. Again, the study showed between **306** and Cys-19, stabilised by hydrogen bonds between the nitro group of the nitrofuroic acid moiety and residues Arg-228 and Tyr-89 (Figure 5.12).<sup>277</sup>



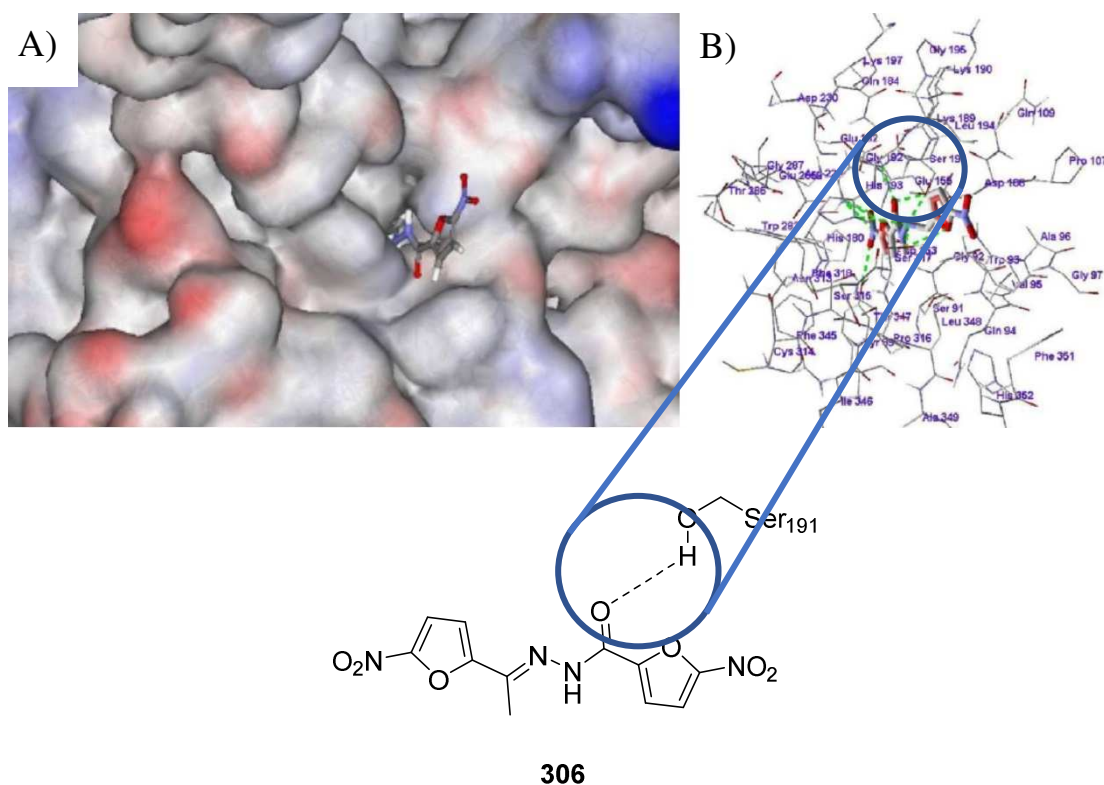


**Figure 5.12** Docked inhibitor **306** within ICL (Cys-191 mutated to Ser-191). **A)** Electrostatic surface map; **B)** Inhibitor binding mode with key hydrogen bonds represents in green.<sup>277</sup>

In 2022, the activity of N-phenylitaconamides on ICL was reported. These compounds are analogues of itaconate **307**, one of the first ICL inhibitors discovered in 1977.<sup>291,292</sup> Compound **308** (Figure 5.13) is the most potent of this series.<sup>291</sup>

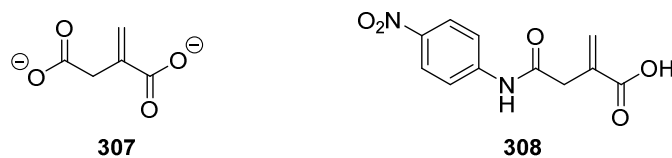


**Figure 5.13** Structures of the first inhibitor of ICL, itaconate **307** discovered in 1977 and of the most potent, N-phenylitaconamide **308**.<sup>291</sup>

Compound **308** gave a 36% rate of inhibition at 10  $\mu\text{M}$  inhibitor concentration. A docking study suggested multiple interactions with residues Ser-91, Thr-347, His-393, Gln-394, Trp-93, Arg-228 and Ser-317 (Figure 5.14).<sup>291</sup>

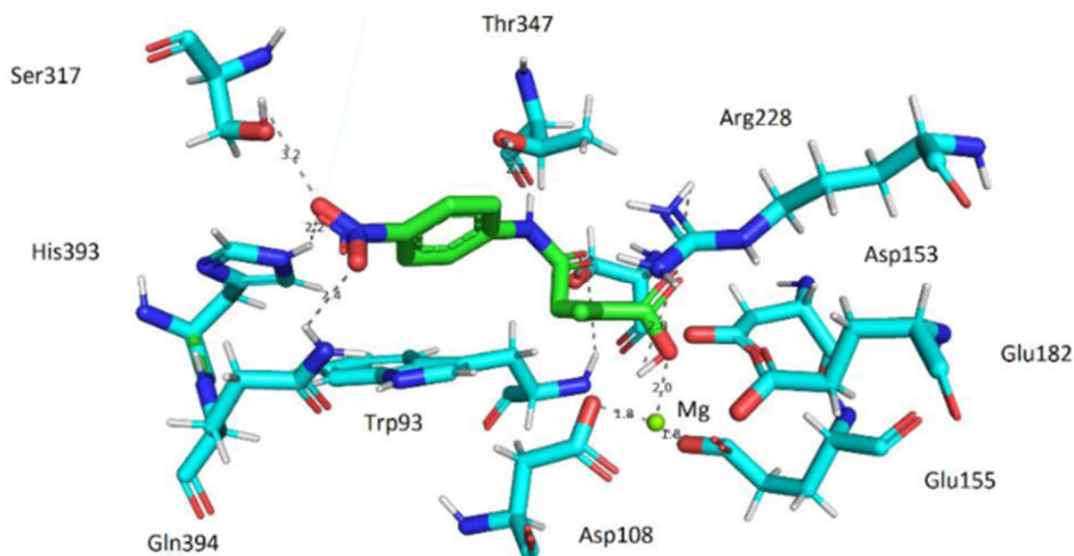


**Figure 5.14** Binding mode of **308** with ICL showing key interactions.<sup>291</sup>

This study also demonstrated a comparison with derivative **309** (Figure 5.15).

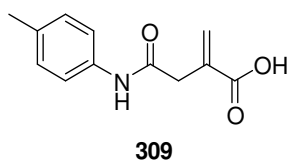


**Figure 5.15** N-Phenylitaconamide **309** a modest inhibitor of ICL.

But **309** has a lower activity on ICL (< 10% inhibition rate at 10  $\mu\text{M}$ ), and this was explained by reduced interactions with amino acid residues of the enzyme, where **309** only interacts now with Trp-93, Thr-347 and Gln-394 (Figure 5.16).<sup>291</sup>

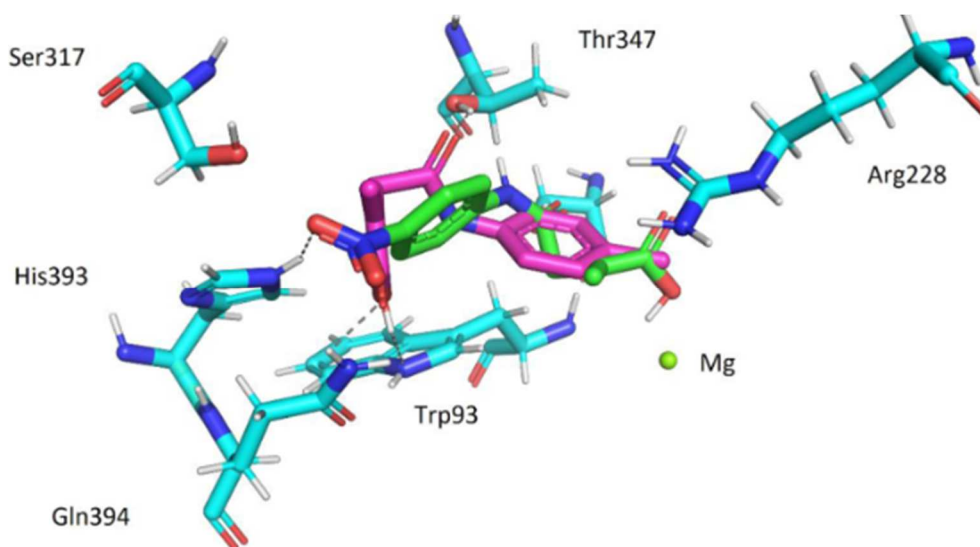


**Figure 5.16** Binding mode of **309** on ICL.<sup>291</sup>

### 5.1.2.2 Covalent inhibitors of ICL

Recently there has been a growing interest towards the development of covalent binding inhibitors of ICL rather than competitive inhibition. In this context analogues of D-isocitrate **192** and succinate **195** are described (Figure 5.17).



**Figure 5.17** Structure of D-isocitrate **192** and succinate **195**.

In 2017 Pham *et al.* reported 2-vinyl-D-isocitrate **310** (2-VIC) as the first mechanism-based inhibitor of ICL<sub>1</sub> and ICL<sub>2</sub> (Figure 5.18).<sup>293</sup>

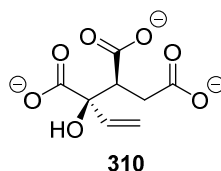
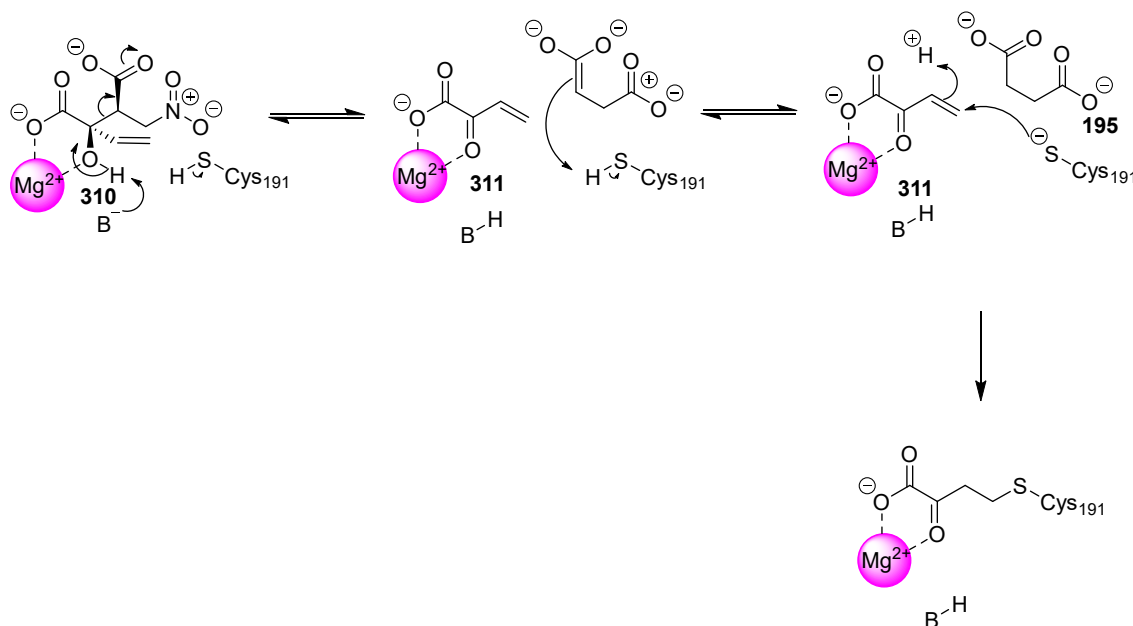


**Figure 5.18** Structure of 2-VIC **310** a mechanism-based inhibitor of ICL.

When 2-VIC binds within the active site in place of D-isocitrate, it is cleaved to generate succinate **195** and 2-vinylglyoxlate **311** (Scheme 5.3).<sup>293</sup>



**Scheme 5.3** Mechanism of ICL inhibition by 2-VIC **310**.<sup>293</sup>

*In-situ* generated **311** is a sufficiently reactive electrophile to become covalently bound to the Cys-191 residue in the enzyme active site (Scheme 3). The level of inhibition on ICL<sub>1</sub> was 65% after 65 min of incubation with 2-VIC **310** (0-40 μM). Some activity was also observed on ICL<sub>2</sub>, and kinetic analysis showed that deactivation was slower than the reaction of ICL on D-isocitrate **192**. Further investigation of the efficiency of **310** explored the partition ratio. The partition ratio is the fraction of bound **310** that's dissociated from the enzyme versus bound **310** that forms a covalent adduct with the

enzyme. Here the partition ratio for ICL<sub>1</sub> was  $P = 0.24 \pm 0.04$  indicating that 1.2 molecules of **310** is required to inhibit 1.0 molecules of enzyme. For ICL<sub>1</sub> it was shown that the enzyme retained around 10% of its activity even if the concentration of **310** was higher than the concentration of ICL<sub>1</sub>. Also, at room temperature the enzyme recovers 50% of its activity after 24h. The retention and recovery of activity indicate that the covalent adduct is reversibly binding to the enzyme. Regarding ICL<sub>2</sub> the partition ratio was higher ( $P = 0.6$ ), showing that ICL<sub>2</sub> in presence of vinylglyoxalate will tend to dissociate instead of forming a covalent adduct; accordingly ICL<sub>2</sub> has a better recovery than ICL<sub>1</sub>.

An interesting aspect of the inhibition study of **310** was the lack of cytotoxicity after 72h of exposition with a concentration of **310** below 400  $\mu\text{M}$ , on human dermal fibroblast (cell type present in skin connective tissue), even though similar inhibition activity of **310** on ICL was observed on human IDH ( $\text{IC}_{50} = 10 \pm 1.3\mu\text{M}$ ). The formation of a covalent bond between the Cys-191 residue and 2-vinylglyoxalate **311** was observed by mass spectrometry analysis with a difference in mass of the enzyme before (48787 Da) and after (48887 Da) of 99 amu. Covalent bond formation was further confirmed through X-ray crystal structure analysis of sufficient resolution (Figure 5.19).<sup>293</sup>

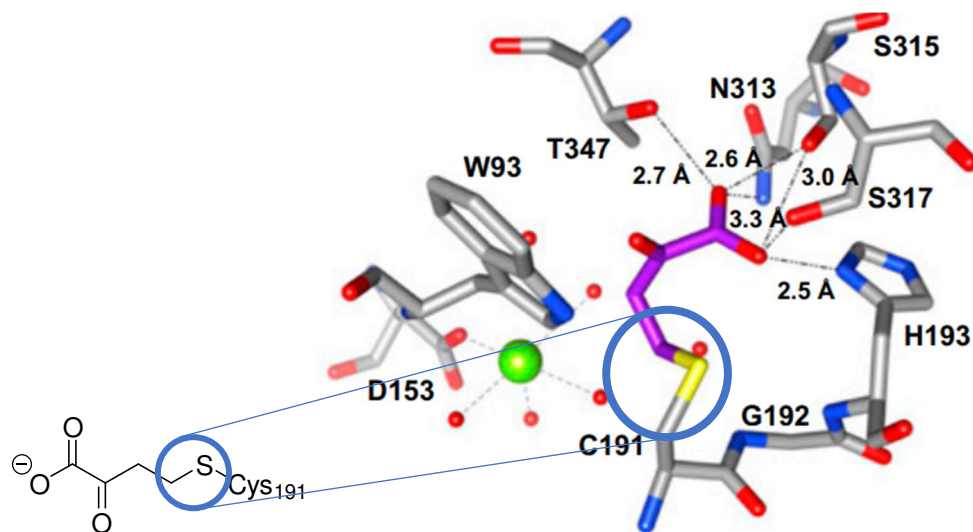


**Figure 5.19** Crystal structure of the covalent adduct of 2-VIC **310** and ICL through Cys-191.<sup>293</sup>

In 2021 Mellott *et al.* reported another D-isocitrate analogue, (2*R*,3*S*)-2-hydroxy-3-(nitromethyl)succinate **312** as a mechanism-based inhibitor of ICL (Figure 5.20).<sup>294</sup>

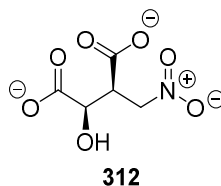
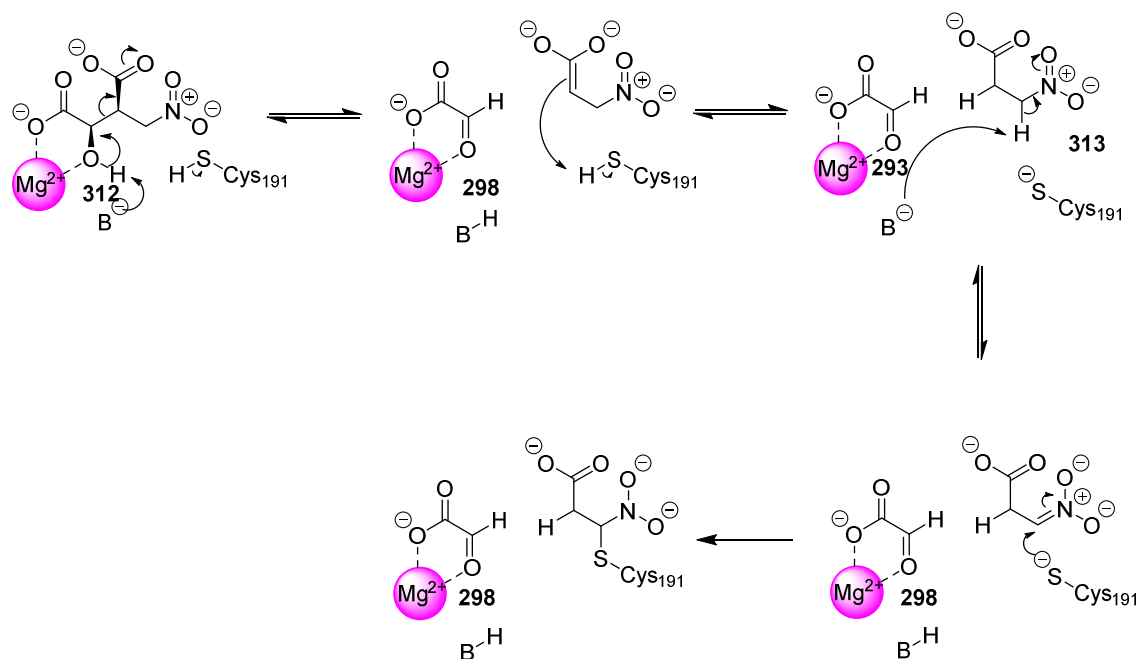


**Figure 5.20** (2*R*,3*S*), 2-Hydroxy-3-(nitromethyl)succinate **312**, a mechanism-based inhibitor of ICL.<sup>294</sup>

The structure of **312** contains a nitro group in place of a carboxylate which reduces the overall charge on the molecule, increasing permeability across cell membranes relative to D-isocitrate **192**. Complete inhibition of ICL<sub>1</sub> was observed after 1000s incubation at 10 μM of **312**. Compound **312** was also observed to be ~20 times more potent than the previously established inhibitor **310**. Results of the inhibition study revealed **312** an irreversible covalent inhibition of ICL. This was rationalised as the result of the formation of 3-NP **313** from cleavage of **312** by ICL (Scheme 5.4).



**Scheme 5.4** Mechanism of ICL inhibition by **312**.<sup>294</sup>

3-NP **312** is a known inhibitor of ICL and has been shown recently to form a covalent adduct to Cys191 of ICL.<sup>290,295</sup> For **312**, it was shown that more than one equivalent (1.25 mol %) was required to inhibit the enzyme and it was suggested that some D-isocitrate **192** was still bound into the active site of ICL<sub>1</sub>. A covalent bond between 3-NP **313** and Cys-191 was confirmed by mass spectrometry analysis with a difference of 101 amu between the native (48787 Da) and modified ICL (48890 Da). Covalent bond formation was subsequently confirmed by X-ray crystal structure of the inactivated enzyme (Figure 5.21).<sup>294</sup>

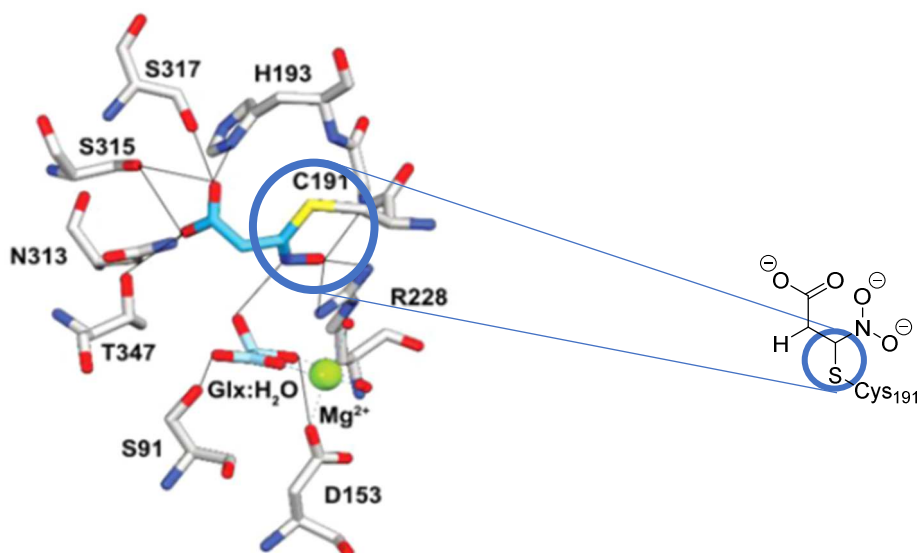


**Figure 5.21** X-ray crystal structure showing adduct **312** covalently bound to Cys-191.<sup>294</sup>

On the succinate analogue side, itaconate **307** (Figure 5.22) was shown to be an inhibitor of ICL.<sup>292</sup>

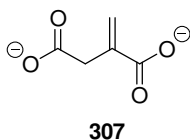


**Figure 5.22** Structure of itaconate **307** an inhibitor of ICL.

Recently the binding mode of itaconate to ICL<sub>1</sub> was reported to be formed by intermolecular electrostatic interactions. In 2021, Kwai *et al.* reported itaconate **307** as a mechanism-based inhibitor of ICL<sub>1</sub> forming a covalent adduct with Cys-191 in the ICL active site.<sup>296</sup> A covalent bond between itaconate **307** and Cys-191 was confirmed again by mass spectrometry with a mass difference of 130 amu between native and inhibited ICL<sub>1</sub>.<sup>296</sup> Covalent bond formation was again confirmed by X-ray structure analysis (Figure 5.23).



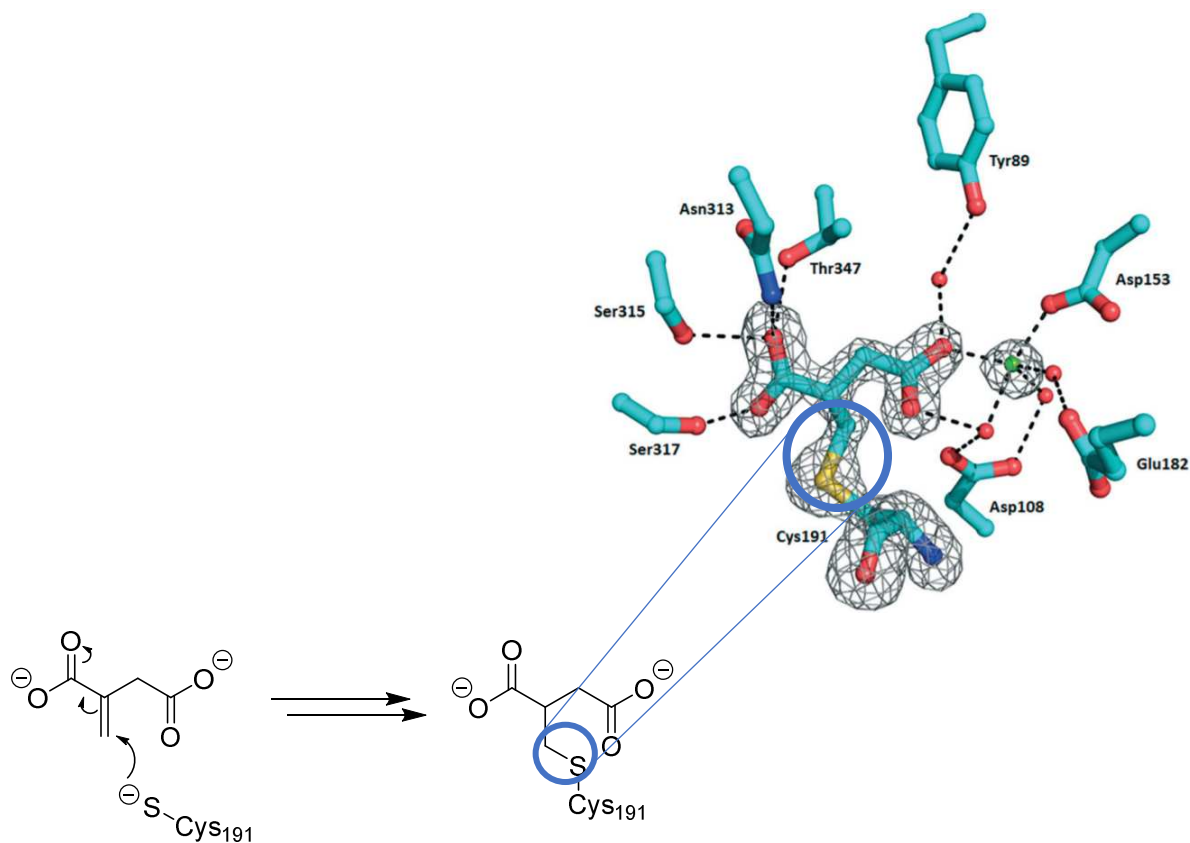
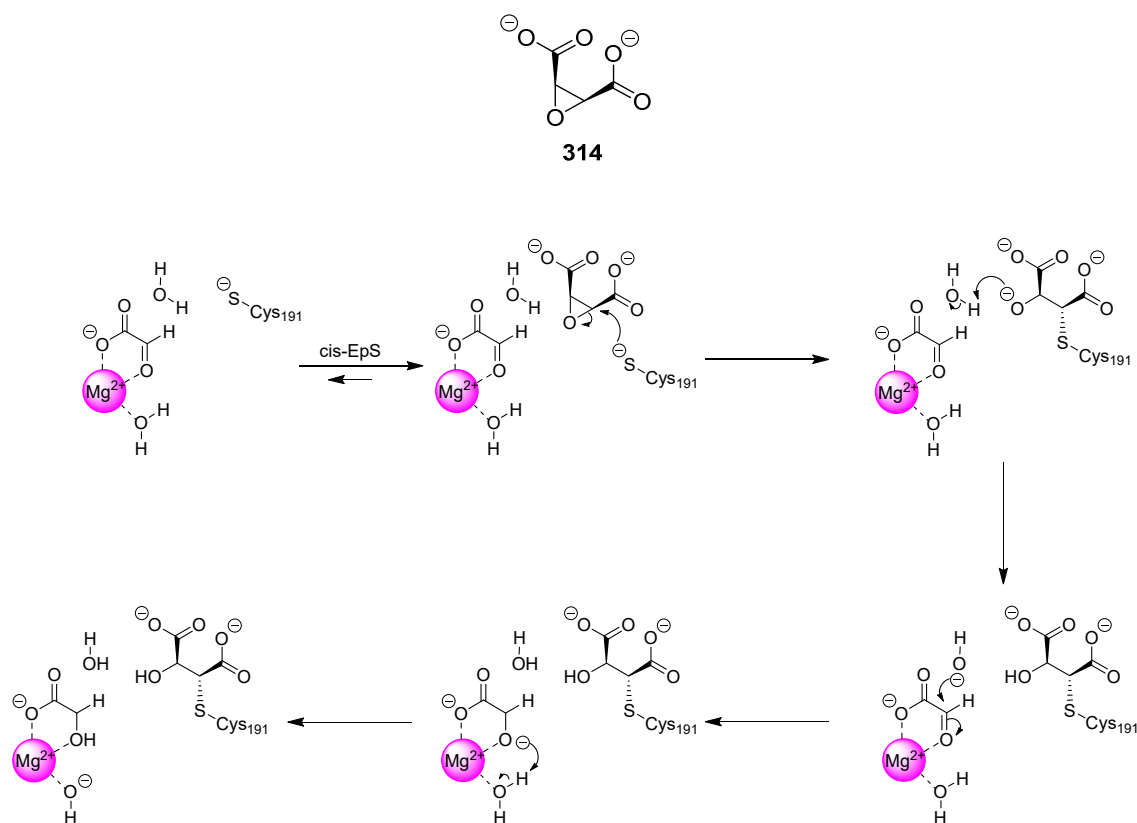


**Figure 5.23** X-Ray structure of the ICL<sub>1</sub> active site showing the covalent adduct of **307** bound to Cys-191.<sup>297</sup>

Further study highlighted the implication of glyoxalate towards formation of the covalent adduct. The hypothesis was that itaconate (analogue of succinate), in the presence of glyoxalate, may facilitate the formation of the covalent adduct with ICL. This study showed that glyoxalate did increase the rate of covalent adduct formation with ICL but did not impact the binding affinity of itaconate in the active site. It was concluded that glyoxalate may help to lock a favoured orientation of itaconate for covalent adduct formation, while in the absence of glyoxalate itaconate might bind in multiple orientations and with a reduced capacity to inhibit ICL.<sup>296</sup> Formation of the covalent adduct was slow with only 50% formed after 75 min of incubation and with full conversion requiring 5 h.<sup>296</sup>

Finally, in 2021, another succinate analogue *cis*-2,3-epoxy-succinate **314** was shown to be a mechanism-based inactivator of ICL forming a covalent adduct to the Cys-191 residue (Scheme 5.5).<sup>297</sup>



**Scheme 5.5** Mechanism of ICL inhibition by *cis*-2,3-epoxy-Succinate **314**.<sup>297</sup>

The *cis* configuration of the epoxide was first explored guided by the activity of maleate, which proved to be more potent than the *trans* isomer, fumarate. Epoxide **314** was found to be an irreversible time-dependent inhibitor of ICL, with better affinity observed with ICL<sub>1</sub> compared to ICL<sub>2</sub>.<sup>297</sup> Epoxide **314** was also shown to be 35 times more potent than 3-bromopyruvate and 750 times more potent than the initial mechanism-based inhibitor 2-VIC **310**.<sup>289,297</sup> The covalent bond between **314** and Cys-191 was again confirmed by mass spectrometry showing a difference in the mass of ICL<sub>1</sub> of 132 amu before and after inhibition.<sup>297</sup> A covalent bond was identified too by X-ray crystallography of the enzyme (Figure 5.24).

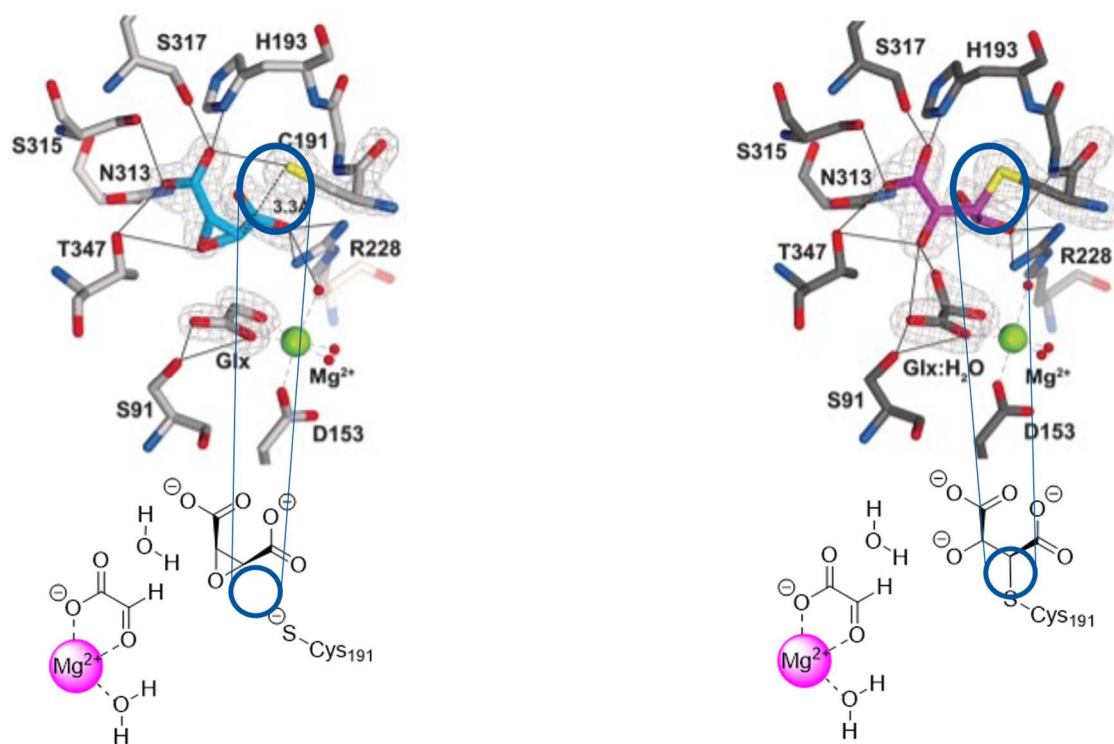
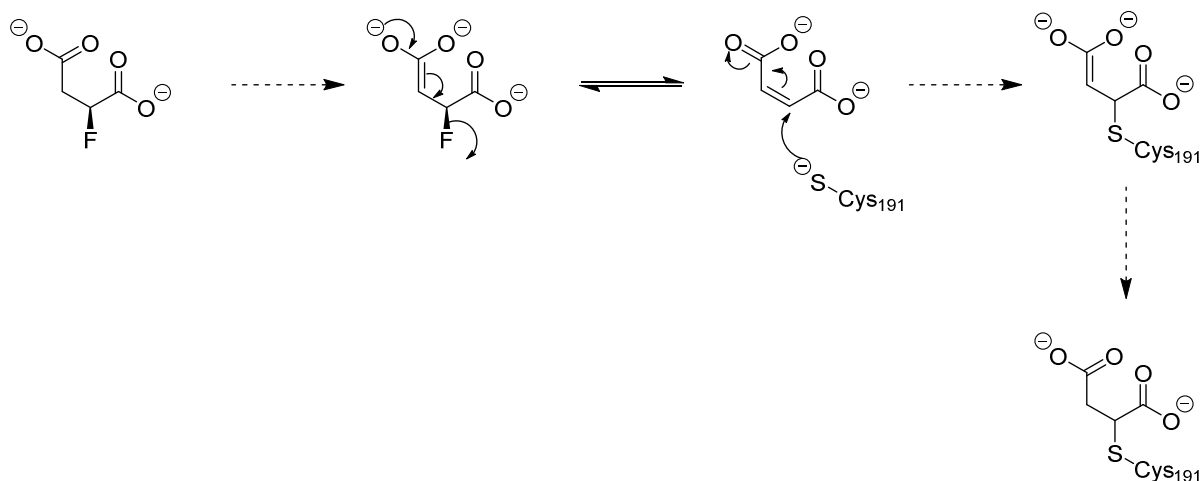


**Figure 5.24** Crystal structure of ICL showing **314** covalently bound into the active site through Cys-191.<sup>297</sup>

## 5.2. Synthesis and assay of potential inhibitors

Considering the structures over-viewed above it appeared that fluorinated succinate derivatives may act as mechanism-based inhibitors of ICL. This would require elimination of HF and then conjugate addition of the thiol of Cys-191. A putative mechanism is illustrated in Scheme 5.6.

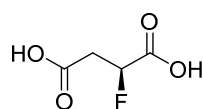


**Scheme 5.6** Putative mechanism for inhibition of ICL with a mono fluorosuccinic acid.

The project aimed to prepare some selectively fluorinated succinic acids for assay with ICL to determine their potency, if any, as inhibitors.

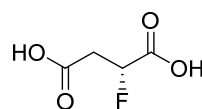
### 5.2.1 Synthesis of fluorosuccinic acid targets

In this project different synthesis routes were explored to the fluorosuccinic acids (**S**)-**315**, (**R**)-**315**, **316** and **317**, as potential ICL inhibitors (Figure 5.25).



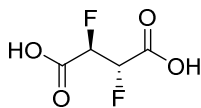
(S)-315

(S)-2-fluorosuccinic acid



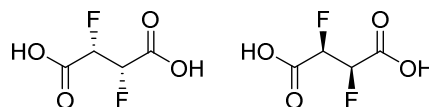
(R)-315

(R)-2-fluorosuccinic acid



316

*meso erythro*-(2*R*,3*S*)-2,3-difluorosuccinic acid



317

racemic *threo*-2,3-difluorosuccinic acid

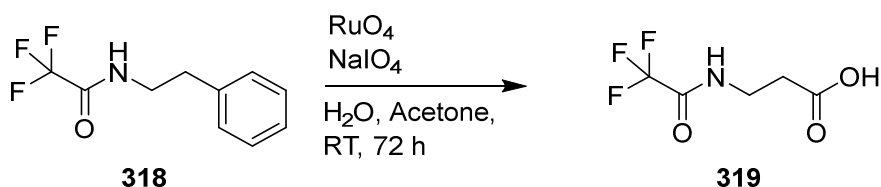
### Scheme 5.25

### Target fluorosuccinic acids 315 – 317

For the synthesis of the two mono fluorosuccinic acids (*S*)-315 and (*R*)-315, the strategy involved an asymmetric  $\alpha$ -fluorination of an aryl-aldehyde, using the MacMillan protocol discussed in Chapter II. This would then be developed by a subsequent oxidation of both the  $\beta$ -fluoro alcohol moiety and the aryl ring to the terminal carboxylic acid moieties using ruthenium tetroxide ( $\text{RuO}_4$ ) as an exhaustive oxidising reagent.

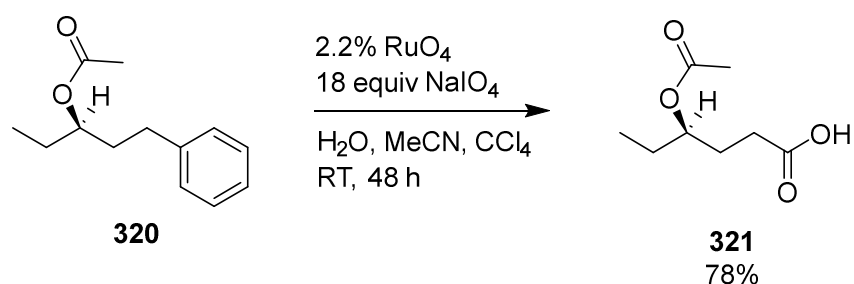
For the synthesis of *erythro*-316 and *threo*-2,3-difluorosuccinic 317 acids, the strategy was taken from previous work in the group by Martin Schueler (St Andrews Ph.D, 2006) starting from the difluorination of stilbene followed by the oxidation of the both phenyl rings with  $\text{RuO}_4$  as the oxidation agent.

$\text{RuO}_4$  is an oxidant in organic chemistry that was investigated as a replacement of osmium tetroxide in 1953 by Djerassi *et al.*<sup>298</sup> Since its discovery it has been widely used for the oxidation of many chemical groups such as olefins, diols, cyclic allylic alcohols, unsaturated ketones, oxidation of primary alcohols and finally exhaustive oxidation of phenyl groups to carboxylic acids (Scheme 5.7).<sup>299</sup>



**Scheme 5.7** Example of an early phenyl oxidation with  $\text{RuO}_4$  and  $\text{NaIO}_4$ , reported in 1984 by Hill *et al.*<sup>299</sup>

Sharpless *et al.*<sup>300</sup> explored the oxidation of aryl rings to afford carboxylic acids with catalytic  $\text{RuO}_4$  in stoichiometric  $\text{NaIO}_4$  in 1981, however the reaction proved challenging due to the sluggishness in reoxidising the reduced  $\text{RuO}_4$  with periodate, as the periodate was insoluble in organic solvents. To solve the problem they carried out a biphasic study using, water, tetrachloromethane and acetonitrile as solvents.<sup>300</sup> Acetonitrile was used due to the ability of nitrile groups to resist oxidation and its ability in ligating lower valent transition metals.<sup>300</sup> There was no conversion to carboxylic acids observed without acetonitrile.<sup>300</sup> In the study on aryl oxidation of **320** to afford carboxylic acid **321**, there was no impact on the stereogenic center in progressing from substrate to product (Scheme 5.8).<sup>300</sup>



**Scheme 5.8** Oxidation of **320** to afford carboxylic acid **321** reported by Sharpless *et al.* in 1981.<sup>300</sup>

Nowadays the oxidation of aryl groups to carboxylic acids is still widely used. The ruthenium tetroxide is now generally generated *in situ* from ruthenium trichloride ( $\text{RuCl}_3$ ) and sodium metaperiodate as the co-oxidant.<sup>301,302</sup> Also tetrachloromethane has been

replaced, for the most of recent syntheses, by dichloromethane to reduced the hazardous aspect of the solvent.<sup>301,302</sup>

### 5.2.1.1 Mono fluorosuccinic acids

Mono fluorosuccinic acids (*S*)-**315** and (*R*)-**315** were developed starting from optimised MacMillan<sup>114</sup>  $\alpha$ -fluorination of aldehydes developed in Section 2.3.<sup>112</sup>

Here the synthesis started from phenylpropanal **164**. Accordingly, aldehyde **164** was fluorinated using MacMillan catalyst (*S*)-**Cat** (for the synthesis of (*S*)-**315**) and (*R*)-**Cat** (for the synthesis of (*R*)-**315**) (Figure 5.26), with NFSI **62** as the electrophilic fluorination reagent. Reactions were stirred overnight at -10°C (Scheme 5.9).

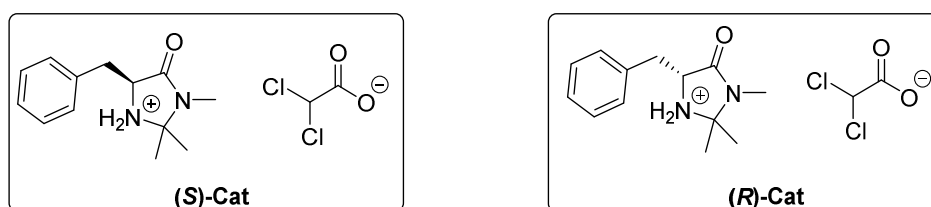
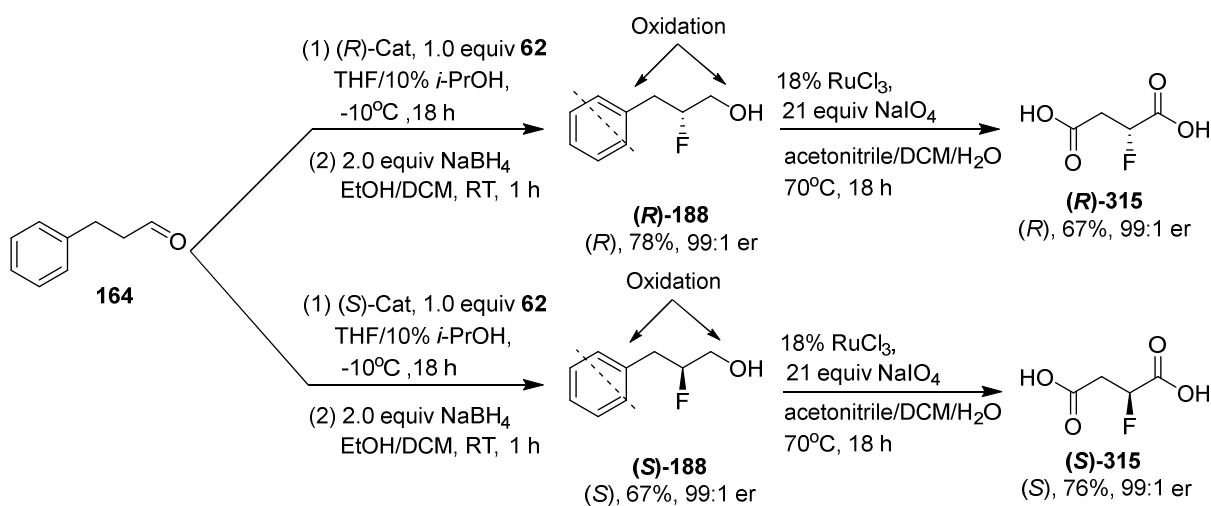


**Figure 5.26** MacMillan catalysts (*S*)-**Cat** and (*R*)-**Cat**.

After a quick work up, due to the instability of the  $\alpha$ -fluoroaldehydes, the crude product was reduced with NaBH<sub>4</sub> at 0°C for 1h and was then quenched with ammonium chloride solution.  $\beta$ -Fluoroalcohols (*R*)-**188** and (*S*)-**188** were recovered after chromatography in 78% yield and 99:1 er for (*R*)-**188** and 67% yield and 99:1 er for (*S*)-**188** (Scheme 5.9).



**Scheme 5.9** Synthetic route to (*R*) and (*S*)-2-fluorosuccinic acids.

The enantiomeric ratios were determined using the <sup>19</sup>F{<sup>1</sup>H}-NMR experiment described in Section 2.4. In Figure 5.26, two <sup>19</sup>F{<sup>1</sup>H}-NMR spectra are illustrated for both enantiomers (**R**)-**188** and (**S**)-**188** after addition of 10 equivalent of L-lactic acid **189**. Only one isomer could be observed in each case. A third experiment was carried out with a mixture of both enantiomers showing a clear resolution of the <sup>19</sup>F{<sup>1</sup>H}-NMR signals indicating that the L-lactic acid experiment is able to resolve the enantiomers. (Figure 5.26). This <sup>19</sup>F{<sup>1</sup>H}-NMR indicates with a good degree of confidence that (**R**)-**188** and (**S**)-**188** are enantiomerically pure.



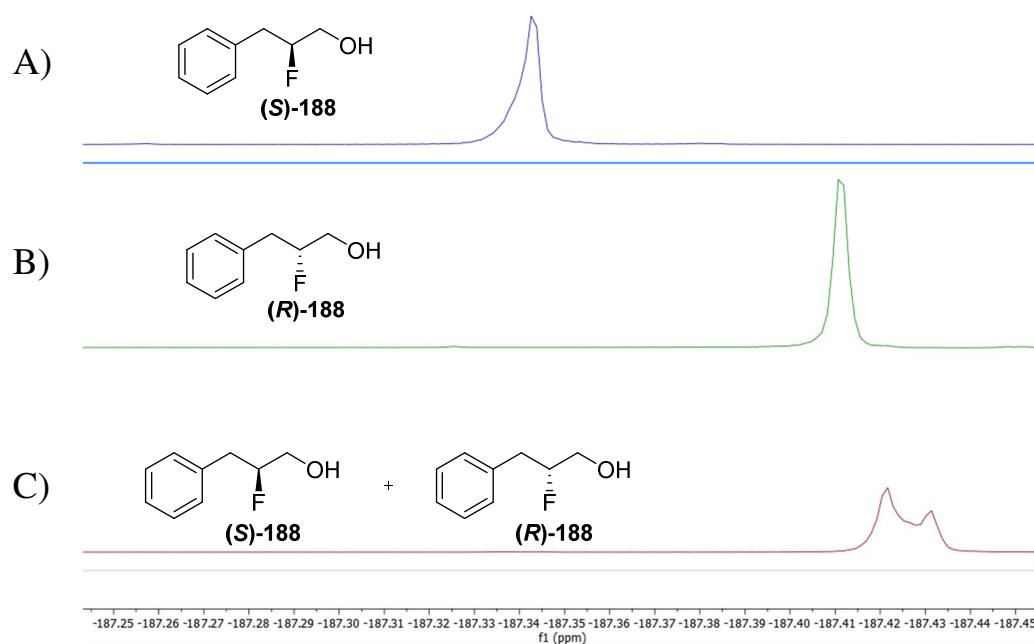


**Figure 5.26**  $^{19}\text{F}\{^1\text{H}\}$ -NMR of : **A)** (*S*)-2-Fluoro-3-phenylpropan-1-ol (**S**)-**188** with 10 equiv. of L-lactic Acid **189** ; **B)** (*R*)-2-fluoro-3-phenylpropan-1-ol (**R**)-**188** with 10 equiv. of L-lactic acid **189** ; **C)** (*R*)-2-fluoro-3-phenylpropan-1-ol (**R**)-**188** + (*S*)-2-fluoro-3-phenylpropan-1-ol (**S**)-**188** with 10 equiv. of L-lactic acid **189**.

The resultant fluoro alcohols were then exhaustively oxidised with  $\text{RuCl}_3$  and  $\text{NaIO}_4$ , in a biphasic solution of acetonitrile, water and dichloromethane, and the reactions were stirred overnight at  $70^\circ\text{C}$  to generate (**S**)-**315** and (**R**)-**315**. This is a biphasic reaction where the periodate oxidises  $\text{RuCl}_3$  to  $\text{RuO}_4$ . The  $\text{RuO}_4$  is soluble in the organic solvent and acts to oxidise the organic substrate, and when it becomes reduced, the  $\text{RuO}_2$  returns to the aqueous phase, where it is reoxidised to  $\text{RuO}_4$  again. The oxidation step simultaneously oxidises the phenyl group and the alcohol to carboxylic acids (Scheme 5.9). After purification by sublimation, (*S*)-2-fluorosuccinic acids (**S**)-**315** was afforded in a 67% yield, and (*R*)-2-fluorosuccinic acid (**R**)-**315** was afforded in 76% yield (Figure 5.27).



**Figure 5.27** Sublimation apparatus with (*S*)-2-fluorosuccinic acid (**S**)-**315** solid on the cold finger.

A side product was observed even after sublimation and was identified as succinic acid **195** (12.5%) (Figure 5.28). Given the observation of Sharpless *et al.*<sup>300</sup> and other reports, the enantioselectivity is assumed to be unchanged before and after oxidation.

The resultant yield was modest to good and with good enantioselectivity in each case. Exhaustive oxidation of the fluorinated products represented a direct and efficient approach to the fluoro-succinate enantiomers. This strategy managed to afford 155 mg of (*S*)-2-fluorosuccinic acid (**S**)-**315** and 144 mg of (*R*)-2-fluorosuccinic acid (**R**)-**315**. The resultant <sup>1</sup>H NMR of (*S*)-2-fluorosuccinic acid is shown in Figure 5.28 and confirmed the formation of the mono fluorosuccinic acid by the clear proton-fluorine coupling of <sup>2</sup>J<sub>HF</sub> = 47 Hz at 5.23 ppm, corresponding to the expected J<sup>2</sup><sub>HF</sub> coupling constant (46-50 Hz).<sup>303</sup> For the diastereotopic protons at 3.00 ppm, corresponding to the protons vicinal to fluorine, The <sup>3</sup>J<sub>HF</sub> values are 24.8 Hz and 6.6 Hz, both in the expected range (21-27 Hz, and 9-6 Hz). These protons have separate signals within this ABX system, but they are overlapping (Figure 5.28).<sup>303</sup>

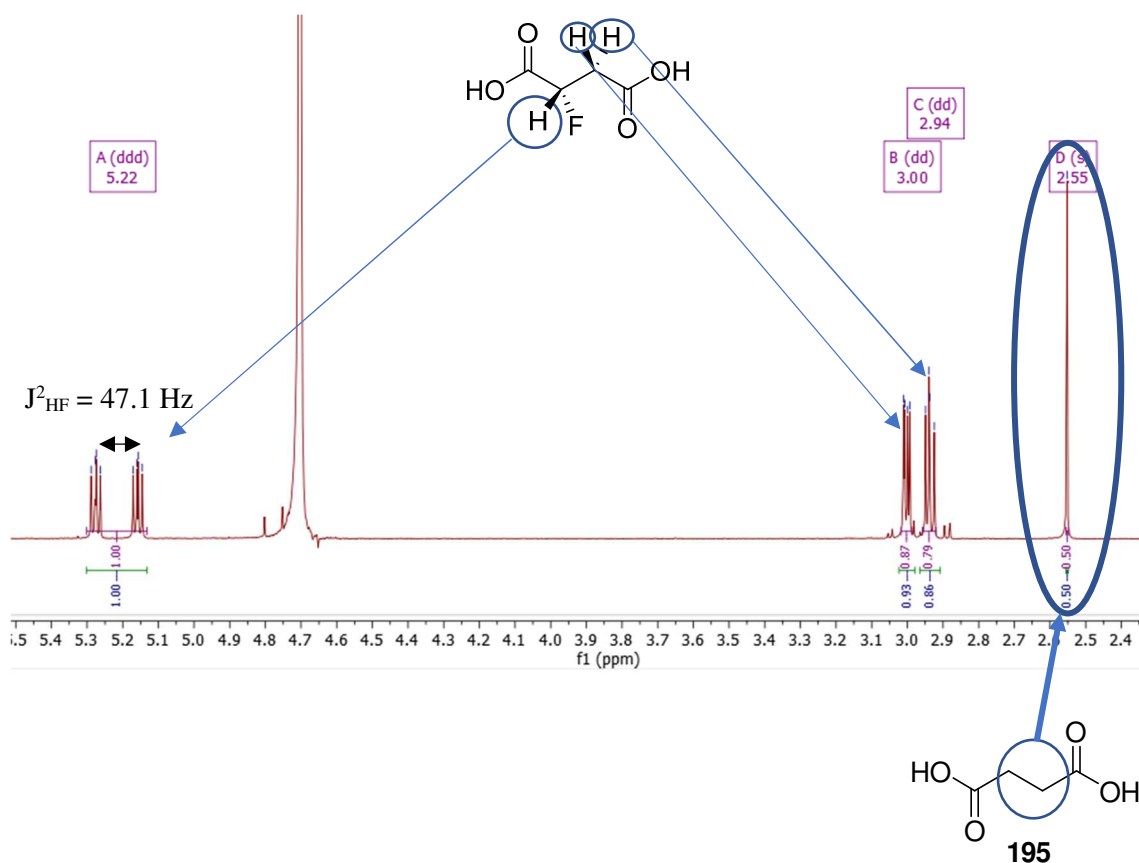
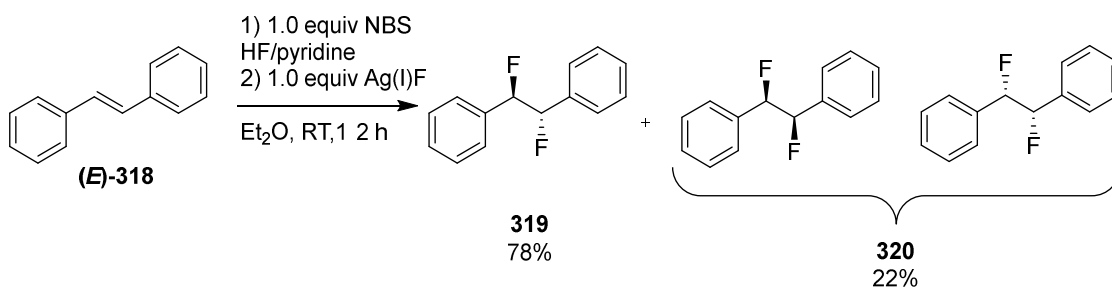


**Figure 5.28**  $^1\text{H}$  NMR of  $(S)$ -2-fluorosuccinic acid (**S**)-**315** in  $\text{D}_2\text{O}$  also highlighting the side product succinic acid **195**.

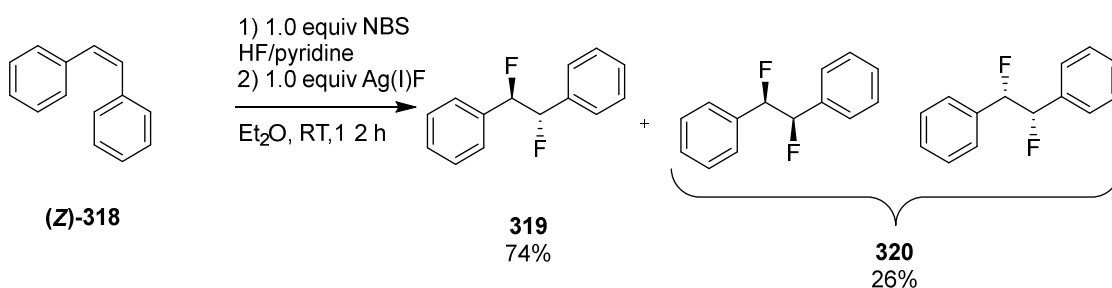
### 5.2.1.2 Difluorosuccinic acids

With the mono fluorosuccinic acid enantiomers  $(S)$ -**315** and  $(R)$ -**315** in hand, the focus of the project moved to the synthesis of *erythro*-2,3-difluoro-succinic acid **316**. This compound had previously been prepared in the group (Martin Schueler PhD, 2006). The strategy started from a one pot difluorination procedure of  $(E)$ -stilbene (**E**)-**318**, using *N*-bromosuccinamide with Olah's reagent, and then stirring for 12 h at room temperature. This was followed by the addition of silver fluoride and again the reaction was left for another 12 h at RT (Scheme 5.10). This procedure afforded the two diastereoisomers **319** and **320** (78:22).<sup>304</sup> Isomer **319** was isolated from **320** by multiple recrystallisations in methanol and petroleum ether.<sup>304</sup>



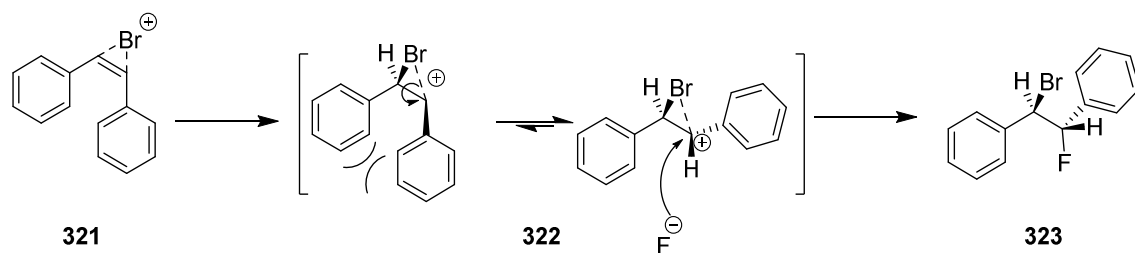
**Scheme 5.10** Difluorination of (*E*)-stilbene (**(E)-318**) to stereoisomers of *erythro*-1,2-difluoro-1,2-diphenylethane **319** and *threo*-**320**.<sup>304</sup>

An alternative approach was taken to obtain isomer **320**, by replacing (*E*)-stilbene (**(E)-318**) with (*Z*)-stilbene (**(Z)-318**) (Scheme 5.11).



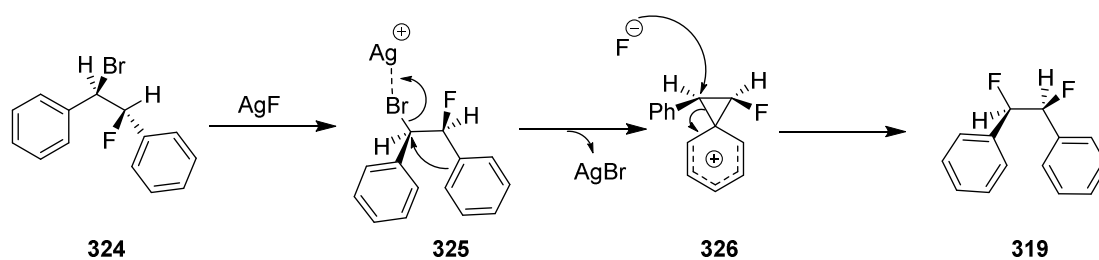
**Scheme 5.11** Difluorination of (*Z*)-stilbene (**(Z)-318**) to stereoisomers of *erythro*-1,2-difluoro-1,2-diphenylethane **319** and *threo*-**320**.<sup>304</sup>

Again, the major product obtained was **319**, but the ratio (74:26) showed a slightly higher production of isomer **320**. The constant bias toward the formation of **319** can be explained by internal rotation of the central C-C bond caused by the steric repulsion of the phenyl groups, after the formation of bromonium ion **321** (Scheme 5.12).<sup>304</sup> The carbocation is shielded on one side by bromine forcing fluoride attack to the opposite face to generate **323** (Scheme 5.12).<sup>304</sup>



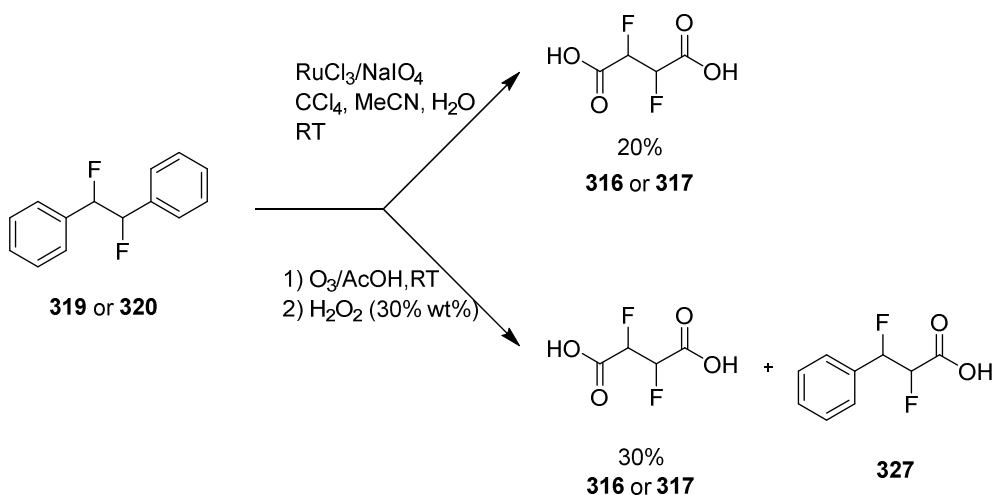
**Scheme 5.12** Proposed mechanism of bromofluorination of (*Z*)-stilbene **321** following an *anti* addition mechanism to generate **323**.

The bromine in **323** is then activated by silver cations to form complex **324** which evolves to the stabilised phenonium ion **325**, and fluoride will then attack from the top face affording isomer **319** (Scheme 5.13).<sup>304</sup>



**Scheme 5.13** Proposed mechanism of *erythro* **319** formation from intermediate **323**.

The difluoro isomers **319** and **320** were then oxidised to afford the difluorosuccinic acids **316** or **317**, but it was observed that only partial conversion of the starting materials 2,3-difluoro-1,2-diphenylethane (**319** or **320**) had occurred, with the formation of unidentified side products (Scheme 5.14).



**Scheme 5.14** Synthesis of 2,3-difluorosuccinic acids **316** or **317** by oxidation of 2,3-difluoro-1,2-diphenylethane (**319** or **320**).<sup>304</sup>

The reaction produced a lot of solid waste because of the loading of NaIO<sub>4</sub> (30-40 equiv.). After several unsuccessful attempts at purification by sublimation, it was decided to move to a different oxidation strategy.<sup>304</sup> The alternative strategy involved ozonolysis (Scheme 5.14). This ozonolysis strategy worked previously for Schueler on both isomers **319** and **320** with a yield of 45% for *erythro*-2,3-difluorosuccinic acid **316** and 30% for *threo*-2,3-difluorosuccinic acid **317**.<sup>304</sup> In light of these previous results it was decided to explore the same approach.

A first reaction involved treating (*E*)-stilbene (*E*)-**318** with HF/pyridine, N-bromosuccinamide and silver fluoride to afford **320**. The results obtained were similar to that reported by Schueler, and with a similar ratio of isomers (77:23) (Figure 5.29, A). Both isomers were isolated after recrystallisation in methanol and followed by a second recrystallisation from petrol to afford pure *erythro*-**319** (Figure 5.29, B).

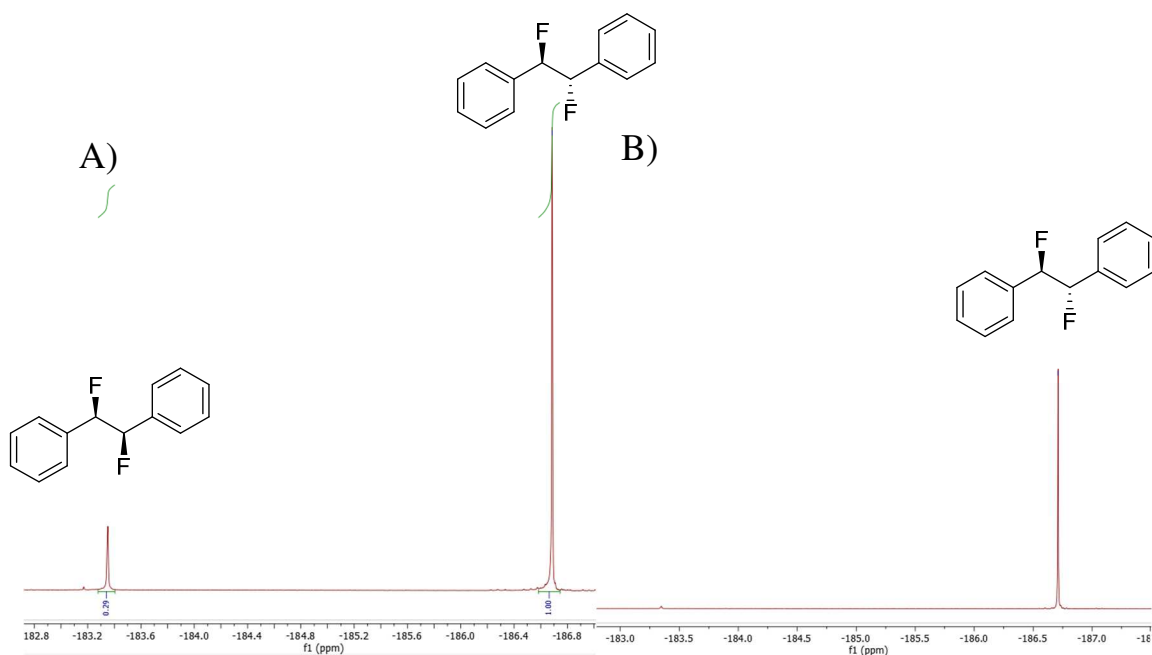
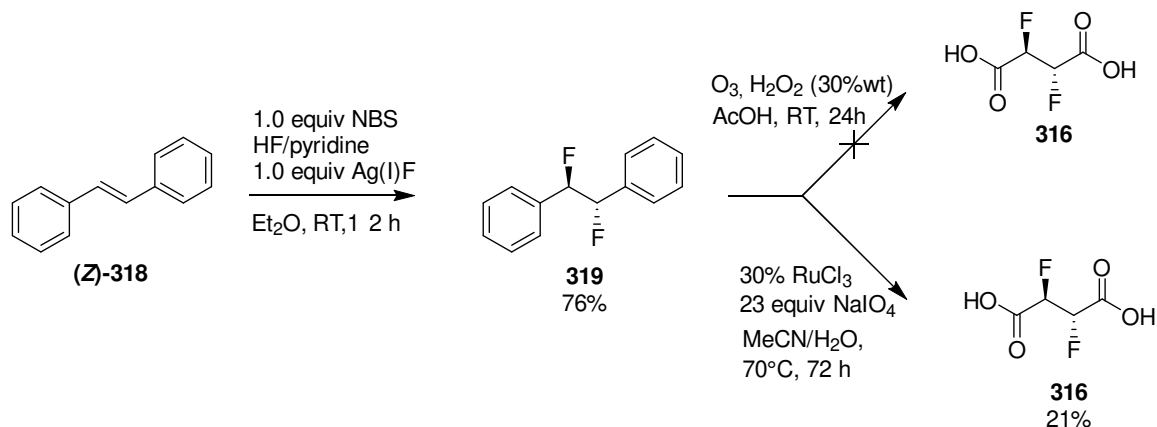


**Figure 5.29** A)  $^{19}\text{F}\{^1\text{H}\}$ -NMR before separation of the major *erythro*-1,2-difluoro-1,2-diphenylethane **319** from *threo*-1,2-difluoro-1,2-diphenylethane **320** (77:23); B)  $^{19}\text{F}\{^1\text{H}\}$ -NMR of recrystallised *erythro*-1,2-difluoro-1,2-diphenylethane **319**.

An attempt was then made to oxidise the phenyl groups with ozone to afford **316** (Scheme 5.15) as described by Schueler *et al.* Unfortunately, the oxidation with ozone caused elimination of the fluorines. As an alternative approach aryl oxidation with  $\text{RuCl}_3/\text{NaIO}_4$  was explored, following our experience with aryl oxidations to access the mono fluoro-succinic acids (Scheme 5.15).



**Scheme 5.15** Synthesis approaches of *erythro*-2,3-difluorosuccinic acid **316**.

This proved successful with a yield of 21%; however, a major side product was observed at 2.00 ppm (Figure 5.30).

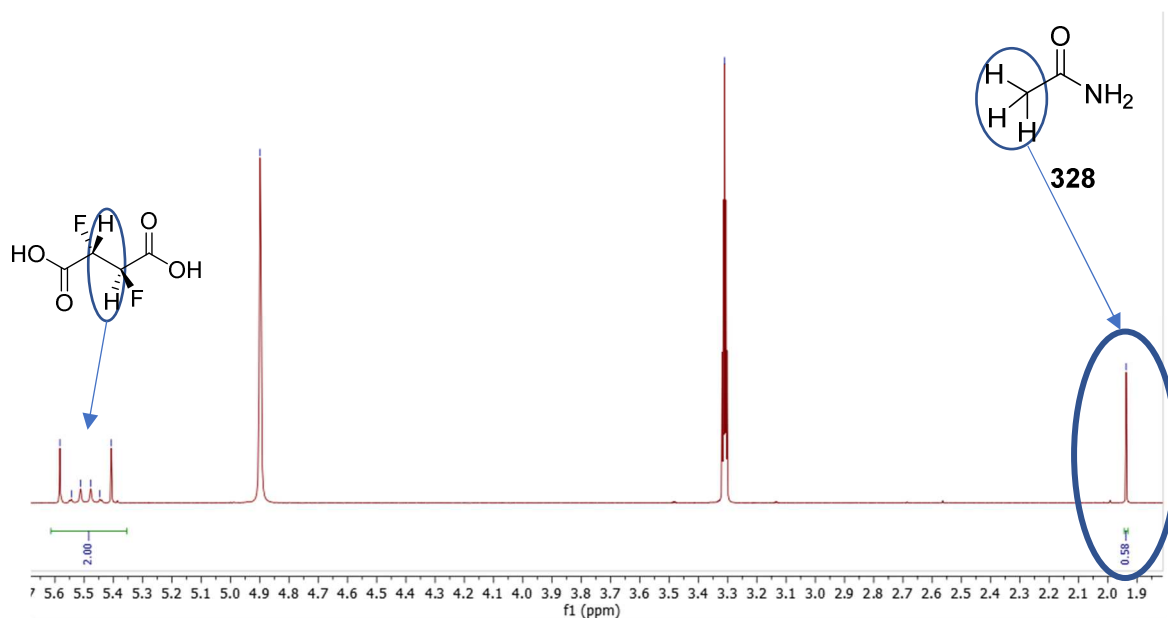
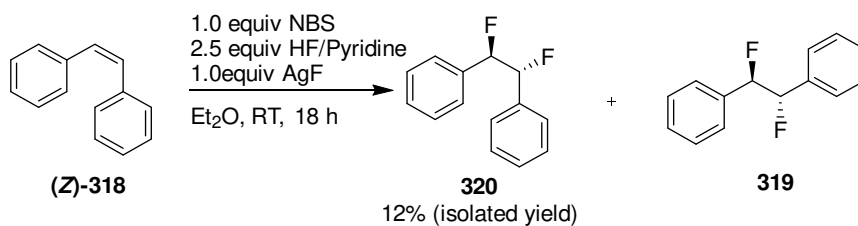


**Figure 5.30** <sup>1</sup>H NMR of isolated *erythro* 1,2-difluorosuccinic acid **316** highlighting a contamination with acetamide **328**.

The side product was identified as acetamide **328** (19%) and can be explained by the hydrolysis of acetonitrile to acetamide under the conditions. Despite many attempts to separate acetamide from the succinic acid *via* sublimation, the acetamide formed a thick stable paste containing *erythro*-2,3-difluorosuccinic acid **316**, and could not be removed.

With *erythro*-2,3-difluorosuccinate in hand, the project moved to the synthesis of *threo*-2,3-difluorosuccinic acid. This is more challenging in terms of stereochemistry as the *threo* isomer has two enantiomers and if the synthesis is successful both enantiomers will result. Also, any ideal route required to be free of any co-formed *erythro* isomer. The route began from the (*Z*)-stilbene (**Z**)-**318** instead of the (*E*)-stilbene (**E**)-**318** (Scheme 5.16) in order to prepare the desired diastereoisomeric series.





**Scheme 5.16** Difluorination of (*Z*)-stilbene (**(Z)-318**) that lead to *erythro* and *threo* (70:30) isomers of **320** and **319**.

Again, the ratio of the two isomers was identical to that observed by Schueler *et al.* (69:31) (Figure 5.31, A).

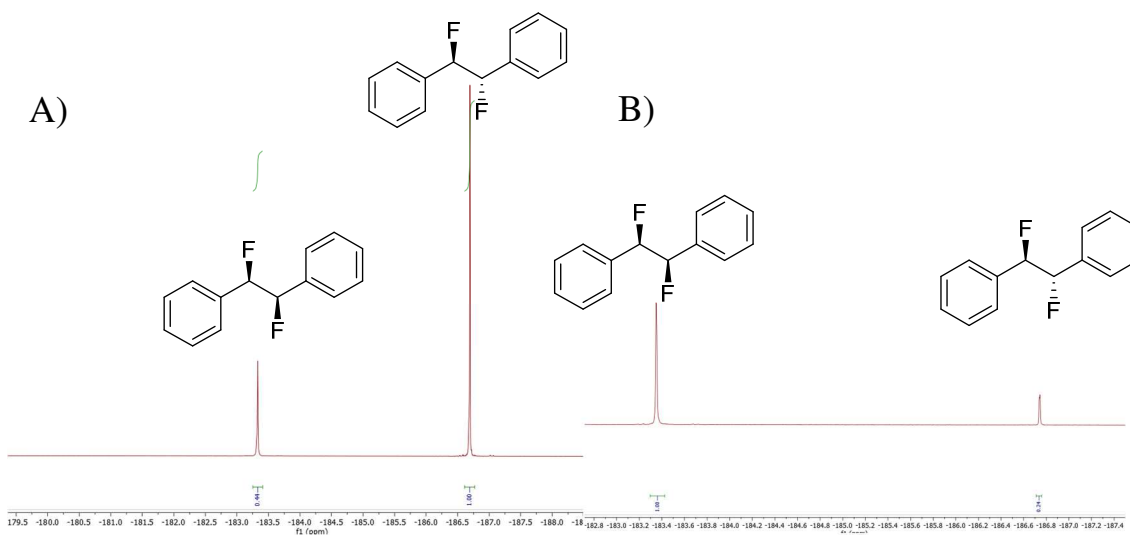


**Figure 5.31** **A)** <sup>19</sup>F{<sup>1</sup>H}- NMR after difluorination of (*Z*)-stilbene (**(Z)-318**) showing product ratios. **B)** <sup>19</sup>F{<sup>1</sup>H}- NMR after recrystallisation of **320** showing an improved *threo* ratio (41:59).

Purification of the *threo*-**320** from the *erythro*-**319** isomer involved recrystallisation in methanol. The filtrate contained more *threo* (60%) than *erythro* (40%) showing a slight improvement of the ratio before crystallisation that contained 31% of *threo* and 69% of *erythro* (Figure 5.31, B). The crystals obtained after recrystallisation contained only the *erythro*-**319** isomer. The 40:60 ratio mixture (Figure 5.31, B), was purified by column chromatography using hexane and ethyl acetate as eluant, again this purification helped to significantly reduce the *erythro*-**319** isomer giving a ratio of 25:75 in favour of *threo*-**320** (Figure 5.32).

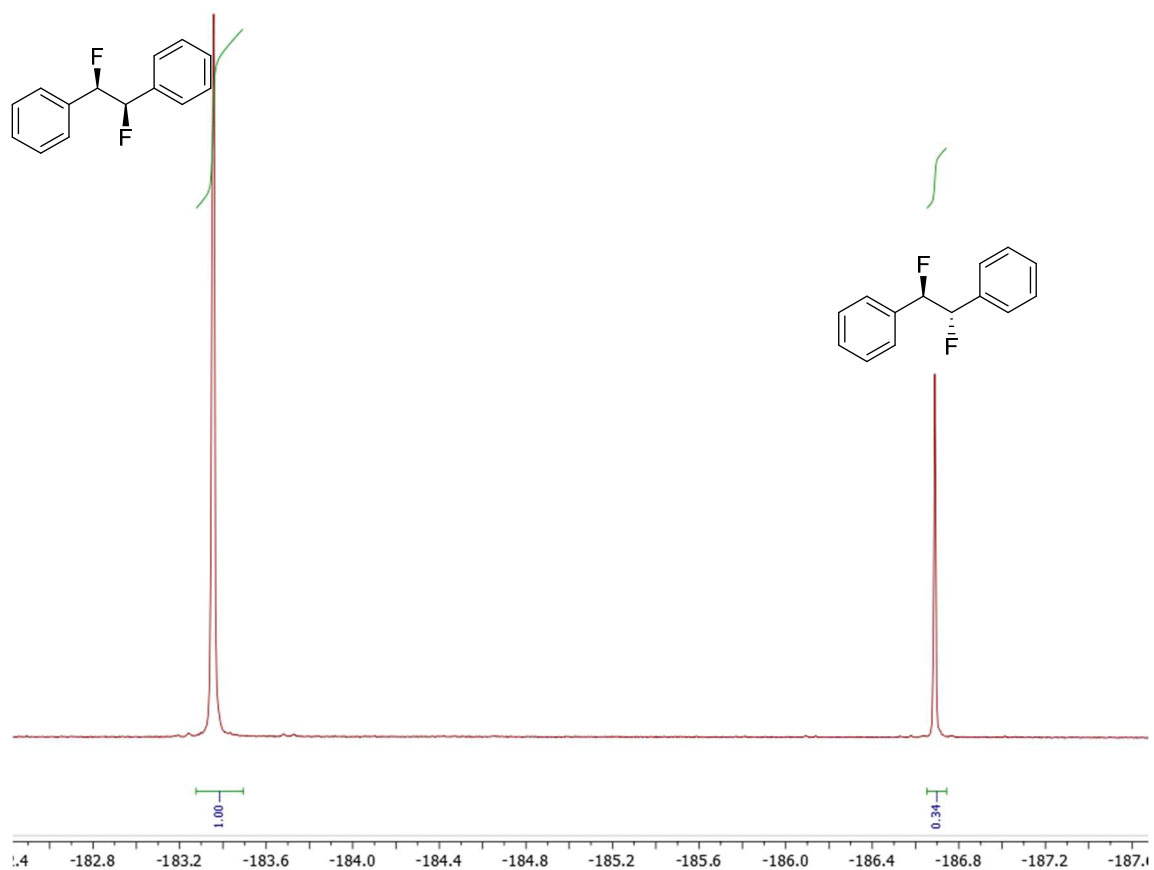


**Figure 5.32**  $^{19}\text{F}\{^1\text{H}\}$ NMR after chromatography gave an improved *threo*- **320** to *erythro*-**319** ratio (41:59).

Finally the *threo* product **320** was recrystallised in hexane and afforded a yellow amorphous solid and with an improvement in the isomer ratio (**319:320** : 20:80) (Figure 5.33).

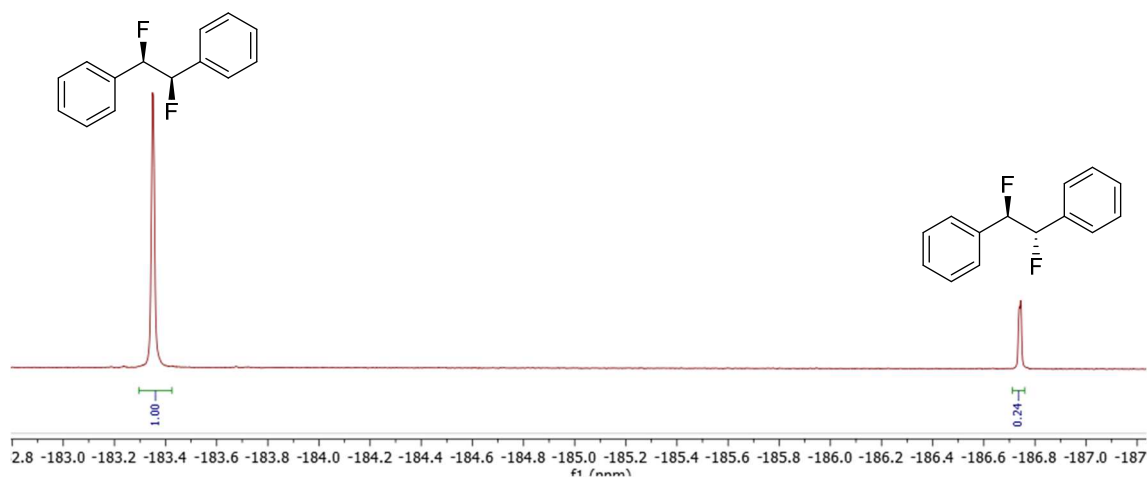
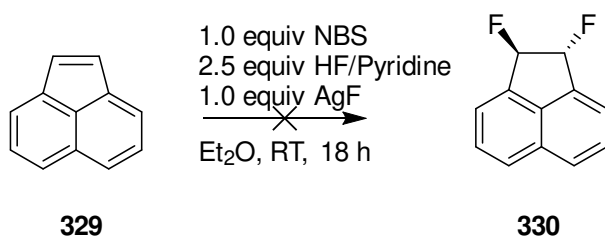


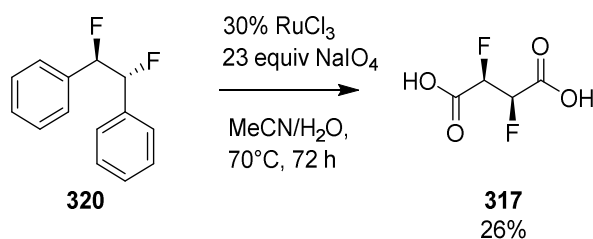
**Figure 5.33**  $^{19}\text{F}\{^1\text{H}\}$ -NMR after recrystallisation in petroleum ether showing an improved ratio toward *threo*-1,2-difluoro-1,2-diphenylethane **320** (20:80).

However, each purification process led to a significant decrease in material recovery, and this became a challenge. In order to improve the overall recovery of **320** an alternative route was explored with acenaphthylene **329** (Scheme 5.17).



**Scheme 5.17** Approach to isomer **330** from acenaphthylene **329**.

The idea behind using acenaphthylene **329** was to avoid C-C rotation during the bromination step (Scheme 5.12) to afford *threo*-**330** and avoid the production of any *erythro* isomer. Unfortunately, no conversion was observed while using acenaphthylene **329**.



**Scheme 5.18** Oxidation of *threo*-1,2-difluoro-1,2-diphenylethane **320** to *threo*-2,3-difluorosuccinic acid **317**.

In the final step *threo*-**320** was oxidised with RuCl<sub>3</sub>, NaIO<sub>4</sub> to obtain the desired *threo*-2,3-difluorosuccinic acid **317** (Scheme 5.18) in a similar yield (26%) to that for the synthesis of *erythro*-2,3-difluorosuccinic acid **316**. This oxidation proved to be successful with a yield of 26%; however, the production of acetamide was observed (59%) in the mixture (Figure 5.34) and again this resulted in a viscous liquid, and it proved impossible to purify by sublimation or any other method.

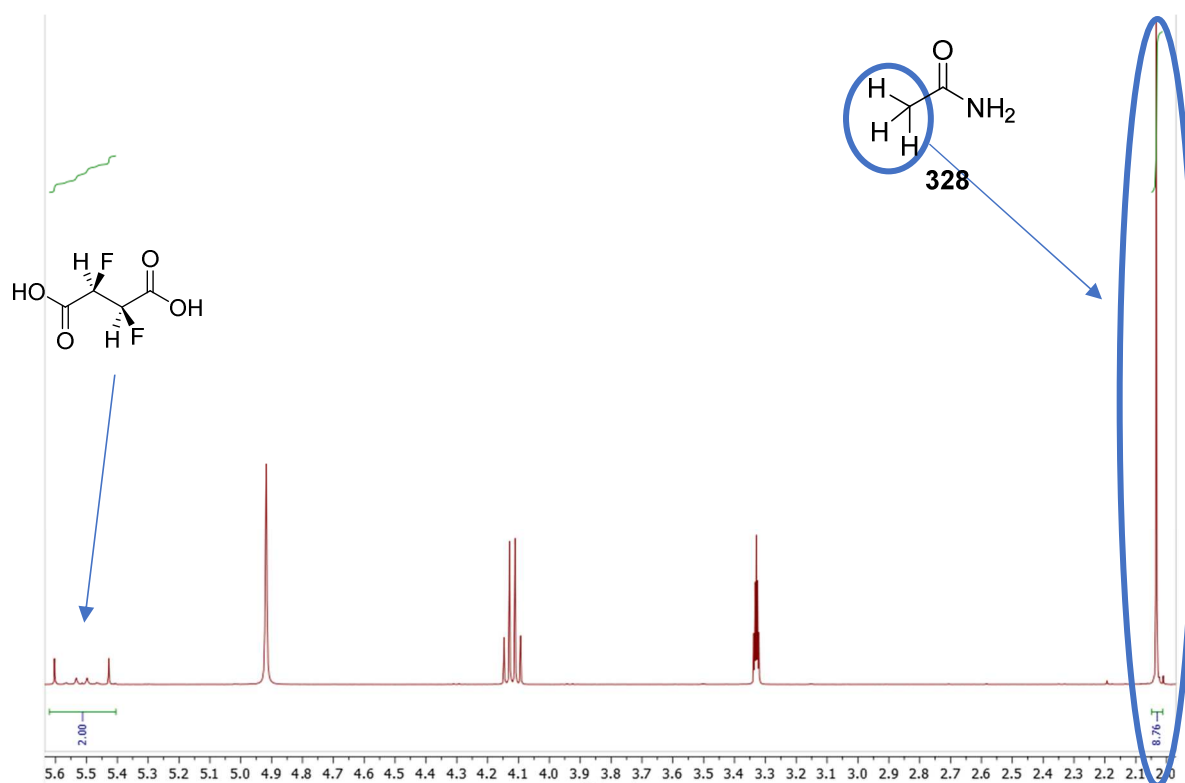


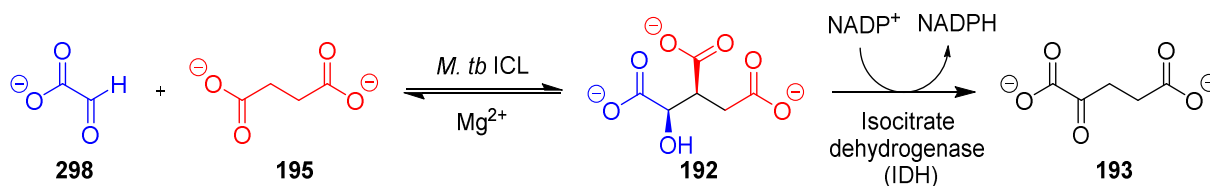
**Figure 5.34** <sup>1</sup>H NMR of isolated *threo*-1,2-difluorosuccinic acid **317** highlighting the contamination with acetamide **328**.

In conclusion the synthesis of *erythro*-1,2-difluorosuccinic acid **316** was accomplished in an overall yield of 16%. However, the synthesis of *threo*-1,2-difluorosuccinic acid **317** was less successful, as fluorination gave a mixture of diastereoisomers which needed to be separated from contaminating acetamide. In addition, the *threo*-1,2-difluorosuccinic acid **317** product was racemic. Thus, this last compound was not progressed to ICI assays.

### 5.3. ICL assay experiments

#### 5.3.1. Enzyme assay of (S)/(R)-2-F-succinic acids

Following the synthesis of the two mono fluorosuccinic acids (**S**)-**315** and (**R**)-**315**, the two enantiomers were assayed at the University at Buffalo in the laboratory of Prof. Andrew Murkin. An ICL-IDH (Scheme 5.19) coupled assay was conducted varying (**R**)-2-fluorosuccinate (**S**)-**315** or (**S**)-2-fluorosuccinate concentrations (**R**)-**315** (0.02 – 0.2 mM). ICL were coupled to IDH for two reasons, first as IDH has a higher rate than ICL leading to the direct consumption of the D-isocitrate **192** produced to  $\alpha$ -ketoglutarate **193** (when the concentration of IDH is in excess to the concentration of ICL). Secondly IDH is an enzyme that requires the reduction of NADP<sup>+</sup> to NADPH, and this can be followed in real time by UV. The production of NADPH correlates to the production of  $\alpha$ -ketoglutarate. The reaction was initiated using ICL (50 nM) and the change in absorbance at 340 nm was measured for 40 mins.



**Scheme 5.19** ICL-IDH Coupled assay is followed by NADPH formation at 340 nm.

In this assay, the better the inhibitor the less NADPH and  $\alpha$ -ketoglutarate **193** is produced. In the event both enantiomers proved to be inhibitors with similar magnitudes in each case. Figure 5.35 illustrates reactivity profiles, with 50, 100 and 150  $\mu$ M concentration of each inhibitor. The inhibition of the enzyme was evaluated over 30 min. For the (**S**) enantiomer inhibition started around 2.20 min, whereas for the (**R**) enantiomer the inhibition started around 3.45 min. Clearly both fluoro-succinate enantiomers are time dependant inhibitors with the (**S**) enantiomer (**S**)-**315** showing a moderately better inhibition profile.

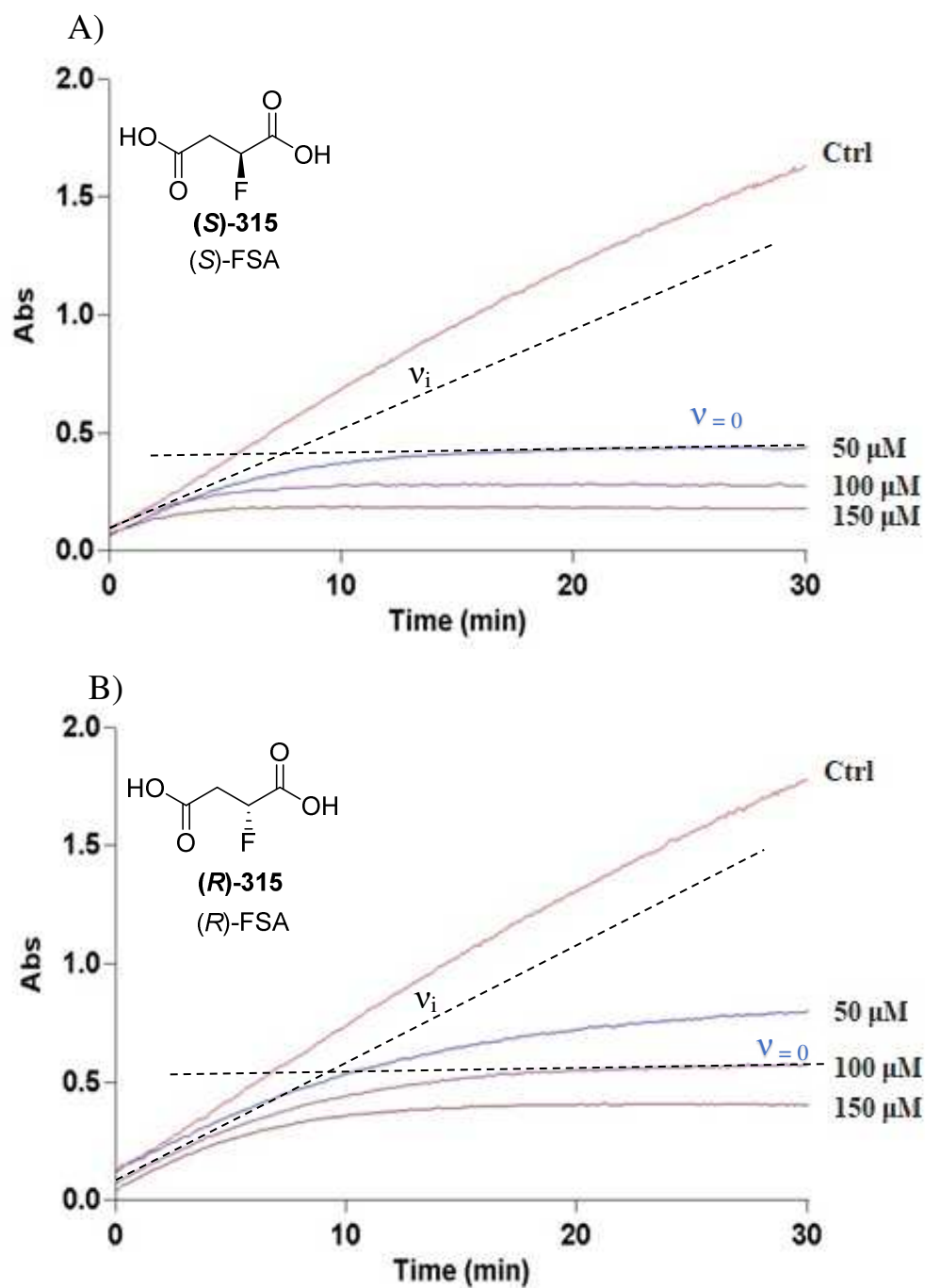


**Figure 5.35** A) Absorbance at 340 nm versus time for the continuous monitoring of the ICL-IDH coupled assay at 1 mM succinate, varying : **A)** (*S*)-2-fluorosuccinate concentrations **(S)-315**. ; **B)** (*R*)-2-fluorosuccinate **(R)-315** concentrations. With the initial rate ( $v_i$ ) and  $v$  the rate of the enzymatic reaction over time.

Figure 5.35, illustrates that the reaction is completely inhibited by (*S*)-**315** at 50  $\mu\text{M}$  (Figure 5.35, A) and (*R*)-**315** at 100  $\mu\text{M}$  (Figure 5.35, B). There is no recovery of the enzyme activity with time demonstrating that both of these fluorosuccinic acids are irreversible inhibitors of ICL. Full inhibition of the enzyme was observed at 1mM for both enantiomers as illustrated in Figure 5.36.

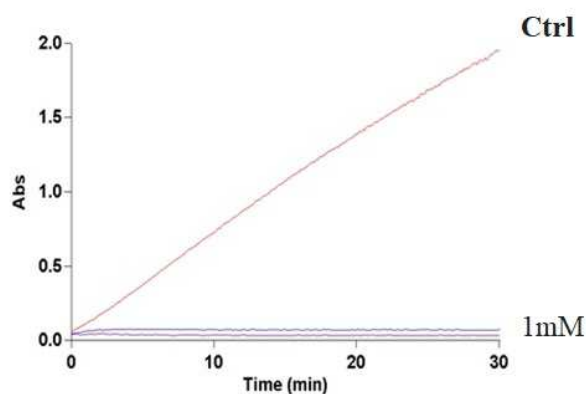


**Figure 5.36** Absorbance at 340 nm versus time for the continuous monitoring of the ICL-IDH coupled assay 1 mM succinate concentrations for both mono fluorosuccinates (*S*)-**315** and (*R*)-**315** at 1 mM concentration.

A difference in potency is also observed in the data in Figure 5.37, where  $k_{obs}$  is the observed rate of inhibition, confirming an inactivation potency of (*S*)-2-F-succinic acid (*S*)-**315** of  $53.3 \text{ M}^{-1} \cdot \text{s}^{-1}$  versus (*R*)-2-F-succinic acid (*R*)-**315** at  $20.0 \text{ M}^{-1} \cdot \text{s}^{-1}$ .



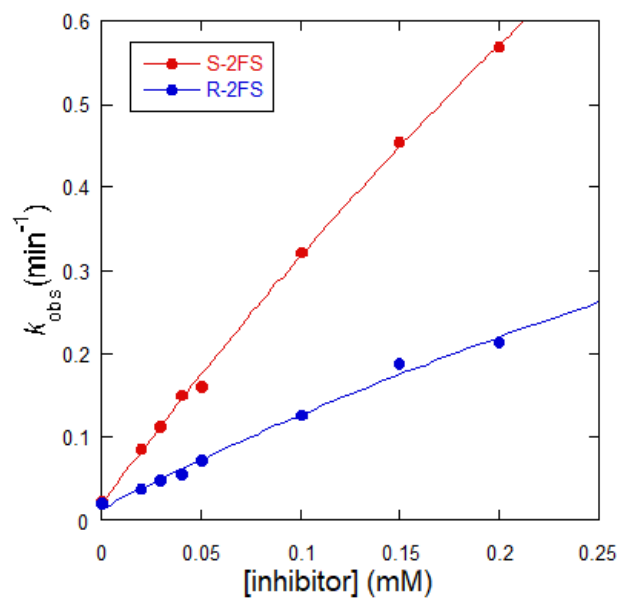


**Figure 5.37** Rate ( $k_{obs}$ ) versus inhibitor concentration of (*S*)-2-fluorosuccinate (**S**-315 (red)) and (*R*)-2-fluorosuccinate (**R**-315 (blue)).

It became an objective to determine the binding mode of inhibition. Itaconate **307** and *cis*-2,3-epoxy-succinic acid **314** are already known to be covalent inhibitors, as previously discussed (Section 5.1.2.2.).<sup>296,297</sup> In that context the reaction products were examined by <sup>1</sup>H-NMR and maleate was observed to accumulate in the incubations (Figure 5.38).

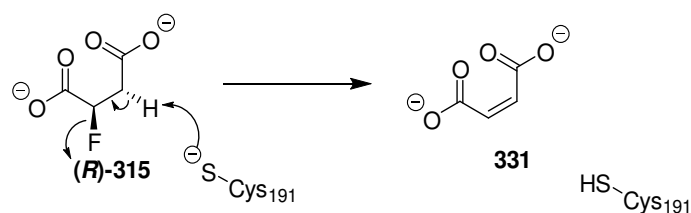
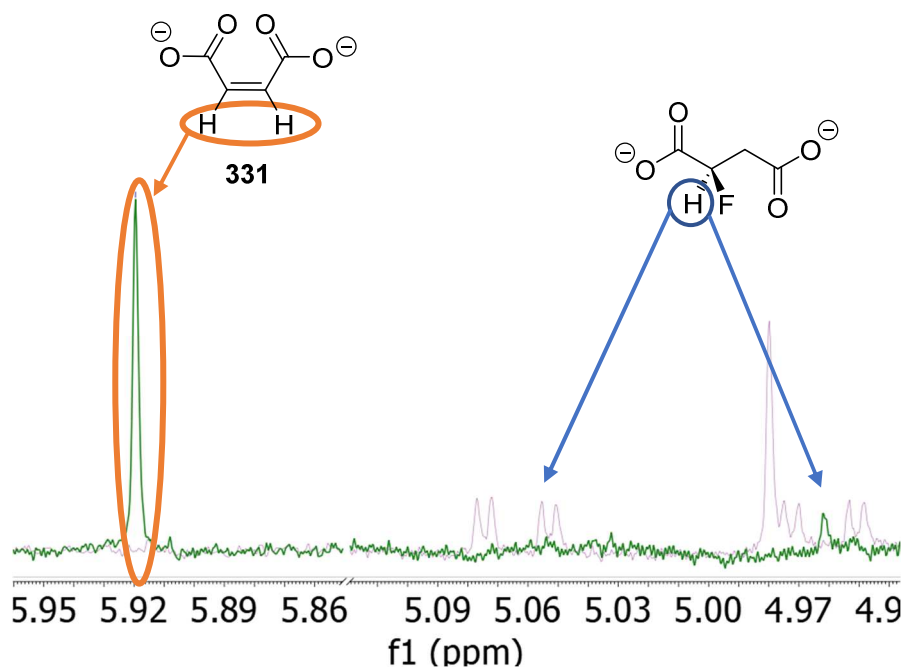


**Figure 5.38** (Blue)  $^1\text{H}$  NMR of ICL + (*R*)-2-fluorosuccinate before incubation (*R*)-**315**. (Green)  $^1\text{H}$  NMR after 9h at  $37^\circ\text{C}$  of ICL + (*R*)-2-fluorosuccinate (*R*)-**315** incubation showing the formation of maleate **331**.

Previous studies from Murkin and co-worker on maleate proved that maleate is a slow time dependant irreversible inhibitor of ICL that forms a covalent adduct with the enzyme. The binding mode of maleate was determined *via* mass spectrometry analysis and showed a mass increase of the enzyme corresponding to maleic acid (116 amu). However, despite the presence of maleate in the assay, there was no such ion in the mass spectrum of the isolated enzyme. Confusingly there was some indication of a mass ion at with an increase of 132 amu. One formal possibility is a maleate adduct (+116) and then an oxygen atom (+16), although this does not fit any obvious structure. Perhaps a sulfoxide of the adduct formed during manipulation, although this remains speculative and the origin may be an artefact, which remains to be resolved (Figure 5.39).

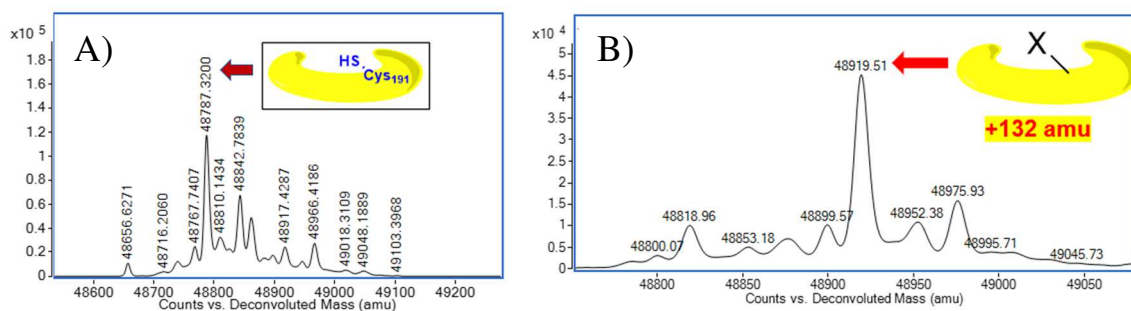


**Figure 5.39** Mass Spec of : **A)** ICL before introduction of (*R*)-2-fluorosuccinate or (*S*)-2-fluorosuccinate; **B)** ICL after introduction of (*R*)-2-fluorosuccinate or (*S*)-2-fluorosuccinate showing a mass increase of 132 amu confirming the formation of a covalent adduct.

### 5.3.2. Enzyme assay of *erythro*-2,3-difluorosuccinic acid

The sample of *erythro*-2,3-difluorosuccinic acid **316** had an acetamide contamination, therefore at the outset it was important to determine that acetamide **328** did not influence inhibition of the enzyme. This was determined by combining ICL-IDH and acetamide with glyoxalate and succinate. First the control contained 1mM of glyoxalate and succinate with 10 nM of ICL, second test contained the same concentration of ICL, succinate and glyoxalate and with 3 mM of acetamide. The results highlighted in Figure 5.40 shows no evidence of any inhibition as the rate of change of absorbance measured does not change.

Reagents	Concentrations	
	Control (1)	Test (2)
Succinate 195	1 mM	1 mM
Glyoxalate 298	1 mM	1 mM
Acetamide 328	0	3 mM
ICL	10 nM	10 nM
IDH	300 nM	300 nM

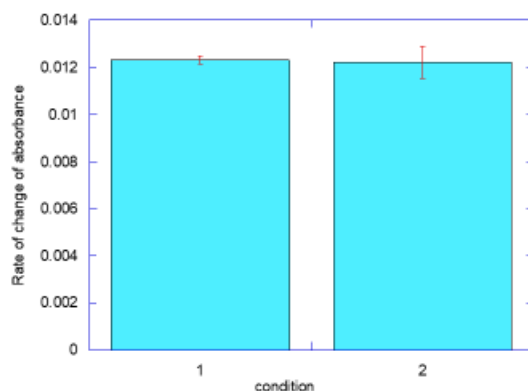


**Figure 5.40** Assay on ICL-IDH system to study acetamide inhibition, showing no impact of acetamide on ICL activity.

*Erythro*-2,3-difluorosuccinate **316** was explored as an inhibitor of ICL in the D-isocitrate synthesis direction. This was conducted by carrying out the ICL-IDH coupled assay and following the reduction of NADP<sup>+</sup> (2 mM) by monitoring at 340 nm. The reaction was initiated by adding 10 nM ICL and the concentrations of *erythro*-2,3-difluorosuccinate studied were between 0.05-1.0 mM.

*Erythro*-2,3-difluorosuccinate **316** proved to be a relatively poor inhibitor with almost no inhibition at 0.05 mM. There is clear inhibition at higher concentrations; however, even at 1 mM the enzyme retained some activity (Figure 5.41). It is clear from the assay that *erythro*-2,3-difluorosuccinate **316** is a much poorer inhibitor than the monofluorosuccinate enantiomers.

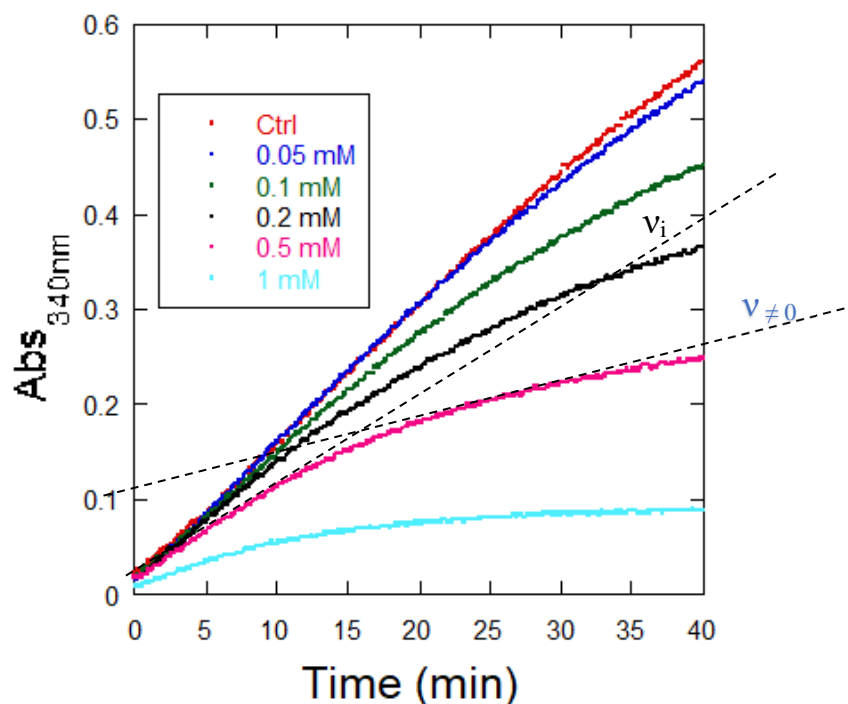


**Figure 5.41** Graph of absorbance at 340 nm versus time (min) for ICL-IDH coupled assay at a fixed concentrations of succinate and varying the *erythro*-2,3-difluorosuccinate **316** concentration.

As for the mono fluorosuccinate, the plot of the absorbance over time gives information regarding the binding mode of *erythro*-2,3-difluorosuccinate (Figure 5.41). Here we cannot observe the velocity of the enzymatic reaction reaching 0 ( $v \neq 0$ ) even at the highest inhibitor concentration of 1mM. This suggests that the enzyme is able to recover over time from any inhibition, with dissociation of the inhibitor from the enzyme active site. Accordingly, it is deduced that *erythro*-2,3-difluorosuccinate **316** is a slow reversible inhibitor of ICL.

The  $k_{obs}$  rate was plotted against the concentration of *erythro*-2,3-difluorosuccinate (Figure 5.42). The hyperbolic shape of the curve indicates that although **316** does not form a covalent adduct with the enzyme, it shows some inhibitory interaction.

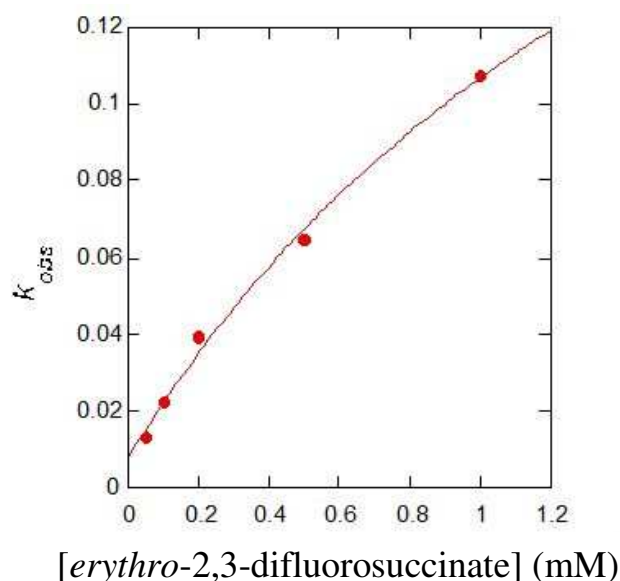


**Figure 5.42** Graph of  $k_{obs}$  obtained from ICL-IDH coupled assay versus *erythro*-2,3-difluorosuccinate **316** concentration.

Figure 5.43 represent a double reciprocal plot for *erythro*-2,3-difluorsuccinate **316** constructed from initial rates of inhibition with varying succinate and inhibitor concentrations. This graph gives two important insights for each of the systems observed. First when the straight line function crosses the ordinate axes the value corresponds to  $\frac{1}{v_{max}}$  and when it crosses the absciss axes the value correspond to  $\frac{1}{Km}$ .  $K_m$ , is the Michaelis constant. It is defined as the enzyme substrate concentration where the reaction rate is at half of its maximum value ( $v_{max}$ ). If all the functions converge on the absciss axes the inhibitor is defined as non-competitive, however if they converge on the ordinate axes then whatever the concentration of the inhibitor, the enzymatic reaction has the same  $v_{max}$  showing a competitive inhibition. Finally, if the functions never converge the inhibitor is defined as uncompetitive.

In this case succinate was the substrate and *erythro*-2,3-difluorsuccinate **316** was explored as an inhibitor. The concentration of **316** was varied between 0 to 0.5 mM and the succinate concentration between 0.1 to 10 mM. It is observed in Figure 5.43 that all the functions on the graph converge on the ordinate axis. This is consistent with **316** as a competitive inhibitor of ICL.

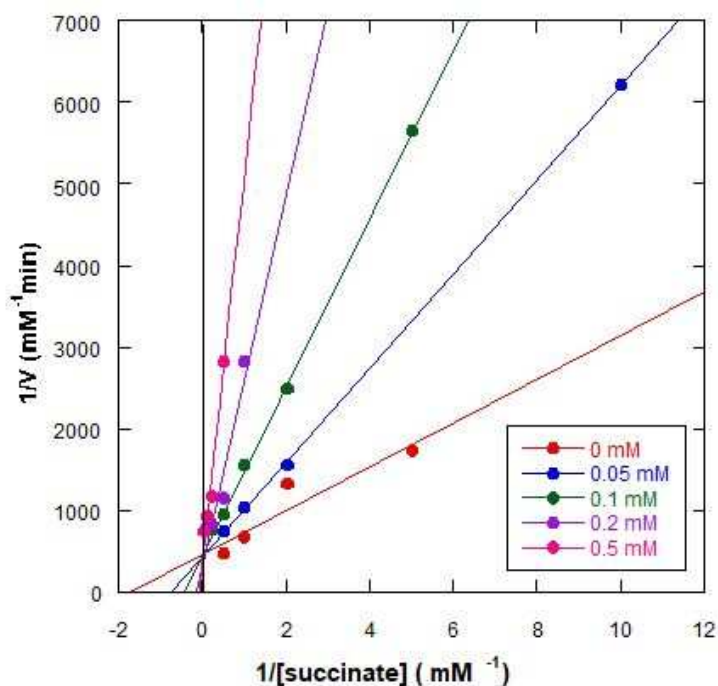
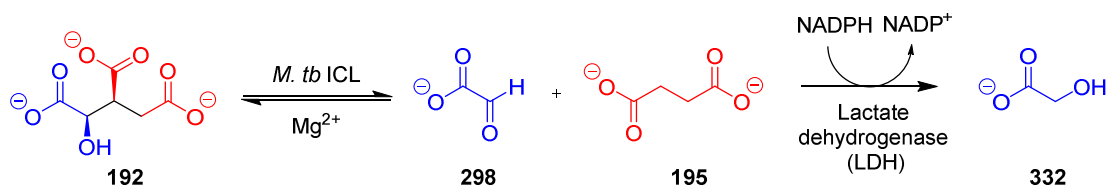


**Figure 5.43** Double reciprocal plot for *erythro*-2,3-difluorsuccinate **316** constructed from initial rates of inhibition with varying succinate and inhibitor concentrations.

Finally, to confirm previously established results with *erythro*-2,3-difluorsuccinate **316**, an ICL-LDH (Scheme 5.20) coupled assay was carried out to study the inhibition potency of **316** for the isocitrate cleavage direction. The reaction was monitored at a fixed isocitrate concentration of 2 mM. Oxidation of NADH (0.2 mM) was measured after varying the *erythro*-2,3-difluorsuccinate **316** concentrations between 0.1–2.0 mM, and following the absorbance at 340 nm. The reaction was initiated with 1 nM of ICL.



**Scheme 5.20** ICL mediated cleavage of isocitrate followed by reaction with lactate dehydrogenase (LDH), transforming glyoxalate to glycolic acid **332**.

Figure 5.44 highlights the inhibition pattern of **316** on ICL for the cleavage to isocitrate. Again **316** shows a clear but slow inhibition, and with some activity being retained at 1 mM. The concentration at which  $v \neq 0$  is not observed even at the highest inhibitor concentration (1mM). This is indicative of the enzyme's ability to recover activity and that *erythro*-difluorosuccinate **316** is a reversible inhibitor of ICL.

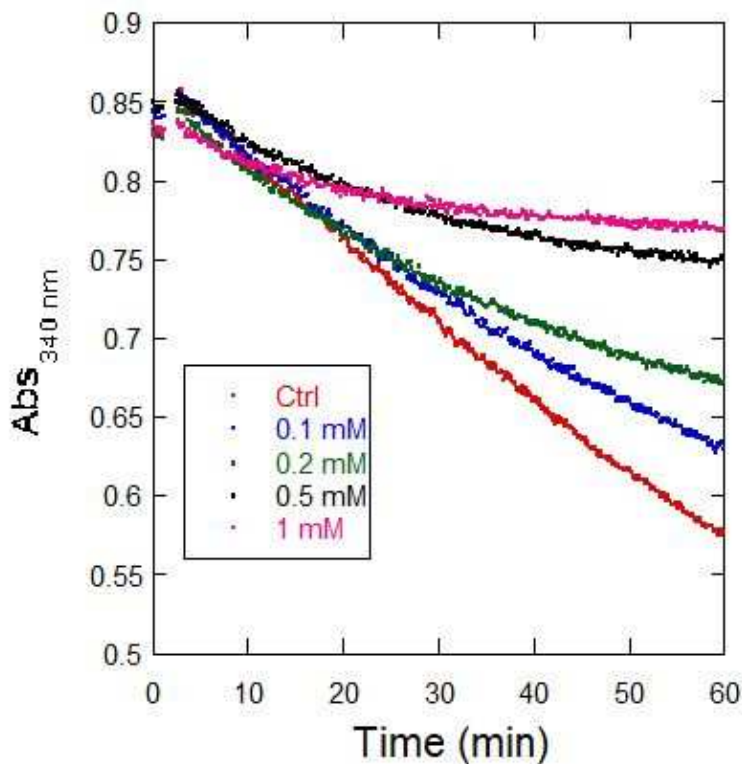


**Figure 5.44** Graph of absorbance at 340 nm versus time (min) for ICL-LDH coupled assay at a fixed concentration of isocitrate with varying *erythro*-2,3-difluorosuccinate **316** concentrations.

In overview *erythro*-2,3-difluorosuccinic acid **316** is a slow-binding reversible inhibitor of ICL, that does not create a covalent adduct with the enzyme. It has a lower inhibition potency than both monofluoro enantiomers (*S*)-**315** and (*R*)-**315**.



## 5.4. Conclusion

In conclusion, four different mono/difluorosuccinic acids were successfully synthesised. Among these four succinic acids, three ((*S*)-**315**, (*R*)-**315** and **316**) were assayed as inhibitors of isocitrate lyases at the University of Buffalo. The bioassays revealed that all three of the succinic acids are inhibitors of ICL. The most potent is (*S*)-2-F-succinic acid (*S*)-**315**. It was observed in the assay that maleate is formed, presumably by an enzyme mediated hydrogen fluoride elimination, and maleate is known to form a covalent adduct with the enzyme. The nature of any covalent adduct in these experiments have not been confirmed, although analysis is ongoing. Finally, *erythro*-2,3-difluorosuccinic acid **316** was observed to be a slow-binding reversible inhibitor of ICL but there was no evidence of covalent modification (Figure 5.45).

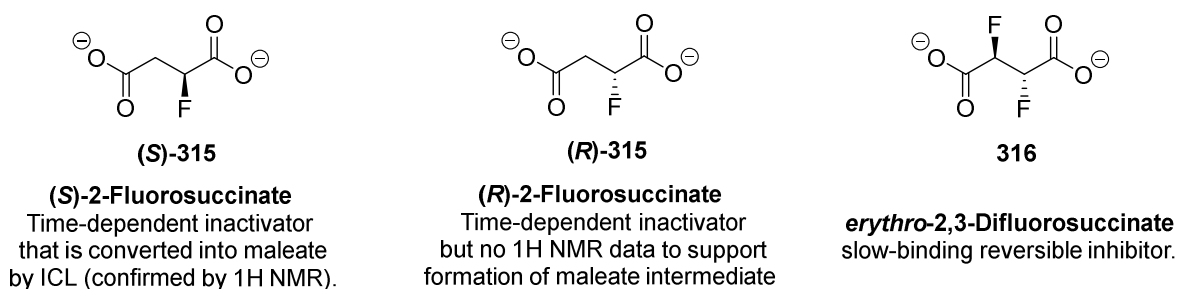


**Figure 5.45** Summary of the F-succinic acids and their modes of inhibition with ICL.

## Chapter VI Experimental

### 6.1 General experimental

All air and moisture sensitive reactions were carried out under inert atmosphere (Argon or Nitrogen atmosphere) and oven-dried glassware. Room temperature (RT) was 18-25 °C. Solvents and reagents were purchased from, Alfa Aesar, TCI, Apollo, Fluorochem, Sigma-Aldrich, and used as received. Anhydrous solvents (DCM, diethyl ether, THF) were dispensed from an MBraun MB SPS-800 solvent purification system by filtration through two drying columns under argon atmosphere. Flash column chromatography was performed using Merk Geduran silica gel 60 Å (250-400 mesh), used either on manual glass column or on Biotage Selekt 2 automatic column eluting with solvents as reported.

Melting points were recorded on an Electrothermal 9100 melting point apparatus and (dec) refers to decomposition. IR were recorded on a Shimadzu IRAffinity-1S spectrometer with a diamond ATR attachment. Spectra were recorded of either thin films or solids, with characteristic absorption wavenumbers ( $\nu_{\max}$ ) reported in  $\text{cm}^{-1}$ .

$^1\text{H}$ ,  $^{13}\text{C}$  and  $^{19}\text{F}$  Nuclear Magnetic Resonance (NMR) spectra were recorded at 298 K on a Bruker Avance 400 MHz spectrometer, at ambient temperature in  $\text{CDCl}_3$ ,  $\text{CD}_3\text{OD}$  or  $\text{D}_2\text{O}$ . Chemical shift ( $\delta$ ) are reported in parts per million (ppm), relative to the residual proton(s) of the following solvents  $\text{CDCl}_3$  (7.26 ppm for  $^1\text{H}$  and 77.00 ppm for  $^{13}\text{C}$ ),  $\text{CD}_3\text{OD}$  (3.31 ppm for  $^1\text{H}$  and 49.00 ppm  $^{13}\text{C}$ ) or  $\text{D}_2\text{O}$  (4.79 ppm for  $^1\text{H}$ ). For  $^1\text{H}$  and  $^{13}\text{C}$ , chemical shift refers to an external calibration using tetramethyl silane ( $\delta = 0.00$  ppm). For  $^{19}\text{F}$ , chemical shift refers to an external calibration using  $\text{CFCl}_3$  ( $\delta = 0.00$  ppm). Data for  $^1\text{H}$  are reported as: chemical shift, multiplicity (s = singlet, d = doublet, t = triplet, m = multiplet), coupling constants J) in Hz and integration. NMR data were processed using MestReNova 12.0.0.

Enantiomeric excess (ee) was determined with addition of 5 to 10 equivalent of L-lactic acid to the isolated compound sonicated with  $\text{CDCl}_3$  in the NMR tube. Enantiomeric excess (ee) was calculated with integration of  $^{19}\text{F}\{^1\text{H}\}$  NMR signals corresponding to both enantiomers. Diastereoisomeric excess (de) was determined by integration of the 2 diastereoisomers signal by  $^{19}\text{F}\{^1\text{H}\}$  NMR.

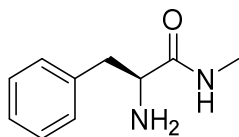
Mass Spectrometry was performed at the University of St Andrews by electrospray ionisation (ESI). Spectra were obtained by Carolyn Horsburgh at the University of St Andrews and Alan Taylor at the University of Edinburgh. Electrospray ionisation was carried out using a Micromass GCT spectrometer. Results reported in m/z values and have units of Dalton (Da).

Optical rotation was performed using a Perkin Elmer Model 341 polarimeter, values were recorded at 20°C and 589 nm using a 1 dm cell,  $[\alpha]_D^{20}$  values are reported in units of  $10^{-1} \text{ deg.cm}^2.\text{g}^{-1}$ .

Single Crystal X-Ray analysis was carried out by Dr David Cordes at University of St Andrews, using a molybdenum or copper X-Ray source. The copper X-Ray source utilised an MM-007 high-brilliance generator with an AFC/Saturn 92 detector. The molybdenum source utilised an MM-007 high-brilliance generator with VariMax optics and either an AFC/Mercury or AGC/Saturne 70 detector.

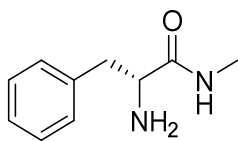
## 6.2 Synthetic procedure and characterisation of compounds

### (S)-2-Amino-N-methyl-3-phenylpropanamide (171)



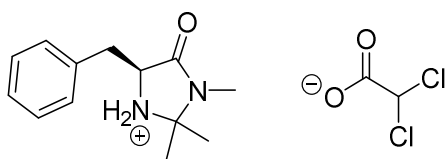
Following a procedure adapted from reference,<sup>305</sup> (*S*)-ethyl 2-amino-3-phenylpropionate hydrochloride salt **169** (1.0 equiv, 2.5 g, 11 mmol) was added to a solution of methylamine in ethanol (33%) (7.0 equiv, 95 mL, 77 mmol). The mixture was stirred for 48 h at RT. The reaction mixture was concentrated *in vacuo*. The resulting oil was then dissolved in CHCl<sub>3</sub> (50 mL), washed with saturated aqueous K<sub>2</sub>CO<sub>3</sub> (50 mL), the aqueous layer was extracted with CHCl<sub>3</sub> (3 x 50 mL) and the resulted organic layer was dried over MgSO<sub>4</sub>, filtered and concentrated *in vacuo*. This material was used without further purification. According to the reference<sup>305</sup> and the NMR data the desired product **171**, was obtained as a white solid with 95% yield (1.85 g). m.p.(Chloroform): 55 °C. [ $\alpha$ ]<sub>D</sub><sup>20</sup> -11.5 (c 0.69, CHCl<sub>3</sub>). IR  $\nu_{\text{max}}/\text{cm}^{-1}$  2822, 1735, 1498, 1228, 1209, 702. <sup>1</sup>H NMR (400 MHz, CDCl<sub>3</sub>)  $\delta$  7.20 – 7.31 (m, 5H, Ph), 3.66 (dd, *J* = 9.5, 4.0 Hz, 1H, CH), 3.28 (dd, *J* = 13.7, 4.0 Hz, 1H, CH<sub>2</sub>), 2.80 (d, *J* = 4.9 Hz, 3H, CH<sub>3</sub>), 2.72 (dd, *J* = 13.7, 9.1 Hz, 1H, CH<sub>2</sub>).

**(R)-2-Amino-N-methyl-3-phenylpropanamide (172)**



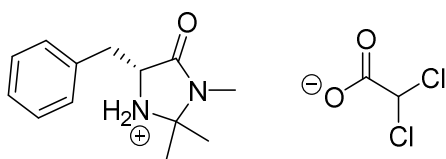
Following a procedure adapted from reference,<sup>305</sup> (*R*)-ethyl 2-amino-3-phenylpropionate hydrochloride salt **170** (1.0 equiv, 2.5 g, 11 mmol) was added to a solution of methylamine in ethanol (33%) (7.0 equiv, 95 mL, 77 mmol). The mixture was stirred for 48 h at RT. The reaction mixture was concentrated *in vacuo*. The resulting oil was then dissolved in CHCl<sub>3</sub> (50 mL), washed with saturated aqueous K<sub>2</sub>CO<sub>3</sub> (50 mL), the aqueous layer was extracted with CHCl<sub>3</sub> (3 x 50 mL) and the resulted organic layer was dried over MgSO<sub>4</sub>, filtered and concentrated *in vacuo*. This material was used without further purification. According to the reference,<sup>305</sup> and the NMR data the desired product **171**, was obtained as a white solid with 93% yield (1.81 g). m.p.(chloroform): 54 °C. [ $\alpha$ ]<sub>D</sub><sup>20</sup> +10.9 (c 0.81, CHCl<sub>3</sub>). **IR**  $\nu_{\text{max}}/\text{cm}^{-1}$  2825, 1738, 1453, 1233, 1224, 1213, 704. **<sup>1</sup>H NMR (400 MHz, CDCl<sub>3</sub>)**  $\delta$  7.34 – 7.27 (m, 2H, Ph), 7.25 – 7.19 (m, 3H, Ph), 3.68 – 3.63 (m, 1H, CH-NH<sub>2</sub>), 3.28 (dd, *J* = 13.7, 4.0 Hz, 1H, CH<sub>2</sub>), 2.80 (d, *J* = 4.9 Hz, 3H, N-CH<sub>3</sub>), 2.72 (dd, *J* = 13.7, 9.1 Hz, 1H, CH<sub>2</sub>).

**(S)-5-Benzyl-2,2,3-trimethylimidazolidin-4-one dichloroacetic acid ((S)-Cat)**



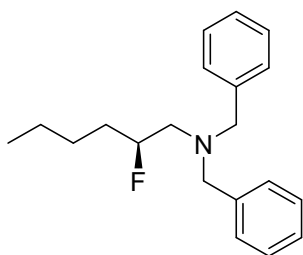
Following a procedure adapted from reference,<sup>306</sup> (S)-2-amino-N-methyl-3-phenylpropanamide **172** (1.0 equiv, 652 mg, 3.66 mmol) and *p*-toluenesulfonic acid monohydrate (10 mol%, 70 mg, 0.37 mmol) was added to anhydrous EtOH (80 mL) and anhydrous acetone (15 mL). The mixture was stirred for 18 h under reflux. The reaction was then cooled down to RT and concentrated *in vacuo*. The crude product was purified by flash column chromatography with silica gel eluting with EtOAc/acetone (1:1). The desired imidazole **173**, was obtained as a yellow oil with 85% yield (0.68 g, 3.11 mmol). The compound was then converted into a salt by addition of dichloroacetic acid (1.0 equiv, 256  $\mu$ L, 3.11 mmol), and recrystallised from DCM/petroleum ether (1:1) to afford **(S)-Cat** (1.08 g).  $[\alpha]^{20}_{\text{D}}$  -42.9 (c 0.92, CHCl<sub>3</sub>). IR  $\nu_{\text{max}}/\text{cm}^{-1}$  2988, 2361, 1720, 1651, 1591, 1427, 1369, 1240, 698. <sup>1</sup>H NMR (400 MHz, CDCl<sub>3</sub>)  $\delta$  7.15 – 7.36 (m, 5H, Ph), 3.79 (dd, *J* = 6.6, 4.5 Hz, 1H, CH), 3.15 (dd, *J* = 14.2, 4.5 Hz, 1H, CH<sub>2</sub>), 3.01 (dd, *J* = 14.2, 6.6 Hz, 1H, CH<sub>2</sub>), 2.75 (s, 3H, CH<sub>3</sub>-N), 1.26 (s, 3H, CH<sub>3</sub>), 1.16 (s, 3H, CH<sub>3</sub>). ESI-MS calculated for C<sub>13</sub>H<sub>19</sub>ON<sub>2</sub> [M+H<sup>+</sup>] = 219.1492, observed [M+H<sup>+</sup>] = 219.1491.

**(R)-5-Benzyl-2,2,3-trimethylimidazolidin-4-one dichloroacetic acid ((R)-Cat)**



Procedure adapted from reference,<sup>306</sup> (*R*)-2-amino-*N*-methyl-3-phenylpropanamide **172** (1 equiv, 652 mg, 3.66 mmol) and *p*-toluenesulfonic acid monohydrate (10 mol%, 70 mg, 0.37 mmol) was added to anhydrous EtOH (80 mL) and anhydrous acetone (15 mL). The mixture was stirred for 18 h under reflux. The reaction was then cooled down to RT and concentrated *in vacuo*. The crude product was purified by flash column chromatography with silica gel eluting with EtOAc/acetone (1:1). The desired imidazole **174**, was obtained as a yellow oil with 95% yield (0.76 g, 3.48 mmol). The compound was then converted into a salt by addition of dichloroacetic acid (1.0 equiv, 286  $\mu$ L, 3.48 mmol), and recrystallised from DCM/petroleum ether (1:1) to afford (*S*)-**Cat** (1.21 g). [ $\alpha$ ]<sub>D</sub><sup>20</sup> +43.7 (c 0.70, CHCl<sub>3</sub>). IR  $\nu_{\text{max}}/\text{cm}^{-1}$  2988, 2359, 1720, 1651, 1591, 1427, 1367, 1242, 698. <sup>1</sup>H NMR (400 MHz, CDCl<sub>3</sub>)  $\delta$  7.35 – 7.26 (m, 4H, Ph), 7.25 – 7.23 (m, 1H, Ph), 4.17 – 4.12 (m, 1H, CH-C=O), 3.26 (d, *J* = 5.7 Hz, 2H, CH<sub>2</sub>), 2.79 (s, 3H, N-CH<sub>3</sub>), 1.44 (s, 3H, CH<sub>3</sub>), 1.29 (s, 3H, CH<sub>3</sub>). ESI-MS calculated for C<sub>13</sub>H<sub>19</sub>ON<sub>2</sub> [M+H<sup>+</sup>] = 219.1492, observed [M+H<sup>+</sup>] = 219.1494.

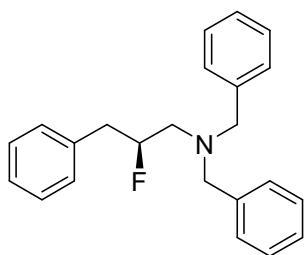
**(S)-N,N-Dibenzyl-2-fluorohexan-1-amine (178)**



1-(S)-5-Benzyl-2,2,3,-trimethylimidazolidin-4-one dichloroacetic acid salt (**S**)-**Cat** (20 mol%, 67 mg, 0.2 mmol) and N-fluorobenzenesulfonimide **62** (5.0 equiv, 1.57 g, 5 mmol) were added to THF (12.5 mL) and *i*-PrOH (1.3 mL). The mixture was stirred at RT until a homogeneous mixture was formed. Then, the reaction was cooled to -10 °C. Hexanal (1.0 equiv, 123  $\mu$ L, 1.0 mmol) was added and the reaction mixture was stirred for 12 h at -10 °C. The reaction was then cooled to -78 °C, diluted with Et<sub>2</sub>O (25 mL) and filtered through a pad of silica gel, eluting with Et<sub>2</sub>O. Dimethyl sulfide (DMS) (12.5 mL) was added, forming a white precipitate. The resulting mixture was washed with saturated aqueous NaHCO<sub>3</sub> (3 x 30 mL), brine (30 mL) and the combined organic layers were dried over MgSO<sub>4</sub>, filtered and concentrated *in vacuo*. The resulting fluorinated aldehyde was dissolved in DCE (22 mL), followed by the addition of dibenzylamine **176** (1.1 equiv, 210  $\mu$ L, 1.1 mmol), and NaBH(OAc)<sub>3</sub> (2.0 equiv, 424 mg, 2.0 mmol). The reaction was stirred for 18 h at RT. The reaction was quenched with saturated aqueous NaHCO<sub>3</sub> (20 mL) and the aqueous layer was extracted with EtOAc (3 x 20 mL). The combined organic layers were dried over MgSO<sub>4</sub>, filtered, and concentrated *in vacuo*. The crude product was purified by flash column chromatography on silica gel eluting with hexane/EtOAc. The desired product **178**, was obtained as a yellow oil with 43% yield (129 mg, er 90:10). [ $\alpha$ ]<sup>20</sup><sub>D</sub> -3.95 (c 2.2, MeOH). <sup>1</sup>H NMR (400 MHz, CDCl<sub>3</sub>)  $\delta$  7.43 – 7.28 (m, 8H, Ph), 7.26 – 7.20 (m, 2H, Ph), 4.74 – 4.53 (m, 1H, CHF), 3.66 (s, 4H, N-CH<sub>2</sub>-benzyl), 1.62 – 1.44 (m, 2H, CH<sub>2</sub>), 1.35 – 1.14 (m, 4H, CH<sub>2</sub>), 0.86 (t, *J* = 7.0 Hz, 3H, CH<sub>3</sub>). <sup>13</sup>C NMR (101 MHz, CDCl<sub>3</sub>)  $\delta$  139.6 (C<sub>Arom</sub>), 129.0 (C<sub>Arom</sub>), 128.3 (C<sub>Arom</sub>), 127.1 (C<sub>Arom</sub>), 93.6 (d, *J* = 169.8 Hz, CHF), 59.2 (CH<sub>2</sub>), 57.1 (d, *J* = 21.2 Hz, CH<sub>2</sub>), 33.1 (d, *J* = 21.2 Hz, CH<sub>2</sub>), 27.13 (CH<sub>2</sub>), 22.63 (CH<sub>2</sub>), 14.07 (CH<sub>3</sub>). <sup>19</sup>F NMR (376 MHz, CDCl<sub>3</sub>)  $\delta$  -180.91. ESI-MS calculated for C<sub>20</sub>H<sub>27</sub>NF [M+H<sup>+</sup>] = 300.2127, observed [M+H<sup>+</sup>] = 300.2113.

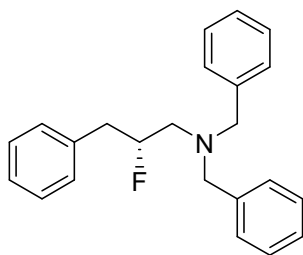


**(S)-N,N-Dibenzyl-2-fluoro-3-phenylpropan-1-amine ((S)-180)**



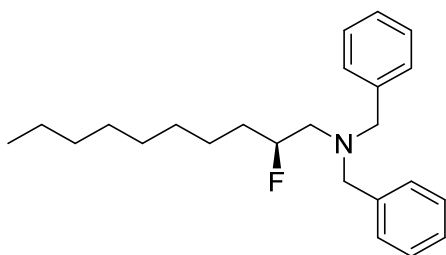
1-(S)-5-Benzyl-2,2,3,-trimethylimidazolidin-4-one dichloroacetic acid salt **(S)-Cat** (20 mol%, 67 mg, 0.2 mmol) and N-fluorobenzenesulfonimide **62** (5.0 equiv, 1.57 g, 5 mmol) were added to THF (12.5 mL) and *i*-PrOH (1.3 mL). The mixture was stirred at RT until a homogeneous mixture was formed. Then, the reaction was cooled to -10 °C. Phenylpropanal (1.0 equiv, 130  $\mu$ L, 1.0 mmol) was added and the reaction mixture was stirred for 12 h at -10 °C. The reaction was then cooled to -78 °C, diluted with Et<sub>2</sub>O (25 mL) and filtered through a pad of silica gel, eluting with Et<sub>2</sub>O. Dimethyl sulfide (DMS) (12.5 mL) was added, forming a white precipitate. The resulting mixture was washed with saturated aqueous NaHCO<sub>3</sub> (3 x 30 mL), brine (30 mL) and the combined organic layers were dried over MgSO<sub>4</sub>, filtered and concentrated *in vacuo*. The resulting fluorinated aldehyde was dissolved in DCE (22 mL), followed by the addition of dibenzylamine **176** (1.1 equiv, 210  $\mu$ L, 1.1 mmol), and NaBH(OAc)<sub>3</sub> (2.0 equiv, 424 mg, 2.0 mmol). The reaction was stirred for 18 h at RT. The reaction was quenched with saturated aqueous NaHCO<sub>3</sub> (20 mL), and the aqueous layer was extracted with EtOAc (3 x 20 mL). The combined organic layers were dried over MgSO<sub>4</sub>, filtered, and concentrated *in vacuo*. The crude product was purified by flash column chromatography on silica gel eluting with hexane/EtOAc. The desired product **180**, was obtained as a yellow oil with 39% yield (130 mg, er 88:12).  $[\alpha]_D^{20}$  -4.04 (c 4.9, MeOH). IR  $\nu_{\text{max}}/\text{cm}^{-1}$  3028, 2929, 2799, 1494, 1452, 1028, 736, 696. <sup>1</sup>H NMR (400 MHz, CDCl<sub>3</sub>)  $\delta$  7.50 – 7.24 (m, 13H, Ph), 7.22 – 7.15 (m, 2H, Ph), 5.02 – 4.79 (m, 1H, CHF), 3.75 (s, 4H, N-CH<sub>2</sub>-benzyl), 3.02 – 2.70 (m, 4H, CH<sub>2</sub>). <sup>13</sup>C NMR (101 MHz, CDCl<sub>3</sub>)  $\delta$  139.4 (C<sub>Arom</sub>), 129.4 (C<sub>Arom</sub>), 129.0 (C<sub>Arom</sub>), 128.4 (C<sub>Arom</sub>), 127.1 (C<sub>Arom</sub>), 126.6 (C<sub>Arom</sub>), 93.6 (d, *J* = 172.5 Hz, CHF), 59.2 (CH<sub>2</sub>), 56.7 (d, *J* = 21.2 Hz, CH<sub>2</sub>), 39.9 (d, *J* = 23.4 Hz, CH<sub>2</sub>). <sup>19</sup>F NMR (376 MHz, CDCl<sub>3</sub>)  $\delta$  -179.86. ESI-MS calculated for C<sub>23</sub>H<sub>25</sub>NF [M+H<sup>+</sup>] = 334.1960, observed [M+H<sup>+</sup>] = 334.1961.

**(R)-N,N-Dibenzyl-2-fluoro-3-phenylpropan-1-amine ((R)-180)**



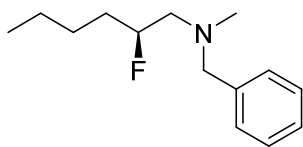
1-(*R*)-5-Benzyl-2,2,3,-trimethylimidazolidin-4-one dichloroacetic acid salt (**R**)-Cat (20 mol%, 67 mg, 0.2 mmol) and N-fluorobenzenesulfonimide **62** (5.0 equiv, 1.57 g, 5 mmol) were added to THF (12.5 mL) and *i*-PrOH (1.3 mL). The mixture was stirred at RT until a homogeneous mixture was formed. Then, the reaction was cooled to -10 °C. Phenylpropanal (1.0 equiv, 130  $\mu$ L, 1.0 mmol) was added and the reaction mixture was stirred for 12 h at -10 °C. The reaction was then cooled to -78 °C, diluted with Et<sub>2</sub>O (25 mL) and filtered through a pad of silica gel, eluting with Et<sub>2</sub>O. Dimethyl sulfide (DMS) (12.5 mL) was added, forming a white precipitate. The resulting mixture was washed with saturated aqueous NaHCO<sub>3</sub> (3 x 30 mL), brine (30 mL) and the combined organic layers were dried over MgSO<sub>4</sub>, filtered and concentrated *in vacuo*. The resulting fluorinated aldehyde was dissolved in DCE (22 mL), followed by the addition of dibenzylamine **176** (1.1 equiv, 210  $\mu$ L, 1.1 mmol), and NaBH(OAc)<sub>3</sub> (2.0 equiv, 424 mg, 2.0 mmol). The reaction was stirred for 18 h at RT. The reaction was quenched with saturated aqueous NaHCO<sub>3</sub> (20 mL) and the aqueous layer was extracted with EtOAc (3 x 20 mL). The combined organic layers were dried over MgSO<sub>4</sub>, filtered, and concentrated *in vacuo*. The crude product was purified by flash column chromatography on silica gel eluting with hexane/EtOAc. The desired product (**R**)-**180**, was obtained as a yellow oil with 39% yield (130 mg, er 93:7). IR  $\nu_{\text{max}}/\text{cm}^{-1}$  3028, 2929, 2799, 1494, 1452, 1028, 736, 696. <sup>1</sup>H NMR (400 MHz, CDCl<sub>3</sub>)  $\delta$  7.37 – 7.21 (m, 13H, Ph), 7.12 – 7.08 (m, 2H, Ph), 4.92 – 4.73 (m, 1H, CHF), 3.67 (s, 4H, N-CH<sub>2</sub>-benzyl), 2.89 – 2.65 (m, 4H, CH<sub>2</sub>). <sup>19</sup>F NMR (376 MHz, CDCl<sub>3</sub>)  $\delta$  -180.06. ESI-MS calculated for C<sub>23</sub>H<sub>25</sub>NF [M+H<sup>+</sup>] = 334.1966, observed [M+H<sup>+</sup>] = 334.1969.

**(S)-N,N-Dibenzyl-2-fluorodecan-1-amine (181)**



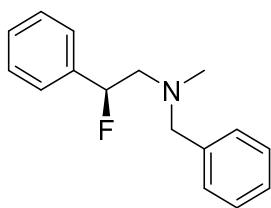
1-(S)-5-Benzyl-2,2,3,-trimethylimidazolidin-4-one dichloroacetic acid salt (**S**)-**Cat** (20 mol%, 67 mg, 0.2 mmol) and N-fluorobenzenesulfonimide **62** (5.0 equiv, 1.57 g, 5 mmol) were added to THF (12.5 mL) and *i*-PrOH (1.3 mL). The mixture was stirred at RT until a homogeneous mixture was formed. Then, the reaction was cooled to -10 °C. Decanal (1.0 equiv, 190  $\mu$ L, 1.0 mmol) was added and the reaction mixture was stirred for 12 h at -10 °C. The reaction was then cooled to -78 °C, diluted with Et<sub>2</sub>O (25 mL) and filtered through a pad of silica gel, eluting with Et<sub>2</sub>O. Dimethyl sulfide (DMS) (12.5 mL) was added, forming a white precipitate. The resulting mixture was washed with saturated aqueous NaHCO<sub>3</sub> (3 x 30 mL), brine (30 mL) and the combined organic layers were dried over MgSO<sub>4</sub>, filtered and concentrated *in vacuo*. The resulting fluorinated aldehyde was dissolved in DCE (22 mL), followed by the addition of dibenzylamine **176** (1.1 equiv, 210  $\mu$ L, 1.1 mmol), and NaBH(OAc)<sub>3</sub> (2.0 equiv, 424 mg, 2.0 mmol). The reaction was stirred for 18 h at RT. The reaction was quenched with saturated aqueous NaHCO<sub>3</sub> (20 mL) and the aqueous layer was extracted with EtOAc (3 x 20 mL). The combined organic layers were dried over MgSO<sub>4</sub>, filtered, and concentrated *in vacuo*. The crude product was purified by flash column chromatography on silica gel eluting with hexane/EtOAc. The desired product **181**, was obtained as a yellow oil with 34% yield (121 mg, er 92:8).  $[\alpha]_D^{20}$  -2.92 (c 2.5, MeOH). <sup>1</sup>H NMR (400 MHz, CDCl<sub>3</sub>)  $\delta$  7.39 – 7.28 (m, 8H, Ph), 7.26 – 7.21 (m, 2H, Ph), 4.76 – 4.51 (m, 1H, CHF), 3.66 (s, 4H, N-CH<sub>2</sub>-benzyl), 2.77 – 2.51 (m, 2H, CH<sub>2</sub>), 1.56 – 1.43 (m, 2H, CH<sub>2</sub>), 1.38 – 1.18 (m, 12H, CH<sub>2</sub>), 0.88 (t, *J* = 6.9 Hz, 3H, CH<sub>3</sub>). <sup>13</sup>C NMR (101 MHz, CDCl<sub>3</sub>)  $\delta$  139.6 (C<sub>Arom</sub>), 129.0 (C<sub>Arom</sub>), 128.3 (C<sub>Arom</sub>), 127.1 (C<sub>Arom</sub>), 93.6 (d, *J* = 169.8 Hz, CHF), 59.2 (CH<sub>2</sub>), 57.1 (d, *J* = 24.9 Hz, CH<sub>2</sub>), 33.5 – 33.3 (d, *J* = 18.6 Hz, CH<sub>2</sub>), 32.0 (CH<sub>2</sub>), 29.6 (d, *J* = 2.3 Hz, CH<sub>2</sub>), 29.4 (CH<sub>2</sub>), 25.0 (d, *J* = 4.1 Hz, CH<sub>2</sub>), 22.8 (CH<sub>2</sub>), 14.3 (CH<sub>3</sub>). <sup>19</sup>F NMR (376 MHz, CDCl<sub>3</sub>)  $\delta$  -180.88. ESI-MS calculated for C<sub>24</sub>H<sub>35</sub>NF [M+H<sup>+</sup>] = 356.2753, observed [M+H<sup>+</sup>] = 356.2737.

**(S)-N-Benzyl-2-fluoro-N-methylhexan-1-amine (182)**



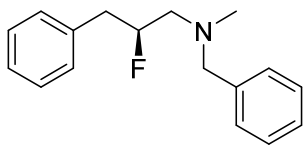
1-(S)-5-Benzyl-2,2,3-trimethylimidazolidin-4-one dichloroacetic acid salt (**S**)-**Cat** (20 mol%, 67 mg, 0.2 mmol) and N-fluorobenzenesulfonimide **62** (5.0 equiv, 1.57 g, 5 mmol) were added to THF (12.5 mL) and *i*-PrOH (1.3 mL). The mixture was stirred at RT until a homogeneous mixture was formed. Then, the reaction was cooled to -10 °C. Hexanal (1.0 equiv, 123  $\mu$ L, 1.0 mmol) was added and the reaction mixture was stirred for 12 h at -10 °C. The reaction was then cooled to -78 °C, diluted with Et<sub>2</sub>O (25 mL) and filtered through a pad of silica gel, eluting with Et<sub>2</sub>O. Dimethyl sulfide (DMS) (12.5 mL) was added, forming a white precipitate. The resulting mixture was washed with saturated aqueous NaHCO<sub>3</sub> (3 x 30 mL), brine (30 mL) and the combined organic layers were dried over MgSO<sub>4</sub>, filtered and concentrated *in vacuo*. The resulting fluorinated aldehyde was dissolved in DCE (22 mL), followed by the addition of N-methylbenzylamine **177** (1.1 equiv, 140  $\mu$ L, 1.1 mmol), and NaBH(OAc)<sub>3</sub> (2.0 equiv, 424 mg, 2.0 mmol). The reaction was stirred for 18 h at RT. The reaction was quenched with saturated aqueous NaHCO<sub>3</sub> (20 mL) and the aqueous layer was extracted with EtOAc (3 x 20 mL). The combined organic layers were dried over MgSO<sub>4</sub>, filtered, and concentrated *in vacuo*. The crude product was purified by flash column chromatography with silica gel eluting with hexane/EtOAc. The desired product **182**, was obtained as a yellow oil with 39% yield (85 mg, er 95:5). [ $\alpha$ ]<sub>D</sub><sup>20</sup> +3.37 (c 1.9, MeOH). <sup>1</sup>H NMR (400 MHz, CDCl<sub>3</sub>)  $\delta$  7.32 (d, *J* = 4.4 Hz, 4H, Ph), 7.26 – 7.21 (m, 1H, Ph), 4.76 – 4.57 (m, 1H, CHF), 3.58 (s, 2H, N-CH<sub>2</sub>-benzyl), 2.71 – 2.43 (m, 2H, CH<sub>2</sub>), 2.29 (s, 3H, N-CH<sub>3</sub>), 1.83 – 1.21 (m, 6H, CH<sub>2</sub>), 0.90 (t, *J* = 7.1 Hz, 3H, CH<sub>3</sub>). <sup>13</sup>C NMR (101 MHz, CDCl<sub>3</sub>)  $\delta$  138.9 (C<sub>Arom</sub>), 129.2 (C<sub>Arom</sub>), 128.4 (C<sub>Arom</sub>), 127.2 (C<sub>Arom</sub>), 93.1 (d, *J* = 160.8 Hz, CHF), 62.9 (CH<sub>2</sub>), 60.0 (d, *J* = 21.2 Hz, CH<sub>2</sub>), 43.2 (N-CH<sub>3</sub>), 33.3 (d, *J* = 20.4 Hz, CH<sub>2</sub>), 27.3 (d, *J* = 4.4 Hz, CH<sub>2</sub>), 22.7 (CH<sub>2</sub>), 14.1 (CH<sub>3</sub>). <sup>19</sup>F NMR (376 MHz, CDCl<sub>3</sub>)  $\delta$  -181.12. ESI-MS calculated for C<sub>14</sub>H<sub>23</sub>NF [M+H<sup>+</sup>] = 224.1814, observed [M+H<sup>+</sup>] = 224.1803.

**(S)-N-Benzyl-2-fluoro-N-methyl-2-phenylethan-1-amine (183)**



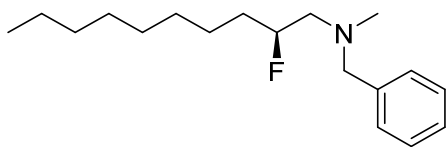
1-(S)-5-Benzyl-2,2,3,-trimethylimidazolidin-4-one dichloroacetic acid salt (**S**)-**Cat** (20 mol%, 67 mg, 0.2 mmol) and N-fluorobenzenesulfonimide **62** (5 equiv, 1.57 g, 5 mmol) were added to THF (12.5 mL) and *i*-PrOH (1.3 mL). The mixture was stirred at RT until a homogeneous mixture was formed. Then, the reaction was cooled to -10 °C. Phenylacetaldehyde (1.0 equiv, 111  $\mu$ L, 1.0 mmol) was added and the reaction mixture was stirred for 12 h at -10 °C. The reaction was then cooled to -78 °C, diluted with Et<sub>2</sub>O (25 mL) and filtered through a pad of silica gel, eluting with Et<sub>2</sub>O. Dimethyl sulfide (DMS) (12.5 mL) was added, forming a white precipitate. The resulting mixture was washed with saturated aqueous NaHCO<sub>3</sub> (3 x 30 mL), brine (30 mL) and the combined organic layers were dried over MgSO<sub>4</sub>, filtered and concentrated *in vacuo*. The resulting fluorinated aldehyde was dissolved *in* DCE (22 mL), followed by the addition of N-methylbenzylamine **177** (1.1 equiv, 140  $\mu$ L, 1.1 mmol), and NaBH(OAc)<sub>3</sub> (2.0 equiv, 424 mg, 2.0 mmol). The reaction was stirred for 18 h at RT. The reaction was quenched with saturated aqueous NaHCO<sub>3</sub> (20 mL) and the aqueous layer was extracted with EtOAc (3 x 20 mL). The combined organic layers were dried over MgSO<sub>4</sub>, filtered, and concentrated *in vacuo*. The crude product was purified by flash column chromatography with silica gel eluting with hexane/EtOAc. The desired product **183**, was obtained as a yellow oil with 15% yield (37 mg, er 99:1). [ $\alpha$ ]<sup>20</sup><sub>D</sub> +26.5 (c 4.3, MeOH). <sup>1</sup>H NMR (400 MHz, CDCl<sub>3</sub>)  $\delta$  7.44 – 7.12 (m, 10H, Ph), 5.66 – 5.46 (m, 1H, CHF), 3.68 (d, *J* = 3.3 Hz, 2H, N-CH<sub>2</sub>-benzyl), 2.99 – 2.88 (m, 1H, CH<sub>2</sub>), 2.80 – 2.57 (m, 1H, CH<sub>2</sub>), 2.41 (s, 3H, N-CH<sub>3</sub>). <sup>13</sup>C NMR (101 MHz, CDCl<sub>3</sub>)  $\delta$  129.0 (C<sub>Arom</sub>), 128.4 (C<sub>Arom</sub>), 128.3 (C<sub>Arom</sub>), 127.1 (C<sub>Arom</sub>), 125.6 (C<sub>Arom</sub>), 93.1 (d, *J* = 171.5 Hz, CHF), 63.1 (CH<sub>2</sub>), 62.6 (CH<sub>2</sub>), 31.1 (N-CH<sub>3</sub>). <sup>19</sup>F NMR (376 MHz, CDCl<sub>3</sub>)  $\delta$  -178.15. ESI-MS calculated for C<sub>16</sub>H<sub>19</sub>NF [M+H<sup>+</sup>] = 244.1501, observed [M+H<sup>+</sup>] = 244.1493

**(S)-N-Benzyl-2-fluoro-N-methyl-3-phenylpropan-1-amine (184)**



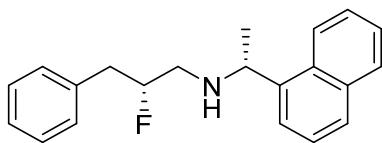
1-(S)-5-Benzyl-2,2,3-trimethylimidazolidin-4-one dichloroacetic acid salt (**S**)-**Cat** (20 mol%, 67 mg, 0.2 mmol) and N-fluorobenzenesulfonimide **62** (5.0 equiv, 1.57 g, 5 mmol) were added to THF (12.5 mL) and *i*-PrOH (1.3 mL). The mixture was stirred at RT until a homogeneous mixture was formed. Then, the reaction was cooled to -10 °C. Phenyl propanal (1.0 equiv, 190  $\mu$ L, 1.0 mmol) was added and the reaction mixture was stirred for 12 h at -10 °C. The reaction was then cooled to -78 °C, diluted with Et<sub>2</sub>O (25 mL) and filtered through a pad of silica gel, eluting with Et<sub>2</sub>O. Dimethyl sulfide (DMS) (12.5 mL) was added, forming a white precipitate. The resulting mixture was washed with saturated aqueous NaHCO<sub>3</sub> (3 x 30 mL), brine (30 mL) and the combined organic layers were dried over MgSO<sub>4</sub>, filtered and concentrated *in vacuo*. The resulting fluorinated aldehyde was dissolved in DCE (22 mL), followed by the addition of N-methylbenzylamine **177** (1.1 equiv, 210  $\mu$ L, 1.1 mmol), and NaBH(OAc)<sub>3</sub> (2.0 equiv, 424 mg, 2.0 mmol). The reaction was stirred for 18 h at RT. The reaction was quenched with saturated aqueous NaHCO<sub>3</sub> (20 mL) and the aqueous layer was extracted with EtOAc (3 x 20 mL). The combined organic layers were dried over MgSO<sub>4</sub>, filtered, and concentrated *in vacuo*. The crude product was purified by flash column chromatography on silica gel eluting with hexane/EtOAc. The desired product **184**, was obtained as a yellow oil with 28% yield (72 mg, er 99:1). [ $\alpha$ ]<sub>D</sub><sup>20</sup> +1.06 (c 4.7, MeOH). <sup>1</sup>H NMR (400 MHz, CDCl<sub>3</sub>)  $\delta$  7.33 – 7.17 (m, 10H, Ph), 4.96 – 4.77 (m, 1H, CHF), 3.57 (s, 2H, N-CH<sub>2</sub>-benzyl), 3.01 – 2.90 (m, 2H, CH<sub>2</sub>), 2.72 – 2.54 (m, 2H, CH<sub>2</sub>), 2.29 (s, 3H, N-CH<sub>3</sub>). <sup>13</sup>C NMR (101 MHz, CDCl<sub>3</sub>)  $\delta$  138.8 (C<sub>Arom</sub>), 129.4 (C<sub>Arom</sub>), 129.0 (C<sub>Arom</sub>), 128.5 (C<sub>Arom</sub>), 128.3 (C<sub>Arom</sub>), 126.6 (C<sub>Arom</sub>), 127.1 (C<sub>Arom</sub>), 93.2 (d, *J* = 172.7 Hz, CHF), 62.7 (CH<sub>2</sub>), 60.1 (d, *J* = 20.7 Hz, CH<sub>2</sub>), 39.8 (CH<sub>2</sub>), 43.1 (N-CH<sub>3</sub>). <sup>19</sup>F NMR (376 MHz, CDCl<sub>3</sub>)  $\delta$  -179.91. ESI-MS calculated for C<sub>17</sub>H<sub>21</sub>NF [M+H<sup>+</sup>] = 258.1658, observed [M+H<sup>+</sup>] = 258.1646.

**(S)-N-Benzyl-2-fluoro-N-methyldecane-1-amine (185)**



1-(S)-5-Benzyl-2,2,3-trimethylimidazolidin-4-one dichloroacetic acid salt (**S-Cat**) (20%, 67 mg, 0.2 mmol) and N-fluorobenzenesulfonimide **62** (5.0 equiv, 1.6 g, 5.0 mmol) were added to THF (12.5 mL) and *i*-PrOH (1.3 mL). The mixture was stirred at RT until a homogeneous mixture was formed. Then, the reaction was cooled to -10 °C. Decanal (1.0 equiv, 190  $\mu$ L, 1.0 mmol) was added and the reaction mixture was stirred for 12 h at -10 °C. The reaction was then cooled to -78 °C, diluted with Et<sub>2</sub>O (25 mL) and filtered through a pad of silica gel, eluting with Et<sub>2</sub>O. Dimethyl sulfide (DMS) (12.5 mL) was added, forming a white precipitate. The resulting mixture was washed with saturated aqueous NaHCO<sub>3</sub> (3 x 30 mL), brine (30 mL) and dried over MgSO<sub>4</sub>, filtered and concentrated *in vacuo*. The resulting fluorinated aldehyde was dissolved in DCE (22 mL), followed by the addition of N-methylbenzylamine **177** (1.1 equiv, 140  $\mu$ L, 1.1 mmol), and NaBH(OAc)<sub>3</sub> (2.0 equiv, 424 mg, 2.0 mmol). The reaction was stirred for 18 h at RT. The reaction was quenched with saturated aqueous NaHCO<sub>3</sub> (20 mL) and the aqueous layer was extracted with EtOAc (3 x 20 mL). The combined organic layers were dried over MgSO<sub>4</sub>, filtered, and concentrated *in vacuo*. The crude product was purified by flash column chromatography on silica gel eluting with hexane/EtOAc. The desired product **185**, was obtained as a yellow oil with 47% yield (131 mg, er 92:8).  $[\alpha]_D^{20} +2.68$  (c 1.9, MeOH). IR  $\nu_{\text{max}}/\text{cm}^{-1}$  3028, 2929, 2799, 1494, 1452, 1028, 736, 696. <sup>1</sup>H NMR (400 MHz, CDCl<sub>3</sub>)  $\delta$  7.41 – 7.16 (m, 5H, Ph), 4.79 – 4.56 (m, 1H, CHF), 3.58 (s, 2H, N-CH<sub>2</sub>-benzyl), 2.72 – 2.43 (m, 2H, CH<sub>2</sub>), 2.30 (s, 3H, N-CH<sub>3</sub>), 1.69 – 1.18 (m, 14H, CH<sub>2</sub>), 0.89 (t, *J* = 7.0 Hz, 3H, CH<sub>3</sub>). <sup>13</sup>C NMR (101 MHz, CDCl<sub>3</sub>)  $\delta$  138.8 (C<sub>Arom</sub>), 129.2 (C<sub>Arom</sub>), 128.4 (C<sub>Arom</sub>), 127.2 (C<sub>Arom</sub>), 93.0 (d, *J* = 171.0 Hz, CHF), 62.89 (CH<sub>2</sub>), 60.0 (d, *J* = 21.3 Hz, CH<sub>2</sub>), 43.2 (N-CH<sub>3</sub>), 33.6 (d, *J* = 23.5 Hz, CH<sub>2</sub>), 32.0 (CH<sub>2</sub>), 29.6 (CH<sub>2</sub>), 29.4 (CH<sub>2</sub>), 25.1 (CH<sub>2</sub>), 22.8 (CH<sub>2</sub>), 14.3 (CH<sub>3</sub>). <sup>19</sup>F NMR (377 MHz, CDCl<sub>3</sub>)  $\delta$  -181.08. ESI-MS calculated for C<sub>18</sub>H<sub>31</sub>NF [M+H<sup>+</sup>] = 280.2440, observed [M+H<sup>+</sup>] = 280.2427.

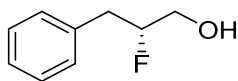
**(R)-2-Fluoro-N-((R)-1-(naphthalen-1-yl)ethyl)-3-phenylpropan-1-amine (187)**



1-(R)-5-Benzyl-2,2,3-trimethylimidazolidin-4-one dichloroacetic acid salt (**R**)-Cat (30%, 210 mg, 0.63 mmol) was added to a solution of THF (18 mL) and *i*-PrOH (1.8 mL). The reaction was cooled to -10 °C. 3-Phenylpropanal **164** (1.0 equiv, 266  $\mu$ L, 2.0 mmol) was added. N-fluorobenzenesulfonimide **62** (1.0 equiv, 0.60 g, 2.0 mmol) solution in THF was then added slowly in over 30 min. The reaction mixture was stirred for 12 h at -10 °C. The reaction was then cooled to -78 °C, quenched with Et<sub>2</sub>O (15 mL) and filtered through a pad of silica gel, eluting with Et<sub>2</sub>O. Dimethyl sulfide (DMS) (1.0 mL) was added. The resulting mixture was washed with saturated aqueous NaHCO<sub>3</sub> (3 x 30 mL), brine (30 mL) and the combined organic layers were dried over MgSO<sub>4</sub>, filtered and concentrated *in vacuo*. The resulting fluorinated aldehyde was dissolved in DCE (22 mL), followed by the addition of (R)-(1-naphthyl)ethylamine **231** (1.1 equiv, 350  $\mu$ L, 2.2 mmol), and NaBH(OAc)<sub>3</sub> (2.0 equiv, 848 mg, 4.0 mmol). The reaction was stirred for 18 h at RT. The reaction was quenched with saturated aqueous NaHCO<sub>3</sub> (20 mL) and the aqueous layer was extracted with EtOAc (3 x 20 mL). The combined organic layers were dried over MgSO<sub>4</sub>, filtered, and concentrated *in vacuo*. The crude product was purified by flash column chromatography on silica gel eluting with hexane/EtOAc. The desired product **187** was obtained as a yellow oil with 71% yield (436 mg, dr 98:2). [ $\alpha$ ]<sub>D</sub><sup>20</sup> -30.6 (c 0.64, CHCl<sub>3</sub>). IR  $\nu_{\text{max}}/\text{cm}^{-1}$  3031, 2926, 2362, 1454, 1029, 777, 698. <sup>1</sup>H NMR (400 MHz, CDCl<sub>3</sub>)  $\delta$  8.18 (d, *J* = 8.2 Hz, 1H, Ph), 7.92 – 7.84 (m, 1H, Ph), 7.76 (dq, *J* = 8.2, 1.9, 1.5 Hz, 1H, Ph), 7.71 – 7.63 (m, 1H, Ph), 7.57 – 7.44 (m, 3H, Ph), 7.35 – 7.13 (m, 5H, Ph), 4.99 – 4.74 (m, 1H, CHF), 4.65 (q, *J* = 6.6 Hz, 1H, CH-N), 3.09 – 2.66 (m, 4H, CH<sub>2</sub>), 1.52 (d, *J* = 6.6 Hz, 3H, CH<sub>3</sub>). <sup>13</sup>C NMR (101 MHz, CDCl<sub>3</sub>)  $\delta$  129.3 (C<sub>Arom</sub>), 129.0 (C<sub>Arom</sub>), 128.5 (C<sub>Arom</sub>), 127.4 (C<sub>Arom</sub>), 126.6 (C<sub>Arom</sub>), 125.9 (C<sub>Arom</sub>), 125.7 (C<sub>Arom</sub>), 125.4 (C<sub>Arom</sub>), 122.9 (C<sub>Arom</sub>), 122.8 (C<sub>Arom</sub>), 94.0 (d, *J* = 171.1 Hz, CHF), 53.5 (CH-N), 51.0 (d, *J* = 20.0 Hz, CH<sub>2</sub>), 39.3 (d, *J* = 21.3 Hz, CH<sub>2</sub>), 23.7 (CH<sub>3</sub>). <sup>19</sup>F NMR (376 MHz, CDCl<sub>3</sub>)  $\delta$  -184.09. ESI-MS calculated for C<sub>21</sub>H<sub>23</sub>NF [M+H<sup>+</sup>] = 308.1809, observed [M+H<sup>+</sup>] = 308.1629.

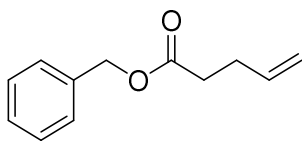


**(R)-2-Fluoro-3-phenylpropan-1-ol ((R)-188)**



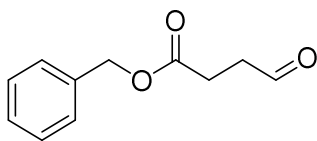
1-(R)-5-Benzyl-2,2,3,-trimethylimidazolidin-4-one dichloroacetic acid salt (**R**)-Cat (30%, 420 mg, 1.26 mmol) was added to THF (18.0 mL) and *i*-PrOH (1.8 mL). The reaction was cooled to -10 °C. Phenylpropanal **164** (1.0 equiv, 530  $\mu$ L, 4.0 mmol) was added. N-fluorobenzenesulfonimide (1.0 equiv, 1.2 g, 4.0 mmol) solution in THF was then added slowly in over 30 min. The resulting reaction mixture was stirred for 12 h at -10 °C. The reaction was then cooled to -78 °C, diluted with Et<sub>2</sub>O (30 mL) and filtered through a pad of silica gel, eluting with Et<sub>2</sub>O. Dimethyl sulfide (2.0 mL) was added. The resulting mixture was washed with saturated aqueous NaHCO<sub>3</sub> (3 x 30 mL), brine (30 mL) and the combined organic layers were dried over MgSO<sub>4</sub>, filtered and concentrated *in vacuo*. The resulting fluorinated aldehyde was dissolved in DCM (24 mL) an ethanol (16 mL), followed by the addition NaBH<sub>4</sub> (2.0 equiv, 303 mg, 5.0 mmol). The reaction was stirred for 30 min at 0°C. The reaction was quenched with saturated ammonium chloride (308 mL), loved to RT and stirred for an extra 1 h. The reaction was the mixture was extracted with DCM (3 x 30 mL). The combined organic layers were washed with aqueous NaHCO<sub>3</sub> (30 mL), brine (30 mL) and the combined organic layers were dried over MgSO<sub>4</sub>, filtered, and concentrated *in vacuo*. The crude product was purified by flash column chromatography on silica gel eluting with hexane/EtOAc. The desired product (**R**)-**188** was obtained as a yellow oil with 78% yield (481 mg, er 99:1). [ $\alpha$ ]<sup>20</sup><sub>D</sub> +8.52 (c 0.91, CHCl<sub>3</sub>). IR  $\nu_{\text{max}}/\text{cm}^{-1}$  3379, 2927, 2360, 1454, 1049, 698. <sup>1</sup>H NMR (400 MHz, CDCl<sub>3</sub>)  $\delta$  7.35 – 7.28 (m, 2H, Ph), 7.28 – 7.18 (m, 3H, Ph), 4.78 (dm, *J* = 48.7, Hz, 1H, CHF), 3.84 – 3.61 (m, 2H, CH<sub>2</sub>), 3.12 – 2.86 (m, 2H, CH<sub>2</sub>). <sup>13</sup>C NMR (101 MHz, CDCl<sub>3</sub>)  $\delta$  129.4 (C<sub>Arom</sub>), 128.7 (C<sub>Arom</sub>), 128.5(C<sub>Arom</sub>), 128.5 (C<sub>Arom</sub>), 126.9 (C<sub>Arom</sub>), 126.0 (C<sub>Arom</sub>), 94.7 (d, *J* = 172.2 Hz, CHF), 64.3 (d, *J* = 20.8 Hz, CH<sub>2</sub>), 37.6 (d, *J* = 20.6 Hz, CH<sub>2</sub>). <sup>19</sup>F NMR (376 MHz, CDCl<sub>3</sub>)  $\delta$  -187.66. ESI-MS calculated for C<sub>9</sub>H<sub>12</sub>OF [M+H<sup>+</sup>] = 155.0788, observed [M+H<sup>+</sup>] = 155.0788.

### Benzyl pent-4-enoate (**224**)



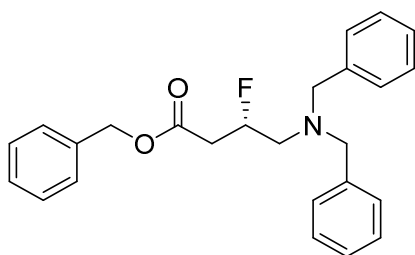
Following a procedure adapted from reference,<sup>307</sup> to a round-bottom flask, equipped with a magnetic stir bar and a Dean Stark apparatus, and charged with pent-4-enoic acid (1.0 equiv, 1.02 mL, 10 mmol), *p*-toluenesulfonic acid (10%, 190 mg, 1 mmol) and benzyl alcohol (1.5 equiv, 1.55 mL, 15 mmol) was added toluene (30 mL). The mixture was stirred under reflux (180 °C). After collection in the Dean Stark, of 1 equiv of water. The reaction was cooled down to RT and concentrated *in vacuo*. The crude product was purified by flash column chromatography with silica gel eluting with hexane/EtOAc (3:7). According to the reference<sup>307</sup> and the NMR The desired product **224**, was obtained as a yellow oil with 74% yield (1.90 g). **IR**  $\nu_{\text{max}}/\text{cm}^{-1}$  3034, 2358, 1734, 1159, 696. **<sup>1</sup>H NMR (400 MHz, CDCl<sub>3</sub>)**  $\delta$  7.30 – 7.41 (m, 5H, Ph), 5.76 – 5.89 (m, 1H, CH), 5.12 (s, 2H, CH<sub>2</sub>-Ph), 4.97 – 5.10 (m, 2H, =CH<sub>2</sub>), 2.35 – 2.51 (m, 4H, CH<sub>2</sub>). **<sup>13</sup>C NMR (101 MHz, CDCl<sub>3</sub>)**  $\delta$  173.03 (C=O), 136.73 (CH=), 128.7 (C<sub>Arom</sub>), 128.5 (C<sub>Arom</sub>), 128.4 (C<sub>Arom</sub>), 127.9 (C<sub>Arom</sub>), 127.8 (C<sub>Arom</sub>), 115.7 (CH<sub>2</sub>=), 66.4 (CH<sub>2</sub>-O), 33.7 (CH<sub>2</sub>), 29.0(CH<sub>2</sub>). **ESI-MS** calculated for C<sub>12</sub>H<sub>15</sub>O<sub>2</sub> [M+H<sup>+</sup>] = 191.0988, observed [M+H<sup>+</sup>] = 191.0991.

### Benzyl 4-oxobutanoate (**225**)



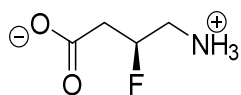
Following a procedure adapted from reference,<sup>308</sup> to a three-necked round-bottom flask, equipped with a magnetic stir bar was passed ozone through a solution of benzyl 4-pentenoate **224** (1.0 equiv, 461 mg, 2.47 mmol) in DCM (25 mL) at -78 °C until the solution became blue. To the reaction was added NEt<sub>3</sub> (0.7 mL) and the reaction was warmed to RT. The mixture was washed with aqueous HCl (1M, 2.25 mL), aqueous NaHCO<sub>3</sub> (5%, 1.15 mL) and the combined organic layers were dried over MgSO<sub>4</sub>, filtered, and concentrated *in vacuo*. This material was used without further purification. According to the reference<sup>308</sup> and the NMR the desired product **225**, was obtained with a yield of 90% (427 mg). **IR**  $\nu_{\text{max}}/\text{cm}^{-1}$  2927, 1726, 1683, 1257, 1170, 941, 696. **<sup>1</sup>H NMR (400 MHz, CDCl<sub>3</sub>)**  $\delta$  9.82 (s, 1H, CHO), 7.33 – 7.38 (m, 5H, Ph), 5.13 (s, 2H, OCH<sub>2</sub>), 2.75 – 2.66 (m, 4H, CH<sub>2</sub>). **<sup>13</sup>C NMR (101 MHz, CDCl<sub>3</sub>)**  $\delta$  200.2 (C=O<sub>Aldehyde</sub>), 172.1 (CO<sub>2</sub>), 135.8 (C<sub>Arom</sub>), 128.7 (C<sub>Arom</sub>), 128.4 (C<sub>Arom</sub>), 128.32 (C<sub>Arom</sub>), 127.9 (C<sub>Arom</sub>), 66.8 (CH<sub>2</sub>-O), 38.6 (CH<sub>2</sub>-CHO), 29.0 (CH<sub>2</sub>). **ESI-MS** calculated for C<sub>11</sub>H<sub>13</sub>O<sub>3</sub> [M+H<sup>+</sup>] = 193.0781, observed [M+H<sup>+</sup>] = 193.0789.

**Benzyl (S)-4-(dibenzylamino)-3-fluorobutanoate ((S)-226)**



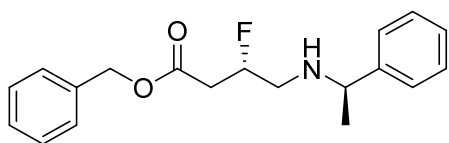
1-(S)-5-Benzyl-2,2,3-trimethylimidazolidin-4-one dichloroacetic acid salt (**S**)-**Cat** (30%, 420 mg, 1.26 mmol) was added to a solution of THF (36 mL) and *i*-PrOH (3.6 mL). The reaction was cooled to  $-10\text{ }^{\circ}\text{C}$ . Benzyl 4-oxobutanoate **225** (1.0 equiv, 769 mg, 4.0 mmol) was added. A N-fluorobenzenesulfonimide (1.0 equiv, 1.26 g, 4.0 mmol) solution in THF was then added slowly in over 30 min. The reaction mixture was stirred for 12 h at  $-10\text{ }^{\circ}\text{C}$ . The reaction was then cooled to  $-78\text{ }^{\circ}\text{C}$ , quenched with Et<sub>2</sub>O (25 mL) and filtered through a pad of silica gel, eluting with Et<sub>2</sub>O. Dimethyl sulfide (DMS) (2.0 mL) was added. The resulting mixture was washed with saturated aqueous NaHCO<sub>3</sub> (3 x 30 mL), brine (30 mL) and the combined organic layers were dried over MgSO<sub>4</sub>, filtered and concentrated *in vacuo*. The resulting fluorinated aldehyde was dissolved in DCE (40 mL), followed by the addition of dibenzylamine **176** (1.1 equiv, 560  $\mu\text{L}$ , 4.4 mmol), and NaBH(OAc)<sub>3</sub> (4.0 equiv, 1.69 g, 8.0 mmol). The reaction was stirred for 18 h at RT. The reaction was quenched with saturated aqueous NaHCO<sub>3</sub> (20 mL) and the aqueous layer was extracted with EtOAc (3 x 20 mL). The combined organic layers were dried over MgSO<sub>4</sub>, filtered, and concentrated *in vacuo*. The crude product was purified by flash column chromatography with silica gel eluting with hexane/DCM. The desired product (**S**)-**226** was obtained as a yellow oil with 52% yield (814 mg, er 89:11).  $[\alpha]_D^{20}$  -1.02 (c 2.1, CHCl<sub>3</sub>). IR  $\nu_{\text{max}}/\text{cm}^{-1}$  3030, 2802, 2360, 1735, 1170, 736, 696. <sup>1</sup>H NMR (400 MHz, CDCl<sub>3</sub>)  $\delta$  7.54 – 7.09 (m, 15H, Ph), 5.25 – 5.13 (m, 1H), 5.18 (s, 2H, O-CH<sub>2</sub>-benzyl), 3.73 (qd,  $J = 13.7, 2.9\text{ Hz}$ , 4H, N-CH<sub>2</sub>-benzyl), 2.79 – 2.60 (m, 4H, CH<sub>2</sub>). <sup>13</sup>C NMR (101 MHz, CDCl<sub>3</sub>)  $\delta$  139.1 (C=O), 129.0 (C<sub>Arom</sub>), 128.7 (C<sub>Arom</sub>), 128.3 (C<sub>Arom</sub>), 127.2 (C<sub>Arom</sub>), 89.5 (d,  $J = 175.6\text{ Hz}$ ), 66.6 (CH<sub>2</sub>O), 59.2 (CH<sub>2</sub>-PH), 56.0 (d,  $J = 19.5\text{ Hz}$ , CH<sub>2</sub>), 38.5 (d,  $J = 28.4\text{ Hz}$ , CH<sub>2</sub>). <sup>19</sup>F NMR (376 MHz, CDCl<sub>3</sub>)  $\delta$  -181.4. ESI-MS calculated for C<sub>25</sub>H<sub>27</sub>O<sub>2</sub>NF [M+H<sup>+</sup>] = 392.2026, observed [M+H<sup>+</sup>] = 392.2020.

**(S)-4-Amino-3-fluorobutanoic acid (3-F-GABA, 16)**



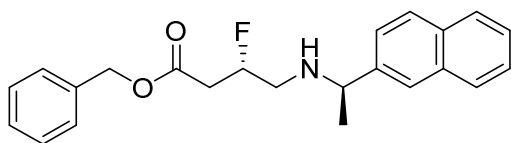
Benzyl (*S*)-4-(dibenzylamino)-3-fluorobutanoate (**S**)-**226** (1.0 equiv, 65 mg, 0.16 mmol) and Pd(OH)<sub>2</sub>/C 20 wt.% (2.8%, 20mg, 0.005 mmol) was added to MeOH (5 mL) under inert atmosphere. The mixture was stirred for 46 h at RT under a H<sub>2</sub> atmosphere (1 atm). The reaction was filtered through a pad of celite<sup>®</sup> and concentrated *in vacuo*. The resulting mixture was dissolved in water (5 mL) and washed with Et<sub>2</sub>O (5 mL). This was purified by reverse phase column chromatography on silica gel (C18) eluting with water. According to the reference<sup>28</sup> and the NMR, the desired product **16** was obtained as a white solid with a 90% yield (18 mg, er 89:11). <sup>1</sup>H NMR (400 MHz, D<sub>2</sub>O) δ 5.05 – 5.30 (m, 1H, CHF), 3.18 – 3.40 (m, 2H, CH<sub>2</sub>), 2.47 – 2.72 (m, 2H, CH<sub>2</sub>). <sup>13</sup>C NMR (101 MHz, D<sub>2</sub>O) δ 129.7 (CO<sub>2</sub>), 129.5(CO<sub>2</sub>), 88.9 (CHF), 87.3 (d, *J* = 171.5, CHF), 51.3 (d, *J* = 20.6 Hz, N-CH<sub>2</sub>), 47.6 (d, *J* = 22.4 Hz, CH<sub>2</sub>-CO<sub>2</sub>). <sup>19</sup>F NMR (376 MHz, D<sub>2</sub>O) δ -185.6.

### Benzyl (S)-3-fluoro-4-((R)-1-phenylethyl)amino)butanoate (233)



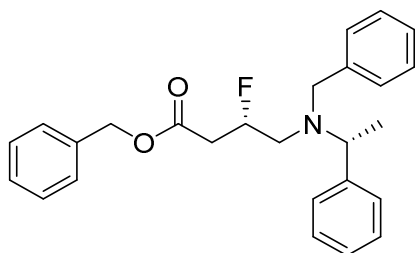
1-(S)-5-Benzyl-2,2,3-trimethylimidazolidin-4-one dichloroacetic acid salt (**S**)-Cat (30%, 420 mg, 1.26 mmol) was added to a solution of THF (36 mL) and *i*-PrOH (3.6 mL). The reaction was cooled to  $-10\text{ }^{\circ}\text{C}$ . Benzyl 4-oxobutanoate **225** (1.0 equiv, 769 mg, 4.0 mmol) was added. A N-fluorobenzenesulfonimide (1.0 equiv, 1.26 g, 4.0 mmol) solution in THF was then added slowly in over 30 min. The reaction mixture was stirred for 12 h at  $-10\text{ }^{\circ}\text{C}$ . The reaction was then cooled to  $-78\text{ }^{\circ}\text{C}$ , quenched with Et<sub>2</sub>O (25 mL) and filtered through a pad of silica gel, eluting with Et<sub>2</sub>O. Dimethyl sulfide (DMS) (2.0 mL) was added. The resulting mixture was washed with saturated aqueous NaHCO<sub>3</sub> (3 x 30 mL), brine (30 mL) and the combined organic layers were dried over MgSO<sub>4</sub>, filtered and concentrated *in vacuo*. The resulting fluorinated aldehyde was dissolved in DCE (40 mL), followed by the addition of (*R*)-methylbenzylamine **230** (1.1 equiv, 560  $\mu\text{L}$ , 4.4 mmol), and NaBH(OAc)<sub>3</sub> (4.0 equiv, 1.69 g, 8.0 mmol). The reaction was stirred for 18 h at RT. The reaction was quenched with saturated aqueous NaHCO<sub>3</sub> (20 mL) and the aqueous layer was extracted with EtOAc (3 x 20 mL). The combined organic layers were dried over MgSO<sub>4</sub>, filtered, and concentrated *in vacuo*. The crude product was purified by flash column chromatography with silica gel eluting with hexane/DCM. The desired product **233** was obtained as a yellow oil with 5% yield (63 mg, dr 93:7).  $[\alpha]_{\text{D}}^{20} +75.10$  (c 0.57, CHCl<sub>3</sub>). <sup>1</sup>H NMR (400 MHz, CDCl<sub>3</sub>)  $\delta$  7.40 – 7.27 (m, 10H, Ph), 5.12 (s, 2H, CH<sub>2</sub>-O), 5.08 (dm,  $J = 49.5$  Hz, 1H, CHF), 3.80 (q,  $J = 6.5$  Hz, CH-N), 2.92 – 2.53 (m, 4H, CH<sub>2</sub>), 1.35 (t,  $J = 6.5$  Hz, 3H, CH<sub>3</sub>). <sup>13</sup>C NMR (101 MHz, CDCl<sub>3</sub>)  $\delta$  129.3 (C<sub>Arom</sub>), 128.7 (C<sub>Arom</sub>), 128.6 (C<sub>Arom</sub>), 128.3 (C<sub>Arom</sub>), 127.7 (C<sub>Arom</sub>), 127.6 (C<sub>Arom</sub>), 127.0 (C<sub>Arom</sub>), 126.8 (C<sub>Arom</sub>), 86.1 (d,  $J = 175.8$  Hz, CHF), 65.43 (N-CH), 49.6 (d,  $J = 24.2$  Hz, OCH<sub>2</sub>), 39.32 (d,  $J = 22.6$  Hz, CH<sub>2</sub>), 16.39 (CH<sub>3</sub>). <sup>19</sup>F NMR (376 MHz, CDCl<sub>3</sub>)  $\delta$  -173.96. ESI-MS calculated for C<sub>19</sub>H<sub>22</sub>O<sub>2</sub>N [M-F<sup>-</sup>] = 296.1654, observed [M-F<sup>-</sup>] = 296.1646.

**Benzyl (S)-3-fluoro-4-(((R)-1-(naphthalen-2-yl)ethyl)amino)butanoate (234)**



1-(S)-5-Benzyl-2,2,3-trimethylimidazolidin-4-one dichloroacetic acid salt (**S**)-**Cat** (30%, 420 mg, 1.26 mmol) was added to a solution of THF (36 mL) and *i*-PrOH (3.6 mL). The reaction was cooled to  $-10\text{ }^{\circ}\text{C}$ . Benzyl 4-oxobutanoate **225** (1.0 equiv, 769 mg, 4.0 mmol) was added. A N-fluorobenzenesulfonimide (1.0 equiv, 1.26 g, 4.0 mmol) solution in THF was then added slowly in over 30 min. The reaction mixture was stirred for 12 h at  $-10\text{ }^{\circ}\text{C}$ . The reaction was then cooled to  $-78\text{ }^{\circ}\text{C}$ , quenched with Et<sub>2</sub>O (25 mL) and filtered through a pad of silica gel, eluting with Et<sub>2</sub>O. Dimethyl sulfide (DMS) (2.0 mL) was added. The resulting mixture was washed with saturated aqueous NaHCO<sub>3</sub> (3 x 30 mL), brine (30 mL) and the combined organic layers were dried over MgSO<sub>4</sub>, filtered and concentrated *in vacuo*. The resulting fluorinated aldehyde was dissolved in DCE (40 mL), followed by the addition of (*R*)-naphthylethylamine **231** (1.1 equiv, 706  $\mu\text{L}$ , 4.4 mmol), and NaBH(OAc)<sub>3</sub> (4.0 equiv, 1.69 g, 8.0 mmol). The reaction was stirred for 18 h at RT. The reaction was quenched with saturated aqueous NaHCO<sub>3</sub> (20 mL) and the aqueous layer was extracted with EtOAc (3 x 20 mL). The combined organic layers were dried over MgSO<sub>4</sub>, filtered, and concentrated *in vacuo*. The crude product was purified by flash column chromatography with silica gel eluting with hexane/DCM. The desired product **234** was obtained as a yellow oil with 22% yield (322 mg, dr 85:15).  $[\alpha]_{\text{D}}^{20} +130.00$  (c 0.02, H<sub>2</sub>O). **<sup>1</sup>H NMR (400 MHz, CDCl<sub>3</sub>)**  $\delta$  8.18 (m, 1H, Ph), 7.87 (m, 1H, Ph), 7.74 (m, 1H, Ph), 7.67 – 7.58 (m, 1H, Ph), 7.54 – 7.42 (m, 3H, Ph), 7.34 (m, 5H, Ph), 5.17 – 5.13 (dm,  $J = 48.2\text{ Hz}$ , 1H, CHF), 5.11 (s, 2H, O-CH<sub>2</sub>), 5.08 – 4.99 (m, 1H), 4.65 (q,  $J = 6.4\text{ Hz}$ , 1H, CH-N), 2.95 – 2.58 (m, 4H, CH<sub>2</sub>), 1.50 (t,  $J = 6.4\text{ Hz}$ , 3H, CH<sub>3</sub>). **<sup>13</sup>C NMR (101 MHz, CDCl<sub>3</sub>)**  $\delta$  129.0 (C<sub>Arom</sub>), 128.6 (C<sub>Arom</sub>), 128.3 (C<sub>Arom</sub>), 128.3 (C<sub>Arom</sub>), 127.4 (C<sub>Arom</sub>), 125.8 (C<sub>Arom</sub>), 125.7 (C<sub>Arom</sub>), 125.4 (C<sub>Arom</sub>), 122.9 (C<sub>Arom</sub>), 122.8 (C<sub>Arom</sub>), 89.8 (d,  $J = 167.8\text{ Hz}$ , CHF), 66.6 (OCH<sub>2</sub>), 53.5 (N-CH), 50.7 (d,  $J = 21.2\text{ Hz}$ , CH<sub>2</sub>), 38.1 (d,  $J = 24.3\text{ Hz}$ , CH<sub>2</sub>), 23.8 (CH<sub>3</sub>). **<sup>19</sup>F NMR (376 MHz, CDCl<sub>3</sub>)**  $\delta$  -185.68. **ESI-MS** calculated for C<sub>23</sub>H<sub>24</sub>O<sub>2</sub>N [M-F] = 346.1802, observed [M-F] = 346.1799.

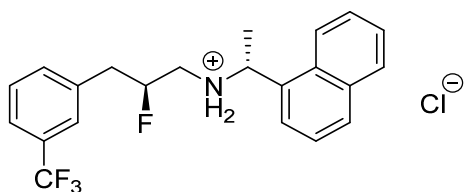
### Benzyl (S)-4-(benzyl((R)-1-phenylethyl)amino)-3-fluorobutanoate (235)



1-(S)-5-Benzyl-2,2,3,-trimethylimidazolidin-4-one dichloroacetic acid salt (**S**)-Cat (30%, 420 mg, 1.26 mmol) was added to a solution of THF (36 mL) and *i*-PrOH (3.6 mL). The reaction was cooled to  $-10\text{ }^{\circ}\text{C}$ . Benzyl 4-oxobutanoate **225** (1.0 equiv, 769 mg, 4.0 mmol) was added. A N-fluorobenzenesulfonimide (1.0 equiv, 1.26 g, 4.0 mmol) solution in THF was then added slowly in over 30 min. The reaction mixture was stirred for 12 h at  $-10\text{ }^{\circ}\text{C}$ . The reaction was then cooled to  $-78\text{ }^{\circ}\text{C}$ , quenched with Et<sub>2</sub>O (25 mL) and filtered through a pad of silica gel, eluting with Et<sub>2</sub>O. Dimethyl sulfide (DMS) (2.0 mL) was added. The resulting mixture was washed with saturated aqueous NaHCO<sub>3</sub> (3 x 30 mL), brine (30 mL) and the combined organic layers were dried over MgSO<sub>4</sub>, filtered and concentrated *in vacuo*. The resulting fluorinated aldehyde was dissolved in DCE (40 mL), followed by the addition of (*R*)-N-(1-Phenylethyl)benzylamine **232** (1.1 equiv, 870  $\mu\text{L}$ , 4.4 mmol), and NaBH(OAc)<sub>3</sub> (4.0 equiv, 1.7 g, 8.0 mmol). The reaction was stirred for 18 h at RT. The reaction was quenched with saturated aqueous NaHCO<sub>3</sub> (20 mL) and the aqueous layer was extracted with EtOAc (3 x 20 mL). The combined organic layers were dried over MgSO<sub>4</sub>, filtered, and concentrated *in vacuo*. The crude product was purified by flash column chromatography with silica gel eluting with hexane/DCM. The desired product **235** was obtained as a yellow oil with 18% yield (292 mg, dr 87:13).  $[\alpha]_{\text{D}}^{20} -31.1$  (c 0.55, CHCl<sub>3</sub>). **<sup>1</sup>H NMR (400 MHz, CDCl<sub>3</sub>)**  $\delta$  7.34 – 7.20 (m, 15H, Ph), 5.09 (d,  $J = 2.5$  Hz, 2H, O-CH<sub>2</sub>), 5.04 – 4.84 (m, 1H, CHF), 3.97 (qd,  $J = 6.9, 3.1$  Hz, 1H, N-CH), 3.62 (s, 2H, N-CH<sub>2</sub>), 2.90 – 2.50 (m, 4H, CH<sub>2</sub>), 1.39 (dd,  $J = 6.9, 3.1$  Hz, 3H, CH<sub>3</sub>). **<sup>13</sup>C NMR (101 MHz, CDCl<sub>3</sub>)**  $\delta$  128.9 (C<sub>Arom</sub>), 128.7 (C<sub>Arom</sub>), 128.4 (C<sub>Arom</sub>), 128.4 (C<sub>Arom</sub>), 128.3 (C<sub>Arom</sub>), 128.1 (C<sub>Arom</sub>), 127.1 (C<sub>Arom</sub>), 127.1 (C<sub>Arom</sub>), 90.0 (d,  $J = 171.3$  Hz, CHF), 66.6 (OCH<sub>2</sub>), 58.5 (N-CH), 55.7 (N-CH), 52.6 (d,  $J = 21.2$  Hz, CH<sub>2</sub>), 38.6 (d,  $J = 23.8$  Hz, CH<sub>2</sub>), 14.7 (CH<sub>3</sub>). **<sup>19</sup>F NMR (376 MHz, CDCl<sub>3</sub>)**  $\delta$  -181.90. **IR**  $\nu_{\text{max}}/\text{cm}^{-1}$  2970, 2360, 1734, 1170, 746, 696. **ESI-MS** calculated for C<sub>26</sub>H<sub>30</sub>O<sub>2</sub>N [M+2H<sup>+</sup>-F] = 388.2271, observed [M+2H<sup>+</sup>-F] = 388.2272.

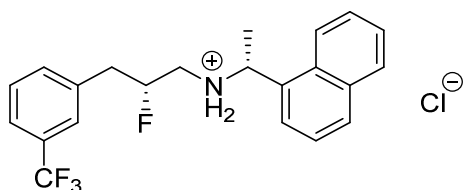


**(<sup>F</sup>S,<sup>R</sup>)-F-Cinacalcet ((<sup>F</sup>S,<sup>R</sup>)-276)**



1-(*S*)-5-Benzyl-2,2,3-trimethylimidazolidin-4-one dichloroacetic acid salt (**S**)-**Cat** (30%, 210 mg, 0.63 mmol) was added to a solution of THF (18 mL) and *i*-PrOH (1.8 mL). The reaction was cooled to -10 °C. 3-(Trifluoromethyl)benzenepropanal **271** (1.0 equiv, 340 μL, 2.0 mmol) was added. *N*-Fluorobenzenesulfonimide (1.0 equiv, 0.60 mg, 2.0 mmol) solution in THF was then added slowly in over 30 min. The reaction mixture was stirred for 12 h at -10 °C. The reaction was then cooled to -78 °C, quenched with Et<sub>2</sub>O (15 mL) and filtered through a pad of silica gel, eluting with Et<sub>2</sub>O. Dimethyl sulfide (DMS) (1.0 mL) was added. The resulting mixture was washed with saturated aqueous NaHCO<sub>3</sub> (3 x 30 mL), brine (30 mL) and the combined organic layers were dried over MgSO<sub>4</sub>, filtered and concentrated *in vacuo*. The resulting fluorinated aldehyde was dissolved in DCE (22 mL), followed by the addition of (*R*)-(1-naphthyl)ethylamine **231** (1.1 equiv, 350 μL, 2.2 mmol), and NaBH(OAc)<sub>3</sub> (2.0 equiv, 848 mg, 4.0 mmol). The reaction was stirred for 18 h at RT. The reaction was quenched with saturated aqueous NaHCO<sub>3</sub> (20 mL) and the aqueous layer was extracted with EtOAc (3 x 20 mL). The combined organic layers were dried over MgSO<sub>4</sub>, filtered, and concentrated *in vacuo*. The crude product was purified by flash column chromatography on silica gel eluting with hexane/EtOAc. The desired product (**F**<sup>S</sup>,**R**)-**269** was obtained as a yellow oil with 28% yield (199 mg, dr 99:1). (**F**<sup>S</sup>,**R**)-**269** was then converted to a salt with the addition of HCl in diethyl ether (1M, 0.56 mmol) and recrystallised in acetone/DCM to afford (**F**<sup>S</sup>,**R**)-**276** as a white solid (231 mg). [ $\alpha$ ]<sup>20</sup><sub>D</sub> -47.0 (c 0.54, CHCl<sub>3</sub>). IR  $\nu_{\text{max}}/\text{cm}^{-1}$  2957, 2684, 1585, 1452, 1329, 1161, 1120, 1072, 800, 779. **1H NMR** (400 MHz, MeOD)  $\delta$  8.15 – 7.22 (m, 10H, Ph), 4.76 (dm, *J* = 48.8 Hz, 1H, CHF), 4.66 (q, *J* = 6.7 Hz, 1H, N-CH), 2.96 – 2.62 (m, 4H, CH<sub>2</sub>), 1.47 (d, *J* = 6.7 Hz, 3H, CH<sub>3</sub>). **13C NMR** (101 MHz, MeOD)  $\delta$  132.9 (C<sub>Arom</sub>), 129.6 (C<sub>Arom</sub>), 129.0 (C<sub>Arom</sub>), 127.2 (C<sub>Arom</sub>), 126.2 (C<sub>Arom</sub>), 125.2 (C<sub>Arom</sub>), 121.5 (C<sub>Arom</sub>), 89.8 (d, *J* = 173.0 Hz, CHF), 53.25 (CH-N), 48.9 (d, *J* = 20.6 Hz, CH<sub>2</sub>), 37.7 (d, *J* = 19.2 Hz, CH<sub>2</sub>), 18.91 (CH<sub>3</sub>). **19F NMR** (377 MHz, MeOD)  $\delta$  -63.9 (CF<sub>3</sub>), -186.2 (CHF). **ESI-MS** calculated for C<sub>22</sub>H<sub>22</sub>NF [M+H<sup>+</sup>] = 376.1688, observed [M+H<sup>+</sup>] = 376.1678.

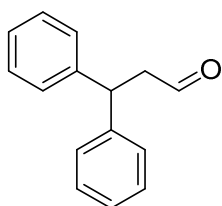
**(<sup>F</sup>R,R)-F-Cinacalcet ((<sup>F</sup>R,R)-276)**



1-(*R*)-5-Benzyl-2,2,3-trimethylimidazolidin-4-one dichloroacetic acid salt (**R**)-Cat (30%, 210 mg, 0.63 mmol) was added to a solution of THF (18 mL) and *i*-PrOH (1.8 mL). The reaction was cooled to -10 °C. 3-(Trifluoromethyl)benzenepropanal **271** (1.0 equiv, 340 μL, 2.0 mmol) was added. *N*-Fluorobenzenesulfonimide (1.0 equiv, 0.60 mg, 2.0 mmol) solution in THF was then added slowly in over 30 min. The reaction mixture was stirred for 12 h at -10 °C. The reaction was then cooled to -78 °C, quenched with Et<sub>2</sub>O (15 mL) and filtered through a pad of silica gel, eluting with Et<sub>2</sub>O. Dimethyl sulfide (DMS) (1.0 mL) was added. The resulting mixture was washed with saturated aqueous NaHCO<sub>3</sub> (3 x 30 mL), brine (30 mL) and the combined organic layers were dried over MgSO<sub>4</sub>, filtered and concentrated *in vacuo*. The resulting fluorinated aldehyde was dissolved in DCE (22 mL), followed by the addition of (*R*)-(1-naphthyl)ethylamine **231** (1.1 equiv, 350 μL, 2.2 mmol), and NaBH(OAc)<sub>3</sub> (2.0 equiv, 848 mg, 4.0 mmol). The reaction was stirred for 18 h at RT. The reaction was quenched with saturated aqueous NaHCO<sub>3</sub> (20 mL) and the aqueous layer was extracted with EtOAc (3 x 20 mL). The combined organic layers were dried over MgSO<sub>4</sub>, filtered, and concentrated *in vacuo*. The crude product was purified by flash column chromatography on silica gel eluting with hexane/EtOAc. The desired product (<sup>F</sup>R,R)-**269** was obtained as a yellow oil with 50% yield (375 mg, dr 99:1). (<sup>F</sup>R,R)-**269** was then converted to a salt with the addition of HCl in diethyl ether (1M, 1.0 mmol) and recrystallised in acetone/DCM to afford (<sup>F</sup>R,R)-**276** as a white solid (412 mg).  $[\alpha]^{20}_{\text{D}}$  -15.4 (c 0.37, CHCl<sub>3</sub>). IR  $\nu_{\text{max}}/\text{cm}^{-1}$  2957, 2679, 1454, 1327, 1161, 1119, 1072, 800, 777. <sup>1</sup>H NMR (400 MHz, MeOD)  $\delta$  8.17 (d, *J* = 8.4 Hz, 1H, Ph), 7.88 – 7.82 (m, 1H, Ph), 7.74 (d, *J* = 8.2 Hz, 1H, Ph), 7.62 (d, *J* = 7.2 Hz, 1H, Ph), 7.53 – 7.28 (m, 8H, Ph), 4.86 (dm, *J* = 50.1 Hz, 1H, CHF), 4.66 (q, *J* = 6.6 Hz, 1H, CH-N) 3.01– 2.57 (m, 4H, CH<sub>2</sub>), 1.47 (d, *J* = 6.6 Hz, 3H, CH<sub>3</sub>). <sup>13</sup>C NMR (101 MHz, MeOD)  $\delta$  132.9 (C<sub>Arom</sub>), 129.63, 129.0 (C<sub>Arom</sub>), 128.9 (C<sub>Arom</sub>), 127.1 (C<sub>Arom</sub>), 126.2 (C<sub>Arom</sub>), 125.2 (C<sub>Arom</sub>), 123.5 (C<sub>Arom</sub>), 121.7 (C<sub>Arom</sub>), 89.9 (d, *J* = 176.6 Hz, CHF), 53.31 (CH-N), 49.0 (d, *J* = 18.1 Hz, CH<sub>2</sub>), 37.7 (d, *J* = 18.6 Hz, CH<sub>2</sub>), 18.58 (CH<sub>3</sub>). <sup>19</sup>F NMR (376 MHz, MeOD)  $\delta$  -64.1, -

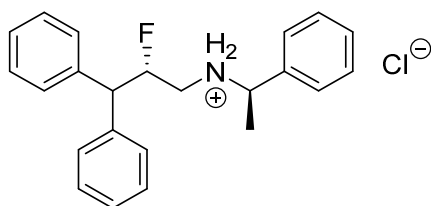
185.94. **ESI-MS** calculated for  $C_{22}H_{22}NF$   $[M+H^+] = 376.1688$ , observed  $[M+H^+] = 376.1679$ .

### 3,3-Diphenylpropanal (279)



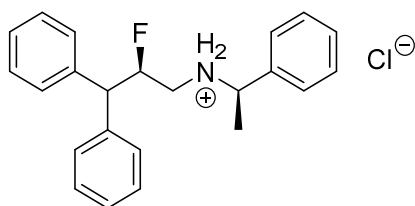
Following a procedure adapted from reference,<sup>309</sup> NaHCO<sub>3</sub> (4.5 equiv, 1.89 g, 22.5 mmol), Dess-Martin periodinane (1.5 equiv, 3.2 g, 7.5 mmol), was added to a solution at 0 °C of dichloromethane (100 mL) containing 3,3-diphenyl-1-propanol **278** (1.0 equiv, 1 mL, 5 mmol). The reaction mixture was stirred for 1 h at 0 °C. The reaction was warmed to RT and was washed with saturated aqueous K<sub>2</sub>CO<sub>3</sub> (50 mL) and saturated aqueous NaHCO<sub>3</sub> (50 mL). The aqueous layer was extracted with EtOAc (3 x 70 mL). The combined organic layers were dried over MgSO<sub>4</sub>, filtered, and concentrated *in vacuo*. This material was used without further purification. According to the reference<sup>309</sup> and the NMR the desired product **279**, was obtained as a yellow oil with a 70% yield (736 mg). **IR**  $\nu_{\text{max}}/\text{cm}^{-1}$  2918, 2358, 1697, 1454, 987, 758, 746, 692. **<sup>1</sup>H NMR (400 MHz, CDCl<sub>3</sub>)**  $\delta$  9.76 (s, 1H, CHO), 7.41 – 7.09 (m, 10H, Ph), 3.20 (dd,  $J = 7.8, 1.9$  Hz, 2H, CH<sub>2</sub>), 1.37 (t,  $J = 6.9$  Hz, 1H, CH). **ESI-MS** calculated for C<sub>15</sub>H<sub>15</sub>O [M+H<sup>+</sup>] = 211.1117, observed [M+H<sup>+</sup>] = 211.1116.

**(<sup>F</sup>S,*R*)-F-Fendiline ((<sup>F</sup>S,*R*)-287)**



1-(*S*)-5-Benzyl-2,2,3-trimethylimidazolidin-4-one dichloroacetic acid salt (**S**)-**Cat** (30%, 210 mg, 0.63 mmol) was added to a solution of THF (18 mL) and *i*-PrOH (1.8 mL). The reaction was cooled to -10 °C. 3,3-Diphenylpropanal **279** (1.0 equiv, 421 mg, 2.0 mmol) was added. *N*-Fluorobenzenesulfonimide (1.0 equiv, 0.60 mg, 2.0 mmol) solution in THF was then added slowly in over 30 min. The reaction mixture was stirred for 12 h at -10 °C. The reaction was then cooled to -78 °C, quenched with Et<sub>2</sub>O (15 mL) and filtered through a pad of silica gel, eluting with Et<sub>2</sub>O. Dimethyl sulfide (DMS) (1.0 mL) was added. The resulting mixture was washed with saturated aqueous NaHCO<sub>3</sub> (3 x 30 mL), brine (30 mL) and the combined organic layers were dried over MgSO<sub>4</sub>, filtered and concentrated *in vacuo*. The resulting fluorinated aldehyde was dissolved in DCE (22 mL), followed by the addition of (*R*)- $\alpha$ -methylbenzylamine **230** (1.1 equiv, 280  $\mu$ L, 2.2 mmol), and NaBH(OAc)<sub>3</sub> (2.0 equiv, 848 mg, 4.0 mmol). The reaction was stirred for 18 h at RT. The reaction was quenched with saturated aqueous NaHCO<sub>3</sub> (20 mL) and the aqueous layer was extracted with EtOAc (3 x 20 mL). The combined organic layers were dried over MgSO<sub>4</sub>, filtered, and concentrated *in vacuo*. The crude product was purified by flash column chromatography on silica gel eluting with hexane/EtOAc. The desired product (**F**<sup>S</sup>,*R*)-**280** was obtained as a yellow oil with 56% yield (373 mg, dr 90:10). (**F**<sup>S</sup>,*R*)-**280** was then converted to a salt with the addition of HCl in diethyl ether (1M, 1.12 mmol) and recrystallised in acetone/DCM to afford (**F**<sup>S</sup>,*R*)-**287** as a white solid (414 mg). [ $\alpha$ ]<sub>D</sub><sup>20</sup> +17.2 (c 0.57, CHCl<sub>3</sub>). IR  $\nu_{\text{max}}/\text{cm}^{-1}$  2959, 2747, 1578, 1452, 1082, 1029, 762, 738, 698. <sup>1</sup>H NMR (400 MHz, MeOD)  $\delta$  7.46 – 7.35 (m, 5H, Ph), 7.34 – 7.17 (m, 10H, Ph), 5.57 (dm, *J* = 48.4 Hz, 1H, CHF), 4.41 (q, *J* = 6.9 Hz, 1H, CH), 4.20 (dd, *J* = 16.9, 8.2 Hz, 1H, N-CH), 3.02 – 2.92 (m, 2H, CH<sub>2</sub>), 1.63 (d, *J* = 6.9 Hz, 3H, CH<sub>3</sub>). <sup>13</sup>C NMR (101 MHz, MeOD)  $\delta$  129.3 (C<sub>Arom</sub>), 129.2 (C<sub>Arom</sub>), 128.7 (C<sub>Arom</sub>), 128.2 (C<sub>Arom</sub>), 127.8 (C<sub>Arom</sub>), 127.1 (C<sub>Arom</sub>), 126.8 (C<sub>Arom</sub>), 90.2 (d, *J* = 183.5 Hz, CHF), 58.1 (CH-N), 53.5 (d, *J* = 19.5 Hz, CH<sub>2</sub>), 18.7 (CH<sub>3</sub>). <sup>19</sup>F NMR (376 MHz, MeOD)  $\delta$  -189.9. ESI-MS calculated for C<sub>23</sub>H<sub>25</sub>NF [M+H<sup>+</sup>] = 334.1971, observed [M+H<sup>+</sup>] = 334.1956.

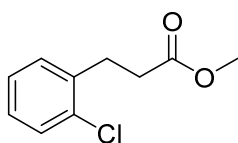
**(<sup>F</sup>R,R)-F-Fendiline ((<sup>F</sup>R,R)-287)**



1-(*R*)-5-Benzyl-2,2,3-trimethylimidazolidin-4-one dichloroacetic acid salt (**R**)-**Cat** (30%, 210 mg, 0.63 mmol) was added to a solution of THF (18 mL) and *i*-PrOH (1.8 mL). The reaction was cooled to -10 °C. 3,3-Diphenylpropanal **279** (1.0 equiv, 421 mg, 2.0 mmol) was added. *N*-Fluorobenzenesulfonimide (1.0 equiv, 0.60 mg, 2.0 mmol) solution in THF was then added slowly in over 30 min. The reaction mixture was stirred for 12 h at -10 °C. The reaction was then cooled to -78 °C, quenched with Et<sub>2</sub>O (15 mL) and filtered through a pad of silica gel, eluting with Et<sub>2</sub>O. Dimethyl sulfide (DMS) (1.0 mL) was added. The resulting mixture was washed with saturated aqueous NaHCO<sub>3</sub> (3 x 30 mL), brine (30 mL) and the combined organic layers were dried over MgSO<sub>4</sub>, filtered and concentrated *in vacuo*. The resulting fluorinated aldehyde was dissolved in DCE (22 mL), followed by the addition of (*R*)- $\alpha$ -methylbenzylamine **230** (1.1 equiv, 280  $\mu$ L, 2.2 mmol), and NaBH(OAc)<sub>3</sub> (2.0 equiv, 848 mg, 4.0 mmol). The reaction was stirred for 18 h at RT. The reaction was quenched with saturated aqueous NaHCO<sub>3</sub> (20 mL) and the aqueous layer was extracted with EtOAc (3 x 20 mL). The combined organic layers were dried over MgSO<sub>4</sub>, filtered, and concentrated *in vacuo*. The crude product was purified by flash column chromatography on silica gel eluting with hexane/EtOAc. The desired product (**F**,**R**,**R**)-**280** was obtained as a yellow oil with 50% yield (333 mg, dr 95:5). (**F**,**R**,**R**)-**280** was then converted to a salt with the addition of HCl in diethyl ether (1M, 1.0 mmol) and recrystallised in acetone/DCM to afford (**F**,**R**,**R**)-**287** as a white crystals (370 mg). [ $\alpha$ ]<sup>20</sup><sub>D</sub> +20.7 (c 0.45, CHCl<sub>3</sub>). IR  $\nu_{\text{max}}/\text{cm}^{-1}$  2974, 2747, 1577, 1452, 1082, 1029, 764, 739, 698. <sup>1</sup>H NMR (400 MHz, MeOD)  $\delta$  7.52 – 7.40 (m, 7H, Ph), 7.38 – 7.18 (m, 9H, Ph), 5.51 (dm, *J* = 50.0, 1H, CHF), 4.44 (m, 1H, CH), 4.24 (dd, *J* = 18.4, 7.8 Hz, 1H, N-CH), 3.26 (dt, *J* = 13.8, 10.8 Hz, 1H, CH<sub>2</sub>), 2.92 (ddd, *J* = 35.8, 13.8, 1.9 Hz, 1H, CH<sub>2</sub>), 1.67 (t, *J* = 7.8 Hz, 3H, CH<sub>3</sub>). <sup>13</sup>C NMR (101 MHz, MeOD)  $\delta$  129.4 (C<sub>Arom</sub>), 129.2 (C<sub>Arom</sub>), 128.6 (C<sub>Arom</sub>), 128.3 (C<sub>Arom</sub>), 128.3 (C<sub>Arom</sub>), 127.7 (C<sub>Arom</sub>), 127.3 (C<sub>Arom</sub>), 127.1 (C<sub>Arom</sub>), 126.9 (C<sub>Arom</sub>), 90.7(d, *J* = 179.1 Hz, CHF), 58.8 (CH-N), 53.5 (d, *J* = 21.1 Hz, CH<sub>2</sub>), 17.98 (CH<sub>3</sub>). <sup>19</sup>F NMR (377 MHz, MeOD)  $\delta$  -189.8. ESI-MS calculated for C<sub>23</sub>H<sub>25</sub>NF [M+H<sup>+</sup>] = 334.1971, observed [M+H<sup>+</sup>] = 334.1957.

Crystal data for  $C_{23}H_{25}ClFN$ ,  $M = 369.89 \text{ g.mol}^{-1}$ , colourless prism, crystal dimensions  $0.11 \times 0.08 \times 0.05 \text{ mm}$ , orthorhombic, space group  $P 2_12_12_1$ ,  $a = 9.62111(9)$ ,  $b = 9.94701(9)$ ,  $c = 20.1391(2)$ ,  $V = 1924.34(3) \text{ \AA}^3$ ,  $Z = 4$ ,  $T = 173 \text{ K}$ ,  $R_I = 0.0237$ ,  $wR_2 = 0.0640$ , for 20184 reflections with  $I > 2\sigma(I)$ . Data were collected using Rigaku MM-007HF High Brilliance RA generator/confocal optics with XtaLAB P100 diffractometer [Cu  $K\alpha$  radiation ( $\lambda = 1.54187 \text{ \AA}$ )] (Annexe1).

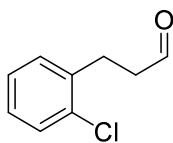
### Methyl 3-(2-chlorophenyl)propanoate (**283**)



Following a procedure adapted from reference,<sup>310</sup> 3-(2-chlorophenyl)propionic acid **282** (1.0 equiv, 6.2 g, 34 mmol) was added to MeOH (60 mL). The mixture was stirred at rt until a homogeneous mixture was formed. To this solution was added thionyl chloride (0.36 equiv, 0.9 mL, 12 mmol). The mixture was stirred for 2 h under reflux before the addition of further thionyl chloride (0.36 equiv, 0.9 mL, 12 mmol). The reaction was then stirred for a further 2 h under reflux. The reaction was cooled down to RT and concentrated *in vacuo*. The resulting oil was dissolved in DCM (60 mL) and washed with saturated aqueous NaHCO<sub>3</sub> (60 mL). The combined organic layers were dried over MgSO<sub>4</sub>, filtered, and concentrated *in vacuo*. This material was used without further purification. According to the reference<sup>310</sup> and the NMR the desired product **283**, was obtained as a yellow oil with 99% yield (6.60 g). **IR**  $\nu_{\text{max}}/\text{cm}^{-1}$  2951, 1734, 1436, 1157, 1053, 750. **<sup>1</sup>H NMR (400 MHz, CDCl<sub>3</sub>)**  $\delta$  7.39 – 7.11 (m, 4H, Ph), 3.68 (s, 3H, O-CH<sub>3</sub>), 3.07 (dd,  $J = 8.4, 7.2$  Hz, 2H, CH<sub>2</sub>), 2.66 (dd,  $J = 8.4, 7.2$  Hz, 2H, CH<sub>2</sub>). **<sup>13</sup>C NMR (101 MHz, CDCl<sub>3</sub>)**  $\delta$  173.29 (CO<sub>2</sub>), 138.14 (C<sub>Arom</sub>), 130.59 (C<sub>Arom</sub>), 129.70 (C<sub>Arom</sub>), 128.00 (C<sub>Arom</sub>), 127.05 (C<sub>Arom</sub>), 51.82 (OCH<sub>3</sub>), 33.89 (CH<sub>2</sub>), 29.08 (CH<sub>2</sub>). **ESI-MS** calculated for C<sub>10</sub>H<sub>12</sub>O<sub>2</sub>Cl [M+H<sup>+</sup>] = 199.0520, observed [M+H<sup>+</sup>] = 199.0520.

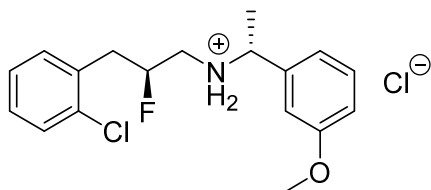


### 3-(2-Chlorophenyl)propanal (**284**)



Following a procedure adapted from reference,<sup>311</sup> to a solution of methyl 3-(2-chlorophenyl)propanoate **283** (1.0 equiv, 8.25 mmol) in anhydrous Et<sub>2</sub>O (82.5 mL) and cooled to -78 °C, was added diisobutylaluminum hydride solution (1.0 M in hexane, 9.4 mL, 9.4 mmol) dropwise under a nitrogen atmosphere. The reaction mixture was stirred for 1 h at -78 °C. The reaction was quenched by the addition of water (1.22 mL). The mixture was warmed up to RT and the organic layer was dried over MgSO<sub>4</sub>, filtered and concentrated *in vacuo*. This material was used without further purification. According to the reference<sup>311</sup> and the NMR the desired product **284**, was obtained as a yellow oil with as 80% yield (1.11 g). <sup>1</sup>H NMR (400 MHz, CDCl<sub>3</sub>) δ 9.82 (s, 1H, CHO), 7.40 – 7.04 (m, 4H, Ph), 3.05 (t, *J* = 7.6 Hz, 2H, CH<sub>2</sub>), 2.79 (t, *J* = 7.6 Hz, 2H, CH<sub>2</sub>).

**(<sup>F</sup>S,*R*)-F-Tecalcet ((<sup>F</sup>S,*R*)-288)**

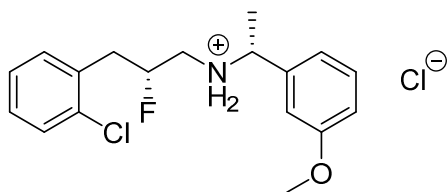


1-(*S*)-5-Benzyl-2,2,3,-trimethylimidazolidin-4-one dichloroacetic acid salt (**S**)-**Cat** (30%, 210 mg, 0.63 mmol) was added to a solution of THF (18 mL) and *i*-PrOH (1.8 mL). The reaction was cooled to -10 °C. 3-(2-Chlorophenyl)propanal **284** (1.0 equiv, 337 mg, 2.0 mmol) was added. N-Fluorobenzenesulfonimide (1.0 equiv, 0.60 mg, 2.0 mmol) solution in THF was then added slowly in over 30 min. The reaction mixture was stirred for 12 h at -10 °C. The reaction was then cooled to -78 °C, quenched with Et<sub>2</sub>O (15 mL) and filtered through a pad of silica gel, eluting with Et<sub>2</sub>O. Dimethyl sulfide (DMS) (1 mL) was added. The resulting mixture was washed with saturated aqueous NaHCO<sub>3</sub> (3 x 30 mL), brine (30 mL) and the combined organic layers were dried over MgSO<sub>4</sub>, filtered and concentrated *in vacuo*. The resulting fluorinated aldehyde was dissolved in DCE (22 mL), followed by the addition of (*R*)-3-methoxy- $\alpha$ -methylbenzylamine **285** (1.1 equiv, 365  $\mu$ L, 2.2 mmol), and NaBH(OAc)<sub>3</sub> (2.0 equiv, 848 mg, 4.0 mmol). The reaction was stirred for 18 h at RT. The reaction was quenched with saturated aqueous NaHCO<sub>3</sub> (20 mL) and the aqueous layer was extracted with EtOAc (3 x 20 mL). The combined organic layers were dried over MgSO<sub>4</sub>, filtered, and concentrated *in vacuo*. The crude product was purified by flash column chromatography on silica gel eluting with hexane/EtOAc. The desired product (**F***S*,*R*)-**281** was obtained as a yellow oil with 54% yield (347 mg, dr 93:7). (**F***S*,*R*)-**281** was then converted to a salt with the addition of HCl in diethyl ether (1M, 1.08 mmol) and recrystallised in acetone/DCM to afford (**F***S*,*R*)-**288** as a white crystals (386 mg). [ $\alpha$ ]<sub>D</sub><sup>20</sup> +22.6 (c 0.67, CHCl<sub>3</sub>). IR  $\nu_{\text{max}}/\text{cm}^{-1}$  2965, 2621, 1595, 1469, 1255, 1055, 1036, 860, 799, 752, 704. <sup>1</sup>H NMR (400 MHz, MeOD)  $\delta$  7.44 – 7.34 (m, 2H, Ph), 7.33 – 7.24 (m, 3H, Ph), 7.06 – 6.97 (m, 3H, Ph), 5.11 (dm, *J* = 49.5 Hz, 1H, CHF), 4.35 (q, *J* = 6.5 Hz, 1H, CH-N), 3.85 (s, 3H, O-CH<sub>3</sub>), 3.21 – 2.93 (m, 4H, CH<sub>2</sub>), 1.65 (t, *J* = 6.5 Hz, 3H, CH<sub>3</sub>). <sup>13</sup>C NMR (101 MHz, MeOD)  $\delta$  131.7 (C<sub>Arom</sub>), 130.2 (C<sub>Arom</sub>), 129.3 (C<sub>Arom</sub>), 128.7 (C<sub>Arom</sub>), 126.9 (C<sub>Arom</sub>), 119.1 (C<sub>Arom</sub>), 114.3 (C<sub>Arom</sub>), 112.8 (C<sub>Arom</sub>), 88.8 (d, *J* = 174.7 Hz, CHF), 58.31 (CH-N), 54.44 (CH<sub>3</sub>-O), 48.8 (d, *J* = 17.8 Hz, CH<sub>2</sub>), 36.0 (d, *J* = 19.9 Hz,

CH<sub>2</sub>), 19.06 (CH<sub>3</sub>). **<sup>19</sup>F NMR (377 MHz, MeOD)** δ -186.8. **ESI-MS** calculated for C<sub>18</sub>H<sub>22</sub>ONClF [M+H<sup>+</sup>] = 322.1374, observed [M+H<sup>+</sup>] = 322.1365.

Crystal data for C<sub>8</sub>H<sub>8</sub>Cl<sub>2</sub>O<sub>8</sub>, *M* = 358.26 g.mol<sup>-1</sup>, colourless needles, crystal dimensions 0.16 x 0.03 x 0.01 mm, orthorhombic, space group P 2<sub>1</sub>2<sub>1</sub>2<sub>1</sub>, *a* = 7.3528(4), *b* = 10.6598(5), *c* = 23.949(2), *V* = 1877.1(2) Å<sup>3</sup>, *Z* = 4, *T* = 173 K, *R*<sub>1</sub> = 0.0453, *wR*<sub>2</sub> = 0.1183, for 19872 reflections with *I* > 2σ(*I*). Data were collected using Rigaku MM-007HF High Brilliance RA generator/confocal optics with XtaLAB P100 diffractometer [Cu Kα radiation (λ = 1.54187 Å)] (Annexe 2).

**(<sup>F</sup>R,R)-F-Tecalcet ((<sup>F</sup>R,R)-288)**

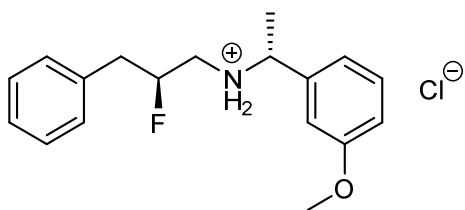


1-(*R*)-5-Benzyl-2,2,3,-trimethylimidazolidin-4-one dichloroacetic acid salt (*R*)-Cat (30%, 210 mg, 0.63 mmol) was added to a solution of THF (18 mL) and *i*-PrOH (1.8 mL). The reaction was cooled to -10 °C. 3-(2-Chlorophenyl)propanal **284** (1.0 equiv, 337 mg, 2.0 mmol) was added. N-Fluorobenzenesulfonimide (1.0 equiv, 0.60 mg, 2.0 mmol) solution in THF was then added slowly in over 30 min. The reaction mixture was stirred for 12 h at -10 °C. The reaction was then cooled to -78 °C, quenched with Et<sub>2</sub>O (15 mL) and filtered through a pad of silica gel, eluting with Et<sub>2</sub>O. Dimethyl sulfide (DMS) (1 mL) was added. The resulting mixture was washed with saturated aqueous NaHCO<sub>3</sub> (3 x 30 mL), brine (30 mL) and the combined organic layers were dried over MgSO<sub>4</sub>, filtered and concentrated *in vacuo*. The resulting fluorinated aldehyde was dissolved in DCE (22 mL), followed by the addition of (*R*)-3-methoxy- $\alpha$ -methylbenzylamine **285** (1.1 equiv, 365  $\mu$ L, 2.2 mmol), and NaBH(OAc)<sub>3</sub> (2.0 equiv, 848 mg, 4.0 mmol). The reaction was stirred for 18 h at RT. The reaction was quenched with saturated aqueous NaHCO<sub>3</sub> (20 mL) and the aqueous layer was extracted with EtOAc (3 x 20 mL). The combined organic layers were dried over MgSO<sub>4</sub>, filtered, and concentrated *in vacuo*. The crude product was purified by flash column chromatography on silica gel eluting with hexane/EtOAc. The desired product (<sup>F</sup>R,R)-**281** was obtained as a yellow oil with 56% yield (360 mg, dr 93:7). (<sup>F</sup>R,R)-**281** was then converted to a salt with the addition of HCl in diethyl ether (1M, 1.12 mmol) and recrystallised in acetone/DCM to afford (<sup>F</sup>R,R)-**288** as a white crystals (401 mg). [ $\alpha$ ]<sub>D</sub><sup>20</sup> -27.4 (c 0.50, CHCl<sub>3</sub>). IR  $\nu_{\text{max}}/\text{cm}^{-1}$  2943, 2648, 1585, 1489, 1259, 1049, 786, 746, 704. <sup>1</sup>H NMR (400 MHz, MeOD)  $\delta$  7.44 – 7.34 (m, 3H), 7.34 – 7.15 (m, 6H), 7.07 – 7.00 (m, 3H), 4.97 (dm, *J* = 48.4 Hz 1H, CHF), 3.84 (s, 3H, O-CH<sub>3</sub>), 3.61 (t, *J* = 6.5 Hz, 1H, CH-N), 3.23 – 2.95 (m, 2H, CH<sub>2</sub>), 2.90 – 2.78 (m, 2H, CH<sub>2</sub>), 1.70 (d, *J* = 6.5 Hz, 3H, CH<sub>3</sub>). <sup>13</sup>C NMR (101 MHz, MeOD)  $\delta$  131.7 (C<sub>Arom</sub>), 130.4 (C<sub>Arom</sub>), 129.3 (C<sub>Arom</sub>), 129.0 (C<sub>Arom</sub>), 128.8 (C<sub>Arom</sub>), 127.4 (C<sub>Arom</sub>), 127.2 (C<sub>Arom</sub>), 126.9 (C<sub>Arom</sub>), 126.7 (C<sub>Arom</sub>), 119.2 (C<sub>Arom</sub>), 114.7 (C<sub>Arom</sub>), 113.1 (C<sub>Arom</sub>), 88.8 (d, *J* = 176.9 Hz, CHF), 58.96 (N-CH), 54.48 (O-CH<sub>3</sub>), 48.7 (d, *J* = 12.2 Hz, CH<sub>2</sub>), 35.8 (d, *J* = 16.9 Hz, CH<sub>2</sub>),

32.3, 29.5, 17.9 (CH<sub>3</sub>). **<sup>19</sup>F NMR (377 MHz, MeOD)**  $\delta$  -186.4. **ESI-MS** calculated for C<sub>18</sub>H<sub>22</sub>ONClF [M+H<sup>+</sup>] = 322.1374, observed [M+H<sup>+</sup>] = 322.1366.

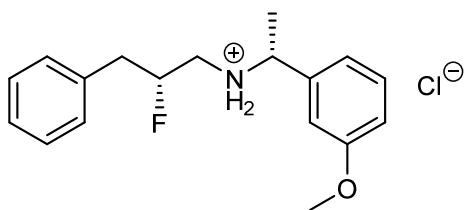
Crystal data for C<sub>8</sub>H<sub>8</sub>Cl<sub>2</sub>O<sub>8</sub>,  $M = 358.26 \text{ g}\cdot\text{mol}^{-1}$ , colourless prism, crystal dimensions 0.20 x 0.02 x 0.02 mm, tetragonal, space group P 4<sub>1</sub>,  $a = 16.6794(7)$ ,  $c = 7.1292(4)$ ,  $V = 1983.4(2) \text{ \AA}^3$ ,  $Z = 4$ ,  $T = 173 \text{ K}$ ,  $R_I = 0.0556$ ,  $wR_2 = 0.1559$ , for 12142 reflections with  $I > 2\sigma(I)$ . Data were collected using a Rigaku FR-X Ultrahigh Brilliance Microfocus RA generator/confocal optics with XtaLAB P200 diffractometer [Mo K $\alpha$  radiation ( $\lambda = 0.71073 \text{ \AA}$ )] (Annexe 3).

**(<sup>F</sup>S,*R*)-F-NPS R-467 (<sup>F</sup>S,*R*)-289**



1-(*S*)-5-Benzyl-2,2,3,-trimethylimidazolidin-4-one dichloroacetic acid salt (**S**)-**Cat** (30%, 210 mg, 0.63 mmol) was added to a solution of THF (18 mL) and *i*-PrOH (1.8 mL). The reaction was cooled to -10 °C. 3-Phenylpropanal **164** (1.0 equiv, 266  $\mu$ L, 2.0 mmol) was added. N-Fluorobenzenesulfonimide (1.0 equiv, 0.60 mg, 2.0 mmol) solution in THF was then added slowly in over 30 min. The reaction mixture was stirred for 12 h at -10 °C. The reaction was then cooled to -78 °C, quenched with Et<sub>2</sub>O (15 mL) and filtered through a pad of silica gel, eluting with Et<sub>2</sub>O. Dimethyl sulfide (DMS) (1 mL) was added. The resulting mixture was washed with saturated aqueous NaHCO<sub>3</sub> (3 x 30 mL), brine (30 mL) and the combined organic layers were dried over MgSO<sub>4</sub>, filtered and concentrated *in vacuo*. The resulting fluorinated aldehyde was dissolved in DCE (22 mL), followed by the addition of (*R*)-3-methoxy- $\alpha$ -methylbenzylamine **285** (1.1 equiv, 365  $\mu$ L, 2.2 mmol), and NaBH(OAc)<sub>3</sub> (2.0 equiv, 848 mg, 4.0 mmol). The reaction was stirred for 18 h at RT. The reaction was quenched with saturated aqueous NaHCO<sub>3</sub> (20 mL) and the aqueous layer was extracted with EtOAc (3 x 20 mL). The combined organic layers were dried over MgSO<sub>4</sub>, filtered, and concentrated *in vacuo*. The crude product was purified by flash column chromatography on silica gel eluting with hexane/EtOAc. The desired product (<sup>F</sup>S,*R*)-**286**, was obtained as a yellow oil with 47% yield (270 mg, dr 85:15). (<sup>F</sup>S,*R*)-**286** was then converted to a salt with the addition of HCl in diethyl ether (1M, 0.94 mmol) and recrystallised in acetone/DCM to afford (<sup>F</sup>S,*R*)-**289** as a white solid (304 mg). [ $\alpha$ ]<sub>D</sub><sup>20</sup> +28.9 (c 0.23, CHCl<sub>3</sub>). IR  $\nu_{\text{max}}/\text{cm}^{-1}$  2972, 2746, 1577, 1496, 1452, 1056, 1029, 738, 698. <sup>1</sup>H NMR (400 MHz, MeOD)  $\delta$  7.39 (t, *J* = 7.9 Hz, 1H, Ph), 7.34 – 7.16 (m, 4H, Ph), 7.09 – 6.97 (m, 3H, Ph), 5.08 (dm, *J* = 50.9 Hz, 1H, CHF), 4.13 (q, *J* = 6.6 Hz, 1H, N-CH), 3.84 (d, *J* = 1.7 Hz, 3H, O-CH<sub>3</sub>), 3.28 – 2.87 (m, 4H, CH<sub>2</sub>), 1.68 (dd, *J* = 6.6, 3.1 Hz, 3H, CH<sub>3</sub>). <sup>13</sup>C NMR (101 MHz, MeOD)  $\delta$  130.4 (C<sub>Arom</sub>), 129.0 (C<sub>Arom</sub>), 128.3 (C<sub>Arom</sub>), 126.8 (C<sub>Arom</sub>), 119.1 (C<sub>Arom</sub>), 114.7 (C<sub>Arom</sub>), 112.9 (C<sub>Arom</sub>), 89.7 (d, *J* = 168.5 Hz, CHF), 58.5 (N-CH), 54.5 (O-CH<sub>3</sub>), 48.5 (d, *J* = 21.2 Hz, CH<sub>2</sub>), 38.1 (d, *J* = 17.6 Hz, CH<sub>2</sub>), 18.4 (CH<sub>3</sub>). <sup>19</sup>F NMR (377 MHz, MeOD)  $\delta$  -186.3. ESI-MS calculated for C<sub>18</sub>H<sub>23</sub>ONF [M+H<sup>+</sup>] = 288.1764, observed [M+H<sup>+</sup>] = 288.1757.

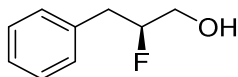
**(<sup>F</sup>R,R)-F-NPS R-467 ((<sup>F</sup>R,R)-289)**



1-(*R*)-5-Benzyl-2,2,3,-trimethylimidazolidin-4-one dichloroacetic acid salt (*R*)-Cat (30%, 210 mg, 0.63 mmol) was added to a solution of THF (18 mL) and *i*-PrOH (1.8 mL). The reaction was cooled to -10 °C. 3-Phenylpropanal **164** (1.0 equiv, 266  $\mu$ L, 2.0 mmol) was added. *N*-Fluorobenzenesulfonimide (1.0 equiv, 0.60 mg, 2.0 mmol) solution in THF was then added slowly in over 30 min. The reaction mixture was stirred for 12 h at -10 °C. The reaction was then cooled to -78 °C, quenched with Et<sub>2</sub>O (15 mL) and filtered through a pad of silica gel, eluting with Et<sub>2</sub>O. Dimethyl sulfide (DMS) (1 mL) was added. The resulting mixture was washed with saturated aqueous NaHCO<sub>3</sub> (3 x 30 mL), brine (30 mL) and the combined organic layers were dried over MgSO<sub>4</sub>, filtered and concentrated *in vacuo*. The resulting fluorinated aldehyde was dissolved in DCE (22 mL), followed by the addition of (*S*)-3-methoxy- $\alpha$ -methylbenzylamine **285** (1.1 equiv, 365  $\mu$ L, 2.2 mmol), and NaBH(OAc)<sub>3</sub> (2.0 equiv, 848 mg, 4.0 mmol). The reaction was stirred for 18 h at RT. The reaction was quenched with saturated aqueous NaHCO<sub>3</sub> (20 mL) and the aqueous layer was extracted with EtOAc (3 x 20 mL). The combined organic layers were dried over MgSO<sub>4</sub>, filtered, and concentrated *in vacuo*. The crude product was purified by flash column chromatography on silica gel eluting with hexane/EtOAc. The desired product (<sup>F</sup>*R,R*)-**286**, was obtained as a yellow oil with 62% yield (356 mg, dr 84:16). (<sup>F</sup>*R,R*)-**286** was then converted to a salt with the addition of HCl in diethyl ether (1M, 1.2 mmol) and recrystallised in acetone/DCM to afford (<sup>F</sup>*R,R*)-**289** as a white solid (401 mg). [ $\alpha$ ]<sup>20</sup><sub>D</sub> +42.6 (c 0.96, CHCl<sub>3</sub>). IR  $\nu_{\text{max}}/\text{cm}^{-1}$  2968, 2731, 1583, 1490, 1454, 1259, 1049, 786, 698. <sup>1</sup>H NMR (400 MHz, MeOD)  $\delta$  7.40 – 7.34 (m, 1H, Ph), 7.33 – 7.18 (m, 6H, Ph), 7.04 – 6.94 (m, 3H, Ph), 4.82 (dm, *J* = 50.6 Hz, 1H, CHF), 4.27 (q, *J* = 6.8 Hz, 1H, CH-N), 3.83 (d, *J* = 2.2 Hz, 3H, O-CH<sub>3</sub>), 3.15 (td, *J* = 13.3, 9.7 Hz, 1H, CH<sub>2</sub>), 3.04 – 2.85 (m, 3H, CH<sub>2</sub>), 1.62 (d, *J* = 6.8 Hz, 3H, CH<sub>3</sub>). <sup>13</sup>C NMR (101 MHz, MeOD)  $\delta$  130.1 (C<sub>Arom</sub>), 129.0 1 (C<sub>Arom</sub>), 128.2 1 (C<sub>Arom</sub>), 126.7 1 (C<sub>Arom</sub>), 119.1 1 (C<sub>Arom</sub>), 114.2 1 (C<sub>Arom</sub>), 112.8 1 (C<sub>Arom</sub>), 90.8 (d, *J* = 174.5 Hz, CHF), 58.74 (CH-N), 54.42 (O-CH<sub>3</sub>), 49.0 (d, *J* = 20.0 Hz, CH<sub>2</sub>), 38.4 (d, *J* = 20.0 Hz, CH<sub>2</sub>), 18.85 (CH<sub>3</sub>). <sup>19</sup>F NMR (377 MHz, MeOD)  $\delta$

-185.9. **ESI-MS** calculated for C<sub>18</sub>H<sub>23</sub>ONF [M+H<sup>+</sup>] = 288.1764, observed [M+H<sup>+</sup>] = 288.1756.

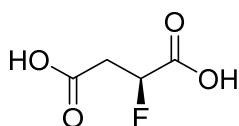
**(S)-2-Fluoro-3-phenylpropan-1-ol ((S)-188)**



1-(S)-5-Benzyl-2,2,3,-trimethylimidazolidin-4-one dichloroacetic acid salt (**S**)-**Cat** (30%, 420 mg, 0.200 mmol) was added to THF (18.0 mL) and *i*-PrOH (1.8 mL). The mixture was stirred at rt until a homogeneous mixture was formed. Then, the reaction was cooled to -10 °C. Phenylpropanal **164** (1.0 equiv, 530 μL, 4.0 mmol) was added. N-Fluorobenzenesulfonimide (1.0 equiv, 1.2 g, 4.0 mmol) solution in THF was then added slowly in over 30 min. The resulting reaction mixture was stirred for 12 h at -10 °C. The reaction was then cooled to -78 °C, diluted with Et<sub>2</sub>O (30 mL) and filtered through a pad of silica gel, eluting with Et<sub>2</sub>O. Dimethyl sulfide (DMS) (2.0 mL) was added, forming a white precipitate. The resulting mixture was washed with saturated aqueous NaHCO<sub>3</sub> (3 x 30 mL), brine (30 mL) and the combined organic layers were dried over MgSO<sub>4</sub>, filtered and concentrated *in vacuo*. The resulting fluorinated aldehyde was dissolved in DCM (24 mL) an ethanol (16 mL), followed by the addition NaBH<sub>4</sub> (2.0 equiv, 303 mg, 8.0 mmol). The reaction was stirred for 30 min at 0°C. The reaction was quenched with saturated aqueous ammonium chloride (308 mL), loved to RT and stirred for an extra 1 h. The reaction was the mixture was extracted with DCM (3 x 30 mL). The combined organic layers were washed with aqueous NaHCO<sub>3</sub> (1 x 30 mL), brine (1 x 30 mL) and dried over MgSO<sub>4</sub>, filtered, and concentrated *in vacuo*. The crude product was purified by flash column chromatography on silica gel eluting with hexane/EtOAc. The desired product (**S**)-**188** was obtained as a yellow oil with 71% yield (438 mg, er 99:1). [α]<sub>D</sub><sup>20</sup> -8.35 (c 1.27, CHCl<sub>3</sub>). **IR** ν<sub>max</sub>/cm<sup>-1</sup> 3350, 2916, 2360, 1454, 1049, 698. **<sup>1</sup>H NMR (400 MHz, CDCl<sub>3</sub>)** δ 7.34 – 7.28 (m, 2H, Ph), 7.27 – 7.19 (m, 3H, Ph), 4.78 (dm, *J* = 48.7 Hz, 1H), 3.85 – 3.61 (m, 2H), 3.11 – 2.86 (m, 2H). **<sup>13</sup>C NMR (101 MHz, CDCl<sub>3</sub>)** δ 130.4 (C<sub>Arom</sub>), 129.3 (C<sub>Arom</sub>), 128.6 (C<sub>Arom</sub>), 126.8 (C<sub>Arom</sub>), 94.6 (d, *J* = 172.7 Hz, CHF), 64.5 (d, *J* = 25.3 Hz, CH<sub>2</sub>), 37.6 (d, *J* = 21.6, CH<sub>2</sub>). **<sup>19</sup>F NMR (376 MHz, CDCl<sub>3</sub>)** δ -187.67. **ESI-MS** calculated for C<sub>9</sub>H<sub>12</sub>OF [M+H<sup>+</sup>] = 155.0788, observed [M+H<sup>+</sup>] = 155.0789.

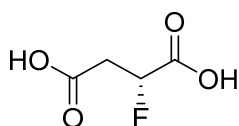


**(S)-2-Fluorosuccinic acid ((S)-315)**



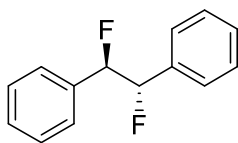
(S)-2-Fluoro-3-phenylpropan-1-ol (**(S)-188**) (1.0 equiv, 231 mg, 1.5 mmol) was added MeCN (5.9 mL), DCE (5.9 mL), H<sub>2</sub>O (14.8 mL), RuCl<sub>3</sub> (20%, 60 mg, 0.3 mmol) and NaIO<sub>4</sub> (21.0 equiv, 6.8 g, 31.5 mmol). The reaction mixture was stirred for 16 h at 70°C. The reaction was then cooled down to RT and filtered through a pad of celite<sup>®</sup>. The resulted mixture was extracted with H<sub>2</sub>O (3 x 15 mL). The combined aqueous layers were washed with DCM (3 x 10 mL) and concentrated in *vacuo*. The resulted solid was extracted with EtOAc (3 x 20 mL) and the combined organic layers were concentrated *in vacuo*. The crude product was purified by sublimation. The desired product (**(S)-315**) was obtained as a white solid with 76% yield (155 mg, er 99:1). m.p.: 131 °C. [ $\alpha$ ]<sub>D</sub><sup>20</sup> -199.47 (c 0.19, H<sub>2</sub>O). IR  $\nu_{\text{max}}/\text{cm}^{-1}$  2877, 2657, 2542, 2360, 1685, 1408, 1274, 1049, 923, 646. <sup>1</sup>H NMR (400 MHz, D<sub>2</sub>O)  $\delta$  5.19 (dm, *J* = 46.9 Hz, 1H, CHF), 3.03 – 2.86 (m, 2H, CH<sub>2</sub>). <sup>19</sup>F NMR (376 MHz, D<sub>2</sub>O)  $\delta$  -188.20. ESI-MS calculated for C<sub>4</sub>H<sub>4</sub>O<sub>4</sub>FNa [M+Na<sup>+</sup>] = 159.0064, observed [M+Na<sup>+</sup>] = 159.0060.

**(R)-2-Fluorosuccinic acid ((R)-315)**



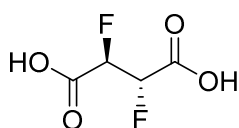
(R)-2-Fluoro-3-phenylpropan-1-ol (**R**)-**188** (1.0 equiv, 231 mg, 1.5 mmol) was added MeCN (5.9 mL), DCE (5.9 mL), H<sub>2</sub>O (14.8 mL), RuCl<sub>3</sub> (20%, 60 mg, 0.3 mmol) and NaIO<sub>4</sub> (21.0 equiv, 6.8 g, 31.5 mmol). The reaction mixture was stirred for 16 h at 70°C. The reaction was then cooled down to RT and filtered through a pad of celite<sup>®</sup>. The resulted mixture was extracted with H<sub>2</sub>O (3 x 15 mL). The combined aqueous layers were washed with DCM (3 x 10 mL) and concentrated in *vacuo*. The resulted solid was extracted with EtOAc (3 x 20 mL) and the combined organic layers were concentrated *in vacuo*. The crude product was purified by sublimation. The desired product (**R**)-**315** was obtained as a white solid with 67% yield (137 mg, er 99:1). m.p.: 124 °C. [ $\alpha$ ]<sub>D</sub><sup>20</sup> +198.90 (c 0.73, H<sub>2</sub>O). IR  $\nu_{\text{max}}/\text{cm}^{-1}$  2983, 2650, 2542, 1699, 1417, 1282, 1047, 925, 628. <sup>1</sup>H NMR (400 MHz, D<sub>2</sub>O)  $\delta$  5.21 (dm,  $J = 47.1$ , 1H, CHF), 3.03 – 2.90 (m, 2H, CH<sub>2</sub>). <sup>19</sup>F NMR (376 MHz, D<sub>2</sub>O)  $\delta$  -188.89. <sup>13</sup>C NMR (101 MHz, D<sub>2</sub>O)  $\delta$  85.7 (d,  $J = 180.5$  Hz, 1H, CHF), 36.9 – 36.7 (d,  $J = 22.1$  Hz, 2H, CH<sub>2</sub>). ESI-MS calculated for C<sub>4</sub>H<sub>4</sub>O<sub>4</sub>FNa [M+Na<sup>+</sup>] = 159.0064, observed [M+Na<sup>+</sup>] = 159.0058.

**(1*R*,2*S*)-1,2-Difluoro-1,2-diphenylethane (319)**



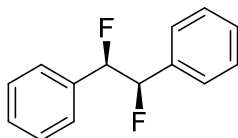
(*E*)-Stilbene (***E***-**318**) (1.0 equiv, 3.6 g, 20 mmol) and N-bromosuccinimide (1.0 equiv, 3.6 g, 20 mmol), were added to dry Et<sub>2</sub>O (20 mL) and HF/Pyridine (70% solution, 20 mL, 770 mmol). The reaction mixture was stirred at RT for 3 h. To the reaction mixture was added Ag(I)F (1.0 equiv, 2.5 g, 20 mmol). The reaction mixture was stirred at RT for an extra 12 h. The reaction was quenched with H<sub>2</sub>O (20 mL) and the mixture was extracted with Et<sub>2</sub>O (3 x 20 mL). The combined organic layers were washed with saturated aqueous NaHCO<sub>3</sub> (10 mL), H<sub>2</sub>O (10 mL), brine (10 mL) and the combined organic layers were dried over MgSO<sub>4</sub>, filtered and concentrated *in vacuo*. The crude product was recrystallised from MeOH followed by a second recrystallisation from petroleum ether. According to the reference<sup>304</sup> and the NMR, the desired product **319** was obtained as white crystals with 76% yield (3.3 g). m.p. (Petroleum ether): 97°C. **IR**  $\nu_{\text{max}}/\text{cm}^{-1}$  2958, 2358, 1496, 1456, 1242, 1207, 997, 829, 758, 596. **<sup>1</sup>H NMR (400 MHz, CDCl<sub>3</sub>)**  $\delta$  7.36 – 7.30 (m, 6H, Ph), 7.21 – 7.15 (m, 4H, Ph), 5.78 – 5.59 (m, 2H, CHF). **<sup>19</sup>F NMR (376 MHz, CDCl<sub>3</sub>)**  $\delta$  -186.70. **ESI-MS** calculated for C<sub>14</sub>H<sub>11</sub>F<sub>2</sub>Na [M+Na<sup>+</sup>] = 241.0799, observed [M+Na<sup>+</sup>] = 241.0798.

***erythro*-2,3-Difluorosuccinic acid (316)**



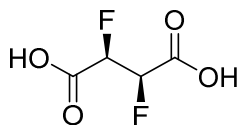
To *erythro*-1,2-difluoro-1,2-diphenylethane **319** (1.0 equiv, 1.0 g, 6.5 mmol) were added MeCN (14.1 mL), DCE (14.1 mL), H<sub>2</sub>O (35.8 mL), RuCl<sub>3</sub> (20%, 273.4 mg, 1.3 mmol) and NaIO<sub>4</sub> (16.0 equiv, 22.8 g, 106.5 mmol). The reaction mixture was stirred for 72 h at 70°C. The reaction was then cooled down to RT and filtered through a pad of celite. The resulted solution was the mixture was extracted with H<sub>2</sub>O (3 x 60 mL). The combined aqueous layer was washed with DCM (3 x 45 mL) and the combined aqueous layers were concentrated *in vacuo*. The resulting solid was extracted with EtOAc (3 x 90 mL) and comibined organic layers were concentrated in *vacuo*. The crude product was purified by sublimation. According to the reference<sup>304</sup> and the NMR, the desired product **316** was obtained as a white solid with 21% yield ( 210 mg). **IR**  $\nu_{\text{max}}/\text{cm}^{-1}$  3504, 3410, 2441, 1695, 1280, 1070, 827. **<sup>1</sup>H NMR (400 MHz, MeOD)**  $\delta$  5.62 – 5.41 (m, 2H, CHF). **<sup>19</sup>F NMR (376 MHz, MeOD)**  $\delta$  -202.01. **ESI-MS** calculated for C<sub>4</sub>H<sub>5</sub>O<sub>4</sub>F<sub>2</sub> [M+H<sup>+</sup>] = 155.0072, observed [M+H<sup>+</sup>] = 155.0073.

### 1,2-Difluoro-1,2-diphenylethane (**320**, racemic)



(*Z*)-stilbene (**Z**)-**318** (1.0 equiv, 3.6 g, 20 mmol) and *N*-bromosuccinimide (1.0 equiv, 3.6 g, 20 mmol), was added dry Et<sub>2</sub>O (20 mL) and HF/Pyridine (70% solution, 20 mL, 770 mmol). The reaction mixture was stirred at RT for 3 h. To the reaction mixture was added Ag(I)F (1.0 equiv, 2.5 g, 20 mmol). The reaction mixture was stirred at RT for an extra 12 h. The reaction was quenched with H<sub>2</sub>O (20 mL) and the mixture was extracted with Et<sub>2</sub>O (3 x 20 mL). The combined organic layers were washed with saturated aqueous NaHCO<sub>3</sub> (10 mL), H<sub>2</sub>O (10 mL), brine (10 mL) and the combined organic layers were dried over MgSO<sub>4</sub>, filtered and concentrated *in vacuo*. The crude product was recrystallised from MeOH, followed by a column chromatography hexane/DCM (20:1) and finally, recrystallised from petroleum ether. According to the reference<sup>304</sup> and the NMR, the desired product **320** was obtained as white crystals with 12% yield (521 mg). m.p.(Petroleum ether): 81 °C. **IR**  $\nu_{\text{max}}/\text{cm}^{-1}$  2972, 2360, 1494, 1454, 1001, 756, 696. **<sup>1</sup>H NMR (400 MHz, CDCl<sub>3</sub>)**  $\delta$  7.37 – 7.27 (m, 5H, Ph), 7.20 – 7.16 (m, 3H, Ph), 7.14 – 7.10 (m, 2H, Ph), 5.76 – 5.59 (m, 2H, CHF). **<sup>19</sup>F NMR (376 MHz, CDCl<sub>3</sub>)**  $\delta$  -186.71. **ESI-MS** calculated for C<sub>14</sub>H<sub>11</sub>F<sub>2</sub>Na [M+Na<sup>+</sup>] = 241.0799, observed [M+Na<sup>+</sup>] = 241.0799.

### 2,3-Difluorosuccinic acid (**317**, racemic)



To 1,2-difluoro-1,2-diphenylethane **320** (1.0 equiv, 185 mg, 0.85 mmol) was added MeCN (3.3 mL), DCE (3.3 mL), H<sub>2</sub>O (8.4 mL), RuCl<sub>3</sub> (20%, 35 mg, 0.17 mmol) and NaIO<sub>4</sub> (21.0 equiv, 3.83 g, 17.9 mmol). The reaction mixture was stirred for 72 h at 70°C. The reaction was then cooled down to RT and filtered through a pad of celite. The resulted mixture was extracted with H<sub>2</sub>O (3 x 10 mL). The combined aqueous layers were washed with DCM (3 x 5 mL) and the combined aqueous layers were concentrated *in vacuo*. The resulting solid was extracted with EtOAc (3 x 11 mL) and the combined organic layers were concentrated *in vacuo*. The crude product was purified by sublimation. According to the reference<sup>304</sup> and the NMR, the desired product **317** was obtained as a white solid with 26% yield (34 mg). **IR**  $\nu_{\text{max}}/\text{cm}^{-1}$  3504, 3410, 2441, 1695, 1280, 1070, 827. **<sup>1</sup>H NMR (400 MHz, D<sub>2</sub>O)**  $\delta$  5.42 – 5.19 (m, 2H, CHF). **<sup>19</sup>F NMR (376 MHz, D<sub>2</sub>O)**  $\delta$  -201.05. **ESI-MS** calculated for C<sub>4</sub>H<sub>4</sub>O<sub>4</sub>F<sub>2</sub> [M+H<sup>+</sup>] = 154.0788, observed [M+H<sup>+</sup>] = 154.0788.

## References

- 1 H. Abdeyazdan, H. Edris, M. H. Abbasi, *Int. J. ISSI*, 2011, **8**, 5–8.
- 2 H. Moissan, *Recherche sur l'isolement du fluor*, 1887.
- 3 H. Moissan, *La Nat.*, 1886, **875**, 363–366.
- 4 E. Desbeaux, *Physique populaire*, 1891.
- 5 J. M. Hamilton, *Adv. Fluor. Chem.*, 1963, **3**, 117–180.
- 6 T. Okazoe, *Proc. Japan Acad. Ser. B Phys. Biol. Sci.*, 2009, **85**, 276–289.
- 7 R. E. Banks, J. C. Taltow, *J. Fluor. Chem.*, 1986, **33**, 71–108.
- 8 T. Midley, A. L. Henne, *Ind. Eng. Chem.*, 1930, **22**, 542–545.
- 9 H. S. Booth, W. L. Mong, P. E. Burchfield, *Ind. Eng. Chem.*, 1932, **24**, 328–331.
- 10 H. G. Locke, W. R. Brode, A. L. Henne, *J. Am. Chem. Soc.*, 1934, **56**, 1726–1728.
- 11 H. Goldwhite, *J. Fluor. Chem.*, 1986, **33**, 109–132.
- 12 H. Ukiashi, M. Yamabe, H. Hiyake, *Prog. Polym. Sci.*, 1987, **12**, 229–270.
- 13 M. Yamabe, S. Munekata, I. Kaneko, H. Ukihashi, *J. Fluor. Chem.*, 1999, **94**, 65–68.
- 14 M. J. Molina, F. S. Rowland, *Nature*, 1974, **249**, 810–812.
- 15 United Nations Environment Programme, The Montreal Protocol, <https://www.unep.org/ozonaction/who-we-are/about-montreal-protocol>.
- 16 T. Okazoe, K. Watanabe, M. Itoh, D. Shirakawa, H. Okamoto, *Adv. Synth. Catal.*, 2001, **343**, 215–219.
- 17 T. Okazoe, K. Watanabe, M. Itoh, D. Shirakawa, S. Tatematsu, *J. Fluor. Chem.*, 2001, **112**, 109–116.
- 18 J. K. Nigell, *J. Am. Chem. Soc.*, 1990, **112**, 4740.
- 19 D. O'Hagan, D. Chambers, F. R. S. He, *Chem. Soc. Rev.*, 2008, **37**, 308–319.
- 20 W. R. Dolbier, A. C. Alty, O. P. Phanstiel, *J. Am. Chem. Soc.*, 1987, **109**, 3046–3050.
- 21 S. N. Pieniazek, K. N. Houk, *Angew. Chem. Int. Ed.*, 2006, **45**, 1442–1445.
- 22 E. Baciocchi, R. Ruzziconi, G. V. Sebastiani, *J. Org. Chem.*, 1982, **47**, 3237–3241.

- 23 L. Goodman, H. Gu, V. Pophristic, *J. Phys. Chem.*, 2005, **109**, 1223–1229.
- 24 I. Kuprov, J. C. Martin, B. Linclau, *Chem. Commun.*, 2018, **54**, 5118–5121.
- 25 N. E. J. Gooseman, D. O'Hagan, M. J. G. Peach, A. M. Z. Slawin, D. J. Tozer, R. J. Young, *Angew. Chem. Int. Ed.*, 2007, **46**, 5904–5908.
- 26 E. Arunan, G. R. Desiraju, R. A. Klein, J. Sadlej, S. Scheiner, I. Alkorta, D. C. Clary, R. H. Crabtree, J. J. Dannenberg, P. Hobza, H. G. Kjaergaard, A. C. Legon, B. Mennucci, D. J. Nesbitt, *Pure Appl. Chem.*, 2011, **83**, 1637–1641.
- 27 A. Sun, D. C. Lankin, K. Hardcastle, J. P. Snyder, *Chem. Eur. J.*, 2005, **11**, 1579–1591.
- 28 G. Deniau, A. M. Z. Slawin, T. Lebl, F. Chorki, J. P. Issberner, T. Van Mourik, J. M. Heygate, J. J. Lambert, L. Etherington, K. T. Sillar, D. O'Hagan, *ChemBioChem*, 2007, **8**, 2265–2274.
- 29 D. A. Ellis, T. M. Cahill, S. A. Mabury and I. T. Cousins, *Partitioning of Organofluorine Compounds*, 2005.
- 30 A. Borodin, *Compt. Rend.*, 1862, **55**, 553–556
- 31 J. Dumas, E. Péligot, *Ann. Pharm.*, 1835, **15**, 246.
- 32 P. Lebeau, A. Damiens, *Compt. Rend*, 1926, **182**, 1340–1342.
- 33 O. Ruff, R. Keim, *Z. Anorg. Allg. Chem.*, 1930, **192**, 249–256.
- 34 K. Tanaka, M. Ohsuga, Y. Sugimoto, Y. Okafuji, K. Mitshuhashi, *J. Fluor. Chem.*, 1988, **39**, 39–45.
- 35 Á. Gutiérrez-Bonet, W. Liu, *Org. Lett.*, 2023, **25**, 483–487.
- 36 J. A. Cuculo, L. A. Bigelow, *J. Am. Chem. Soc.*, 1952, **74**, 710–713.
- 37 D. A. Wynn, M. M. Rothe, B. D. Pollard, *Talanta*, 1984, **31**, 1063–1040.
- 38 D. W. Kim, H. Jeong, S. T. Lim, M. Sohn, *Tetrahedron Lett.*, 2010, **51**, 432–434.
- 39 G. A. Olah, J. T. Welch, Y. D. Vankar, M. Nojima, I. Kerekes, J. A. Olah, *J. Org. Chem.*, 1979, **44**, 3872–3881.
- 40 V. A. Brunet, A. M. Z. Slawin and D. O'Hagan, *Beilstein J. Org. Chem.*, 2009, **5**, 61.
- 41 O. E. Okoromoba, J. Han, G. B. Hammond, B. Xu, *J. Am. Chem. Soc.*, 2014, **136**, 14381–14384.
- 42 E. M. Woerly, S. M. Banik, E. N. Jacobsen, *J. Am. Chem. Soc.*, 2016, **138**, 13858–13861.
- 43 P. Daumar, B. M. Zeglis, N. Ramos, V. Divilov, K. K. Sevak, N. Pillarsetty, J. S. Lewis, *Eur. J. Med. Chem.*, 2014, **86**, 769–781.



- 44 M. Kaźmierczak, M. Bilska-Markowska, *Eur. J. Org. Chem.*, 2021, **41**, 5585–5604.
- 45 M. K. Nielsen, C. R. Ugaz, W. Li, A. G. Doyle, *J. Am. Chem. Soc.*, 2015, **137**, 9571–9574.
- 46 A. Lheureux, F. Beaulieu, C. Bennett, D. R. Bill, S. Clayton, F. Laflamme, M. Mirmehrabi, S. Tadayon, D. Tovell, M. Couturier, *J. Org. Chem.*, 2010, **75**, 3401–3411.
- 47 J. Baudoux, D. Cahard, *Org. React.*, 2007, **69**, 347–672.
- 48 R. E. Banks, R. G. Syvretb, *J. Chem. Soc., Chem. Comm.*, 1992, **8**, 595–596.
- 49 R. E. Banks, *J. Fluor. Chem.*, 1998, **87**, 1–17.
- 50 S. Poorsadeghi, K. Endo, S. Arimitsu, *Org. Lett.*, 2022, **24**, 420–424.
- 51 F. A. Davis, W. Han, *Tetrahedron Lett.*, 1992, **33**, 1153–1156.
- 52 S. Yuan, W. Zheng, *J. Org. Chem.*, 2022, **87**, 713–720.
- 53 J. G. Hernández, K. J. Ardila-Fierro, D. Barišić and H. Geneste, *Beilstein J. Org. Chem.*, 2022, **18**, 182–189.
- 54 K. J. Ardila-fierro, J. G. Hernandez, *ChemSusChem*, 2021, **14**, 2145–2162.
- 55 Y. Yang, G. B. Hammond, T. Umemoto, *Angew. Chem. Int. Ed.*, 2022, **61**, 1–7.
- 56 H. Deng, D. O’Hagan, C. Schaffrath, *Nat. Prod. Rep.*, 2004, **21**, 773–784.
- 57 D. O’Hagan, R. Perry, J. M. Lock, J. J. M. Meyer, L. Dasaradhi, J. T. G. Hamilton, *Phytochemistry*, 1993, **33**, 1043–1045.
- 58 D. O’Hagan, C. Schaffrath, S. L. Cobb, J. T. G. Hamilton, *Nature*, 2002, **416**, 279.
- 59 D. O’Hagan, H. S. Rzepab, *J. Chem. Soc.*, 1994, 2029–2030.
- 60 H. L. Krebs, H. A. Kornberg, *Nature*, 1957, **179**, 988–991.
- 61 R. A. Peters, R. J. Hall, P. F. V. Ward, *Biochem. J.*, 1960, **77**, 17–22.
- 62 W. Meng, B. S. M. Roberts, A. J. Willetts, *J. Am. Chem. Soc. Perkin Trans.*, 1993, **1**, 1795–1808.
- 63 E. W. Boland, N. E. Headley, *Ann. Rheum. Dis.*, 1954, **13**, 291–296.
- 64 A. Goldfien, J. C. Laidlaw, N. A. Haydar, A. E. Renold, G. W. Thorn, *N. Engl. J. Med.*, 1955, **252**, 415–421.
- 65 Y. Kawasaki, T. Sato, S. Nakano, T. Usui, S. Narumi, T. Ishii, T. Hasegawa, *Clin. Pediatr. Endocrinol.*, 2022, **31**, 93–97.

- 66 V. C. Jordan, *Cancer Res.*, 2016, **76**, 767–768.
- 67 D. B. Longley, D. P. Harkin, P. G. Johnston, *Nat. Rev. Cancer*, 2003, **3**, 330–338.
- 68 L. P. Melean, L. M. Guerrero, L. Lopez, *Oral Maxillofac. Surg.*, 2022, **22**, 1–8.
- 69 M. F. Caminiti, M. El-Rabbany, J. Jeon, G. Bradley, *Pathology*, 2020, **79**, 814–821.
- 70 M. Inoue, Y. Sumii, N. Shibata, *ACS Omega*, 2020, **5**, 10633–10640.
- 71 A. Hill, B. Simmons, D. Gotham, J. Fortunak, *J. Virus Erad.*, 2016, **2**, 28–31.
- 72 M. J. Sofia, D. Bao, W. Chang, J. Du, D. Nagarathnam, S. Rachakonda, P. G. Reddy, B. S. Ross, P. Wang, H. Zhang, S. Bansal, C. Espiritu, M. Keilman, A. M. Lam, H. M. M. Steuer, C. Niu, M. J. Otto, P. A. Furman, *J. Med. Chem.*, 2010, **53**, 7202–7218.
- 73 D. B. Tiz, L. Bagnoli, O. Rosati, F. Marini, L. Sancineto, L. Bagnoli, O. Rosati, F. Marini, L. Sancineto, C. Santi, *Molecules*, 2022, **27**, 1–23.
- 74 J. He, Z. Li, G. Dhawan, W. Zhang, A. E. Sorochinsky, G. Butler, V. A. Soloshonok, J. Han, *Chinese Chem. Lett.*, 2023, **34**, 1–10.
- 75 J. Schoepfer, W. Jahnke, G. Berellini, S. Buonamici, S. Cotesta, S. W. Cowan-jacob, S. Dodd, P. Drueckes, D. Fabbro, T. Gabriel, J. Groell, R. M. Grotzfeld, A. Q. Hassan, V. Iyer, D. Jones, F. Lombardo, A. Loo, P. W. Manley, X. Pelle, G. Rummel, B. Salem, M. Warmuth, A. A. Wylie, T. Zoller, A. L. Marzinzik, P. Furet, *J. Med. Chem.*, 2018, **61**, 8120–8135.
- 76 C. A. Lipinski, F. Lombardo, B. W. Dominy, P. J. Feeney, *Adv. Drug Deliv. Rev.*, 1997, **23**, 3–25.
- 77 J. C. Biffinger, H. W. Kim, S. G. Dimagno, *ChemBioChem*, 2004, **5**, 622–627.
- 78 T. Bechalany, A. Roethlisberger, N. El Tayar, B. Testa, *J. Chromatogr.*, 1989, **473**, 115–124.
- 79 F. A. Gago, J. Alvarez-Builla, J. Elguero, *J. Liq. Chromatogr.*, 1987, **10**, 1031–1047.
- 80 J. E. Garst, *J. Pharm. Sci.*, 1984, **73**, 1623–1629.
- 81 Y. Inel, R. Iseri, *Chemosphere*, 1997, **35**, 993–1002.
- 82 S. H. Yalkowsky, S. C. Valvani, *J. Pharm. Sci.*, 1980, **69**, 912–922.
- 83 H. Böhm, D. Banner, S. Bendels, M. Kansy, B. Kuhn, M. Klaus, U. Obst-sander, M. Stahl, *ChemBioChem*, 2004, **5**, 637–643.
- 84 D. O’Hagan and R. J. Young, *Angew. Chem. Int. Ed.*, 2016, **55**, 3858–3860.
- 85 C. Yu, A. Kütt, G. Rösenthaller, T. Lebl, D. B. Cordes, A. M. Z. Slawin, M. Bühl,

- D. O'Hagan, *Angew. Chem. Int. Ed.*, 2020, **132**, 20077–20081.
- 86 B. Linclau, Z. Wang, G. Compain, V. Paumelle, C. Q. Fontenelle, N. Wells, A. Weymouth-Wilson, *Angew. Chem. Int. Ed.*, 2016, **55**, 674–678.
- 87 B. Jeffries, Z. Wang, H. R. Felstead, J. Y. Le Questel, J. S. Scott, E. Chiarparin, J. Graton, B. Linclau, *J. Med. Chem.*, 2020, **63**, 1002–1031.
- 88 A. P. Dobbs, M. R. Kimberley, *J. Fluor. Chem.*, 2002, **118**, 3–17.
- 89 D. R. Spahn, R. Kocian, *Curr. Pharm. Des.*, 2005, **11**, 4099–4114.
- 90 J. G. Riess, *Artif. Cells. Blood Substit. Immobil. Biotechnol.*, 2005, **33**, 47–63.
- 91 P. Cabrales, B. Y. S. Vaquez, A. C. Negrete, M. Intaglietta, *Transfus. Altern. Transfus. Med.*, 2007, **9**, 294–303.
- 92 J. G. Riess, *Vox Sang.*, 1991, **61**, 225–239.
- 93 O. Y. Cuignet, P. M. Baele, L. J. Van Obbergh, *Anesth. Analg.*, 2002, **95**, 368–372.
- 94 T. H. Shaffer, *Am. Soc. Art. Int. Org. J.*, 2006, **52**, 485–490.
- 95 D. R. Spahn, *Crit. Care*, 1999, **3**, 91–92.
- 96 L. T. Goodnough, M. E. Brecher, M. H. Kanter, J. P. AuBuchon, *New Engl. J. Med.*, 1999, **340**, 438–447.
- 97 W. Caminati, S. Melandri, A. Maris, P. Ottaviani, *Angew. Chem. Int. Ed.*, 2006, **45**, 2438–2442.
- 98 D. O'Hagan, H. S. Rzepa, *Chem. Commun.*, 1997, **7**, 645–652.
- 99 G. M. Dubowchik, V. M. Vrudhula, B. Dasgupta, J. Ditta, T. Chen, S. Sheriff, K. Sipman, M. Witmer, J. Tredup, D. M. Vyas, T. A. Verdoorn, S. Bollini, *Org. Lett.*, 2001, **3**, 17–20.
- 100 M. B. Van Niel, I. Collins, M. S. Beer, H. B. Broughton, S. K. F. Cheng, S. C. Goodacre, A. Heald, K. L. Locker, A. M. Macleod, D. Morrison, C. R. Moyes, D. O. Connor, A. Pike, M. Rowley, M. G. N. Russell, B. Sohal, J. A. Stanton, S. Thomas, H. Verrier, A. P. Watt, *J. Med. Chem.*, 1999, **42**, 2087–2104.
- 101 K. A. Watanabe, U. Reichman, K. Hirota, C. Lopez, J. J. Fox, *J. Med. Chem.*, 1979, **22**, 21–24.
- 102 V. E. Marquez, C. K. Tseng, J. A. Kelley, H. Mitsuya, S. Broder, J. S. Roth, J. S. Driscoll, *Biochem. Pharmacol.*, 1987, **36**, 2719–2722.
- 103 W. Walther, T. Netscher, *Chirality*, 1996, **8**, 397–401.
- 104 K. M. Rentsch, *J. Biochem. Biophys. Methods*, 2002, **54**, 1–9.
- 105 S. V. Rajkumar, *Mayo Clin. Proc.*, 2004, **79**, 899–903.

- 106 W. Rehman, L. M. Arfons, H. M. Lazarus, *Ther. Adv. Hematol.*, 2011, **2**, 291–308.
- 107 T. Eriksson, S. Bjo, P. Höglund, *Eur. J. Clin. Pharmacol.*, 2001, **57**, 365–376.
- 108 W. G. McBride, *Lancet*, 1961, **2**, 1358.
- 109 A. L. Speirs, M. D. Aberd, *Lancet*, 1962, **279**, 303–305.
- 110 C. Tian, P. Xiu, Y. Meng, W. Zhao, Z. Wang, R. Zhou, *Chem. Eur. J.*, 2012, **18**, 14305–14313.
- 111 S. W. Smith, *Toxicol. Sci.*, 2009, **110**, 4–30.
- 112 D. D. Steiner, N. Mase, C. F. Barbas, *Angew. Chem. Int. Ed.*, 2005, **44**, 3706–3710.
- 113 J. Franzén, M. Marigo, D. Fielenbach, T. C. Wabnitz, A. Kjærsgaard and K. A. Jørgensen, *J. Am. Chem. Soc.*, 2005, **127**, 18296–18304.
- 114 T. D. Beeson, D. W. C. Macmillan, *J. Am. Chem. Soc.*, 2005, **127**, 8826–8828.
- 115 S. T. Purrington, N. V. Lazaridis, C. L. Bumgardner, *Tetrahedron Lett.*, 1986, **3**, 2715–2716.
- 116 M. P. Brochu, S. P. Brown, D. W. C. Macmillan, *J. Am. Chem. Soc.*, 2004, **126**, 4108–4109.
- 117 N. Halland, A. Braunton, S. Bachmann, M. Marigo, K. A. Jørgensen, *J. Am. Chem. Soc.*, 2004, **126**, 4790–4791.
- 118 L. Wang, C. Cai, D. P. Curran, W. Zhang, *Synlett*, 2010, **2010**, 433–436.
- 119 O. O. Fadeyi, C. W. Lindsley, *Org. Lett.*, 2009, **11**, 943–946.
- 120 G. Hutchinson, C. Alamillo-ferrer, *J. Am. Chem. Soc.*, 2021, **143**, 6805–6809.
- 121 A. Bazemore, K. A. C. Elliott, E. Florey, *Nature*, 1956, **178**, 1052–1053.
- 122 K. A. C. Elliott, E. Florey, *J. Neuro. Chem.*, 1956, **1**, 181–191.
- 123 S. W. Kuffler, C. Edwards, *J. Neuriphysiol.*, 1957, **21**, 589–610.
- 124 A. M. Abdou, S. Higashiguchi, K. Horie, M. Kim, H. Hatta, H. Yokogoshi, *BioFactors*, 2006, **26**, 201–208.
- 125 P. Nuss, *Neuropsychiatr. Dis. Treat.*, 2015, **11**, 165–175.
- 126 S. Zhang, X. Qian, S. Chang, G. C. Dismukes, D. A. Bryant, *Front. Microbiol.*, 2016, **7**, 1–13.
- 127 K. Kaila, J. Voipio, *Nature*, 1987, **330**, 163–165.
- 128 J. Bormann, O. P. Hamill, B. Sakmann, *J. Physiol.*, 1987, **385**, 243–286.

- 129 N. Rahmati, F. E. Hoebeek, S. Peter, C. I. De Zeeuw, *Front. Cell. Neurosci.*, 2018, **12**, 1–23.
- 130 D. R. Curtis, A. W. Duggan, D. Felix, G. A. R. Johnston, *Nature*, 1970, **228**, 676–677.
- 131 G. A. R. Johnston, *Br. J. Pharma.*, 2013, **169**, 328–336.
- 132 P. S. Miller, A. R. Aricescu, *Nature*, 2015, **512**, 270–275.
- 133 M. Ernst, D. Brauchart, S. Boresch, W. Sieghart, *Neuroscience*, 2003, **119**, 933–943.
- 134 K. Kaupmann, K. Huggel, J. Heid, P. J. Flor, S. Bischoff, S. J. Mickel, G. McMaster, C. Angst, H. Bihiger, W. Froestl, B. Bettler, *Nature*, 1997, **386**, 239–246.
- 135 S. Chuang, D. S. Reddy, *J. Pharmacol. Exp. Ther.*, 2018, **364**, 180–197.
- 136 N. Wongsamitkul, M. C. Maldifassi, X. Simeone, R. Baur, M. Ernst, E. Sigel, *Sci. Rep.*, 2017, **7**, 1–11.
- 137 E. E. Benarroch, *Neurology*, 2012, **78**, 578–584.
- 138 B. M. T. Erunuma, *Proc. Jpn. Acad., Ser. B.*, 2018, **94**, 390–411.
- 139 P. Hudgson, D. Weightman, *Br. Med. J.*, 1971, **4**, 15–17.
- 140 W. Froestl, *Adv. Pharmacol.*, 2010, **58**, 19–62.
- 141 W. Birkmayer, W. Danielczyk, G. Weiler, *Wiener medizinische Wochenschrift*, 1967, **117**, 7.
- 142 P. W. Nathan, E. Pedersen, P. Arlien-Soborg, V. Grynderup, O. Henriksen, *Acta Neurol. Sc.*, 1970, **46**, 257.
- 143 R. F. Jones, D. Burke, J. E. Marosszeky, J. D. Gillies, *J. Neurol. Neurosurg. Psychiat.*, 1970, **33**, 464–468.
- 144 D. J. Hogenkamp, S. H. Tahir, J. E. Hawkinson, R. B. Upasani, M. Alauddin, C. L. Kimbrough, M. Acosta-burrueal, E. R. Whittemore, R. M. Woodward, N. C. Lan, K. W. Gee, M. B. Bolger, *J. Med. Chem.*, 1997, **40**, 61–72.
- 145 D. S. Reddy, R. Woodward, *Drugs Fut.*, 2004, **29**, 227.
- 146 R. B. Carter, P. L. Wood, S. Wieland, J. E. Hawkinson, D. Belelli, J. J. Lambert, H. S. White, H. H. Wolf, S. Mirsadeghi, S. H. Tahir, M. B. Bolger, N. C. Lan, K. W. Gee, *J. Pharmacol. Exp. Ther.*, 1997, **280**, 1284–1295.
- 147 D. S. Reddy, M. A. Rogawski, *Neurotherapeutics*, 2009, **6**, 392–401.
- 148 I. N. Tyurenkov, L. E. Borodkina, V. V. Bagmetova, V. M. Berestovitskaya, O. S. Vasil'eva, *Bull. Exp. Biol. Med.*, 2016, **160**, 465–469.
- 149 R. A. Khaunina, I. P. Lapin, *Khimho-Farmatsevticheskii Zhurnal*, 1976, **10**, 125–127.

- 150 G. K. Talalayenko, A. N. Krivobok, Y. V. Babiy, B. A. Bogdanov, N. N. Perch, *Zh. Vyssh. Nerv. Deyat. Im. I P Pavlova*, 1994, **44**, 1116–1123.
- 151 I. Lapin, *CNS Drug Rev.*, 2001, **7**, 471–481.
- 152 C. R. Doyno, C. M. White, *J. Clin. Pharmacol.*, 2021, **61**, 114–128.
- 153 I. V. Belozertseva, B. V. Andreev, *Zh Vyss. Nerv Deyat Im. I P Pavlov.*, 1997, **47**, 1024–1031.
- 154 R. D. Allan, M. C. Bates, C. A. Drew, R. K. Duke, T. W. Hambley, G. A. R. Johnston, K. N. Mewettl, I. Spencer, *Tetrahedron Lett.*, 1990, **46**, 2511–2524.
- 155 I. P. Lupin, *Vopr. Med. Khim.*, 1997, **43**, 548–556.
- 156 W. Löscher, *Eur. J. Pharmacol.*, 1998, **342**, 1–13.
- 157 R. S. Ryback, L. Brodsky, F. Munasifi, *J. Neuropsychiatry Clin. Neurosci.*, 1997, **9**, 301.
- 158 C. B. Schaffer, L. C. Schaffer, *Am. J. Psychiatry*, 1997, **154**, 291–292.
- 159 J. E. Lavigne, K. Mustian, J. L. Mathews, C. Heckler, O. Palesh, E. Amos, G. R. Morrow, *Breast Cancer Res. Treat.*, 2012, **136**, 479–486.
- 160 B. A. Johnson, R. M. Swift, G. Addolorato, D. A. Ciraulo, H. Myric, *Alcohol Clin. Exp. Res.*, 2005, **29**, 248–254.
- 161 R. E. Appleton, *Neurology*, 1993, **43**, 21–23.
- 162 Z. Wang, R. B. Silverman, *J. Enzyme Inhib. Med. Chem.*, 2004, **19**, 293–301.
- 163 T. Wada, A. Goto, Y. Fukushima, K. Tateyama, *Psychiatry Clin. Neurosci.*, 1961, **15**, 327–335.
- 164 T. Hinton, M. Chebib, G. A. R. Johnston, *Bioorganic Med. Chem. Lett.*, 2008, **18**, 402–404.
- 165 P. Yogeewari, J. V. Ragavendran, D. Sriram, *Recent Pat. CNS Drug Discov.*, 2006, **1**, 113–118.
- 166 J. Kollonitsch, S. Marburg, L. M. Perkins, *J. Org. Chem.*, 1979, **44**, 771–777.
- 167 X. Yang, T. Wu, R. J. Phipps, F. D. Toste, *Chem. Rev.*, 2015, **115**, 826–870.
- 168 S. Bruns, G. Haufe, *J. Fluor. Chem.*, 2000, **104**, 247–254.
- 169 È. Haufe, S. Bruns, M. Runge, *J. Fluor. Chem.*, 2001, **112**, 55–61.
- 170 G. Haufe, S. Bruns, *Adv. Synth. Catal.*, 2002, **344**, 165–171.
- 171 A. M. Forster and A. J. Downs, *J. Chem. Soc. Dalton Trans.*, 1984, **12**, 2827–2834.

- 172 D. Shoback, J. Thatcher, R. Leomeruno, E. Brown, J. C. Melby, *Endocrinology*, 1983, **113**, 424–426.
- 173 E. F. Nemeth, A. Scarpa, *J. Biol. Chem.*, 1987, **262**, 5188–5196.
- 174 D. M. Shoback, L. A. Membreno, J. G. McGhee, *Endocrinology*, 1988, **123**, 382–389.
- 175 O. Kifor, E. M. Brown, *Endocrinology*, 1988, **123**, 2723–2729.
- 176 E. M. Brown, G. Gambatt, D. Riccardi, M. Lombardlt, R. Butters, O. Klfor, A. Suntt, M. A. Hedlgert, J. Lyttont, S. C. Hebertt, *Nature*, 1993, **366**, 575–580.
- 177 E. M. Brown, *Best Pract. Res. Clin. Endocrinol. Metab.*, 2013, **27**, 333–343.
- 178 M. Zaidi, *Biosci. Rep.*, 1990, **10**, 493–507.
- 179 J. A. McKania, A. Chuncharunee, J. Breyer, R. C. Harris, *Kidney Int.*, 1990, **37**, 374–374.
- 180 S. Santhosh, H. Witt, R. H. M. Te Morsche, Z. Nemoda, T. Molnár, A. Pap, J. B. M. J. Jansen, J. P. H. Drenth, *BMC Gastroenterol.*, 2008, **36**, 317–320.
- 181 X. Zhao, Y. Xian, C. Wang, L. Ding, X. Meng, W. Zhu, S. Hang, *J. Vet. Sci.*, 2018, **19**, 179–187.
- 182 B. L. Jones, S. M. Smith, *Front. Physiol.*, 2016, **7**, 1–7.
- 183 R. Xie, B. O. Tang, X. Yong, G. Luo, S. M. Yang, *Int. J. Oncol.*, 2014, **45**, 1355–1362.
- 184 M. M. Dufner, P. Kirchhoff, C. Remy, P. Hafner, M. K. Müller, S. X. Cheng, L. Q. Tang, S. C. Hebert, J. P. Geibel, C. A. Wagner, *Am. J. Physiol. Gastrointest. Liver Physiol.*, 2005, **289**, 1084–1090.
- 185 A. M. Roesler, S. A. Wicher, J. Ravix, R. D. Britt Jr, L. Manlove, J. Teske, K. Cummings, M. A. Thompson, C. Farver, P. MacFarlane, C. M. Pabelick, Y. Prakash, *J. Cell Physiol.*, 2019, **234**, 14187–14197.
- 186 H. R. Toka, M. R. Pollak, P. Houillier, *Physiology*, 2015, **30**, 317–326.
- 187 L. Katie, M. J. Tracy, N. K. Andrew, T. W. Donald, S. M. Rebecca, B. Hans, *Pharmacol Rev.*, 2020, **72**, 558–604.
- 188 J. M. Streeto, *Metabolism*, 1969, **18**, 968–973.
- 189 E. Bellorin-Font, K. J. Martin, *Am. J. Physiol. Ren. Fluid Electrolyte Physiol.*, 1981, **10**, 364–373.
- 190 L. Kantham, S. J. Quinn, O. I. Egbuna, K. Baxi, R. Butters, J. L. Pang, M. R. Pollak, D. Goltzman, E. M. Brown, *Am. J. Physiol. Endocrinol. Metab.*, 2009, **297**, 915–923.
- 191 N. J. Fudge, C. S. Kovacs, *BMC Physiol.*, 2004, **6**, 1–6.

- 192 T. Ohsu, Y. Amino, H. Nagasaki, T. Yamanaka, S. Takeshita, T. Hatanaka, Y. Maruyama, N. Miyamura, Y. Eto, *J. Biol. Chem.*, 2010, **285**, 1016–1022.
- 193 V. N. Babinsky, F. M. Hannan, R. D. Ramracheya, Q. Zhang, M. A. Nesbit, A. Hugill, L. Bentley, T. A. Hough, E. Joynson, M. Stewart, A. Aggarwal, M. Prinz-Wohlgenannt, C. M. Gorvin, E. Källay, S. Wells, R. D. Cox, D. Richards, P. Rorsman, R. V. Thakker, *Endocrinology*, 2017, **158**, 2486–2502.
- 194 P. L. Yarova, A. L. Stewart, V. Sathish, R. D. Britt Jr, M. A. Thompson, A. P. P. Lowe, M. Freeman, B. Aravamudan, H. Kita, S. C. Brennan, M. Schepelmann, T. Davies, S. Yung, Z. Cholisoh, E. J. Kidd, W. R. Ford, K. J. Broadley, K. Rietdorf, W. Chang, M. E. Bin Khayat, D. T. Ward, C. J. Corrigan, J. P. T. Ward, P. J. Kemp, C. M. Pabelick, Y. S. Prakash, D. Riccardi, *Physiol. Behav.*, 2016, **176**, 139–148.
- 195 G. N. Hendy, L. Canaff, D. E. C. Cole, *Best Pract. Res. Clin. Endocrinol. Metab.*, 2013, **27**, 285–301.
- 196 Y. Jiang, E. Minet, Z. Zhang, P. A. Silver, M. Bai, *J. Biol. Chem.*, 2004, **279**, 14147–14156.
- 197 Y. Geng, L. Mosyak, I. Kurinov, H. Zuo, E. Sturchler, T. C. Cheng, P. Subramanyam, A. P. Brown, S. C. Brennan, H. C. Mun, M. Bush, Y. Chen, T. X. Nguyen, B. Cao, D. D. Chang, M. Quick, A. D. Conigrave, H. M. Colecraft, P. McDonald, Q. R. Fan, *Elife*, 2016, **5**, 1–25.
- 198 C. Zhang, T. Zhang, J. Zou, C. L. Miller, R. Gorkhali, J. Y. Yang, A. Schillmiller, S. Wang, K. Huang, E. M. Brown, K. W. Moremen, J. Hu, J. J. Yang, *Sci. Adv.*, 2016, **2**, 1–9.
- 199 S. Chavez-Abiega, I. Mos, P. P. Centeno, T. Elanaf, W. Schlattl, D. T. Ward, J. Goedhart, E. Kallay, *Sensing Extracellular Calcium-An insight into the structure and function of the Calcium Receptor (CaSR).*, 2020, vol. 1131.
- 200 J. Diao, A. Debono, T. M. Josephs, J. E. Bourke, B. Capuano, K. J. Gregory, K. Leach, *ACS Pharmacol. Transl. Sci.*, 2021, **4**, 666–679.
- 201 J. P. Changeux, A. Christopoulos, *Cell*, 2016, **166**, 1084–1102.
- 202 T. M. Josephs, A. N. Keller, E. Khajehali, A. DeBono, C. J. Langmead, A. D. Conigrave, B. Capuano, I. Kufareva, K. J. Gregory, K. Leach, *Br. J. Pharmacol.*, 2020, **177**, 1917–1930.
- 203 P. J. Marie, *Bone*, 2010, **46**, 571–576.
- 204 B. Mayr, D. Schnabel, H. G. N. Dörr, C. Schöfl, *Eur. J. Endocrinol.*, 2016, **174**, R189–R208.
- 205 R. F. Spurney, M. Pi, P. Flannery, L. D. Quarles, *Kidney Int.*, 1999, **55**, 1750–1758.
- 206 Zuzana Saidak, M. Brazier, S. Kamel, R. Mentaverri, *Mol. Pharmacol.*, 2009, **76**, 1131–1144.
- 207 A. Maiti, M. J. Beckman, *J. Steroid Biochem. Mol. Biol.*, 2007, **103**, 504–508.
- 208 A. Maiti, N. C. Hait, M. J. Beckman, *J. Biol. Chem.*, 2008, **283**, 175–183.



- 209 E. F. Nemeth, *Cell Calcium*, 1990, **11**, 323–327.
- 210 E. Brown, P. Enyedi, M. LeBoff, J. Rotberg, J. Preston, C. Chen, *FEBS Lett.*, 1987, **218**, 113–118.
- 211 S. J. Quinn, C. Ye, R. Diaz, O. Kifor, M. Bai, P. Vassilev, M. E. I. Bai, E. Brown, J. Stephen, E. B. The, *Am. J. Physiol. Cell Physiol.*, 1997, **273**, C1315–C1323.
- 212 Ö. Ljunggren, B. B. Fredholm, U. H. Lerner, *Acta Physiol. Scand.*, 1991, **142**, 267–373.
- 213 K. Ray, J. Northup, *J. Biol. Chem.*, 2002, **277**, 18908–18913.
- 214 E. M. Brown, R. Butters, O. K. C. Katz, *Endocrinology*, 1991, **128**, 3047–3054.
- 215 K. M. Krause, A. W. Serio, T. R. Kane, L. E. Connolly, *Cold Spring Harb. Perspect. Med.*, 2016, **6**, 1–18.
- 216 A. D. Conigrave, S. J. Quinn, E. M. Brown, *Proc. Natl. Acad. Sci. U. S. A.*, 2000, **97**, 4814–4819.
- 217 A. D. Conigrave, A. H. Franks, E. M. Brown, S. J. Quinn, *Eur. J. Clin. Nutr.*, 2002, **56**, 1072–1080.
- 218 A. D. Conigrave, H. C. Mun, L. Delbridge, S. J. Quinn, M. Wilkinson, E. M. Brown, *J. Biol. Chem.*, 2004, **279**, 38151–38159.
- 219 S. J. Quinn, M. Bai, E. M. Brown, *J. Biol. Chem.*, 2004, **279**, 37241–37249.
- 220 I. López, E. Aguilera-Tejero, J. C. Estepa, M. Rodríguez, A. J. Felsenfeld, *Am. J. Physiol. Endocrinol. Metab.*, 2004, **286**, 780–785.
- 221 L. A. Fitzpatrick, M. L. Brandi, G. D. Aurbach, *Biochem. Biophys. Res. Commun.*, 1986, **138**, 960–965.
- 222 A. F. Stewart, *N. Engl. J. Med.*, 2004, **351**, 324–326.
- 223 E. F. Nemeth, B. C. Van Wagenen and M. F. Balandrin, *Discovery and Development of Calcimimetic and Calcilytic Compounds*, Elsevier B.V., 1st edn., 2018, vol. 57.
- 224 R. Bayer, R. Mannhold, *Pharmatherapeutica*, 1987, **5**, 103–136.
- 225 FDA, *FULL PRESCRIBING INFORMATION Secondary Hyperparathyroidism Sensipar is indicated for the treatment of secondary hyperparathyroidism ( HPT ) in patients with chronic kidney disease ( CKD ) on dialysis. Parathyroid Carcino*, 2011.
- 226 S. J. Silverberg, M. R. Rubin, C. Faiman, M. Peacock, D. M. Shoback, R. C. Smallridge, L. E. Schwanauer, K. A. Olson, P. Klassen, J. P. Bilezikian, *J. Clin. Endocrinol. Metab.*, 2007, **92**, 3803–3808.
- 227 G. A. Block, D. Zaun, G. Smits, M. Persky, S. Brillhart, K. Nieman, J. Liu, W. L. St Peter, *Kidney Int.*, 2010, **78**, 578–589.

- 228 A. W. Gannon, H. M. Monk, M. A. Levine, *J. Clin. Endocrinol. Metab.*, 2014, **99**, 7–11.
- 229 G. A. Block, D. A. Bushinsky, S. Cheng, *JAMA*, 2017, **317**, 156–164.
- 230 Amgen, AMGEN REPORTS FOURTH QUARTER AND FULL YEAR 2021 FINANCIAL RESULTS, <https://www.prnewswire.com/news-releases/amgen-reports-fourth-quarter-and-full-year-2021-financial-results-301476867.html>.
- 231 M. Gowen, E. F. Nemeth, J. Fox, M. Gowen, G. B. Stroup, R. A. Dodds, I. E. James, B. J. Votta, B. R. Smith, P. K. Bhatnagar, A. M. Lago, J. F. Callahan, E. G. Delmar, M. A. Miller, E. F. Nemeth, J. Fox, *J. Clin. Invest.*, 2000, **105**, 1595–1604.
- 232 E. M. Nemeth, *L. Mol. Endocrinol.*, 2002, **29**, 15–21.
- 233 R. W. Marquis, A. M. Lago, J. F. Callahan, A. Rahman, X. Dong, G. B. Stroup, S. Hoffman, M. Gowen, E. G. Delmar, B. C. Van Wagenen, S. Logan, S. Shimizu, J. Fox, E. F. Nemeth, T. Roethke, B. R. Smith, K. W. Ward, P. Bhatnagar, *J. Med. Chem.*, 2009, **2**, 6599–6605.
- 234 G. Balan, J. Bauman, S. Bhattacharya, M. Castrodad, D. R. Healy, M. Herr, P. Humphries, S. Jennings, A. S. Kalgutkar, B. Kapinos, V. Khot, K. Lazarra, M. Li, Y. Li, C. Neagu, R. Oliver, D. W. Piotrowski, D. Price, H. Qi, H. A. Simmons, J. Southers, L. Wei, Y. Zhang, V. M. Paralkar, *Bioorg. Med. Chem. Lett.*, 2009, **19**, 3328–3332.
- 235 S. Kumar, C. J. Matheny, S. J. Hoffman, R. W. Marquis, M. Schultz, X. Liang, J. A. Vasko, G. B. Stroup, V. R. Vaden, H. Haley, J. Fox, E. G. Delmar, E. F. Nemeth, A. M. Lago, J. F. Callahan, P. Bhatnagar, W. F. Huffman, M. Gowen, B. Yi, T. M. Danoff, L. A. Fitzpatrick, *Bone*, 2010, **46**, 534–542.
- 236 L. A. Fitzpatrick, C. E. Dabrowski, G. Cicconetti, D. N. Gordon, T. Fuerst, K. Engelke, H. K. Genant, *J. Bone Miner. Res.*, 2012, **27**, 255–262.
- 237 M. R. John, E. Harfst, J. Loef, R. Belleli, J. Mason, G. J. M. Bruin, K. Seuwen, L. B. Klickstein, L. Mindeholm, L. Widler, M. Kneissel, *Bone*, 2014, **64**, 204–210.
- 238 A. Phase, J. Halse, S. Greenspan, F. Cosman, G. Ellis, A. Santora, A. Leung, N. Heyden, S. Samanta, S. Doleckyj, E. Rosenberg, A. E. Denker, *J. Clin. Endocrinol. Metab.*, 2014, **99**, 2207–2215.
- 239 P. L. Yarova, P. Huang, M. W. Schepelmann, R. Bruce, R. Ecker, R. Nica, V. Telezhkin, D. Traini, L. Gomes, E. J. Kidd, W. R. Ford, K. J. Broadley, B. M. Kariuki, C. J. Corrigan, J. P. T. Ward, P. J. Kemp, D. Riccardi, *J. Pharmacol. Exp. Ther.*, 2021, **376**, 51–63.
- 240 L. Ardeshirpour, P. Dann, M. Pollak, J. Wysolmerski, J. Vanhouten, *Bone*, 2006, **38**, 787–793.
- 241 K. Leach, K. J. Gregory, I. Kufareva, E. Khajehali, A. E. Cook, R. Abagyan, A. D. Conigrave, P. M. Sexton, A. Christopoulos, *Cell Res.*, 2016, **26**, 574–592.
- 242 S. Kumar, C. Matheny, B. Yi, M. McLaughlin, J. Phillips, L. Skordos, D. Ethgen, *J. Bone Miner. Res.*, 2008, **23**, S50–S50.
- 243 F. Fukumoto, T. Nakamura, Y. Nishizawa, M. Hoyashi, T. Matsumoto, *Endocr. J.*,

- 2010, **57**, S481–S482.
- 244 A. Kessler, H. Faure, C. Petrel, D. Rognan, M. Césario, M. Ruat, P. Dauban, R. H. Dodd, *J. Med. Chem.*, 2006, **49**, 5119–5128.
- 245 C. Petrel, A. Kessler, F. Maslah, P. Dauban, R. H. Dodd, D. Rognan, M. Ruat, *J. Biol. Chem.*, 2003, **278**, 49487–49494.
- 246 C. Petrel, A. Kessler, P. Dauban, R. H. Dodd, D. Rognan, M. Ruat, *J. Biol. Chem.*, 2004, **279**, 18990–18997.
- 247 K. J. Gregory, I. Kufareva, A. N. Keller, E. Khajehali, H. Mun, M. A. Goolam, R. S. Mason, B. Capuano, A. D. Conigrave, A. Christopoulos, K. Leach, *ACS Pharmacol. Transl. Sci.*, 2018, **1**, 96–109.
- 248 P. W. Chia, S. C. Brennan, A. M. Z. Slawin, D. Riccardi, D. O’Hagan, *Org. Biomol. Chem.*, 2012, **10**, 7922–7927.
- 249 S. . Cole, R. Brosch, J. Parkhill, T. Garnier, C. Churcher, D. Harris, S. V. Gordon, K. Eiglmeier, S. Gas, C. E. Barry, F. Tekaiia, K. Badcock, D. Basham, D. Brown, T. Chillingworth, R. Connor, R. Davies, K. Devlin, T. Feltwell, S. Gentles, N. Hamlin, S. Holroyd, T. Hornsby, K. Jagels, A. Krogh, J. McLean, S. Moule, L. Murphy, K. Oliver, J. Osborne, M. A. Quail, M. A. Rajandream, J. Rogers, S. Rutter, K. Seeger, J. Skelton, R. Squares, S. Squares, J. E. Sulston, K. Taylor, S. Whitehead, B. G. Barrell, *Nature*, 1998, **393**, 537–544.
- 250 E. Cambau, M. Drancourt, *Clin. Microbiol. Infect.*, 2014, **20**, 196–201.
- 251 Image taken from: <https://elifesciences.org/digests/41129/tuberculosis-bacteria-thrive-on-a-nitrogen-source-buffet>.
- 252 H. Herbert Fox, *Science.*, 1952, **116**, 129–134.
- 253 M. H. Lepper, H. W. Spies, N. H. Blatt, H. F. Dowling, *J. Clin. Lab. Clin. Med.*, 1952, **40**, 821–822.
- 254 D. A. L. Bowen, D. M. Collins, *Tubercle*, 1952, **33**, 276–278.
- 255 C. L. Joinier, K. S. Maclean, E. K. Pritchard, K. Anderson, M. B. King, P. Collard, R. Knox, *Lancet*, 1952, **263**, 843–849.
- 256 H. M. Blumberg, W. J. Burman, R. E. Chaisson, C. L. Daley, S. C. Etkind, L. N. Friedman, P. Fujiwara, M. Grzemska, P. C. Hopewell, M. D. Iseman, R. M. Jasmer, V. Koppaka, R. I. Menzies, R. J. O’Brien, R. R. Reves, L. B. Reichman, P. M. Simone, J. R. Starke, A. A. Vernon, *Am. J. Respir. Crit. Care Med.*, 2003, **167**, 603–662.
- 257 M. A. Huaman, T. R. Sterling, *Clin. Chest Med.*, 2019, **40**, 839–848.
- 258 G. S. Timmins, S. Master, F. Rusnak, V. Deretic, *Antimicrob. Agents Chemother.*, 2004, **48**, 3006–3009.
- 259 K. Takayama, C. Wang, G. S. Besra, *Clin. Microbiol. Rev.*, 2005, **18**, 81–101.
- 260 K. J. Seung, S. Keshavjee, M. L. Rich, *Handb. Antimicrob. Resist.*, 2015, **5**, 1–11.

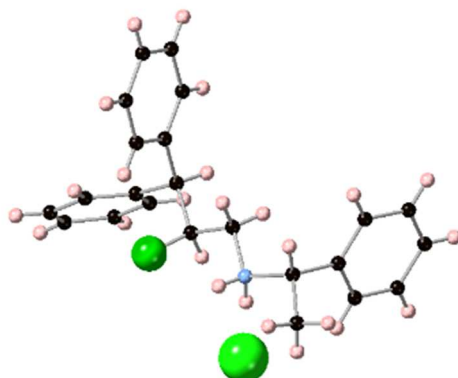
- 261 M. Cumpston, T. Li, M. J. Page, J. Chandler, V. A. Welch, J. P. Higgins, J. Thomas, *Cochrane database Syst. Rev.*, 2019, **10**, ED000142.
- 262 P. Sensi, *Rev. Infect. Dis.*, 1983, **5**, S402–S406.
- 263 C. Calvani, L. Frontali, L. Leoni, G. Tecce, *Nature*, 1965, **207**, 417–418.
- 264 E. A. Campbell, N. Korzheva, A. Mustaev, K. Murakami, S. Nair, A. Goldfarb, S. A. Darst, *Cell*, 2001, **104**, 901–912.
- 265 B. P. Goldstein, *J. Antibiot. (Tokyo)*, 2014, **67**, 625–630.
- 266 R. P. Bhusal, G. Bashiri, B. X. C. Kwai, J. Sperry and I. K. H. Leung, *Drug Discov. Today*, 2017, **22**, 1008–1016.
- 267 L. G. Wayne, K. Y. Lin, *Infect. Immun.*, 1982, **37**, 1042–1049.
- 268 N. K. Dutta, P. C. Karakousis, *Microbiol. Mol. Biol. Rev.*, 2014, **78**, 343–371.
- 269 E. Petruccioli, T. J. Scriba, L. Petrone, M. Hatherill, D. M. Cirillo, S. A. Joosten, T. H. Ottenhoff, C. M. Denking, D. Goletti, *Eur. Respir. J.*, 2016, **48**, 1751–1763.
- 270 J. C. Betts, P. T. Lukey, L. C. Robb, R. A. McAdam, K. Duncan, *Mol. Microbiol.*, 2002, **43**, 717–731.
- 271 K. H. Zu Bentrup, A. Miczak, D. L. Swenson, D. G. Russell, *J. Bacteriol.*, 1999, **181**, 7161–7167.
- 272 V. Sharma, S. Sharma, K. Hoener Zu Bentrup, J. D. McKinney, D. G. Russell, W. R. Jacobs, J. C. Sacchettini, *Nat. Struct. Biol.*, 2000, **7**, 663–668.
- 273 E. J. Muñoz-Elías, J. D. McKinney, *Nat. Med.*, 2005, **11**, 638–644.
- 274 T. A. Gould, H. Van De Langemheen, E. J. Muñoz-Elías, J. D. McKinney, J. C. Sacchettini, *Mol. Microbiol.*, 2006, **61**, 940–947.
- 275 R. P. Bhusal, W. Jiao, B. X. C. Kwai, J. Reynisson, A. J. Collins, J. Sperry, G. Bashiri, I. K. H. Leung, *Nat. Commun.*, 2019, **10**, 1–7.
- 276 D. Sriram, P. Senthilkumar, D. Sangaraju, R. Nelli, P. Bhat, H. Thimmappa, *Chem. Biol. Drug. Des.*, 2010, **75**, 381–391.
- 277 D. Sriram, P. Yogeewari, D. Ravi, K. Vyas, P. Senthilkumar, P. Bhat, M. Srividya, *Bioorganic Med. Chem. Lett.*, 2010, **20**, 4313–4316.
- 278 M. Dinakaran, P. Senthilkumar, P. Yogeewari, A. China, V. Nagaraja, D. Sriram, *Med. Chem.*, 2008, **4**, 482–491.
- 279 R. R. Kumar, S. Perumal, P. Senthilkumar, P. Yogeewari, D. Sriram, *J. Med. Chem.*, 2008, **51**, 5731–5735.
- 280 M. Dinakaran, P. Senthilkumar, P. Yogeewari, *Bioorg. Med. Chem. Lett.*, 2008, **18**, 1229–1236.
- 281 M. Dinakaran, P. Senthilkumar, P. Yogeewari, *Bioorganic Med. Chem.*, 2008, **16**,

- 3408–3418.
- 282 D. Sriram, P. Senthilkumar, M. Dinakaran, P. Yogeewari, *J. Med. Chem.*, 2007, **50**, 6232–6239.
- 283 D. Sriram, P. Yogeewari, M. Dinakaran, *J. Antimicrob. Chemother.*, 2007, **59**, 1194–1196.
- 284 R. R. Kumar, S. Perumal, P. Senthilkumar, P. Yogeewari, D. Sriram, *Bioorg. Med. Chem. Lett.*, 2007, **17**, 6459–6462.
- 285 D. Sriram, P. Yogeewari, *J. Med. Chem.*, 2006, **49**, 3448–3450.
- 286 D. Sriram, P. Yogeewari, P. Senthilkumar, S. Dewakar, N. Rohit, B. Debjani, P. Bhat, B. Veugopal, V. V. S. Pavan, H. M. Thimmappa, *Med. Chem.*, 2009, **5**, 422–422.
- 287 D. Sriram, P. Yogeewari, P. Dhakla, P. Senthilkumar, D. Banerjee, T. H. Manjashetty, *Bioorg. Med. Chem. Lett.*, 2009, **19**, 1152–1154.
- 288 R. P. Tangallapally, R. Yendapally, R. E. Lee, A. J. M. Lenaerts, R. E. Lee, *J. Med. Chem.*, 2005, **48**, 8261–8269.
- 289 Y. Hee Ko, B. A. Mcfadden, *Arch. Biochem. Biophys.*, 1990, **278**, 373–380.
- 290 J. V Schloss, W. W. Cleland, *Biochemistry*, 1982, **21**, 4420–4427.
- 291 M. Krátký, E. Novotná, J. Stolaříková, M. Švarcová, J. Vinšová, *Eur. J. Pharm. Sci.*, 2022, **176**, 106252.
- 292 B. A. Mcfadden, S. Purohit, *J. Bacteriol.*, 1977, **131**, 136–144.
- 293 T. V. Pham, A. S. Murkin, M. M. Moynihan, L. Harris, P. C. Tyler, N. Shetty, J. C. Sacchettini, H. ling Huang, T. D. Meek, *Proc. Natl. Acad. Sci. U. S. A.*, 2017, **114**, 7617–7622.
- 294 D. M. Mellott, D. Torres, I. V. Krieger, S. A. Cameron, Z. Moghadamchargari, A. Laganowsky, J. C. Sacchettini, T. D. Meek, L. D. Harris, *J. Am. Chem. Soc.*, 2021, **143**, 17666–17676.
- 295 S. Ray, D. F. Kreitler, A. M. Gulick, A. S. Murkin, *ACS Chem. Biol.*, 2018, **13**, 1470–1473.
- 296 B. X. C. Kwai, A. J. Collins, M. J. Middleditch, J. Sperry, G. Bashiri, I. K. H. Leung, *RSC Med. Chem.*, 2021, **12**, 57–61.
- 297 T. V. Pham, D. M. Mellott, Z. Moghadamchargari, K. Chen, I. Krieger, A. Laganowsky, J. C. Sacchettini, T. D. Meek, *ACS Chem. Biol.*, 2021, **16**, 463–470.
- 298 B. C. Djerassi, R. R. Engle, *J. Am. Chem. Soc.*, 1953, **75**, 3838–3840.
- 299 R. K. Hill, S. R. Prakash, T. M. Zydowsky, *J. Org. Chem.*, 1984, **49**, 1666–1669.
- 300 P. H. J. Carlsen, T. Katsuki, V. S. Martin, K. B. Sharpless, *J. Org. Chem.*, 1981, **46**, 3936–3938.

- 301 S. Ciceri, P. Grisenti, S. R. Elahi, P. Ferraboschi, *Molecules*, 2018, **23**, 1–11.
- 302 M. Kawasaki, D. Kato, T. Okada, Y. Morita, Y. Tanaka, N. Toyooka, *Tetrahedron*, 2020, **76**, 130984.
- 303 W. R. Dolbier Jr., *Guide to Fluorine NMR for Organic Chemists*, 2016.
- 304 D. O'Hagan, H. S. Rzepa, M. Schüler, A. M. Z. Slawin, *Beilstein J. Org. Chem.*, 2006, **2**, 1–13.
- 305 H. Abas, J. Mas-roselló, M. M. Amer, D. J. Durand, R. R. Groleau, N. Fey, J. Clayden, *Angew. Chem. Int. Ed.*, 2019, **58**, 2418–2422.
- 306 U. Grošelj, A. Beck, W. B. Schweizer, D. Seebach, *Helv. Chim. Acta*, 2014, **97**, 751–796.
- 307 Q. Yue, T. Yang, Y. Yang, C. Zhang, Q. Zhang, D. Li, *Asian J. Org. Chem.*, 2017, **6**, 936–942.
- 308 L. Ghosez, G. Yang, J. R. Cagnon, F. Le Bideau, J. Marchand-Brynaert, *Tetrahedron*, 2004, **60**, 7591–7606.
- 309 H. Huang, C. Yu, Y. Zhang, Y. Zhang, P. S. Mariano, W. Wang, *J. Am. Chem. Soc.*, 2017, **139**, 9799–9802.
- 310 H. Doušová, R. Horák, Z. Růžicková, P. Šimůnek, *Beilstein J. Org. Chem.*, 2015, **11**, 884–892.
- 311 F. Chalyavi, P. H. Gilmartin, A. J. Schmitz, M. W. Fennie, M. J. Tucker, *Angew. Chem. Int. Ed.*, 2018, **57**, 7528–7532.

## Annexe 1

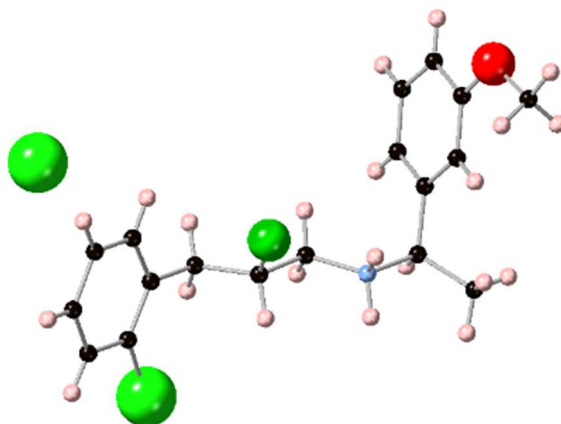
Crystal data and structure refinement for (<sup>F</sup>*R,R*)-287



CCDC number	2259660
formula	C <sub>23</sub> H <sub>25</sub> Cl <sub>2</sub> N
fw	369.89
crystal description	Colourless prism
crystal size [mm <sup>3</sup> ]	0.11×0.08×0.05
space group	<i>P</i> 2 <sub>1</sub> 2 <sub>1</sub> 2 <sub>1</sub>
<i>a</i> [Å]	9.62111(9)
<i>b</i> [Å]	9.94701(9)
<i>c</i> [Å]	20.1391(2)
$\alpha$ [°]	
$\beta$ [°]	
$\gamma$ [°]	
vol [Å <sup>3</sup> ]	1927.34(3)
<i>Z</i>	4
$\rho$ (calc) [g/cm <sup>3</sup> ]	1.275
$\mu$ [mm <sup>-1</sup> ]	1.867
F(000)	784
reflections collected	20184
independent reflections	3502 (0.0274)
( <i>R</i> <sub>int</sub> )	
parameters, restraints	244, 2
GoF on <i>F</i> <sup>2</sup>	1.044
<i>R</i> <sub>1</sub> [ <i>I</i> > 2 $\sigma$ ( <i>I</i> )]	0.0237
<i>wR</i> <sub>2</sub> (all data)	0.0640
largest diff. peak/hole	0.201, -0.132
[e/Å <sup>3</sup> ]	
Flack parameter	-0.019(4)

## Annexe 2

Crystal data and structure refinement for (<sup>F</sup>*F,R*)-288.

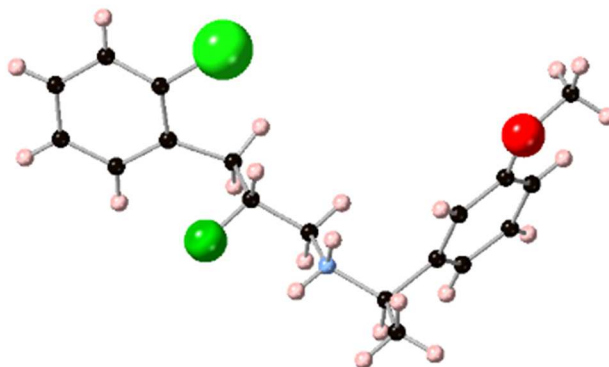


CCDC number	2259658
formula	C <sub>18</sub> H <sub>22</sub> Cl <sub>2</sub> FNO
fw	358.26
crystal description	Colourless needle
crystal size [mm <sup>3</sup> ]	0.16×0.03×0.01
space group	<i>P</i> 2 <sub>1</sub> 2 <sub>1</sub> 2 <sub>1</sub>
<i>a</i> [Å]	7.3528(4)
<i>b</i> [Å]	10.6598(5)
<i>c</i> [Å]	23.949(2)
<i>α</i> [°]	
<i>β</i> [°]	
<i>γ</i> [°]	
vol [Å <sup>3</sup> ]	1877.1(2)
<i>Z</i>	4
<i>ρ</i> (calc) [g/cm <sup>3</sup> ]	1.268
<i>μ</i> [mm <sup>-1</sup> ]	3.215
F(000)	752
reflections collected	19872
independent reflections	3428 (0.0883)
( <i>R</i> <sub>int</sub> )	
parameters, restraints	219, 2
GoF on <i>F</i> <sup>2</sup>	1.017
<i>R</i> <sub>1</sub> [ <i>I</i> > 2σ( <i>I</i> )]	0.0453
<i>wR</i> <sub>2</sub> (all data)	0.1183
largest diff. peak/hole	0.251, -0.250
[e/Å <sup>3</sup> ]	
Flack parameter	-0.001(13)



## Annexe 3

Crystal data and structure refinement for (<sup>F</sup>*R,R*)-288.



CCDC number	2259659
formula	C <sub>18</sub> H <sub>22</sub> Cl <sub>2</sub> FNO
fw	358.26
crystal description	Colourless prism
crystal size [mm <sup>3</sup> ]	0.20×0.02×0.02
space group	<i>P</i> 4 <sub>1</sub>
<i>a</i> [Å]	16.6794(7)
<i>b</i> [Å]	
<i>c</i> [Å]	7.1292(4)
$\alpha$ [°]	
$\beta$ [°]	
$\gamma$ [°]	
vol [Å <sup>3</sup> ]	1983.4(2)
<i>Z</i>	4
$\rho$ (calc) [g/cm <sup>3</sup> ]	1.200
$\mu$ [mm <sup>-1</sup> ]	0.339
F(000)	752
reflections collected	12142
independent reflections	3938 (0.0365)
( <i>R</i> <sub>int</sub> )	
parameters, restraints	282, 276
GoF on <i>F</i> <sup>2</sup>	1.045
<i>R</i> <sub>1</sub> [ <i>I</i> > 2σ( <i>I</i> )]	0.0556
<i>wR</i> <sub>2</sub> (all data)	0.1559
largest diff. peak/hole	0.770, -0.292
[e/Å <sup>3</sup> ]	
Flack parameter	-0.02(3)